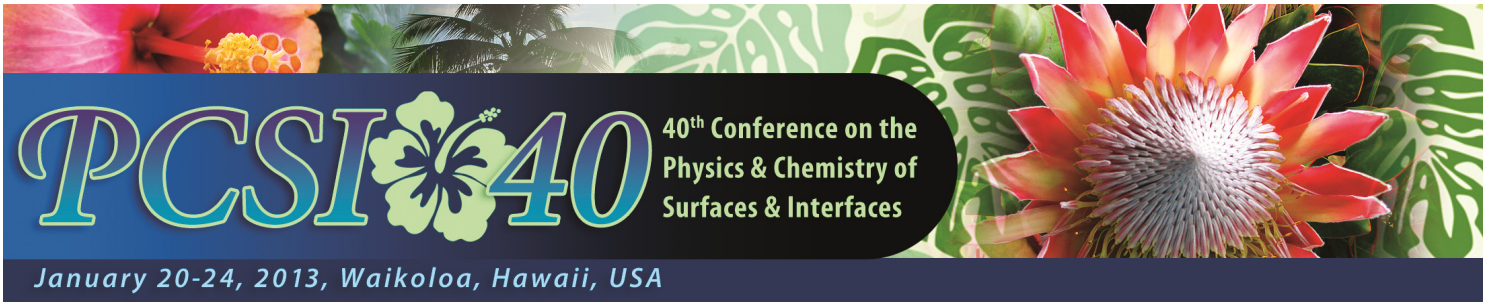

Abstract Book & Schedule

Corporate Gold Sponsors

Omicron
An Oxford Instruments Company

SPECS™

SVT Associates, Inc.

Corporate Silver Sponsors

AMERICAN ELEMENTS

INTEGRATED ENGINEERING SOFTWARE

Kurt J. Lesker® Company

VG SCIENTA

PCSI 40 General Information

Conference Hotel:
Waikoloa Beach Marriott Resort & Spa, Waikoloa, Hawaii

Program Committee:
- Chagaan Baatar, Office of Naval Research
- Anand Bhattacharya, Argonne National Lab
- Leonard Brillson, The Ohio State University
- Alex Demkov, University of Texas, Austin
- Helen Farrell
- Michael Flatté, University of Iowa
- Rachel S. Goldman, University of Michigan
- Jessica Hilton, Omicron NanoTechnology
- Harold Hwang, Stanford University
- Hisao Ishii, Chiba University
- Karen Kavanagh, Simon Fraser University
- Roland Kawakami, University of California, Riverside
- William Lampert, Sustema Research LLC
- Lincoln Lauhon, Northwestern University
- Matthew R. Libera, Stevens Institute of Technology
- Rudy Ludeke
- Chris McConville, Warwick University
- Anders Mikkelsen, Lund University
- Chris J. Palmstrøm, University of California, Santa Barbara
- Henning Riechert, Paul Drude Institute
- Jack Rowe
- Nitin Samarth, Penn State University
- Akira Toriumi, University of Tokyo
- Chakrapani Varanasi, Army Research Office
- Robert Wallace, University of Texas, Dallas
- Ed Yu, University of Texas at Austin

Chair:
Robert Wallace *(University of Texas, Dallas)*
E-mail: rmwallace@utdallas.edu

General Chair:
Chris Palmstrøm
University of California, Santa Barbara
E-mail: cpalmstrom@ece.ucsb.edu

JVST Special Issue Editor:
Rudy Ludeke
E-mail: rudy_ludeke@msn.com

Registration:
Della Miller/Heather Korff
AVS, 110 Yellowstone Dr., Suite 120
Chico, CA 95973
E-mail: della@avs.org /heather@avs.org
Phone: 530-896-0477

Conference Website: www.pcsiconference.org

Presentation Formats:
Invited Talks—25 minute oral presentation, 5 minute discussion, plus poster
Upgraded Talks—17 minute oral presentation, 3 minute discussion, plus poster
Contributed Talks—4 minute oral presentation (max 3 slides, 1 minute discussion, plus poster)
Posters—Displayed all week (46 inches tall x 44 inches wide)

PCSI 40 General Sponsors

AVS

PCSI 40 Corporate Sponsors

Gold

Conference Banquet

Omicron
An Oxford Instruments Company

Monday Dinner

SPECS™

Lunches

SVT Associates, Inc.

Silver

Coffee Breaks

AMERICAN ELEMENTS

INTEGRATED ENGINEERING SOFTWARE

Kurt J. Lesker® Company

VG SCIENTA

PCSI 40 Schedule Overview

Sunday:

Su1400 Registration
Su1455 Welcome Remarks
Su1500 Sunday Afternoon Session: *2-D Materials*
Su1705 Poster Setup
Su1730 Welcome Reception
Su1930 Sunday Evening Session: *Complex Oxides*

Monday:

Mo0730 Registration and Continental Breakfast
Mo0830 Monday Morning Session: *Interface & Surface Magnetism*
Mo1000 Coffee Break and Poster Viewing
Mo1100 Monday Morning Session: *Semiconductor Growth & Surfaces*
Mo1210 Lunch and Poster Viewing
Mo1400 Monday Afternoon Session: *Spintronics with Organics*
Mo1500 Coffee Break and Poster Viewing
Mo1600 Monday Afternoon Session: *Surface Passivation & High-K Dielectrics*
Mo1730 Dinner
Mo1930 Monday Evening Session: *Energy Materials*

Tuesday:

Tu0730 Registration and Continental Breakfast
Tu0830 Tuesday Morning Session: *Contacts & Nanocontacts*
Tu0950 Coffee Break and Poster Viewing
Tu1050 Tuesday Morning Session: *New Tools & Applications*
Tu1215 Free Afternoon
Tu1930 Tuesday Evening Session: *Topological Insulators I*

Wednesday:

We0730 Registration and Continental Breakfast
We0830 Wednesday Morning Session: *Topological Insulators II*
We0945 Coffee Break and Poster Viewing
We1045 Wednesday Morning Session: *Spintronics Inorganic & Organic*
We1210 Lunch and Poster Viewing
We1330 Wednesday Afternoon Session: *Nanowire Growth & Strain Effects*
We1445 Coffee Break and Poster Viewing
We1515 Wednesday Afternoon Session: *Epitaxy & Graphene I*
We1700 Conference Banquet Luau

Thursday:

Th0730 Continental Breakfast
Th0830 Thursday Morning Session: *Spin Torque & Graphene*
Th0930 Coffee Break and Poster Viewing
Th0830 Thursday Morning Session: *Graphene II*
Th1145 Conference Ends

PCSI 40 Schedule

Sunday Afternoon:

Su1400	2:00 p.m.	Registration		
Su1455	2:55 p.m.	Welcome Remarks		
2-D Materials				Session Chair: R. Ludeke
Su1500	3:00 p.m.	INVITED: Silicene: Graphene's Topologically Non-trivial Cousin		G. Le Lay, Aix-Marseille Univ., CNRS-CINaM, Campus de Luminy and CNR-ISM
Su1530	3:30 p.m.	Silicene: From the Formation of Single 2D Layers to Stacks of Graphitic-Si		P. Vogt, Technische Universitaet Berlin; P. De Padova, CNR; T. Bruhn, Technische Universitaet Berlin/ Aix-Marseille Univ., CNRS; A. Resta, Aix-Marseille Univ., CNRS; G. Le Lay, Aix-Marseille Univ., CNRS; CNR
Su1535	3:35 p.m.	UPGRADED: LT-STM/STS Investigation of the Electronic Properties of Epitaxial Silicene		A. Fleurence, JAIST; Y. Yoshida, The Univ. of Tokyo; C-C. Lee, T. Ozaki, JAIST; Y. Hasegawa, The Univ. of Tokyo; Y-Y. Takamura, JAIST
Su1555	3:55 p.m.	UPGRADED: Yttria (Y_2O_3) Growth by Reactive MBE on Graphene		M. Batzill, Univ. of South Florida
Su1615	4:15 p.m.	STM Studies of Sidewall Graphene Nanoribbons		D.B. Torrance, Y. Li, M. Swegan Nevius, J.O. Andrews, B. Zhang, P.N. First, Georgia Tech
Su1620	4:20 p.m.	Ballistic Phonon Thermal Conductance in Graphene Nano-ribbon		H. Tomita, J. Nakamura, The Univ. of Electro-Communications (UEC-Tokyo)
Su1625	4:25 p.m.	Controlled Motion of Freestanding Graphene and Graphene on Graphite via Scanning Tunneling Microscopy		P. Xu, Y. Yang, D. Qi, S.D. Barber, J.K. Schoelz, M.L. Ackerman, L. Bellaiche, P.M. Thibado, Univ. of Arkansas
Su1630	4:30 p.m.	INVITED: Single-layer MoS_2 – Electrical Transport and Devices		A. Kis, EPFL
Su1700	5:00 p.m.	Dynamic Negative Compressibility of Solid Lubricants		B. Neves, A.P. Barboza, H. Chacham, C. Oliveira, T. Fernandes, UFMG; E. Ferreira, B. Archanjo, Inmetro; R. Batista, A. Oliveira, UFOP
Su1705	5:05 p.m.	Poster Setup		
Su1730	5:30 p.m.	Welcome Reception		

Sunday Evening:

Complex Oxides				Session Chair: E. Yu
Su1930	7:30 p.m.	INVITED: Two-dimensional Electron Gas at the Atomically Smooth $LaAlO_3/SrTiO_3$ (111) Interface		C. Eom, Univ. of Wisconsin-Madison
Su2000	8:00 p.m.	Investigation of Interfacial Electronic Properties of $LaAlO_3/SrTiO_3$ Using Scanning Tunneling Microscopy		Y.P. Chiu, B.C. Huang, P.C. Huang, W.C. Wang, National Sun Yat-sen Univ.; V.T. Tra, Institute of Physics, National Chiao Tung Univ., J.C. Yang, National Chiao Tung Univ.; Q. He, Advanced Light Source, Lawrence Berkeley National Laboratory; J.Y. Lin, Institute of Physics, National Chiao Tung Univ., C.S. Chang, Institute of Physics, Academia Sinica; Y.H. Chu, National Chiao Tung Univ.
Su2005	8:05 p.m.	Intrinsic Spin-orbit Effects in $LaAlO_3/SrTiO_3$ interface 2DEGs		C. Sahin, Univ. of Iowa; G. Vignale, Univ. of Missouri; M.E. Flatté, Univ. of Iowa
Su2010	8:10 p.m.	INVITED: Unusual Behavior of Quantum-well Subbands in Transition-metal Oxide Thin Films		H. Kumigashira, KEK/Japan
Su2040	8:40 p.m.	Electric Field Control of the Verwey Transition and Induced Magnetoelectric Effect in Magnetite		J. Wong, A. Swartz, R. Zheng, W. Han, R. Kawakami, UC Riverside
Su2045	8:45 p.m.	Reduced Symmetry and Orbital Order at Perovskite Surfaces and Interfaces		A. Demkov, J. Lee, K. Fredrickson, C. Lin, C. Mitra, The Univ. of Texas
Su2050	8:50 p.m.	Interplay of Native Point Defects in $SrTiO_3$, $BaTiO_3$, and $BaxSr_{1-x}TiO_3/SrTiO_3$ Heterojunctions with Growth Temperature, Oxidation, and Strain		L. Brillson, S. Shen, M. Rutkowski, K. McNicholas, S. Balaz, T. Merz, The Ohio State Univ.; C. Brooks, D. Schlom, Cornell Univ.

Su2055	8:55 p.m.	High Quality $SrVO_3$ Thin Films Grown by Hybrid Molecular Beam Epitaxy		J.A. Moyer, C. Eaton, R. Engel-Herbert, Pennsylvania State Univ.
Su2100	9:00 p.m.	Synthesis and Magnetic Properties of RE Doped $SrFe_{12-x}$ $DyxO_{19}$ Ferrite Nanoparticles		B. Rai, S.R. Mishra, The Univ. of Memphis
Monday Morning:				
Mo0730	7:30 a.m.	Registration and Continental Breakfast		
Interface & Surface Magnetism				Session Chair: L. Brillson
Mo0830	8:30 a.m.	INVITED: Recent Developments in Interface-driven Magnetism		R. Wiesendanger, Univ. of Hamburg
Mo0900	9:00 a.m.	Incorporation of Cr or Mn at the GaAs(001)-c(4×4)α Surface: Structural Stability and Electronic States		K. Okukita, A. Hagiwara, J. Nakamura, The Univ. of Electro-Communications (UEC-Tokyo)
Mo0905	9:05 a.m.	Exchange Bias of the Interface Spin System at the Ferromagnet/Oxide Interface		G. Luepke, Y. Fan, K.J. Smith, The College of William and Mary; A.T. Hanbicki, R. Goswami, C.H. Li, Naval Research Laboratory; H.B. Zhao, Fudan Univ.; B.T. Jonker, Naval Research Laboratory
Mo0910	9:10 a.m.	INVITED: Tunable Control Over Individual Dopants in Semiconductors via STM Positioning of Charged Defects		J. Gupta, Ohio State Univ.
Mo0940	9:40 a.m.	Off-Axis Electron Holography of Ferromagnetic Nanowire Arrays.		A. Akhtari-Zavareh, Simon Fraser Univ.; T. Kasama, Technical Univ. of Denmark; L. Philippe Carignan, A. Yelon, D. Ménard, École Polytechnique de Montréal; R. Herring, Univ. of Victoria; R.E. Dunin-Borkowski, Microscopy and Spectroscopy with Electrons Institute for Microstructure; M.R. McCartney, Arizona State Univ.
Mo0945	9:45 a.m.	Micromagnetic Simulations of GaAs/MnAs Core/Shell Nanowires		A. Paul, J. Liang, N. Samarth, R. Engel-Herbert, The Pennsylvania State Univ.
Mo0950	9:50 a.m.	Influence of Spin-orbit Coupling on the Two-dimensional Fröhlich Polaron		K.A. Vardanyan, A.L. Vartanian, A.A. Kirakosyan, Yerevan State Univ.
Mo1000	10:00 a.m.	Coffee Break and Poster Viewing		
Semiconductor Growth & Surfaces				Session Chair: C. McConville
Mo1100	11:00 a.m.	Atomic Structure and Stoichiometry of Tensile-strained GaAs/GaSb(001) Nanostructures		A. Lenz, J. Schuppang, Technische Universität Berlin; A. Gassenq, T. Taliercio, E. Tournié, Université Montpellier 2; M. Dähne, H. Eisele, Technische Universität Berlin
Mo1105	11:05 a.m.	Influence of Quantum Dot Atomic Structure and Strain Relaxation on GaSb/GaAs Band Offsets		E.S. Zech, A.S. Chang, A.J. Martin, J.C. Canniff, Y.H. Lin, J.M. Millunchick, R.S. Goldman, Univ. of Michigan
Mo1110	11:10 a.m.	In Situ X-ray Diffraction Study of GaAs Growth on Si		M. Takahasi, Japan Atomic Energy Agency; Y. Nakata, Univ. of Hyogo; H. Suzuki, Miyazaki Univ.; K. Ikeda, Toyota Technological Institute; W. Hu, Japan Atomic Energy Agency; M. Kozu, Univ. of Hyogo; Y. Ohshita, Toyota Technological Institute
Mo1115	11:15 a.m.	A Novel Approach for High Performance InAs FinFETs on Silicon		X. Dai, Nanyang Technological Univ.; Y. Hwang, B-M. Nguyen, Center for Integrated Nanotechnologies, Los Alamos National Laboratories; W. Tang, Univ. of California, Los Angeles; C. Soci, Nanyang Technological Univ.; S.A. Dayeh, Los Alamos National Laboratories & U.C. San Diego
Mo1120	11:20 a.m.	Surface Studies of Polytypic InAs Nanowires		M. Hjort, S. Lehmann, J. Knutsson, R. Timm, K. Dick, E. Lundgren, K. Deppert, L. Samuelson, A. Mikkelsen, Lund Univ.
Mo1125	11:25 a.m.	INVITED: Probing Semiconductor Surface Charge Transport Using Crystalline Nanomembranes		M. Lagally, Univ. of Wisconsin-Madison
Mo1155	11:55 a.m.	Trench Structure Formations Around InAs QDs on GaAs(001) Observed by STMBE		T. Toujyou, Center for Collaborative Research, Anan National College of Technology; K. Yamaguchi, Department of Electronic Engineering, The Univ. of Electro-Communications; S. Tsukamoto, Center for Collaborative Research, Anan National College of Technology

Mo1200	12:00 p.m.	Atomic Structure and Electronic Properties of Ringlike Antimony Clusters on the Si(111)7×7 Surface		M. Franz, S. Appelfeller, M. Dähne, Technische Universität Berlin
Mo1205	12:05 p.m.	Strain Analysis of Compositionally Tailored Interfaces in InAs/GaSb Superlattices by Aberration Corrected Transmission Electron Microscopy		K. Mahalingam, UES, Inc; H. Haugan, UTC, Inc; G.J Brown, K.G Eyink, Air Force Research Laboratory
Mo1210	12:10 p.m.	Lunch and Poster Viewing		
Monday Afternoon:				
Spintronics with Organics				Session Chair: L. Lauhon
Mo1400	2:00 p.m.	INVITED: Spin Transport and Carrier-mediated Magnetism in Vanadium Tetracyanoethylene (V[TCNE]~2)		E. Johnston-Halperin, The Ohio State Univ.
Mo1430	2:30 p.m.	Dipole Interactions at the Interface with Ferroelectric Cystalline Polymers		P. Dowben, X. Zhang, Univ. of Nebraska
Mo1435	2:35 p.m.	Manipulating Fermi Level of CuPc Molecules by Dosing Gaseous Oxidant		J.H. Park, S.W. Park, T. Kent, W.C. Trogler, A.C. Kummel, Univ. of California San Diego
Mo1440	2:40 p.m.	Coexistence of Ferromagnetism and Ferroelectric Polarization in Epitaxial NiTiO3 thin films with the $LiNbO_3$-Type Structure		T. Varga, T.C. Droubay, M.E. Bowden, S.A. Chambers, B.C. Kabius, E. Apra, W.A. Shelton, V. Shutthanandan, R.J. Colby, PNNL
Mo1445	2:45 p.m.	Photoluminance, Aging and Magnetization Effect on the Low Temperature Surface Phase Transitions on BiFeO3		A. Anshul, A. Kumar, B.K. Gupta, R.K. Kotnala, National Physical Laboratory, India
Mo1450	2:50 p.m.	Graphene as Substrate for Organic Semiconductor Films		C. Teichert, M. Kratzer, Montanuniversitaet Leoben, Austria; G. Hlawacek, F. Khokhar, R. van Gastel, B. Poelsema, H. Zandvliet, Univ. of Twente, NL; B. Vasić, A. Matković, U. Ralević, R. Gajić, Univ. of Belgrade, Serbia
Mo1455	2:55 p.m.	Optical and Structural Properties of CdZnS Quantum Dots Formed by the Langmuir-Blodgett Technique		A. Milekhin, N. Yeryukov, L. Sveshnikova, T. Duda, D .Protasov, O. Tereshchenko, Institute of Semiconductor Physics, Novosibirsk, Russia; N. Surovtsev, S. Adichtchev, Institute of Automation and Electrometry, Novosibirsk, Russia; C. Himcinschi, TU Bergakademie Freiberg, Freiberg, Germany; V. Dzhagan, V. Lashkaryov Institute of Semiconductor Physics, Kyiv, Ukraine; D.R.T. Zahn, Chemnitz Univ. of Technology, Chemnitz, Germany
Mo1500	3:00 p.m.	Coffee Break and Poster Viewing		
Surface Passivation & High-K Dielectrics				Session Chair: S. Chambers
Mo1600	4:00 p.m.	Characterization of Al_2O_3/GaAs Interface and Film Prepared by ALD		R.E. Sah, R. Driad, F. Bernhard, Fraunhofer Institute for Applied Solid State Physics; V. Naumann, C. Hagendorf, Fraunhofer Center for Photovoltaics CSP; H. Czap, T. Fuchs, M. Mikulla, Fraunhofer Institute for Applied Solid State Physics
Mo1605	4:05 p.m.	Interface Characterization of Epitaxial $SrTiO_3$ on GaAs		R. Droopad, R. Contreras-Guerrero, Texas State Univ.; Q. Qiao, R. Klie, Univ. of Illinois-Chicago
Mo1610	4:10 p.m.	UPGRADED: Passivation of Missing As Defect Sites on InGaAs(001)-(2x4)		M. Edmonds, T. Kent, Univ. of California, San Diego; R. Droopad, Texas State Univ.; E. Chagarov, A.C. Kummel, Univ. of California, San Diego
Mo1630	4:30 p.m.	Impact of Atomic Hydrogen Exposure on the Growth, Interfacial, and Electrical Characteristics of HfO_2 on Al0.25Ga0.75N		X. Qin, S. Anwar, B. Brennan, C.L. Hinkle, R.M. Wallace, Univ. of Texas at Dallas
Mo1635	4:35 p.m.	Controlling the Electrostatic Potential of Gate-Last Ge/High-k/Metal Gate Stacks through Interface Dipole Formation		S. Anwar, J. Burris, C. Buie, C. Hinkle, Univ. of Texas at Dallas
Mo1640	4:40 p.m.	Improvements in Atomic Layer Deposition Nucleation on Ge(100) via HOOH Dosing		T. Kaufman-Osborn, J.S. Lee, A.C. Kummel, Univ. of California, San Diego
Mo1645	4:45 p.m.	Electronic Reconstruction of Sr/Si(001) Zintl Template: Ab-initio Theory and Photoemission		H. Seo, M. Choi, R.C. Hatch, A.B. Posadas, A.A. Demkov, The Univ. of Texas at Austin

Mo1650	4:50 p.m.	Optical Properties of Solution-processed LaAlO/Si Films Using Spectroscopic Ellipsometry		T.J. Kim, Kyung Hee Univ.; S.M. Hwang, Sungkyunkwan Univ.; J.J. Yoon, Korea Institute of Science and Technology; S.Y. Hwang, H.G. Park, J.Y. Kim, J.H. Choi, Y.D. Kim, Kyung Hee Univ.; J. Joo, Sungkyunkwan Univ.
Mo1655	4:55 p.m.	UPGRADED: Selective TiO_2 Deposition on Oxidized and Hydrogen Passivated Silicon		S. McDonnell, R.C. Longo, O. Seitz, G. Mordi, J. Kim, Y.J. Chabal, K. Cho, R.M. Wallace, Univ. of Texas at Dallas
Mo1715	5:15 p.m.	An Atomic View of Trimethylaluminum Nucleation on GaAs/InGaAs (110) Surfaces		T. Kent, M. Edmonds, Univ. of California San Diego; R. Droopad, Texas State Univ.; E. Chagarov, A.C. Kummel, U.C, San Diego
Mo1720	5:20 p.m.	Compensation and Passivation of InN Surface Donors by Mg Dopants and Sulphur		W.M. Linhart, Univ. of Warwick; J. Chai, Univ. of Canerbury; S.M. Durbin, Univ. of Buffalo; T.D. Veal, Univ. of Liverpool; C.F. McConville, Univ. of Warwick
Mo1725	5:25 p.m.	Structure and Optical Properties of Pure and W-doped Gallium Oxide Thin Films		E.J. Rubio, M. Noor-A-Alam, C.D. Barraza, C.V. Ramana, Univ. of Texas at El Paso
Mo1730	5:30 p.m.	Dinner		
Monday Evening:				
Energy Materials				Session Chair: H. Farrell
Mo1930	7:30 p.m.	INVITED: Compound Semiconductor Heterostructure Challenges for Ultrahigh Efficiency Photovoltaics		H. Atwater, California Institute of Technology
Mo2000	8:00 p.m.	Pt-based Catalyst for PEM Fuel Cell: Role of Surfaces and Interfaces in a Novel Plasma Deposition Method		M. Laurent-Brocq, Univ. of Namur; N. Job, Liege Univ.; J-J. Pireaux, Univ. of Namur
Mo2005	8:05 p.m.	The Role of Mobile Ionized Defects in the Aging of Cu_2O/ZnO Nanowire Solar Cells		J.H. Joo, Harvard Univ.; J.J. Richardson, Univ. of California, Santa Barbara; E.L. Hu, Harvard Univ.
Mo2010	8:10 p.m.	INVITED: Semiconductor Nanowires for Solar Energy Conversion		P. Yang, U.C. Berkeley
Mo2040	8:40 p.m.	Investigations on the Electronic and Structural Properties of CdS_CZTS Heterojunction Interface for Improving Solar Cell Efficiency and Stability		R.R. Thankalekshmi, A.C. Rastogi, State Univ. of New York, Binghamton Univ.
Mo2045	8:45 p.m.	Tin Dioxide δ-Doped with Antimony for Thermoelectric Applications: First Principles Calculations		L. Scolfaro, Texas State Univ. - San Marcos; F.G. Pinto, N.S. Castro, D.E.S. Silva, P.D. Borges, Universidade Federal de Viçosa
Mo2050	8:50 p.m.	Interfacial Polymer Ferroelectric Dipole Induced Electric Field Effect on the Photovoltaic Performance of Organic Solar Cells		A.C. Rastogi, Binghamton Univ.
Mo2055	8:55 p.m.	Thermoelectric Effects of a Chain of Coupled Quantum Dots Connected to Metallic Electrodes		D.M.T. Kuo, National Central Univ.
Tuesday Morning:				
Tu0730	7:30 a.m.	Registration and Continental Breakfast		
Contacts & Nanocontacts				Session Chair: K. Kavanagh
Tu0830	8:30 a.m.	UPGRADED: Ultra-low Contact Resistance at an Epitaxial Metal/Oxide Heterojunction through Diffusion-controlled Metallization of the Oxide		S. Chambers, Pacific Northwest National Laboratory; P. Sushko, Univ. College London; M. Gu, Pacific Northwest National Laboratory; H. Yang, Univeristy of California at Davis; C. Wang, N. Browning, Pacific Northwest National Laboratory
Tu0850	8:50 a.m.	Barrier Height Measurement of Metal Contacts to Silicon Nanowires Using Spectrally Resolved Scanning Photocurrent Microscopy		K-H. Yoon, J.K. Hyun, J.G. Connell, S.L. Howell, L.J. Lauhon, Northwestern Univ.
~~Tu0855~~	~~8:55 a.m.~~	~~Understanding of Nanoscale Resistive Switches (Memristors) Based on Transition Metal Oxides~~		~~J.P. Strachan, Hewlett-Packard Laboratories; I. Goldfarb, Tel-Aviv Univ.; J.J. Yang, F. Miao, M. Pickett, M. Zhang, R.S. Williams, Hewlett-Packard Laboratories~~
~~Tu0900~~	~~9:00 a.m.~~	~~Local Multi-probe Measurements of ZnO Nanowires to Isolate the Au Catalyst Interface~~		~~A. Lord, Swansea Univ.; A. Walton, Leeds Univerity; M. Ward, Leeds Univ.; J. Köble, Omicron Germany; T. Maffeis, Swansea Univ.; S. Wilks, Swansea Univ.~~

Tu0905	9:05 a.m.	INVITED: The Nanoelectronics Research Initiative: Prospects for Logic Beyond CMOS		T. Theis, IBM
Tu0935	9:35 a.m.	New Experiments and Applications Made Possible by a Low Temperature 4-Tip STM with UHV-SEM Navigation		B. Guenther, A. Bettac, J. Koeble, J. Hilton, A. Feltz, Omicron NanoTechnology
Tu0940	9:40 a.m.	Surface Characterization of Functionalized Gold Nanoparticles		A. Rafati, S.D. Techane, L.J. Gamble, Univ. of Washington; D.R. Baer, Pacific Northwest National Lab; D.G. Castner, Univ. of Washington
Tu0945	9:45 a.m.	New Milestones in Scanning Probe Microscopy: Graphene on Rh(111) studied by DFT, STM and NC-AFM using KolibriSensorTM and TytoTM		E. Voloshina, Freie Universität Berlin; Y. Dedkov, SPECS Surface Nano Analysis GmbH; T. Schulmeyer, SPECS Surface Nano Analysis Inc; A. Thissen, SPECS Surface Nano Analysis GmbH
Tu0950	9:50 a.m.	Coffee Break and Poster Viewing		
New Tools & Applications				Session Chair: J. Hilton
Tu1050	10:50 p.m.	UPGRADED: In-situ Characterization of Semiconductor Nanostructure Devices		R. Timm, O. Persson, J. Webb, M. Hjort, C. Thelander, L. Samuelson, A. Mikkelsen, Lund Univ.
Tu1110	11:10 a.m.	Ultrafast Spectroscopy of Intermediate Band Solar Cell Prospects		R. Clarke, V. Stoica, R. Goldman, J. Phillips, R. Schaller, Univ. of Michigan
Tu1115	11:15 a.m.	Proximal Probe Characterization of Thermal Conductivity in ErAs/GaAs Superlattice Grown by Molecular Beam Epitaxy		K.W. Park, H.P. Nair, S.R. Bank, E.T. Yu, Univ. of Texas at Austin
Tu1120	11:20 a.m.	Atom Probe Tomography: Applications to Interfaces		D.J. Larson, CAMECA; V. Smentkowski, General Electric; K. Inoue, Tohoku Univ.; D.A. Reinhard, T.J. Prosa, P.H. Clifton, R.M. Ulfig, I. Martin, D. Snoeyenbos, T.F. Kelly, CAMECA
Tu1125	11:25 a.m.	Atom Probe Tomographic Analysis of InGaN Quantum Wells and GdN Nanoislands in GaN		J.R. Riley, Northwestern Univ.; T. Detchprom, Rensselaer Polytechnic Institute; T.F. Kent, R.C. Myers, The Ohio State Univ.; C. Wetzel, Rensselaer Polytechnic Institute; L.J. Lauhon, Northwestern Univ.
Tu1130	11:30 a.m.	Imaging "Invisible" Dopant Atoms in Semiconductor Nanocrystals		A.A. Gunawan, A.W. Wills, Univ. of Minnesota; M.G. Thomas, Cornell Univ.; D.J. Norris, ETH Zürich; K.A. Mkhoyan, Univ. of Minnesota
Tu1135	11:35 a.m.	UPGRADED: Non-contact Electrical Measurements at Selected Inner Sites and Interfaces		H. Cohen, Weizmann
Tu1155	11:55 a.m.	Resonant Coupling For Contactless Measurement of Materials Parameters		R. Ahrenkiel, S.W. Johhston, National Renewable Energy Laboratory
Tu1200	12:00 p.m.	Consequences of the Simplified Bond Hyperpolarizability Model for Second Harmonic Generation for Diamond and Zincblende semiconductors		B. Pesendorfer, H. Hardhienata, D. Stifter, K. Hingerl, Johannes Kepler Univ.
Tu1205	12:05 p.m.	Bulk Dipole Contribution to Second Harmonic Generation in Diamond Lattices Due to Spatial Dispersion		H. Hardhienata, D. Stifter, K. Hingerl, Univ. Linz
Tu1210	12:10 p.m.	Comparison of Cathodoluminescence, Imaging Micro-photoluminescence and Confocal Photoluminescence Microscopy for Determination of Interfacial Defect Densities in Semiconductors		O.C. Noriega, Texas State Univ. - San Marcos
Tu1215	12:15 p.m.	Free Afternoon		
Tuesday Evening:				
Topological Insulators I				Session Chair: N. Samarth
Tu1930	7:30 p.m.	Topological Insulators: An Overview of Experimental Progress		N. Samarth, Penn State Univ.
Tu1950	7:50 p.m.	Topological Quantum Computing with Majorana Particles		R. Lutchyn, Microsoft
Tu2020	8:20 p.m.	Transport Properties of Magnetically Doped Topological Insulator Films		Yayu Wang, Tsinghua Univ.

Wednesday Morning:

We0730	7:30 a.m.	Registration and Continental Breakfast	
Topological Insulators II			**Session Chair: R. Lutchyn**
We0830	8:30 a.m.	INVITED: Angle-Resolved Photoemission Spectroscopy of Correlated Oxide Interfaces and Thin Films	K.M. Shen, E. Monkman, J. Harter, D. Shai, Y. Nie, P. King, M. Uchida, B. Burganov, C. Adamo, A. Melville, L. Maritato, J. Mundy, D. Muller, D. Schlom, Cornell Univ.
We0900	9:00 a.m.	UPGRADED: Limits to Coherent Electronic Transport in Bi_2Se_3 in the Topological Regime	D. Kim, Q. Li, P. Syers, N.P. Butch, J. Paglione, S. Das Sarma, M.S. Fuhrer, Univ. of Maryland
We0920	9:20 a.m.	Periodic Conductance Fluctuations in $Bi2Se_3$ Channels with Self-organized, Correlated Surface Morphology	A. Kandala, A. Richardella, D. Zhang, T. Flanagan, N. Samarth, Penn State Univ.
We0925	9:25 a.m.	Opening a Surface State Gap with Magnetic Heterostructures	A. Richardella, The Pennsylvania State Univ.; A. Kandala, The PennsylvaniaState Univ.; J.S. Lee, D. Zhang, D. Rench, N. Samarth, The Pennsylvania State Univ.
We0930	9:30 a.m.	Epitaxial Growth and Surface Characterization of Zero-Gap Semiconductor, Half Heusler Compound LuPtSb	S. Patel, B.D. Schultz, C. Palmstrom, Univ. of California, Santa Barbara
We0935	9:35 a.m.	Ferromagnetism in Mn-doped Topological Insulator $Bi2Te_3$ Thin-Films	J.S. Lee, A. Richardella, D. Rench, The Pennsylvania State Univ.; D. Zhang, National Institute of Standards and Technology; N. Samarth, The Pennsylvania State Univ.
We0940	9:40 a.m.	Gapless States Between Two Topological Insulators Protected by Mirror Symmetry	R. Takahashi, S. Murakami, Tokyo Institute of Technology
We0945	9:45 a.m.	Coffee Break and Poster Viewing	
Spintronics Inorganic & Organic			**Session Chair: M. Flatté**
We1045	10:45 a.m.	INVITED: Electrical and Thermal Spintronics in Silicon	R. Jansen, National Institute of Advanced Industrial Science and Technology (AIST)
We1115	11:15 a.m.	Efficient Spin Injection with an AlOx Tunnel Barrier Prepared by the Oxidation of an Ultra-thin Al Epitaxial Layer on GaAs	N. Nishizawa, H. Munekata, Tokyo Institute of Technology
We1120	11:20 a.m.	Surface-termination Effect on Nitrogen-Vacancy Charge in Diamond	S. Cui, E. Hu, Harvard Univ.
We1125	11:25 a.m.	Manganese Phthalocyanine on Cobalt: An Interesting Model Interface for Organic Spintronics	F. Haidu, A. Fechner, Chemnitz Univ. of Technology; B. Mahns, IFW Dresden; G. Salvan, Chemnitz Univ. of Technology; M. Knupfer, IFW Dresden; D.R.T. Zahn, Chemnitz Univ. of Technology
We1130	11:30 a.m.	INVITED: Energy Level Alignment and Charge Transport at Metal/Alq_3 Interfaces: Implications for Organic Spintronics	J.S. Jiang, Argonne National Laboratory
We1200	12:00 p.m.	Hysteretic Control of Organic Conductance Due to Remanent Magnetic Fringe Fields	M.E. Flatté, Univ. of Iowa; F. Macia, New York Univ.; F. Wang, N.J. Harmon, M. Wohlgenannt, Univ. of Iowa; A.D. Kent, New York Univ.
We1205	12:05 p.m.	Integrating MBE Materials with Graphene to Induce Novel Spin-based Phenomena	A. Swartz, K. McCreary, W. Han, P. Odenthal, J-R. Chen, Univ. of California, Riverside; Y. Hao, R. Ruoff, Univ. of Texas at Austin; J. Fabian, Univ. of Regensburg; R. Kawakami, Univ. of California, Riverside
We1210	12:10 p.m.	Lunch and Poster Viewing	

Wednesday Afternoon:

Nanowire Growth & Strain Effects			**Session Chair: R. Droopad**
We1330	1:30 p.m.	XPS and PL Investigation of ZnO Nanowire Arrays	D Jones, J Minster-Blondeau, R Brown, T Maffeis, Univ. of Swansea
We1335	1:35 p.m.	Novel InGaAs/GaAs Quantum Dots in a GaP(001) Matrix	H. Eisele, C. Prohl, A. Lenz, D. Roy, J. Schuppang, M. Dähne, G. Stracke, A. Strittmatter, U.W. Pohl, D. Bimberg, Technische Universität Berlin
We1340	1:40 p.m.	MOCVD Regrowth of InP on Hybrid Silicon Substrate	C. Zhang, Univ. of California, Santa Barbara; D. Liang, HP; J.E. Bowers, Univ. of California, Santa Barbara

We1345	1:45 p.m.	News from the Non-polar GaN (10-10) Surface: Hidden Surface States and Intrinsic Versus Extrinsic Fermi-level Pinning		Ph. Ebert, Forschungszentrum Juelich GmbH; L. Lymperakis, Max-Planck-Institut fuer Eisenforschung GmbH; P.H. Weidlich, Forschungszentrum Juelich GmbH; H. Eisele, Technische Universitaet Berlin; M. Schnedler, Forschungszentrum Juelich GmbH; J.-P. Nys, B. Grandidier, D. Stievenard, IEMN; R.E. Dunin-Borkowski, Forschungszentrum Juelich GmbH; J. Neugebauer, Max-Planck-Institut fuer Eisenforschung GmbH
We1350	1:50 p.m.	Atomic Layer Epitaxy of III-N Semiconductors: How Low (in T) Can You Go?		C.R. Eddy, Jr., N. Nepal, N.A. Mahadik, L.O. Nyakiti, S.B. Qadri, M.J. Mehl, J.K. Hite, U.S. Naval Research Laboratory
We1355	1:55 p.m.	INVITED: Polarization-induced Nanowire Light Emitting Diodes with Mid-deep UV Emission		S.C. Carnevale, T.F. Kent, C. Marginean, F. Akyol, Ohio State Univ.; P.J. Phillips, R.F. Klie, Univ. of Illinois at Chicago; S. Rajan, R.C. Myers, Ohio State Univ.
We1425	2:25 p.m.	Morphology and Evolution of Surface Reconstruction of an InAs-GaAs Wetting Layer at High Temperatures		T. Konishi, Anan National College of Technology; G.R. Bell, Univ. of Warwick; S. Tsukamoto, Anan National College of Technology
We1430	2:30 p.m.	Surface Morphology of GaAs and GaSb (111)A Grown by Molecular Beam Epitaxy		J.J.M. Law, Univ. of Cal., Santa Barbara; I. Calderon, Santa Barbara City College; C -Y. Huang, H. Lu, M. J.W. Rodwell, A.C. Gossard, Univ. of Cal., Santa Barbara
We1435	2:35 p.m.	Use of Atomic Hydrogen to Prepare GaSb(211)B and GaSb(100) Substrates for Subsequent ZnTe Growth by MBE		T. Myers, Texas State Univ.- San Marcos
~~We1440~~	~~2:40 p.m.~~	~~High-quality Detachable CdTe (111) Heteroepitaxial Films on $Al2O_3$ (0001)~~		~~K. Meinander, G.A. Devenyi, S.M. Jovanovic, J.L. Carvalho, J.S. Preston, McMaster Univ.~~
We1445	2:45 p.m.	Coffee Break and Poster Viewing		
Epitaxy & Graphene I				Session Chair: R. Kawakami
We1515	3:15 p.m.	Epitaxial Growth and Electronic Band Structure of the Semiconducting Half Heusler Compound CoTiSb		J.K. Kawasaki, Univ. of California Santa Barbara; L.M. Johansson, M. Hjort, R. Timm, T. Balasubramanian, A. Mikkelsen, Lund Univ.; B.D. Schultz, C.J. Palmstrøm, Univ. of California Santa Barbara
We1520	3:20 p.m.	Epitaxial Growth Cubic InN Films via Plasma-Assisted Atomic Layer Epitaxy		N. Nepal, N.A. Mahadik, L.O. Nyakiti, S.B. Qadri, M.J. Mehl, J.K. Hite, C.R. Eddy, Jr., U.S. Naval Research Laboratory
We1525	3:25 p.m.	Single Crystal Zinc Oxide Formed Epitaxially on Single Crystal Gold		K.J. Greenberg, J.H. Joo, M. Baram, D.R. Clarke, E.L. Hu, Harvard Univ.
We1530	3:30 p.m.	INVITED: Quantum Transport and Correlated Phenomena in Bilayer and Trilayer Graphene		J. Lau, Univ. of California, Riverside
We1600	4:00 p.m.	Effects of Surface Geometry on the Wettability of Water on Graphene		T. Yonemaru, H. Shimizu, J. Nakamura, The Univ. of Electro-Communications (UEC-Tokyo)
We1605	4:05 p.m.	Electronic Effects of Non-Covalent Molecular Modification of Graphene NanoElectronic Devices		C.A. Hacker, M.A. Walsh, C.A. Richter, NIST
We1610	4:10 p.m.	Imaging of Electron Beam Induced Current in Epitaxial Graphene		S. Mou, J. Boeckl, W. Lu, J.H. Park, W.C. Mitchel, Air Force Research Laboratory; S. Tetlak, Wyle Laboratories
We1615	4:15 p.m.	Growth of III-N Semiconductors on XeF_2 Functionalized Epitaxial Graphene		N. Nepal, V.D. Wheeler, T.J. Anderson, F.J. Kub, M.A. Mastro, R.L. Myers-Ward, S.C. Hernandez, F. Bezares, J.A. Freitas, L.O. Nyakiti, A.D. Koehler, D.K. Gaskill, K.D. Hobart, C.R. Eddy, Jr., U.S. Naval Research Laboratory
We1620	4:20 p.m.	Finite-ranged Impurity Effect to Hall Conductivity in graphene		M. Noro, S. Murakami, T. Ando, Tokyo Institute of Technology
We1625	4:25 p.m.	Controlled Interface Manipulation for Epitaxial Graphene on 4H- & 6H-SiC using Scanning Tunneling Microscopy		P. Xu, M.L. Ackerman, S.D. Barber, J.K. Schoelz, D. Qi, P.M. Thibado, Univ. of Arkansas; V.D. Wheeler, L.O. Nyakiti, R.L. Myers-Ward, C.R. Eddy, D.K. Gaskill, Naval Research Laboratory
We1630	4:30 p.m.	INVITED: The Evolution of PCSI— A Perspective of the Last 40 Years		D. Ferry, Arizona State Univ.
We1700	5:00 p.m.	Conference Banquet Luau		

Thursday Morning:				
Th0730	7:30 a.m.	Continental Breakfast		
Spin Torque & Graphene				Session Chair: A. Mikkelsen
Th0830	8:30 a.m.	INVITED: Giant Spin Hall Effects and Spin Transfer Torques in Heavy Metal/Ferromagnet Thin Film Devices		D. Ralph, Cornell Univ.
Th0900	9:00 a.m.	INVITED: Multiferroic Tunnel Junctions		A. Chanthbouala, A. Crassous, V. Garcia, K. Bouzehouane, S. Fusil, Unité Mixte de Physique CNRS/Thales; L. Bocher, A.Gloter, Laboratoire de Physique des Solides; C. Deranlot, Unité Mixte de Physique CNRS/Thales; S. Xavier, Thales Research and Technology; N. Mathur, Univ. of Cambridge; M. Bibes, A. Barthélémy, Unité Mixte de Physique CNRS/Thales
Th0930	9:30 a.m.	Coffee Break and Poster Viewing		
Graphene II				Session Chair: R. Wallace
Th1015	10:15 a.m.	INVITED: Graphene Barristor: a New Device Structure for High On- and Off- current Ratio		H. Chong, Samsung Advanced Institute of Technology
Th1045	10:45 a.m.	INVITED: Unique Optoelectronic Applications of Graphene		H. Xing, Univ. of Notre Dame
Th1115	11:15 a.m.	INVITED: Graphene and h-BN at the Interface		R.S. Ruoff, The Univ. of Texas at Austin
Th1145	11:45 a.m.	Conference Ends		

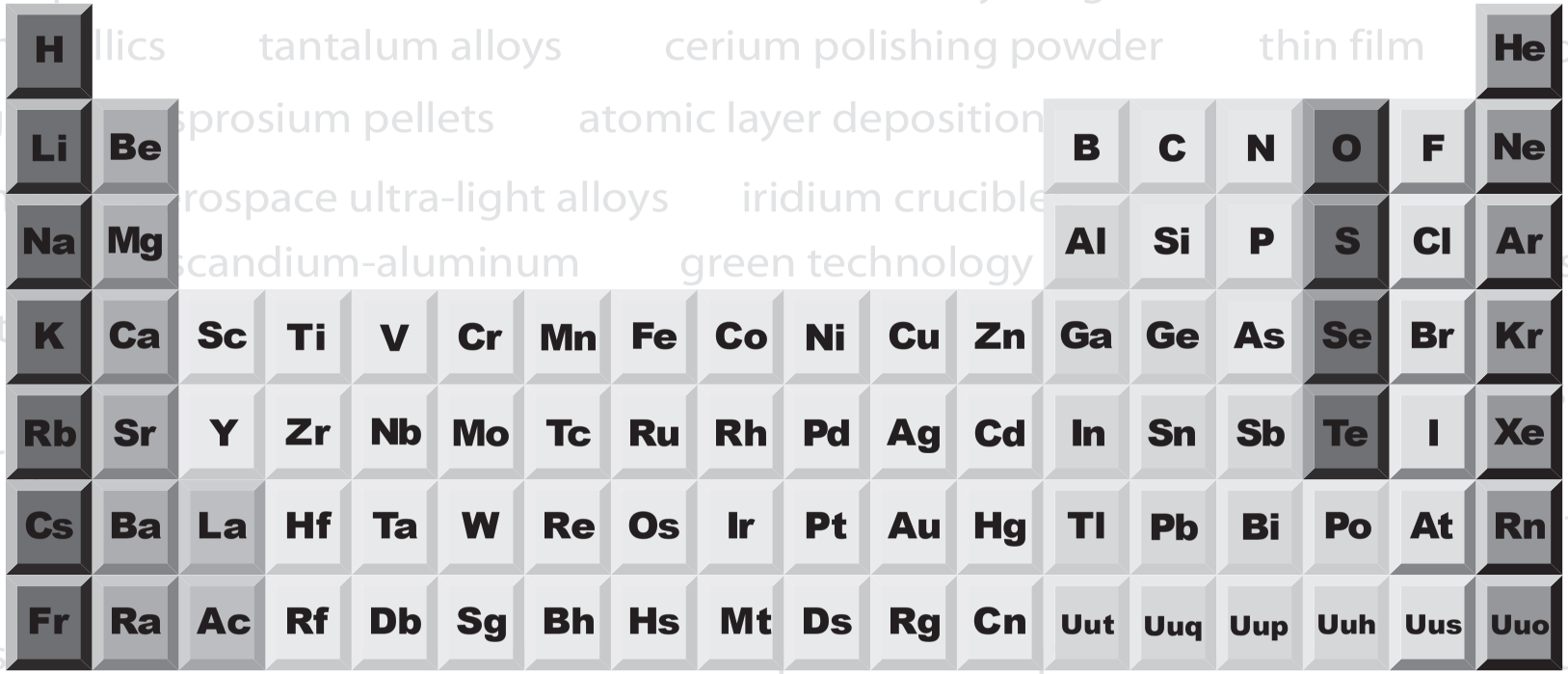

Now Invent.™

AMERICAN ELEMENTS®

The World's Manufacturer of Engineered & Advanced Materials

catalog: americanelements.com

SPM Aarhus 150 NAP

HIGH STABILITY SPM IN SITU MEASUREMENTS AT
NEAR AMBIENT PRESSURE CONDITIONS

KEY FEATURES

- SPM Head with High Stability
- In-Situ Tip Preparation,
- Reactor Cell Gas Volume < 10 ml
- Pressure Range: UHV to 100 mbar
- Temperature Ranges:
  130 K to 900 K in UHV
  300 K to 600 K at 100 mbar

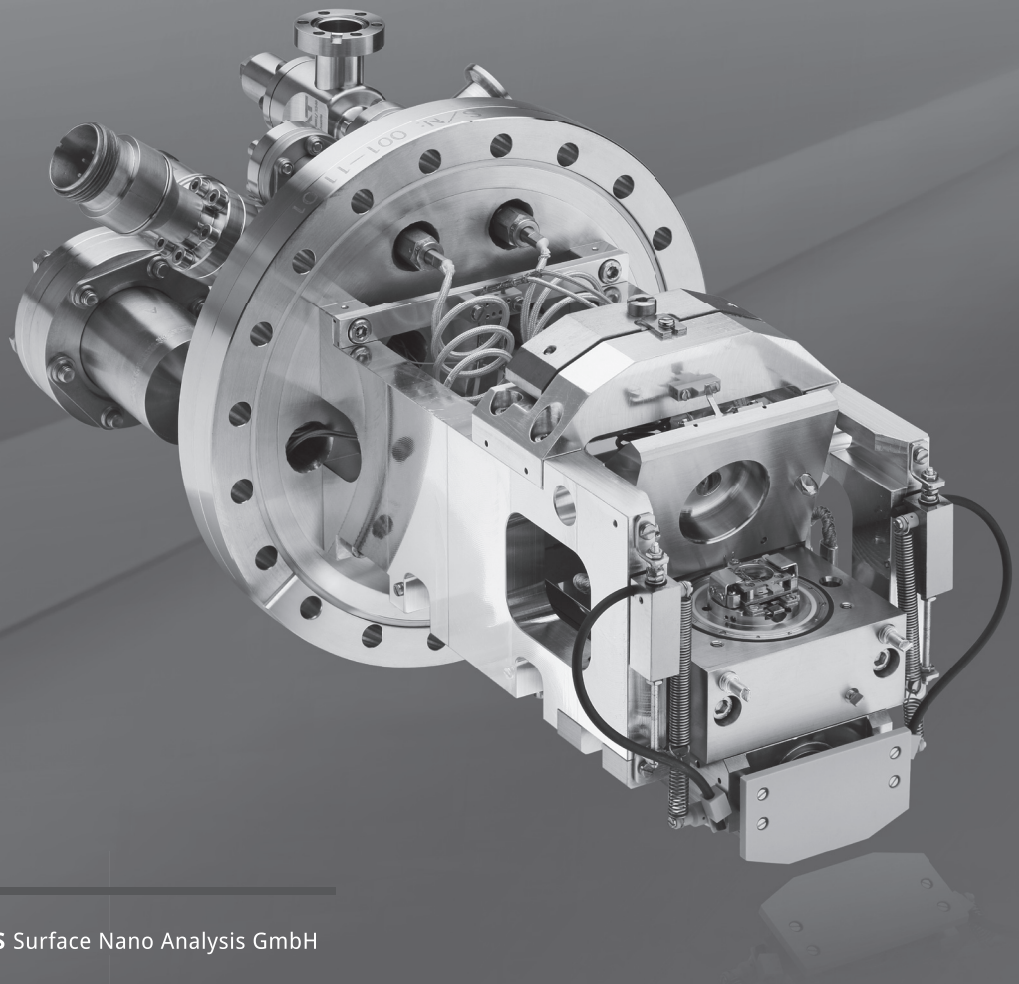

SPECS Surface Nano Analysis GmbH

T +49 30 46 78 24-0
E support@specs.com
H www.specs.com

SPECS™

SVT MBE

SVT Associates offers a variety of versatile, cost effective thin film deposition tools, backed by in-house experts.

SVT Associates Manufacturing and Research Facility in Eden Prairie, MN

For detailed information, visit: **www.svta.com**
or email: **sales@svta.com**

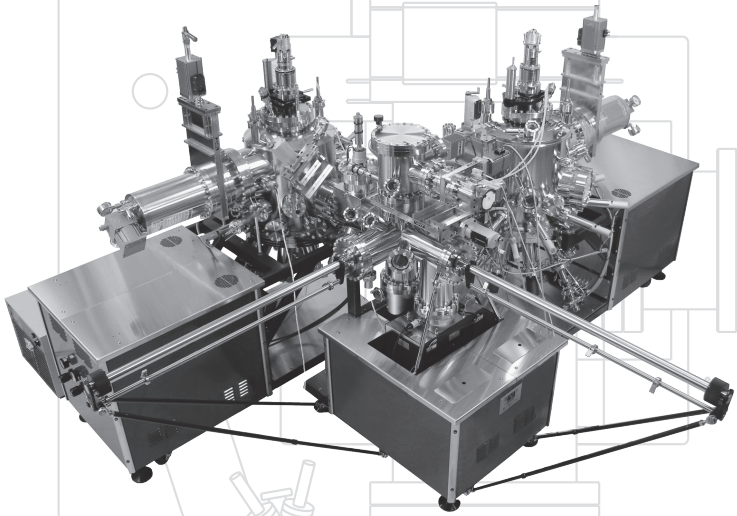

Multiple Material MBE Configurations

SMART MBE/Pulsed Laser Deposition/PVD

NorthStar Atomic Layer Deposition (ALD) Systems

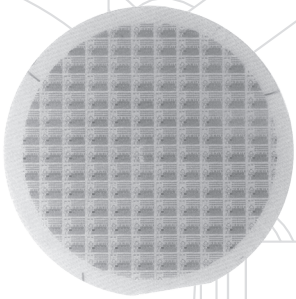

Epi-Wafer Service Available

Ammonia Gas Injectors

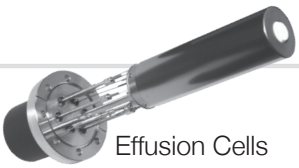

Effusion Cells

NH_3 Injectors

RF Plasma Sources

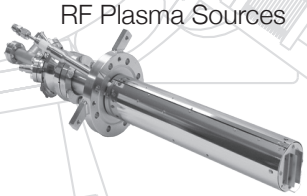

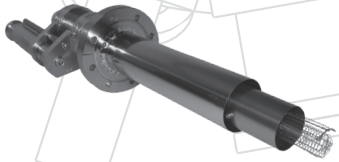

Linear Beam Flux Monitors

SVT MBE

7620 Executive Drive | Eden Prairie, MN 55344-3677 | USA
Phone: 952-934-2100 | *Fax:* 952-934-2737 | *Email:* sales@svta.com | www.svta.com

Sunday

Su1400	Registration
Su1455	Welcome Remarks
Su1500	Sunday Afternoon Session: 2-D Materials
Su1705	Poster Setup
Su1730	Welcome Reception
Su1930	Sunday Evening Session: Complex Oxides

2-D Materials

Silicene: graphene's topologically non-trivial cousin

Guy Le Lay
Aix-Marseille University, CNRS-CINaM, Campus de Luminy, Case 913, 13288, Marseille France.
&
CNR-ISM, via Fosso del Cavaliere 100, Rome, Italy.

Large attention has be paid recently to silicene, the graphene equivalent for silicon, which, however, does not exist in nature.
We have succeeded in providing compelling evidences of its first synthesis upon epitaxial silicon growth on a silver (111) substrate [1]. Of particular interest is the fact that silicene, which hosts Dirac fermions with a 1.3E6 m/s Fermi velocity, is predicted to have non-trivial topological properties.
Since, silicon can be considered the workhorse of electronic industry, this synthesis, which further opens the route to the synthesis of germanene, might have a major impact.
In this talk, I will review the present status of silicene research and draw perspectives in relation with other two-dimensional crystalline materials.

[1] P. Vogt et al., Phys. Rev. Lett. **108**, 155501 (2012).

Acknowledgements: *support from FET-Open grant number 270749 for the project "**2D-NANOLATTICES**"*

Su1530

Silicene: From the formation of single 2D layers to stacks of graphitic-Si

Patrick Vogt[a], Paola De Padova[b], Thomas Bruhn[a,c], Andrea Resta[c], Guy Le Lay[b,c]

[a]Technische Universität Berlin, Hardenbergstrasse 36, 10623 Berlin, Germany.
[b]CNR-ISM, via Fosso del Cavaliere 100, Rome, Italy.
[c]Aix-Marseille University, CNRS-CINaM, Campus de Luminy, Case 913, 13288, Marseille France.

Since the discovery of graphene and the tremendous advancement in this field of research [1] enormous efforts have been invested to search for other similar 2-dimensional materials, especially for silicene. Despite their similarities to graphene, these 2D materials would differ, for example in terms of chemical reactivity or the electronic band gap.
Recently we have succeeded in providing first compelling evidences for the synthesis of monolayer epitaxial silicene on a silver (111) template [2]. Silicene shares essentially the same electronic properties as graphene, namely an electronic linear dispersion resembling that of relativistic Dirac fermions at the K points of the Brillouin-zone, the so-called Dirac points [2,3]. The measured high Fermi velocity of ~1.3×10^6 m/s could open new perspectives for applications, especially due to the compatibility of silicene with Si-based electronics.

Based on these results we have grown multilayer structures: STM observations indicate the presence of large islands exhibiting a honeycomb-like arrangement in STM images. This structure can be explained by stacking of single silicene layers. We will discuss the atomic structure and the electronic properties of this layered system and compare the strong similarities of these silicene stacks to graphite.

We acknowledge financial support by the European Commission, under FET FP7 Grant “2D Nanolattices” No. 270749 and the Deutsche Forschungsgemeinschaft under Grant VO1261/3-1.

[1] A.K. Geim, *Science* **342,** (2009) 1530.
[2] P. Vogt et al., *Phys. Rev. Lett.* **108**, 155501 (2012)
[3] S. Cahangirov et al., *Phys. Rev. Lett.* 1**02**, 236804 (2009)

Su1535 Upgraded

LT-STM/STS investigation of the electronic properties of epitaxial silicene

A. Fleurence[1], Y. Yoshida[2], C.-C. Lee[1], T. Ozaki[1,3], Y. Hasegawa[2], Y. Yamada-Takamura[1]

[1] School of Materials Science, Japan Advanced Institute of Science and Technology

[2] Institute for Solid State Physics, The University of Tokyo

[3] Research Center for Simulation Science, Japan Advanced Institute of Science and Technology

The presence of Dirac cones in the predicted band structure of free-standing silicene, an atom-thick honeycomb structure of silicon with a low-buckled conformation [1], conveys to this two-dimensional material, the nature of a zero-gap semiconductor with massless Dirac fermionic charge carrier. Those astonishing properties together with pioneering experimental observations, triggered in the very recent years, an exponentially increasing interest for this graphene-like form of silicon, both at fundamental level and for applications in high-speed electronics devices.

So far, extensive characterization of silicene has only been carried out on sheets epitaxied on conductive substrates. It has been formed by deposition of Si atoms on silver single crystals [2,3,4], and as we demonstrated, also by the spontaneous segregation of silicon on (0001) surface of zirconium diboride (ZrB_2) thin films epitaxied on Si(111) wafers. The latter gives rise to a wide-scale uniform two-dimensional silicene sheet textured into a 1D array of domain boundaries [5]. Core-level photoelectron spectroscopy using a surface-sensitive synchrotron radiation together with scanning tunneling microscopy (STM) show unambiguously the existence of a single atom thick Si honeycomb mesh. The silicene nature of this 2D structure is emphasized by the observation of a gap-opened π-electronic band centered at the K points of the silicene Brillouin zone by angle-resolved ultraviolet photoelectron spectroscopy (ARUPS). The band gap opening is a result of the specifically imprinted buckling rather than due to the electronic coupling with the diboride layer [5].

Here, we present the results of a low-temperature scanning tunneling spectroscopy (STS) investigation of silicene epitaxied on ZrB_2(0001) thin films. STS, owing to its surface states sensitivity, evidences the n-type semi-conductor properties of silicene, whereas the mapping of the local density of states, together with density functional theory give precious insights on the microscopic origin of the electronic bands of silicene resolved by ARUPS. In particular, it shows the correlation between the degree of sp^2 hybridization of different Si atoms in the internal structure of silicene and the character of the electronic bands. Additionally, the nature of states localized at the domain boundaries texturing the silicene sheet, will be discussed.

[1] S. Cahangirov, *et al.*, “Two- and One-Dimensional Honeycomb Structures of Silicon and Germanium”, Phys. Rev. Lett. **102**, 236804 (2009).

[2] P. De Padova, *et al.*, “Evidence of graphene-like electronic signature in silicene nanoribbons ”, Appl. Phys. Lett., **96**, 261905 (2010).

[3] P. Vogt *et al.*, "Silicene: Compelling Experimental Evidence for Graphene like Two-Dimensional Silicon", Phys. Rev. Lett, **108**, 155501 (2012).

[4] L. Chen *et al.*,,"Evidence for Dirac Fermions in a Honeycomb Lattice Based on Silicon", Phys. Rev. Lett, **109**, 056804 (2012).

[5] A. Fleurence, *et al.*, ”Experimental Evidence for Epitaxial Silicene on Diboride Thin Films” Phys. Rev. Lett, **108**, 245501 (2012).

Su1555 Upgraded

Yttria (Y_2O_3) growth by reactive MBE on graphene

Matthias Batzill

Department of Physics, University of South Florida, Tampa, FL 33620, USA

Integration of graphene into device architectures requires interfacing of graphene with dielectric materials. However, de-wetting and thermal instability of dielectric layers on top of graphene makes fabrication of continuous graphene/dielectric interfaces a materials challenge. Here we report that yttria (Y_2O_3), a high-κ dielectric, forms a complete monolayer on Pt supported graphene. Graphene interacts weakly with Pt thus forming a 'quasi freestanding' graphene layer providing a good model system for fundamental materials characterization studies of graphene.

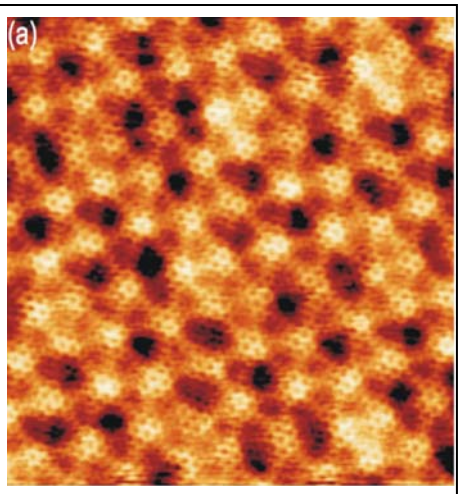

STM image (22x23 nm) of yttria monolayer on Pt supported graphene.

Electron spectroscopy indicates that an yttria-monolayer covered graphene is stable to high annealing temperatures. Furthermore, scanning tunneling microscopy (see Figure) reveals that the yttria monolayer forms an ordered structure upon annealing to above 500 °C and it exhibits a two-dimensional hexagonal lattice rotated by 30° relative to the graphene honeycomb. Charge doping of graphene due to the interface formation is characterized by x-ray photoemission spectroscopy. These measurements indicate a shift of the Fermi-level in graphene upon yttria deposition, suggesting the possible use of dielectric layers for charge doping of metal-supported graphene. Additional studies on other metal substrates indicate that this growth mode of yttria is not unique to the Pt-support but is also observed for graphene supported on iridium and nickel. Ex-situ AFM characterization of the growth of few nanometer thick yttria layers on HOPG and metal supported graphene also indicates a wetting of the substrate, albeit sub-nanometer surface roughness of the yttria film. These studies suggest that yttria may be an excellent dielectric material for graphene and the unexpected monolayer growth of a well-ordered two dimensional yttria layer on graphene may present a potentially transformative advancement in the fabrication of graphene heterostructures.

Su1615

STM studies of sidewall graphene nanoribbons

David B. Torrance, Yuntao Li, Meredith Swegan Nevius,
James O. Andrews, Baiqian Zhang, and Phillip N. First

School of Physics, Georgia Institute of Technology, Atlanta, GA 30332-0430

The potential of strain for tailoring the electronic structure of graphene has been recognized previously, but no credible method has been proposed for designing structures with large strain in a way that could be scaled to millions of devices. Strain of order 10% results in discrete *E(k)* modes separated by energies much larger than k_BT at room temperature. Like magnetic cyclotron states in graphene, the mode energies scale proportional to $\sqrt{N}$, where N is the mode index. We have recently observed these "pseudo-Landau level" states in tunneling conductance spectra of sidewall graphene nanoribbons grown on single-crystal silicon carbide. Strain increases near curved regions where graphene grows over the corner of a step-bunched nanofacet (see Figures 1 and 2). Because graphene grows epitaxially on SiC(0001), this observation could lead to the creation of strained graphene nanostructures with crystallographic control of the strain field through judicious patterning of the SiC prior to graphene growth. Orbitals of the underlying SiC substrate also may contribute density-of-states features to the tunneling conductance spectra, which we observe using room-temperature scanning tunneling spectroscopy. We apply the criterion of electron-hole symmetry in order to separate graphene-specific features from those of the SiC substrate. Smaller density-of-states features with uniform energy scaling may be due to quantum confinement within portions of the nanoribbon.

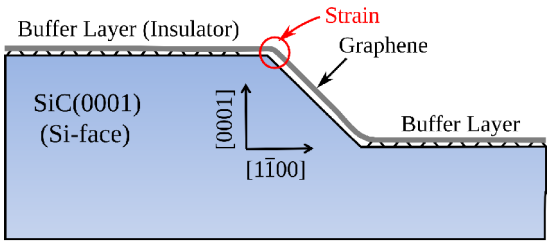

FIG 1: Cross-section of a sidewall graphene nanoribbon with strained region of study labeled.

Work funded in part by NSF (DMR-1106131, DMR-0820382 [MRSEC]) and by NRI-INDEX.

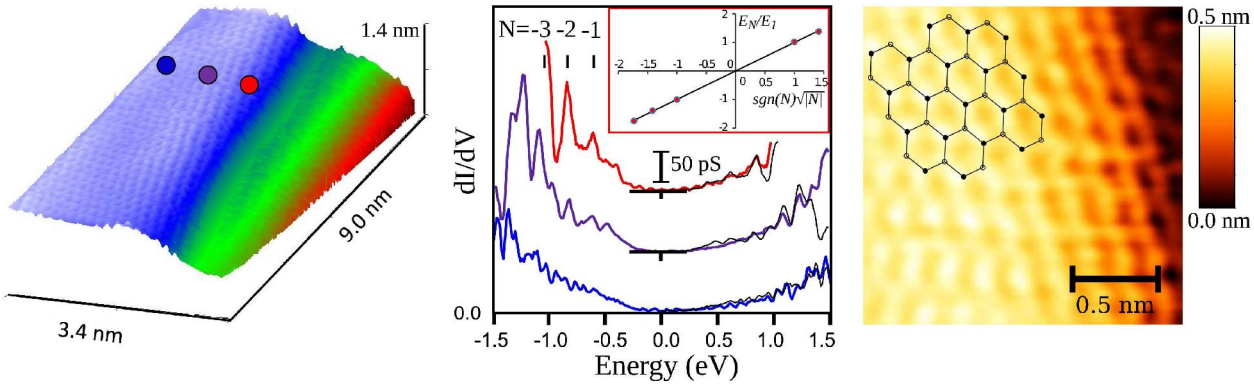

FIG 2: Left: *Epitaxial graphene growing over the top corner of a 15-nm-high step in the SiC substrate.* Middle: *STS at the color-coded points labeled at left (left to right positions correspond to spectra bottom to top). Thin black lines show electron-hole symmetry of spectra.* Middle (inset): *Scaling of strain-induced "pseudo–Landau level" energies with index N.* Right: *Atomic imaging near the position of the labels in the left image. Atom heights in both images have been magnified to enhance visibility on the curved edge; actual corrugation ~2 pm.*

Su1620

Ballistic phonon thermal conductance in graphene nano-ribbon

Hiroki Tomita[1] and *Jun Nakamura[1,2]

[1]*The University of Electro-Communications (UEC-Tokyo), Tokyo, Japan*

[2]*JST-CREST, Saitama, Japan*

In this study, we have explored the ballistic phonon thermal conductance for hydrogenated and dehydrogenated Graphene Nano-Ribbons (GNRs). The phonon dispersion relations are derived from the first-principles calculations within the density functional perturbation theory. The ballistic thermal current of GNRs is evaluated from the Landauer heat flux [1,2].

We have found that the phonon thermal conductance per unit width for GNR (1) is larger than that for graphene and (2) increases with decreasing ribbon width (N), as shown in Fig.1 for the dehydrogenated armchair-GNR (AGNR). This is because the phonon dispersion curves for the two in-plane acoustic modes (LA and TA) remain unchanged with decreasing N, so that these modes become dominant for the phonon thermal conductance of narrower ribbons.

We have also investigated the normalized thermal conductance for the GNR and the single-walled carbon nanotube (SWNT) which has a circumferential length corresponding to the width of GNR. It has been indicated that the GNR has a better thermal conductance compared with SWNT at an extremely-low temperature, since the optical phonon mode localized at the edge emerges in GNR at a low-frequency region. The contribution of such edge modes to the conductance becomes smaller as N decreases (N=4-12).

The phonon modes associated with the C-H bond has been found at the high-frequency region [3], and thus the contribution of these modes to the thermal transport is negligible small at the room temperature. However, we notice that the hydrogenation of edges causes a indirect effect on the thermal conductance: the phonon dispersions of the out-of-plane acoustic modes (ZA and twist [4,5]) become narrower.

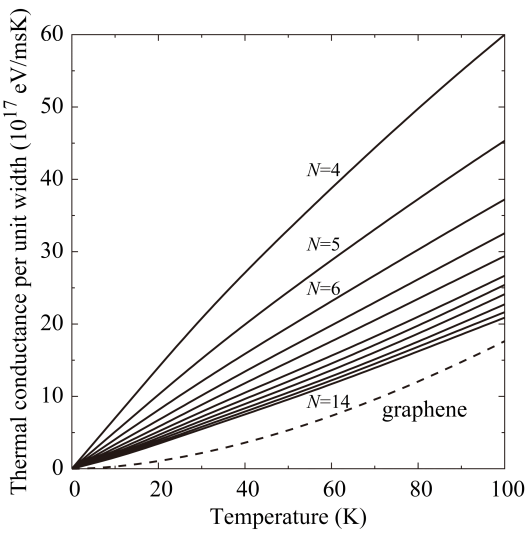

Fig.1: Thermal conductance per unit width, w, for the dehydrogenated-AGNR with *N*=4-14 (solid lines) and graphene (dashed line) as a function of temperature.

References

[1] K.Saito, J.Nakamura, and A.Natori, Phys. Rev. B **76**, 115409 (2007).

[2] E.Watanabe, S.Yamaguchi, J.Nakamura, and A.Natori, Phys. Rev. B **80**, 085404 (2009).

[3] R.Gillen et al., Phys. Rev. B **80**, 155418 (2009).

[4] R.Saito et al., Physical Properties of Carbon Nanotubes (Imperial College Press, 1998).

[5] M.Yamada et al., Phys. Rev. B **77**, 054302 (2008).

*Corresponding author: Jun Nakamura
Department of Engineering Sciences,
The Univ. of Electro-Communications (UEC-Tokyo)
1-5-1 Chofugaoka, Chofu, Tokyo 182-8585,Japan
e-mail : junj@ee.uec.ac.jp
Tel. & FAX : +81-42-443-5156
http://www.natori.ee.uec.ac.jp/~junj/

Su1625

Controlled Motion of Freestanding Graphene and Graphene on Graphite via Scanning Tunneling Microscopy

P. Xu[1] Yurong Yang,[1,2] D. Qi,[1] S. D. Barber,[1] J. K. Schoelz,[1] M. L. Ackerman,[1] L. Bellaiche,[1] and P. M. Thibado[1,*]

[1]*Department of Physics, University of Arkansas, Fayetteville, Arkansas 72701, USA*
[2]*Physics Department, Nanjing University of Aeronautics and Astronautics, Nanjing 210016, China*

A series of measurements using a new technique called electrostatic-manipulation scanning tunneling microscopy (EM-STM) were performed on freestanding graphene and highly-oriented pyrolytic graphite (HOPG). For HOPG, the electrostatic interaction between the tip and sample could be used to produce large-scale movement of the graphite surface. For example, we have altered the local geometry of a 20 nm wide graphite nano-ribbon (not shown). In addition, we have observed a continuous electronic transition from triangular symmetry, where only alternate atoms are imaged, to hexagonal symmetry in the STM images as shown below in Fig. 1(a-c). Density functional theory (DFT) calculations reveal that this transition can be related to vertical displacement of the top layer of graphite relative to the bulk as seen in the simulated STM images shown below in Fig. 1(d-f). At a vertical displacement of ~0.09 nm (not shown), the top layer of graphite has become graphene. At this height and beyond, the top layer electronic structure has transitioned from parabolic bands (i.e., massive electrons) to linear band (i.e., massless electrons). The EM-STM experimental technique therefore, allows for the systematic study of the process by which the electron gains mass. For freestanding graphene, STM and EM-STM can be used to induce a broad range of dynamic movement. Furthermore, the induce curvature locally creates a pseudo-magnetic field, which would modify the electron transport properties. According to our DFT results, with additional displacements, strain enters the lattice creating an electronic band gap as well as a strain-induced pseudo-magnetic field.

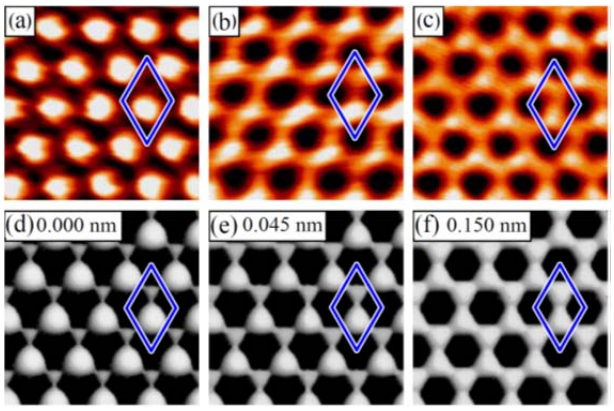

FIG. 1. (a-c) Filled-state atomic-resolution STM images of the HOPG surface taken with a bias voltage of 0.1 V and a setpoint current of 0.2 nA. A unit cell is superimposed on each image. Notice that (a) shows triangular symmetry because only alternate atoms appear in the image, while (c) shows the full hexagonal symmetry. (d-f) Simulated STM images of graphite taken from DFT calculations. The rhombus unit cell is again superimposed on each image, and the top layer's vertical displacement from equilibrium is indicated at top left.

This work is supported in part by ONR grant N00014-10-1-0181, NSF grant DMR-0855358, and ARO grant W911NF-12-1-0085.

* Electronic mail: thibado@uark.edu

Su1630 Invited

Single-layer MoS_2 – electrical transport and devices

Andras Kis, *Ecole Polytechnique Federale de Lausanne (EPFL), Lausanne, Switzerland*

Web site: lanes.epfl.ch

After quantum dots, nanotubes and nanowires, two-dimensional materials in the shape of sheets with atomic-scale thickness represent the newest addition to the diverse family of nanoscale materials. The most widely studied two-dimensional material to date is graphene because of its rich physics, high-mobility and wide variety of potential applications. Pristine graphene is however not a semiconductor and the lack of band gap is a serious problem in many applications, for example in electronics.

I will present here our work on a material similar to graphene – single layer MoS_2, a direct-gap semiconductor that can be produced using the scotch-tape technique commonly associated with the production of graphene. Our nanolayers are mechanically and chemically stable under ambient conditions. We have fabricated transistors based on single-layer MoS_2 which demonstrate that this material has several advantages over silicon or graphene for potential applications in electronics.

Our latest results on MoS_2 show transistors with increased performance that indicate how this material could be used not only in low-power digital but also high-performance analogue electronic applications. Temperature-dependent transport and Hall-effect measurements further yielded new insights into the mobility engineering of this material and the barrier height between gold and monolayer MoS_2.

Su1700

Dynamic Negative Compressibility of Solid Lubricants

Bernardo R. A. Neves†, Ana Paula M. Barboza,† Helio Chacham,† Camilla K. Oliveira,† Thales F. D. Fernandes,† Erlon H. Martins Ferreira,‡ Braulio S. Archanjo,‡ Ronaldo J. C. Batista,§ and Alan B. de Oliveira,§

†Departamento de Física, ICEx, Universidade Federal de Minas Gerais (UFMG), C.P. 702, 30123-970 Belo Horizonte, Brazil
‡Divisão de Metrologia de Materiais, Instituto Nacional de Metrologia, Normalização e Qualidade Industrial, 25250-020 Duque de
Caxias, Brazil
§Departamento de Física, ICEB, Universidade Federal de Ouro Preto (UFOP), 35400-000 Ouro Preto, Brazil

We report a novel mechanical response of solid lubricants (few-layer graphene, h-BN, MoS_2 and talc) to the simultaneous compression and shear by an atomic force microscope (AFM) tip. The response is characterized by the vertical expansion of these two-dimensional (2D) layered materials upon compression. Such effect is proportional to the applied load, leading to vertical strain values (opposite to the applied force) of up to 150%. The effect is null in the absence of shear, increases with tip velocity, and is anisotropic. It also has similar magnitudes in all solid lubricants (few-layer graphene, h-BN, talc and MoS_2), but it is absent in single-layer graphene and in other layered materials (few-layer mica and Bi_2Se_3). We propose a physical mechanism for the effect where the combined compressive and shear stresses from the tip induce dynamical wrinkling on the upper material layers, leading to the observed flake thickening. The new effect (and, therefore, the proposed wrinkling) is reversible in all solid lubricant materials where it is observed.

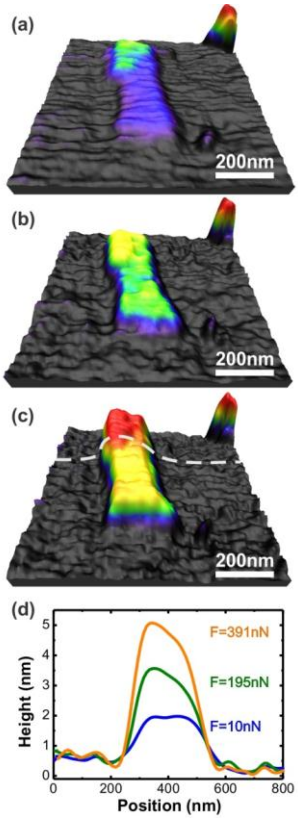

The negative compressibility effect.

3D-rendering topographic AFM images of the same graphene flake acquired in contact mode under increasing tip loads: (a) 10 nN, (b) 195 nN, and (c) 391 nN. (d) Height profiles taken from the images in (a), (b), and (c) evidencing the negative strain of the graphene flake (expansion upon compression). The dashed line in (c) indicates where the profiles were measured. The tip velocity was v = 5 μm/s.

Complex Oxides

Su1930 Invited

Two-dimensional electron gas at the atomically smooth $LaAlO_3/SrTiO_3$ (111) interface

Chang-Beom Eom
Department of Materials Science and Engineering
University of Wisconsin-Madison, Madison, Wisconsin 53706, USA

The two-dimensional electron gas (2DEG) at the $LaAlO_3/SrTiO_3$ (001) heterointerface has been widely investigated due to its diverse functionalities such as conductivity, ferromagnetism, and superconductivity. In this orientation, the $SrTiO_3$ is nonpolar, with charge-neutral AO and BO_2 planes, while +e of charge is transferred between AO and BO_2 planes in the $LaAlO_3$ layer. The (111) orientation is, however, qualitatively different in that the AO_3 and B lattice planes in both materials exhibit charge transfer between layers, and both have in principle a polar character. We have found that $LaAlO_3$ deposited on the (111) $SrTiO_3$ polar surface also supports an interfacial 2DEG. An atomically smooth step and terrace structure of (111) $SrTiO_3$ surface was prepared by buffered-HF and heat treatment. The step height of the treated (111) $SrTiO_3$ is ~2.25Å, which is 1/3 of the diagonal of the cubic $SrTiO_3$ lattice along the [111] direction, consistent with the thickness of one AO_3/B (111) bilayer. $LaAlO_3$ was grown epitaxially in a layer-by-layer growth mode, with one oscillation of the reflection-high energy electron diffraction (RHEED) specular spot corresponding to this single step height. The (111) interfacial 2DEG shows a higher carrier concentration than LAO/STO (001) at room temperature. We find a $LaAlO_3$ critical thickness between 11.3 and 16 Å, with the transition between insulating and conducting regimes broader than that of LAO/STO (001). Surface X-ray diffraction with COherent Bragg Rod Analysis (COBRA) has been carried out to explore the possible structural reconstruction of (111) $SrTiO_3$. We will discuss the origin of 2DEG at this polar-polar interface.

This work has been done in collaboration with S. Ryu, C. W. Bark, T. Hernandez, M. S. Rzchowski, H. Zhou and D. D. Fong, T. R. Paudel and E.Y. Tsymbal

Su2000

Investigation of interfacial electronic properties of $LaAlO_3/SrTiO_3$ using scanning tunneling microscopy

Y. P. Chiu[1], B. C. Huang[1], P. C. Huang[1], W. C. Wang[1], V. T. Tra[2], J. C. Yang[3], Q. He[4], J. Y. Lin[2], C. S. Chang[5], Y. H. Chu[3]

[1]*Department of Physics, National Sun Yat-sen University, Kaohsiung, 804, Taiwan*

[2]*Institute of Physics, National Chiao Tung University, Hsinchu, 300, Taiwan*

[3]*Department of Materials Science and Engineering, National Chiao Tung University, HsinChu, 300, Taiwan*

[4]*Advanced Light Source, Lawrence Berkeley National Laboratory, Berkeley, CA94720, USA*

[5]*Institute of Physics, Academia Sinica, Taipei, 105, Taiwan, ROC*

Recently, unusual electronic structures due to the polarity discontinuity at the heterointerface have attracted much attention. For instance, the quasi-two dimensional electron gas has been found at the interface between two insulating materials $LaAlO_3$ and $SrTiO_3$. To study the uncommon electronic properties at the interface of $LaAlO_3/SrTiO_3$ systems, a combination of cross-sectional scanning tunneling microscopy and scanning tunneling spectroscopy measurements is employed to investigate the localized interfacial band structures at atomic scale. Experimental results indicate that electronic reconstructions and a built-in electric field in the polar $LaAlO_3$ layer induced by the polarity discontinuities are directly mapped out. The band bending as well as the notched band structure in the $SrTiO_3$ adjacent to the interface is clearly revealed.

Su2005

Intrinsic spin-orbit effects in oxide interfaces: $LaAlO_3/SrTiO_3$ 2DEGs

Cuneyt Sahin[1,*], Giovanni Vignale[2], and Michael E. Flatté[1]

[1]Optical Science and Technology Center and Department of Physics and Astronomy, University of Iowa, Iowa City, Iowa 52242, USA
[2]Department of Physics and Astronomy, University of Missouri, Columbia, Missouri 65211, USA
[*]Email: cuneyt-sahin@uiowa.edu

Recent studies have shown that it is possible to create a high-density, high mobility two-dimensional electron gas (2DEG) at the interface between $LaAlO_3$ and $SrTiO_3$. (LAO/STO).[1] Furthermore it is possible to change the electronic features of this strongly correlated 2DEG using strain and different growth techniques [2,3], to realize a metal-insulator transition, superconducitivity, and various spintronic properties (including a large Rashba coefficient). In this study we calculate intrinsic properties due to the spin-orbit interaction, including the spin relaxation time and intrinsic spin Hall conductivity for the 2DEG at the interface of LAO/STO.

In order to calculate intrinsic spin orbit effects address the importance of the tensorial form of the spin-orbit interaction for non-spherical conduction bands. The influence of the spin-orbit interaction can be understood through a proper consideration of the crystal symmetry (the inversion-symmetric space group O_h^1) and bonding properties (through a Slater-Koster [4] tight-binding model for STO [5], in which the carriers predominately reside). STO is a semiconductor with a band gap about 3.22 eV, and has a four-fold-degenerate conduction band when spin-orbit interaction is included. We have extended the tight-binding model for STO by adding spin-orbit interactions (couplings computed from atomic spectra) and uniaxial elastic strain. This results in a single conduction band for the LAO/STO 2DEG, as observed for carrier densities below a critical density.(Supplementary Fig.1) From this model we extract the functional form of the spin-orbit interaction, which we express in terms of a highly symmetric rank-3 tensor. This tensor has also been calculated with a 12 band $\mathbf{k}\cdot\mathbf{p}$ model and we obtained a good agreement between two models.

From the spin-orbit interaction we have calculated the spin relaxation time via the Elliott-Yafet mechanism as a function of temperature. Spin flips occur via mixing of different pseudospin states into the wave functions of eigenstates of different momenta, which produces spin flips as the carriers scatter from interactions with impurities and phonons. We model the scattering as due to point defects, and calculate spin flip scattering probabilities from Fermi's Golden rule. Spin relaxation times (Supplementary Fig.2) have been calculated for different carrier densities and temperatures below the density to occupy the second conduction band. Furthermore, by calculating carrier densities and mobilities at different temperature and comparing it with experimental values in the literature we obtain an estimate of the strength of the impurity potential. Results indicate that 2DEG at the interface of LAO/STO has relatively long spin relaxation times at low temperatures.

We also express the spin Hall conductivity by Kubo formula and evaluate it by calculating Berry curvature in the clean static limit and it is found to be quite large. (Supplementary Fig.3) Moreover the spin Hall conductivity as a function of the strain and spin-orbit splitting in the conduction band has been studied. Modifications due to vertex corrections have been considered and shown to be insignificant. The large spin Hall conductivity and long spin lifetimes suggest the potential for novel spintronic applications of the LAO/STO 2DEG.

This work was supported by an ARO MURI.

Su2010 Invited

Unusual behavior of quantum-well subbands in transition-metal oxide thin films

Hiroshi KUMIGASHIRA[1,2]

[1] *Photon Factory, Institute of Materials Structure Science, KEK, Tsukuba, Japan, 305-0801*

[2] *PRESTO, Japan Science and Technology Agency, Saitama, Japan, 332-0012*

Email: hiroshi.kumigashira@kek.jp

The quantum confinement of strongly correlated electrons in artificial structures provides an ideal platform for studying the behavior of correlated Fermi-liquid states in reduced dimensions, as well as for controlling the extraordinary physical properties of layered complex oxides, such as high-temperature superconductivity in cuprates, triplet superconductivity in ruthenates, and colossal magnetoresistance in manganites. In this talk, we report the creation and control of two-dimensional electron-liquid states in ultrathin films of $SrVO_3$ epitaxially grown on Nb:$SrTiO_3$ substrates, which are artificial oxide structures that can be varied in thickness by single monolayers [1]. Angle-resolved photoemission from the $SrVO_3$/Nb:$SrTiO_3$ samples shows metallic quantum well states that are adequately described by the well-known phase-shift quantization rule, confirming the quantum confinement of strongly correlated electrons in the oxide artificial structures. The observed quantum well states in $SrVO_3$ ultrathin films exhibit distinctive features, such as orbital-selective quantization originating from the anisotropic orbital character of the V 3*d* states and unusual band renormalization of the subbands near the Fermi level, that reflect complex interactions in the quantum well. The successful fabrication of a metallic quantum well structure based on a strongly correlated oxide promises to provide a setting in which to explore the fundamental physics and extraordinary functionalities of strongly correlated oxides.

[1] K. Yoshimatsu *et al*. *Science* **333**, 319 (2011).

Su2040

Electric Field Control of the Verwey Transition and Induced Magnetoelectric Effect in Magnetite

Jared J. I. Wong, Adrian G. Swartz, Renjing Zheng, Wei Han, and Roland K. Kawakami
Department of Physics and Astronomy, University of California, Riverside, CA 92521, USA

ABSTRACT

Electric field control of magnetic and metal-to-insulator transitions in highly correlated materials has generated great interest both scientifically and technologically. Magnetite (Fe_3O_4) is a highly correlated material that undergoes the well-known Verwey transition with sharp changes in the electric, magnetic, and structural properties at a transition temperature of $T_V \sim 120$ K [1–3]. The Verwey transition, discovered in 1939 as one of the first metal-to-insulator transitions generated by electron-electron correlations, has been studied intensively over the past seven decades and the microscopic theory is still under investigation. More recently, theoretical predictions of half-metallic behavior (100% spin polarization) [4] have motivated studies of magnetite thin films and heterostructures for spintronics [5, 6].

In this work [7], we demonstrate that static electric fields can control the Verwey transition in Fe_3O_4 thin films. Our experiments utilize an electrostatic gate to apply a static electric field to a 50 nm magnetite film. It is found that the application of either positive or negative electric fields leads to an increase of the transition temperature (T_V), as shown in Figure 1. This result is quite surprising and intriguing because it was not theoretically predicted despite years of intense research with magnetite and on the Verwey transition. Furthermore, because the Verwey transition is accompanied by a sharp change in magnetization, electric field control of T_V leads to a new mechanism for generating a magnetoelectric effect. Figure 2 shows the magnetization measured by the magneto-optic Kerr effect (MOKE) as a function of applied electric field. The absolute scale of magnetization is calibrated by superconducting quantum interference device (SQUID) magnetometry.

Previous demonstrations of electric field control of magnetic and metal-to-insulator transitions have resulted from various effects including current-induced breakdown of the insulating state [8–10], field-induced changes of carrier concentration [11, 12], field-induced strain generated by growth on piezoelectric substrate (i.e. composite system) [13–16]. The results reported here are significantly distinct from these previous categories. Particularly, while current-induced breakdown is a highly non-equilibrium process, the present effect produces a true change in the equilibrium phase transition. We also find that this effect is not due to changes in carrier concentration, as shown by a symmetric dependence of T_V on gate voltage. Finally, this effect does not rely on external strain provided by adjacent layers. Thus, the electric field control of the Verwey transition represents a new type of electric field control in a highly correlated material.

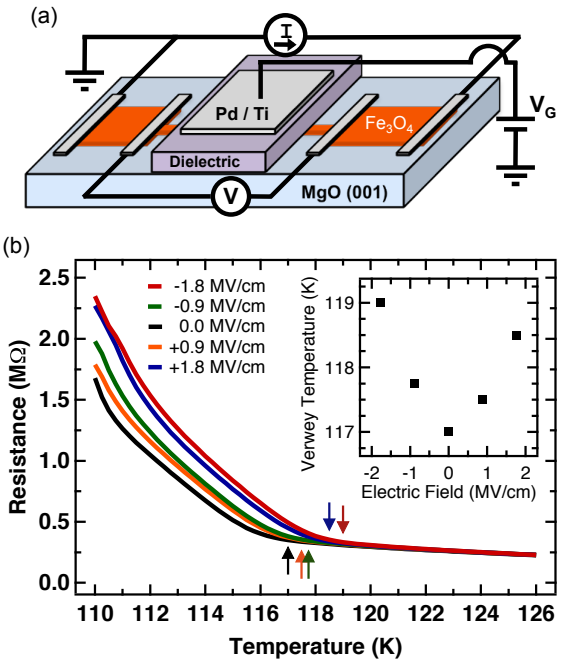

FIG. 1. Electrical gating of a 50 nm Fe_3O_4 film and manipulation of the Verwey transition. (a) A schematic of the sample device structure. The dielectric layer consists of PMMA(900 nm)/Al_2O_3(50 nm)/MgO(10 nm). Positive electric field corresponds to the application of positive voltage to the top gate electrode. (b) Temperature dependence of resistance for applied electric fields of +1.8 MV/cm (blue), +0.9 MV/cm (orange), 0 MV/cm, -0.9 MV/cm (green), -1.8 MV/cm (red). The arrows show T_V for each electric field, which is summarized in the inset.

[1] E. J. W. Verwey, Nature **144**, 327 (1939).
[2] E. J. W. Verwey and P. W. Haayman, Physica **8**, 979 (1941).
[3] F. Walz, J. Phys.: Condens. Matter **14**, R285 (2002).
[4] Z. Zhang and S. Satpathy, Phys. Rev. B **44**, 13319 (1991).
[5] P. Seneor, A. Fert, J.-L. Maurice, F. Montaigne, F. Petroff, and A. Vaures, Appl. Phys. Lett. **74**, 4017 (1999).
[6] Y. Li, W. Han, A. G. Swartz, K. Pi, J. J. I. Wong, S. Mack, D. D. Awschalom, and R. K. Kawakami, Phys.

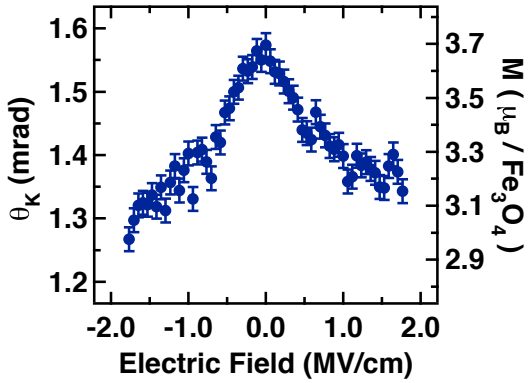

FIG. 2. Magnetization as a function of electric field measured by MOKE and calibrated by SQUID. This demonstrates a magnetoelectric effect induced by electric field control of the Verwey transition.

Rev. Lett. **105**, 167203 (2010).
[7] J. J. I. Wong, A. G. Swartz, R. Zheng, W. Han, and R. K. Kawakami, Phys. Rev. B **86**, 060409(R) (2012).
[8] A. Asamitsu, Y. Tomioka, H. Kuwahara, and Y. Tokura, Nature **388**, 50 (1997).
[9] S. Lee, A. Fursina, J. T. Mayo, C. T. Yavuz, V. L. Colvin, R. G. S. Sofin, I. V. Shvets, and D. Natelson, Nature Mater. **7**, 130 (2008).
[10] F. Wang, C.-H. Li, T. Zou, L. Yi, and Y. Sun, J. Phys.: Condens. Matter **22**, 496001 (2010).
[11] T. Lottermoser, T. Lonkai, U. Amann, D. Hohlwein, J. Ihringer, and M. Fiebig, Nature **430**, 541 (2004).
[12] C. A. F. Vaz, J. Hoffman, Y. Segal, J. W. Reiner, R. D. Grober, Z. Zhang, C. H. Ahn, and F. J. Walker, Phys. Rev. Lett. **104**, 127202 (2010), pRL.
[13] J. Ryu, A. V. Carazo, K. Uchino, and H.-E. Kim, Jpn. J. Appl. Phys. **40**, 4948 (2001).
[14] J. Ryu, S. Priya, K. Uchino, and H.-E. Kim, J. Electroceram. **8**, 107 (2002).
[15] H. Zheng, J. Wang, S. E. Lofland, Z. Ma, L. Mohaddes-Ardabili, T. Zhao, L. Salamanca-Riba, S. R. Shinde, S. B. Ogale, F. Bai, D. Viehland, Y. Jia, D. G. Schlom, M. Wuttig, A. Roytburd, and R. Ramesh, Science **303**, 661 (2004).
[16] L. Yan, Z. Wang, Z. Xing, and J. Li, J. Appl. Phys. **107**, 064106 (2010).

Su2045

Reduced symmetry and orbital order at perovskite surfaces and interfaces

A.A. Demkov, J. Lee, K. Fredrickson, C. Lin and C. Mitra

Department of Physics, The University of Texas at Austin, Austin, Texas 78712, USA

Recent discovery of two-dimensional electron gas at the interface of $SrTiO_3$ (STO) and $LaAlO_3$ (LAO) [1] has spurred an intense research effort aiming to understand the origin of charge and find ways to control it in functional devices. The system has proven to be even more exciting after the discovery of collective ground states such as magnetism, superconductivity and even co-existence of the two [2-8]. Even the surface of STO is now believed to be metallic [9]. Simultaneously with the growing body of experiments, a large number of theoretical contributions describing different aspect of the system's behavior can be found in the literature [10-13]. One may find this attention to STO somewhat surprising as it is a prototypical perovskite that does not possess many of the functional properties of the other members of this group of materials. The Ti *3d* t_{2g}^* band is empty, rendering STO nonmagnetic. Instead of the FE transition observed in $BaTiO_3$, STO is known to undergo an AFD transition corresponding to out-of-phase rotations in neighboring planes of TiO_6 octahedra but only when the temperature drops below 110 K [14-16]. But despite these "shortcomings", STO is proving to be a very interesting material in its own right. In particular, putting charge into the d-shell of Ti is at the heart of all phenomena mentioned above. This however is not a unique feature of the LAO/STO interface, oxygen vacancy or a heterojunction with metal result in charging the perovskite.

In this talk I will compare the behavior of the initially empty d-shell of Ti atoms in STO and ferroelectric $BaTiO_3$ (BTO) in the bulk, bulk with an oxygen vacancy, clean surface, surface with a vacancy and at the interfaces with LAO, Cs and Pt. In summary, the crystal field splitting in these titanates is approximately two eV. And to first order, Ti *d* states do not mix with the *p* states. Once the symmetry is lowered, however, none of this is true. It does though make a difference how exactly the symmetry is lowered. I will discuss the relative significance of the d-p mixing, global symmetry lowering, local distortion, evanescent charge transfer and chemical bond formation. Lattice screening effects manifesting themselves as rumpling will also be discussed as they found to play an important role. We illustrate the difference in Figure 1. At the LAO/STO interface the orbital caring the charge in STO is d_{xy} of the t_{2g}^* band, while at the Cs/STO interface it is $3d_{z^2}$ of the e_g band.

This work is supported by the National Science Foundation under grant DMR-0548182, and the US Department of Energy under grant DE-SC0001878. All calculations are done at the Texas Advanced Computing Center.

Su2050

Interplay of Native Point Defects in $SrTiO_3$, $BaTiO_3$, and $Ba_xSr_{1-x}TiO_3/SrTiO_3$ Heterojunctions with Growth Temperature, Oxidation, and Strain

L.J. Brillson,[1-3] S. Shen,[1] M.M. Rutkowski,[2] K. McNicholas,[1] S. Balaz,[1] T. Merz,[2] C. Brooks,[4] and D.G. Schlom[4]
[1]Departments of Electrical Engineering, [2] Physics, and [3]Center for Materials Research, 205 Dreese Lab, 2015 Neil Ave. The Ohio State University, Columbus, OH 43210-1272
[4] Department of Materials Science & Engineering, Cornell University, Ithaca, NY 14853

Native point defects can have a significant impact on the interface properties of complex oxides, and their accumulation at heterojunctions can severely limit the integration of complex oxides with conventional semiconductor devices. We used depth-resolved cathodoluminescence spectroscopy (DRCLS), X-ray diffraction (XRD), atomic force microscopy (AFM) and surface photovoltage spectroscopy (SPS) to characterize growth-related defects vs. depth through molecular beam epitaxy (MBE) – grown $SrTiO_3$ (STO), $BaTiO_3$ (BTO), and $Ba_{0.5}Sr_{0.5}TiO_3$ (BTO)/ STO heterojunctions. We found correlations between growth parameters, film characteristics and specific defect concentrations across this range, which also relate to RF dielectric permittivity and loss tangents. BST shows strong promise for many RF devices as well as templates for strain-controlled growth of perovskite heterojunctions.

These compounds exhibit multiple DRCLS defect features at energies below their band gaps that can be identified with oxygen vacancies (V_O) and related complexes (V_O-R), Ti^{3+} states, and Ba vacancies (V_{Ba}). 100 nm $SrTiO_3$ grown on LSAT (compressive), DSO (tensile), and $SrTiO_3$ exhibit dramatic differences in defect densities and depend strongly on growth temperature T_G in the range 650 - 1000°C. In general, V_O-R defects increase with increasing T_G while Ti^{3+} defects remain unchanged. Conversely, Ti^{3+} states are very sensitive to strain, increasing with decreasing compressive strain, consistent with lattice expansion due to the lower Ti oxidation state. Well-resolved Ti^{3+} features display a monotonic energy shift to higher energies as substrate lattice constant increases, indicating a defect gauge of strain related to Ti 3d band splitting. Interestingly, 100 nm $SrTiO_3$ / $SrTiO_3$ films exhibit the highest defect densities overall for all T_G and substrates. $BaTiO_3$ films on $SrTiO_3$ display no Ti^{3+} peaks and relatively low V_O-R features, again consistent with effects of lattice compression on these defects. V_O-R features are further reduced by oxygen plasma vs. ambient oxygen growth.

100nm thick $Ba_{0.5}Sr_{0.5}TiO_3$/ $SrTiO_3$(100) epilayers grown at T_G = 700°C to 900°C, P_{O_2} = $3x10^{-8}$ - 10^{-6} Torr, and both O_2 and O plasma ambients display DRCL spectra whose transition energies match with SPS energy levels within the BST band gap. Two of the V_O-R emissions correlate with strain and O ambient. A 1.9 eV peak identified with V_O-V_{Ba} transitions correlates with strain from c-axis parameter XRD, increasing toward the strained interface and decreasing by nearly 10X in partially relaxed films. A 2.95 eV commonly attributed to an intrinsic "self-trapped exciton" is in fact a V_O-related state. This feature increases dramatically with decreasing $P(O_2)$ at the BST/STO interface, identifying the V_O created as O diffuses out of STO into the growing BST epilayer. This effect is confirmed by fully-oxidized BST films (from XPS depth profiles) grown *without any ambient oxygen*, revealing a huge increase in V_O-R emission tens of nm below the BST/STO interface. All these results demonstrate the first-order effect of native point defects on dielectric properties at complex oxide heterostructures and the ability to control them by MBE growth conditions.

This work was supported by the Office of Naval Research (Dan Green), Army Research Office (Marc Ulrich), and the National Science Foundation (Charles Ying).

Su2055

High quality $SrVO_3$ thin films grown by hybrid molecular beam epitaxy

J.A. Moyer[1,2)], C. Eaton [2)], and R. Engel-Herbert[2)]

[1)] Department of Physics, Pennsylvania State University, University Park, Pennsylvania 16802, USA.
[2)] Department of Materials Science and Engineering, Pennsylvania State University, University Park, Pennsylvania 16802, USA.

Complex transition metal oxides with perovskite and related structure exhibit a plethora of properties arising from a complex interplay of spin, charge, lattice and orbital degree of freedom as well as strong electron correlations. $SrVO_3$ is a Mott material with $3d^1$ configuration. Its relatively large band width compared to the on-site Coulombic repulsion enables metallic-like transport. Narrowing the band width by reducing the orbital overlap can be achieved by imposing a tensile epitaxial strain which would tune $SrVO_3$ closer to the metal-to-insulator transition (MIT). However, a mandatory requirement to study the effect of strain on the MIT is the ability to growth high quality, stoichiometric $SrVO_3$ thin films. Nonstoichiometric growth conditions can result in the formation of extended defects. Excess Sr has been reported to get incorporated into perovskite $SrVO_3$ forming SrO planar faults and eventually members of the Ruddlesden-Popper homologous series [1]. Furthermore unintentional defects that are potentially electrically active will change the band filling and therefore affect transport properties.

In this presentation we will demonstrate that the hybrid MBE approach recently developed for complex titanate thin films and successfully applied to the growth of stoichiometric $SrTiO_3$ films [2] can be extended to complex vanadates. $SrVO_3$ thin films were grown on (001) $SrTiO_3$ and (001) $(La_{0.3}Sr_{0.7})(Al_{0.65}Ta_{0.35})O_3$ [LSAT] substrates. The metal-organic precursor vanadium oxo-tri-isopropoxide [VTIP] was used to supply vanadium whereas strontium was evaporated from an effusion cell. Co-supplying VTIP and Sr fluxes in the presence of an oxygen background pressure of 5×10^{-7} Torr at a substrate temperature of 800°C resulted in high quality $SrVO_3$ thin films. The intrinsic film lattice parameter was used to determine the film's stoichiometry. High resolution x-ray diffraction has been performed on a series of samples grown on LSAT with varying VTIP to Sr flux ratio which will be directly correlated with reflection high energy electron diffraction (RHEED) observations and surface morphology. Specific features characteristic of Sr rich and V rich films have been identified and will be discussed. For stoichiometric films rocking curve widths of $SrVO_3$ identical to those of the substrates have been generally found indicating that the structural quality of the film is substrate-limited. Specifically, rocking curve widths of the 002 $SrVO_3$ reflection as narrow as 40 arcsec were achieved on LSAT substrates. Atomic force microscopy revealed atomically smooth surfaces with atomic terraces separated by terrace steps with single unit cell step height. RHEED showed streaky diffractions pattern throughout the growth. The absence of intensity oscillation suggests that films grew in step-flow growth mode. Finally, temperature dependent transport measurements of stoichiometric $SrVO_3$ thin films grown on $SrTiO_3$ (1.7% tensile strain) and LSAT (0.7% tensile strain) will be compared and the applicability of epitaxial strain as a means to modulate the band width in $SrVO_3$ is discussed.

[1] A. Nozaki, H. Yoshikawa, T. Wada, H. Yamauchi, and S. Tanaka, "Layered perovskite compounds $Sr_{n+1}V_nO_{3n+1}$ (n=1, 2, 3, and ∞)", Physical Review B **43**, 181 – 185 (1991).

[2] B. Jalan, R. Engel-Herbert, N. J. Wright, S. Stemmer, "Growth of high-quality $SrTiO_3$ films using a hybrid molecular beam epitaxy approach", Journal of Vacuum Science & Technology A **27**, 461-464 (2009).

Su2100

Title: Synthesis and Magnetic Properties of RE doped $SrFe_{12-x}$ Dy_xO_{19} ferrite nanoparticles.

Binod Kumar Rai, Sanjay Raj Mishra

The University of Memphis, Memphis, TN, 38152.

The M-phase ferrites (Pb, Sr, Ba)$Fe_{12}O_{19}$ with magnetoplumbate structures are commonly known as hexagonal ferrites. The hexagonal ferrites are the first group of ferrites whose coercivity is due to magnetocrystalline anisotropy rather than shape anisotropy. Because of their high magnetization (M_s), Curie temperature (T_c) and Coercivity (H_c), environmental stability, low price for production and corrosion resistivity [1,2] these ferrites have become popular for industrial. In our previous work, substantially large coercivity (18 KOe) [3] was reported for the Al doped hard ferrites ($SrAl_4Fe_8O_{19}$). On the other hand, light rare-earth doped for iron show very low remnant flux density (B_r), abruptly decreasing $(BH)_{max}$ because of low B_r instead of low H_c. In the present study, heavy rare earth (~10μ_B) with large magnetocrystalline anisotropy doped for Fe in SrFe12O19 showed improvement in the B_r and H_c.

Rare Earth (RE) substituted $SrFe_{12-x}RE_xO_{19}$ particles (RE: Dy) were prepared via auto-combustion route. The phase and structure of samples were characterized by using XRD. The magnetic properties of the samples were investigated using VSM and Mossbauer spectroscopy (MS). The Tc was determined using differential scanning calorimetry.

The XRD patterns indicate that as synthesized powders were pure phase hexagonal ferrites upto x = 3. Increment in lattice parameters was observed with increase in concentration of Dy. A significant increment in both M_r (remanence) and M_s is noticed with small concentration of RE doping as compared to pure $SrFe_{12}O_{19}$ which can be attributed to large magnetic moment in RE (~10.62μB for Dy) as compared to small magnetic moment in Fe (~5μB). As supported by MS, these decreases in Ms results from Fe3+ being converted to Fe2+, a concomitant decrease in superexchange interaction between Fe^{3+} ion sites, and increase in spin non-collinearity. A substantial increase in coercivity (Hc~ 28%) as compared to $SrFe_{12}O_{19}$ is observed. The increase in H_c of RE doped ferrite is due to magnetocrystalline anistropy of heavy RE ions.

In conclusion, replacing Fe^{3+} ions by RE^{3+} ion brought ~ 28% increment in H_c with high Ms = 65 emu/g and T_c~733 K. High H_c and M_r/M_s ratio (0.63) of $SrFe_{12-x}RE_xO_{19}$ could find potential application in the field of permanent magnets and nanotechnology.

References [1]. N. Chen, K. Yang, and M. Y. Gu, J. Alloys. Comp. 490 (2010) 609.

[2]. J. Dho, E. K. Lee, J. Y. Park, and N. H. Hur, J. Magn. Magn. Mater. 285 (2005) 164.

[3]. H. Luo, B. K. Rai, S. R. Mishra, V. V. Nguyen, J. P. Liu, J. Mang. Magn. Mater., 324 (2012) 2602.

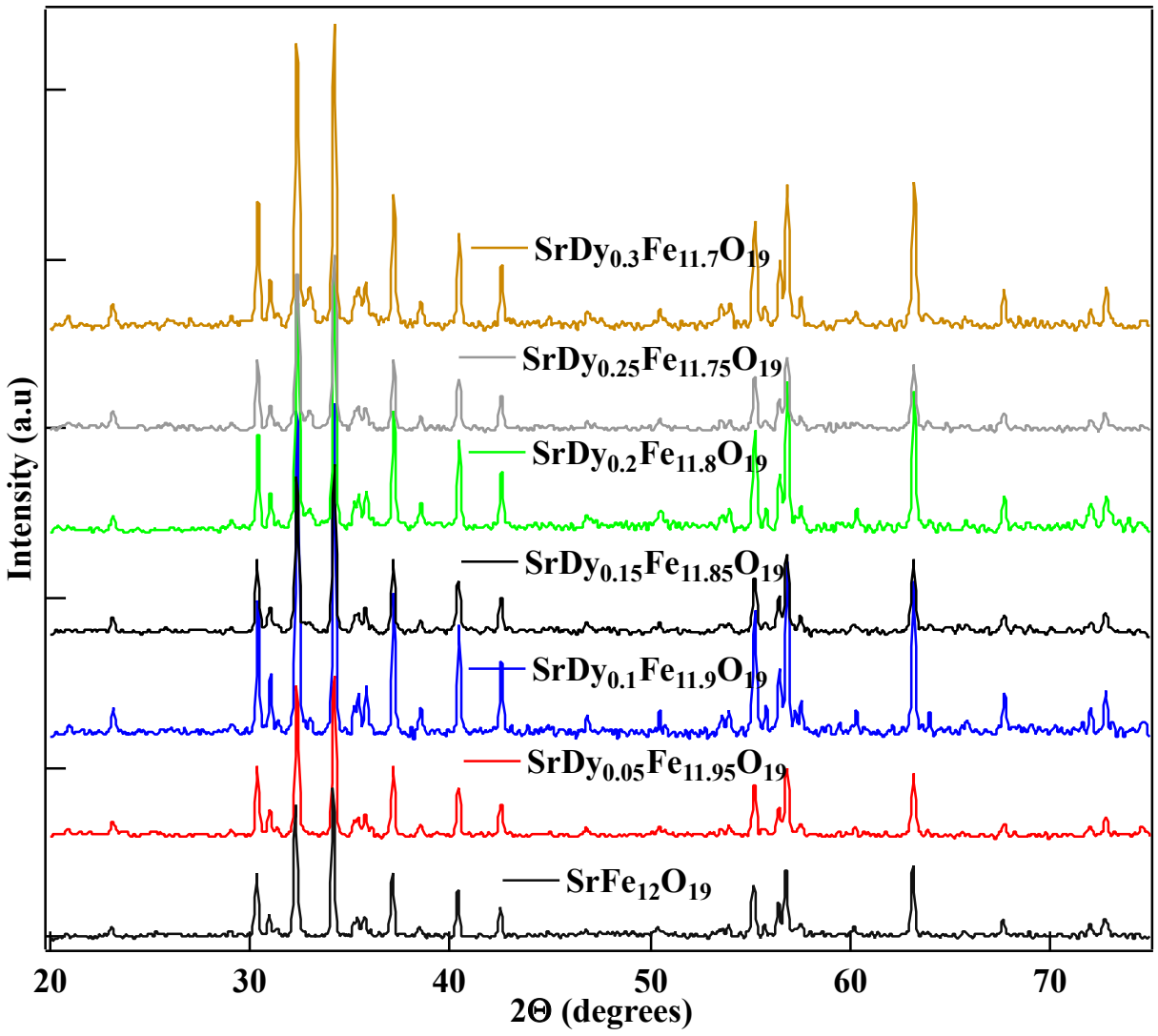

Figure. XRD patterns of Dysprosium doped Strontium Hexaferrite nanoparticles.

Monday

Mo0730	Registration and Continental Breakfast
Mo0830	Monday Morning Session: Interface & Surface Magnetism
Mo1000	Coffee Break and Poster Viewing
Mo1100	Monday Morning Session: Semiconductor Growth & Surfaces
Mo1210	Lunch and Poster Viewing
Mo1400	Monday Afternoon Session: Spintronics with Organics
Mo1500	Coffee Break and Poster Viewing
Mo1600	Monday Afternoon Session: Surface Passivation & High-K Dielectrics
Mo1730	Dinner
Mo1930	Monday Evening Session: Energy Materials

Interface & Surface Magnetism

Mo0830 Invited

Recent Developments in Interface-driven Magnetism

Roland Wiesendanger
Institute of Applied Physics and Interdisciplinary Nanoscience Center Hamburg, University of Hamburg, D-20355 Hamburg, Germany
Email: wiesendanger@physnet.uni-hamburg.de

In the past decades modern condensed matter research has greatly been driven by interface related phenomena. In the field of semiconductor physics, two-dimensional electron systems confined at interfaces of, e.g. GaAs-AlGaAs heterostructures, played a key role for the field of Quantum Hall physics. In the field of magnetism, the atomic-scale control of interfaces in metallic multilayer systems played a crucial role for the discovery of the Giant Magneto-Resistance (GMR) effect. More recently, interfaces were shown to provide a novel playground for superconductivity research with many unexpected observations in various classes of material systems including oxide-based hybrid systems.
By using Spin-Polarized Scanning Tunnelling Microscopy (SP-STM) [1] we have recently discovered a variety of novel interface-driven nanomagnetic states, such as spin spirals [2-4] and nanoskyrmion lattices [5] in single atomic layers of transition metals on particular substrates exhibiting a large spin-orbit coupling. In contrast to spin spiral and skyrmionic states in bulk samples, these novel interface-driven states are stabilized by the Dzyaloshinskii-Moriya interaction combined with the breaking of inversion symmetry at surfaces and interfaces. Following this novel approach, the existence of magnetic skyrmions of ultimate small size, being stable even in zero field, has recently been demonstrated, offering great potential for future nanospintronic devices.

[1] R. Wiesendanger, Rev. Mod. Phys. **81**, 1495 (2009).
[2] M. Bode et al., Nature **447**, 190 (2007).
[3] P. Ferriani et al., Phys. Rev. Lett. **101**, 027201 (2008).
[4] Y. Yoshida et al., Phys. Rev. Lett. **108**, 087205 (2012).
[5] S. Heinze et al., Nature Physics **7**, 713 (2011).

Mo0900

Incorporation of Cr or Mn at the GaAs(001)-c(4×4)α surface: Structural stability and electronic states

Kazuya Okukita, Atsushi Hagiwara, and Jun Nakamura
The University of Electro-Communications (UEC-Tokyo), Tokyo, Japan

Strong ferromagnetic interactions in the two-dimensional system such a MnAs layer or a CrAs layer embedded in GaAs have been predicted theoretically: For example, a MnAs/GaAs superlattice stacked along the <001>-direction exhibits half-metallicity[1]. In order to fabricate such atomically-controlled structures, it is important to understand initial processes of epitaxial growth on the GaAs substrate. Recently, Yagyu *et al.* reported the initial adsorption of Cr atoms on GaAs(001)-c(4×4)α[2] using the scanning tunneling microscopy[3]. However, the stable adsorption site and the magnetic states have not been clarified yet. The purpose of this study is to evaluate the structural stability and the electronic state of a Cr atom on GaAs(001)-c(4×4)α using first-principles calculations based on the spin density functional theory. We also explore the system of a Mn atom on GaAs(001)-c(4×4)α for comparison.

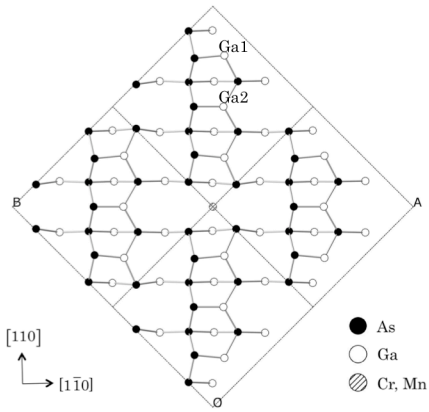

Fig.1 Surface structure of the GaAs(001)-c(4×4)α surface. Stable adsorption sites of Cr and Mn are indicated by shaded circles (interstitial site). Substituted Ga atoms are indicated by Ga1 or Ga2.

It has been found that both Cr and Mn atoms prefer to adsorb at the missing dimer site of the GaAs(001)-c(4×4)α surface (indicated by shaded circles in Fig.1, hereafter referred to as the interstitial site). Next, we examine the possibility of the substitution of Cr or Mn atoms for the surface Ga atoms. Figures 2(a) and 2(b) show the difference in formation energy for the Cr or Mn adsorbed surfaces. It has been found that both the interstitial and substitutional sites can be stable for Cr; interstitial site under As-rich condition and substitutional site under Ga-rich condition. For the Mn-adsorbed surface, on the other hand, only the substitutional site becomes stable irrespective of the chemical potential of Ga. The spin magnetic moments for the interstitial site models are 5.0μ_B/c(4×4) and 6.0μ_B/c(4×4) for Cr and Mn, respectively and those for the substitutional models are 3.0μ_B/c(4×4) and 4.0μ_B/c(4×4) for Cr and Mn, respectively. The magnetic moment for the Mn-substitutional site model is comparable to that for the GaAs(110)-Mn surface[4]. In our presentation, we will discuss in detail the structural stability and the spin states of the Cr- or Mn-adsorbed GaAs(001) surfaces.

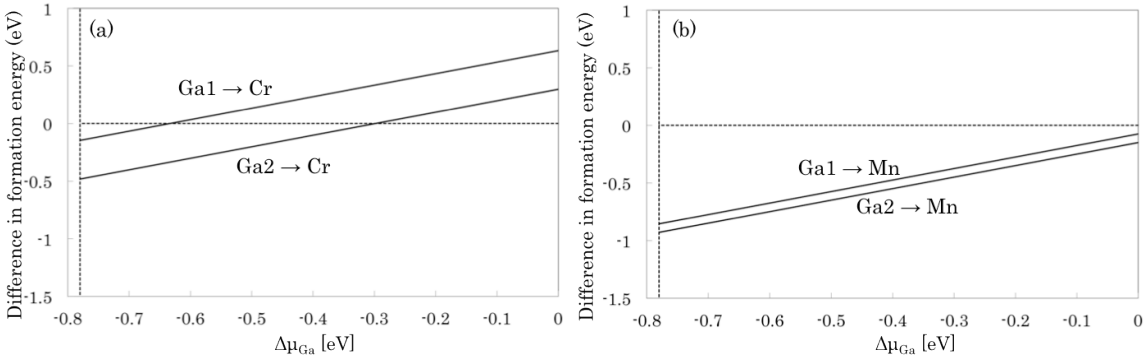

Fig.2 Difference in the formation energy of (a)Cr and (b)Mn on the GaAs(001)-c(4×4)α surface between the interstitial site and substitutional site models. The energy for the interstitial site model is set to be zero. The thermodynamically allowed range is between -0.780 eV (As-rich) and 0.0 eV (Ga-rich).

[1]M. Shirai, T. Ogawa, I. Kitagawa, and N. Suzuki, J. Mag. Mag. Mat. **177**, 1383 (1998).
[2]A. Ohtake, P. Kocan, J. Nakamura, A. Natori, and N. Koguchi, Phys. Rev. Lett. **92**, 236105 (2004).
[3]K. Yagyu, D. Komamiya and J. Yoshino, Physica E **43**, 773 (2011).
[4]M. Hirayama, A. Natori, and J. Nakamura, J. Vac. Sci. Technol. B **27**, 2062 (2009).

Corresponding author : Jun Nakamura
Department of Engineering Sciences, The University of Electro-Communications (UEC-Tokyo)
1-5-1 Chofugaoka, Chofu, Tokyo 182-8585, Japan
E-mail : junj@ee.uec.ac.jp
Tel. & FAX : +81-42-443-5156

Mo0905

Exchange Bias of the Interface Spin System at the Ferromagnet / Oxide Interface

G. Luepke,[1] Y. Fan,[1] K. J. Smith,[1] A. T. Hanbicki,[2] R. Goswami,[2] C. H. Li,[2] H. B. Zhao[3] and B. T. Jonker[2]

1 Department of Applied Science, College of William & Mary, Williamsburg, VA 23187
2 Materials Science & Technology Division, Naval Research Laboratory, Washington, DC 20375
3 Department of Optical Science and Engineering, Fudan University, Shanghai, 200433, China

The ferromagnet/oxide interface is key to the development of emerging multiferroic and spintronic technologies with new functionality. Magnetic tunnel junctions (MTJs) incorporating such interfaces are critical elements in magnetic memory and disk drives, and show promise for much broader application in reprogrammable architectures. Here we use magnetic second-harmonic generation (MSHG) to selectively probe the magnetization at the Fe/MgO interface typically used in MTJs due to band matching symmetries, and discover an exchange bias (EB) not previously observed, and markedly different from its typical manifestation. This reveals the existence of an antiferromagnetic exchange pinning layer at the interface, which we identify as FeO patches that exist even for a nominally "clean" interface. These results demonstrate that atomic moments at the interface are non-collinear with the bulk magnetization, and serve as spin scattering sites, reducing the measured tunneling magnetoresistance. We control the EB magnitude by varying the interface oxygen concentration and Fe-O bonding. Our results identify a new source of spin scattering in this technologically important MTJ system, provide insight into the phenomenon of exchange bias, and suggest new avenues for tuning the operating characteristics of ferromagnet/oxide interface-based devices.

Mo0910 Invited

Tunable control over individual dopants in semiconductors via STM positioning of charged defects

Jay Gupta

Department of Physics, Ohio State University

The scaling of electronic devices such as transistors to nanometer dimensions requires more precise control of individual dopants in semiconductor nanostructures, as statistical fluctuations can impact device performance and functionality. Toward this end, the scanning tunneling microscope (STM) is emerging as a useful tool for its capabilities of atomic manipulation, imaging and tunneling spectroscopy. I will discuss our STM studies of Mn acceptors within the surface layer of a *p*-doped GaAs crystal [1,2,3]. We start by sublimating Mn adatoms (Mn_{ad}) onto the GaAs (110) surface, prepared by cleavage in ultrahigh vacuum. A voltage pulse applied with the STM tip allows us to replace a Ga atom in the surface with the Mn atom, thus forming a single Mn acceptor (Mn_{Ga}) and a Ga adatom (Ga_{ad}). We find that the properties of Mn acceptors can be tuned by control of the local electrostatic landscape. For example, the STM tip can be used to position As vacancies (V_{As}) and other adatoms (e.g. Mn, Ga), all of which are positively charged. Direct Coulomb repulsion causes a reduction in the hole-Mn binding energy as V_{As} is moved nearby. Tunneling spectroscopy allows us to quantify this effect, through the shift of an in-gap acceptor resonance toward lower energy. In addition, defect-induced band bending provides a method for tuning the ionization state of the Mn acceptors, as evidenced by a ring-like feature in STM images. We have extended this work to dimers of Mn acceptors, in the hopes of tuning the spin-spin interaction between them. Tunneling spectra of the dimers reveal six dimer states, representing bonding and anti-bonding combinations of Mn acceptor states. These states systematically shift in energy as charged defects are brought nearby. Comparison of these experimental results with density functional theory calculations provides further insight into the electronic states and properties of the defects. These studies show that tunable control over single dopants in semiconductors is becoming realistic route for next-generation classical- and quantum-based information technologies.

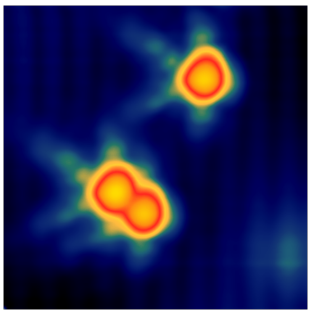

STM image of three Mn acceptors within the 1st layer of a GaAs (110) surface.

[1] D H Lee and J A Gupta, "Tunable Field Control Over the Binding Energy of Single Dopants by a Charged Vacancy in GaAs," *Science* 330, no. 6012 (December 23, 2010): 1807–1810.
[2] Dong-Hun Lee and Jay A Gupta, "Tunable Control Over the Ionization State of Single Mn Acceptors in GaAs with Defect-Induced Band Bending," *Nano Letters* 11, no. 5 (May 11, 2011): 2004–2007.
[3] D H Lee, N M Santagata, and J A Gupta, "Influence of the Local Environment on Zn Acceptors in the GaAs(110) Surface," *Applied Physics Letters* 99, no. 5 (2011): 053124.

Mo0940

Off-Axis Electron Holography of Ferromagnetic Nanowire Arrays

A. Akhtari-Zavareh [1], L.P. Carignan[2] , A. Yelon[2] , D. Ménard[2] , T. Kasama[3] , R. Herring[4], R E Dunin-Borkowski[5] , M. R. McCartney[6] and K. L. Kavanagh[1]

1. Department of Physics, Simon Fraser University, BC, V5A1S6, Canada, 2. Department of Engineering Physics, École Polytechnique de Montréal, Montréal, Québec, Canada. 3. Center for Electron Nanoscopy, Technical University of Denmark, DK-2800 Kongens Lyngby, Denmark. 4. Department of Mechanical Engineering,University of Victoria ,Victoria, B.C., V8W 3P6 Canada. 5. Ernst Ruska-Centre for Microscopy and Spectroscopy with Electrons Institute for Microstructure Research, D-52425 Jülich, Germany. 6. Department of Physics, Arizona State University, Tempe, AZ 85287-1504, USA.

Arrays of ferromagnetic nano-wires (FMNW) have been proposed for high frequency applications [1] and high-density storage media [2]. Understanding the crystallographic and magnetic properties of individual wires is crucial for optimizing the properties of these arrays. For that purpose, the soft and high-saturation magnetization of single-layer CoFeB and periodic CoFeB/Cu NWs were studied as a function of the thickness and period of the magnetic and nonmagnetic layers. All NWs were fabricated by pulsed-current electrodeposition in nanoporous alumina membranes [3].

Electron holography (EH) [4] was used to investigate the local magnetic behavior of a statistical number of these FMNWs and this information compared to the results obtained from magnetostatic and ferromagnetic resonance (FMR) of macroscopic NW arrays [3]. A 300kV STEM equipped with a biprism operating at 150V was used for EH measurements. Holograms were acquired at a remanence magnetic field < 5 Oe (obtained at zero tilt by turning off the objective lens). The magnetization inside the magnetic layers was uniform over most of the wire length, except at their surfaces. Since the wires consist of nanocrystals, it is a reasonable observation that the shape anisotropy dominates the control of the magnetic properties.

The magnetic induction measured by EH for single-layer CoFeB wires ranged from an average of 0.5 T near the tip to 1.5 T in the middle of the wires. This overall magnetization is somewhat smaller than the saturation magnetization extracted from static magnetometry measurements of thin films of electrodeposited CoFeB (1.67 T). The smaller induction near the end of the wires is attributed to the presence of a significant out-of-plane magnetic component, probably since their tips are pointed out of the plane of the sample holder. Additionally, near the tip of the wires, the increased demagnetizing field and thinner sample thickness weakened the induction.

On the other hand, for periodic CoFeB/Cu NWs, the wires had a relatively significant magnetization even at their surfaces. In the Cu layers, the magnetic induction became weaker as a result of demagnetizing field from the magnetic layers. Magnetization components parallel and perpendicular to the applied field from the objective lens were measured as a function of the angle of the NW axis. In some cases, a NW magnetization component transverse to the applied field direction was observed, which was not the case for the arrays. This suggests that the easy axis of each magnetic layer is not always in the same direction as their adjacent layer.

[1] A. Saib, IEEE Trans. Mic. Theory Tech. **53**, 2043 (2005).
[2] C.A. Ross, Annual Rev. Mater. Sci. **31**, 203 (2001).
[3] L.-P. Carignan, A. Yelon, D. Ménard, C. Caloz, IEEE Trans. Mic. Theory Tech. **59**, 2568 (2011).
[4] D. Shindo and Y. Murakami, J. Phys. D: Appl. Phys. **41,** 125 (2008).

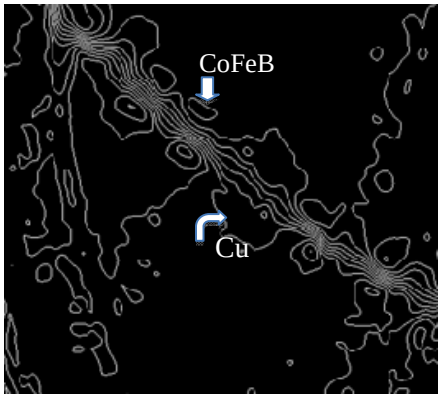

Mo0945

Micromagnetic simulations of GaAs/MnAs core/shell nanowires

A. Paul[1)], J. Liang[2)], N. Samarth[2)], and R. Engel-Herbert[2)]

[1)] Department of Materials Science and Engineering, The Pennsylvania State University, University Park, Pennsylvania 16802, USA.

[2)] Department of Physics, The Pennsylvania State University, University Park, Pennsylvania 16802, USA.

The epitaxial combination of ferromagnetic MnAs with GaAs has attracted wide-spread interest due to its potential to enable spin-dependent functionalities in a semiconductor material. Recently it was demonstrated that hexagonal GaAs/MnAs core/shell nanowires can be synthesized by catalyst-free molecular beam epitaxy [1]. Although the complex magnetic domain structure is well understood in MnAs thin films with different orientations [2,3], the direct extraction of domain arrangement and magnetization reversal properties of GaAs/MnAs nanowires is more difficult. In particular it has been found that although GaAs cores predominantly grow with zinc-blende structure along [111] direction, GaAs nanowire segments with wurtzite structure also occur with the [0001] direction along the wire axis. The nanowire's core crystal structure dictates the magnetic domain structure of the MnAs shell due to the epitaxial relationship between MnAs and the different phases of GaAs, which changes the direction of MnAs magnetocrystalline hard axis with respect to the wire axis.

In this talk micromagnetic simulations of GaAs/MnAs core/shell nanowires are presented. Nanowires with varying geometries, i.e. core radius, shell thickness and wire length have been modeled and magnetic hysteresis curves have been calculated using the finite element solver MAGPAR. The main difference in the magnetization reversal of GaAs/MnAs nanowires with zinc-blende and wurtzite core is found for applied magnetic fields along the wire axis. In contrast to nanowires with GaAs wurtzite core (MnAs hard axis parallel to wire axis) revealing a hard axis loop, for nanowire with zinc-blende core the MnAs hard axis is tilted away from the nanowire axis showing a single domain reversal. Although the reversal of zinc-blende core/shell nanowires are unaffected by the core diameter a monotonic increase of coercive field and decrease of remnant magnetization with decreasing shell width indicates that the magnetization reversal energy barrier height is mainly determined by the shape anisotropy of the MnAs shell.

The simulated hysteresis curves of the core/shell nanowires with zinc-blende structure can explain the measured low field anisotropic magnetoresistance (AMR) transport measured at low temperatures for magnetic fields parallel and perpendicular to the wire. We will present evidence that nanowire segments with zinc-blende core contribute the dominant features of the AMR data [4]. Whereas a single domain reversal mechanism is found for magnetic fields along the wire axis, a two-step reversal process is found for magnetic fields perpendicular to it. Variation of applied field direction perpendicular to the wire suggest that the difference in the switching fields of the two-step reversal process can be attributed to the alignment of the hexagonal facets in the applied field.

[1] N.S. Dellas, J. Liang, B.J. Cooley, N. Samarth and S.E. Mohney, Appl. Phys. Lett. **97**, 072505 (2010).

[2] R. Engel-Herbert, T. Hesjedal, and D. M. Schaadt, Phys. Rev. B **75**, 094430 (2007).

[3] R. Engel-Herbert, T. Hesjedal, D. M. Schaadt, L. Daweritz, and K. H. Ploog, Appl. Phys. Lett. **88**, 052505 (2006).

[4] J. Liang, J. Wang, A. Paul, B.J. Cooley, D.W. Rench, N.S. Dellas, S.E. Mohney, R. Engel-Herbert, and N. Samarth, Applied Physics Letters **100**, 182402 (2012).

Mo0950

Influence of spin-orbit coupling on the two-dimensional Fröhlich polaron

K.A. Vardanyan, A.L. Vartanian*, A.A. Kirakosyan

Department of Solid State Physics, Yerevan State University, Al. Manoogian 1, Yerevan 0025, Armenia

The Rashba and Dresselhaus mechanisms of spin-orbit (SO) coupling of 2D electrons are relevant in two-dimensional systems with zinc-blende structure. Depending on the material characteristics, either of these couplings, or both of them together, can play a leading role in spin-based solid state nanoscale devices, for the intensity of these mechanisms can be controlled by an external electric field and by specific material engineering methods.

Electrons in two-dimensional systems can also couple with phonon modes of nanostructure. In practice, the electron-phonon coupling is essential in understanding a large variety of spin phenomena (transport, coherence, relaxation, etc.) in low-dimensional systems. Over the past years, a lot of studies have focused on the role of SO coupling in the context of electron-polar optical phonon interaction. Particularly, it has been shown that the spin-orbit coupling leads to quite different polaronic effect in two-dimensional semiconductors [1-3]. In these works, an enhancement of polaronic properties has been obtained for a two-dimensional electron gas with Rashba coupling for both short- and long-range electron-phonon interactions. It has also been shown that in a weak electron-phonon coupling regime polaronic binding energy is enhanced by the spin-orbit coupling and the polaronic effective mass varies differently in different Rashba bands [4]. On the contrary, a recent calculation on the 2D tight binding Holstein-Rashba model on the square lattice has shown that a large electron-phonon interaction gets effectively suppressed by Rashba SO coupling [5]. Therefore, at present the role of SO coupling on polaron properties is not clear, and different models and approximations appear to give quite contradicting results.

However, in spite of growing interest in the properties of non-centrosymmetric semiconductors with SO coupling, this is the first time (to our knowledge) that a calculation of polaron energy fully includes the effect of Rashba and Dresselhaus SO couplings. The main objective of this paper is an analytical investigation of the interplay between Rashba and Dresselhaus spin-orbit and electron-phonon interactions in weak-coupling approximation.

We have shown that in the presence of both SO coupling terms the self-energy correction of the electron energy due to the electron–LO-phonon interaction exhibits angular anisotropy unlike the case when only one of the spin-orbit coupling terms (Rashba or Dresselhaus) is considered. A similar behavior is obtained for the polaron effective mass as a function of SO coupling constants. The simultaneous consideration of the Rashba and Dresselhaus mechanisms shows that polaronic effect may become either stronger or weaker depending on directions, a phenomenon which does not occur when the spin-orbit interaction is not taken into account.

[1] E. Cappelluti, C. Grimaldi, F. Marsiglio, Phys. Rev. B **76**, 085334 (2007).
[2] E. Cappelluti, C. Grimaldi, F. Marsiglio, Phys. Rev. Lett. **98**, 167002 (2007).
[3] C. Grimaldi, Phys. Rev. B **77**, 024306 (2008).
[4] Z. Li, Z. Ma, A. R. Wright, C. Zhang, Appl. Phys. Lett. **90,** 112103 (2007).
[5] L. Covaci, M. Berciu, Phys. Rev. Lett. **102,** 186403 (2009).

Corresponding author. A.L. Vartanian, E-mail address: vardan@ysu.am

Semiconductor Growth & Surfaces

Mo1100

Atomic structure and stoichiometry of tensile-strained GaAs/GaSb(001) nanostructures

A. Lenz[1]*, J. Schuppang[1], A. Gassenq[2], T. Taliercio[2], E. Tournié[2], M. Dähne[1], and H. Eisele[1]

[1]Institut für Festkörperphysik, Technische Universität Berlin, 10623 Berlin, Germany

[2]Université Montpellier 2, Institut d'Electronique du Sud, 34095 Montpellier cedex 5, France

*Email address: alenz@physik.tu-berlin.de

The development of III-V semiconductor devices has been concentrated on the compressively-strained material systems, such as InGaAs/GaAs or GaSb/GaAs. In contrast, the Ga(In)As/GaSb(001) material system may act as the model system for tensile-strained nanostructures, being promising for near-to-mid infrared applications. In order to understand the growth process we study the atomic structure and stoichiometry of GaAs depositions on GaSb(001) substrate with varying layer thicknesses by cross-sectional scanning tunneling microscopy (XSTM).

The sample was grown using molecular beam epitaxy with cracker cells, evaporating As_2 and Sb_2. It contains four layers with nominally 1 ML, 2 ML, 3 ML, and 4 ML GaAs, grown at 500°C with a rate of 0.5 ML/s. Prior to each GaAs layer a 5 s growth interruption was applied, but not afterwards.

Within the resulting GaAs/GaSb layers GaAs agglomerations are formed, but without a persistent wetting layer. In the case of 1 ML and 2 ML GaAs deposition, the layer thickness along growth direction extends over 8 ML. The agglomerations for 1 ML and 2 ML GaAs have an averaged lateral size of 5 nm and 6 nm, respectively. In both cases the agglomeration height amounts to about 7 ML and the density is about 1x12 cm^{-2}. The XSTM image contrast within the agglomerations is rather inhomogeneous, indicating an intermixed GaAsSb material. In the case of 3 ML and 4 ML GaAs deposition larger nanostructures develop with base lengths of about 10 nm and 11 nm, respectively, and heights of about 8–11 ML. As compared with the 1 ML and 2 ML GaAs layers the density is decreased to about 4x11 cm^{-2}, while the XSTM image contrast within the agglomerations is increased, indicating a higher GaAs content. In addition, a more quantitative analysis of the local stoichiometry will be shown, which is based on the local distance between neighboring atomic rows along the [001] growth direction and by comparing it with strain relaxation simulations. This method shows that no segregation of GaAs into the GaSb matrix occurs. Furthermore, a maximum As concentration of about 50% in case of 2 ML GaAs is found, while in case of 4 ML GaAs the concentration increases to almost 100% As.

However, in all cases no well-defined shape of these nanostructures, especially no flat bottom boundaries were observed. This is in contrast to the compressively-strained InGaAs/GaAs or GaSb/GaAs systems, exhibiting always a sharp and flat interface at their base. From these results we consider a different growth mode for tensile-strained GaAs/GaSb nanostructures.

Mo1105

Influence of Quantum Dot Atomic Structure and Strain Relaxation on GaSb/GaAs Band Offsets

E. S. Zech[1], A. S. Chang[1], A. J. Martin[1], J. C. Canniff[1], Y.H. Lin[2], J. M. Millunchick[1], R. S. Goldman[1,2,*]
[1]Department of Materials Science and Engineering, [2]Physics, University of Michigan, Ann Arbor, MI 48109-2136, USA
*rsgold@umich.edu

Due to the predicted strain and composition dependence of type I versus type II band offset formation, mixed arsenide-antimonide quantum dots (QDs) have been identified as promising systems for a variety of optoelectronic applications, including light emitters (type I) and photovoltaics and photodetectors (type II). In the case of InGaSb QDs, a composition dependent transition from type I to type II offsets has been reported [1]. Although type II band offsets have been reported for GaSb/GaAs QDs [2], a variety of atomic structures have been observed, ranging from clusters to rings to dots [3]. Furthermore, type I band offsets have been reported for Sb clusters on GaAs surfaces [4]. To date, the precise growth conditions needed for tuning the GaSb/GaAs QD atomic structure and its influence on the presence of type I versus type II band offsets have not been reported. Therefore, we have investigated the influence of growth conditions on the nanoscale structure and band offsets of GaSb/GaAs QDs using a combination of cross-sectional scanning tunneling microscopy, scanning tunneling spectroscopy (STS), and transmission electron microscopy (TEM). The GaSb/GaAs QDs are grown by molecular beam epitaxy on either As-terminated (2 x 4) or Sb-terminated (2 x 8) surfaces [5]. For GaSb/GaAs QD grown on both As- and Sb-terminated surfaces, mostly clusters are observed. STS in the vicinity of the clusters reveals type I offsets with ΔE_C and ΔE_V similar to that of Sb clusters on GaAs [4]. TEM analysis of the GaSb/GaAs QDs showed threading dislocations at the base of the QDs, suggesting strain relaxation within the QDs. This research is supported by the United States Department of Energy, Basic Energy Sciences under contract DE-FG02-06ER46339.

[1] Yu. I. Mazur, V. G. Dorogan, G. J. Salamo, G. G. Tarasov, B. L. Liang, Appl. Phys. Lett. 100, 033102 (2012).
[2] F. Hatami, N. N. Ledentsov, M. Grundmann, J. Böhrer, F. Heinrichsdorff et al., Appl. Phys. Lett. 67, 656 (1995).
[3] E. P. Smakman, J. K. Garleff, R. J. Young, M. Hayne, P. Rambabu, and P. M. Koenraad, Appl. Phys. Lett. 100, 142116 (2012).
[4] R. M. Feenstra and P. Martensson, Phys. Rev. Lett. 61, 447 (1988).
[5] A. J. Martin, T. W. Saucer, K. Sun, S. J. Kim, G. Ran, G. V. Rodriguez, X. Pan, V. Sih, J. Millunchick, J. Vac. Sci. Tech. B 30, 02B112 (2012).

Mo1110

In Situ X-ray Diffraction Study of GaAs Growth on Si

M. Takahasi[1,2], Y. Nakata[2], H. Suzuki[3], K. Ikeda[4], W. Hu[1], M. Kozu[2] and Y. Ohshita[4]

[1]Quantum Beam Science Directorate, Japan Atomic Energy Agency, Hyogo 679-5148, Japan

[2]University of Hyogo, Hyogo 679-1297, Japan

[3]Miyazaki University, Miyazaki 889-2192, Japan

[4]Toyota Technological Institute, Aichi 468-8511, Japan

Epitaxial growth of III-V semiconductors on silicon substrates is a longstanding issue in semiconductor technology including optoelectronics, high-mobility devices and solar cells. The growth of GaAs on Si is known to follow the Volmer-Weber mode, in which three-dimensional (3D) islands are formed from the beginning of the growth. Nucleated islands undergo a considerable redistribution during growth. Some islands grow larger by collecting adatoms floating on the surface. On the other hand, the reservoir of adatoms are refilled by detachment from other islands and the deposition from the environment. General nucleation theory tells that, as a result of the redistribution of the islands, the average size of the islands, r, shows a power law, $r \propto t^n$, where t is the growth time. The exponent is shown to be $n = 1/3$ in the surface-diffusion-limited case whereas it is $n = 1/2$ in the interface-transfer-limited case [1]. Thus, determining the temporal evolution of the islands size during growth can help understand the mechanism of the initial growth of GaAs/Si. In the present work, in situ synchrotron X-ray diffraction was employed to invesigate the mechanism of molecular-beam epitaxial (MBE) growth of GaAs/Si. Experiments were carried out at a synchrotron beamline 11XU at SPring-8 using an MBE chamber integrated with a multi-axis X-ray diffractometer. With this instrument, we have developed a 3D X-ray reciprocal-space mapping technique and successfully applied to high-speed measurements of InGaAs/GaAs(001) growth at a rate of 10 s [2]. As opposed to the conventional X-ray reciprocal mapping, which is a 2D cross section of the intensity distribution of the diffracted X-rays, the present 3D recirocal space mapping technique enables simultaneos determination of the position and extent of the diffraction peak in the in-plane and out-of-plane directions. From these measurements, structural information, such as strains, crystalline domain size and defects, can be obtained. GaAs was grown on Si(001) and Si(111) at a substrate temperature of 550°C at a rate of 150 nm/h in an As pressure of 2.5×10^{-4} Pa. Figure 1 shows part of a series of the 3D X-ray reciprocal-space mappings near the Si 022 Bragg point during growth. Isointensity surfaces are drawn in the reciprocal space. From the extent of the GaAs 022 peak, evolution of the crystalline grain size was evaluated as shown in Fig. 2. While the average grain size increases with growth time as $t^{1/2}$ for GaAs/Si(001), GaAs/Si(111) shows a time dependence of $t^{1/3}$. It is concluded, therefore, that growth processes of GaAs on Si(001) and Si(111) are limited by interface transfer and surface diffusion, respectively. Deviation from the power law at a later stage of growth is atttibuted to coalescence of islands and increase in dislocations inside individual islands.

[1] B. K. Chakraverty, J. Phys. Chem. Solids 28, 2413 (1967).

[2] W. Hu, H. Suzuki, T. Sasaki, M. Kozu and M. Takahasi, J. Appl. Cryst. 45, 1046 (2012).

Mo1115

A Novel Approach for High Performance InAs FinFETs on Silicon

Xing Dai,[1] Yoontae Hwang,[2] Binh-Minh Nguyen,[2] Wei Tang,[2] Cesare Soci[1] and Shadi A. Dayeh[2,3]

[1]Nanyang Technological University, School of Physical and Mathematical Sciences
[2]Center for Integrated Nanotechnologies, Los Alamos National Laboratory
[3]Department of Electrical and Computer Engineering, University of California, San Diego

Si CMOS performance boosters such as stressors, high-k dielectrics, metal gates, and recently 3D architectures have allowed Si to deliver performance not inherent to its material capabilities. A viable approach for cultivating enhanced performance per unit area is the heterointegration of the higher capable III-V materials on a Si platform. Hybrid integration using wafer bonding is a potential route for such integration. However, popular wafer bonding techniques such as smart-cut, BCB, and epitaxial lift-off require high processing costs and has limited thermal budgets. We have developed a fab-compatible process that allows integration of III-V materials to Si and (i) is CMOS compatible, (ii) has a wide thermal budget, (iii) can be applied to patterned substrates, and (iv) overcomes the shortcomings of eutectic bonding and the high costs and limitations of smart-cut and epitaxial lift-off. This bonding technique relies on the formation of a nickel-silicide layer at a temperature as low as 300 °C and can applied to a wide range of bonded materials with the insertion of thin dielectric layer between the Si and the bonded structure. We have utilized this integration scheme to fabricate 3D InAs FinFET transistors with deeply scaled channel lengths down to 20 nm.

Panel (a) shows a transmission electron microscope (TEM) image of the bonded structure with an inset of high-resolution TEM displaying single crystal transferred InAs layers on insulator on Si. Panel (b) shows an SEM image of etched Fin structures on SiN_x on Si with a raised InAs body for better electrostatic gate coupling to the channel. Panel (c) shows an SEM image of a completed device on a single InAs Fin on a reference bulk InAs substrate. This device features raised source-drain contacts for lower source-drain leakage current in the off-state. In addition to the central conformal gate, two external conformal gates are used to deplete the InAs channel below the source/drain regions and reduce leakage currents through the InAs bulk layers. Panel (d) shows a multi-Fin device structure. Panel (e) shows an energy-balance Silvaco/Atlas simulation of the carrier transport in the InAs channel. The inset text describes details of the simulated structure and material characteristics while the top-left inset in panel (e) shows the off-state electron distribution on a $2x10^{17}$ cm^{-3} p-doped sample. This transfer curve demonstrates that our device approach can result in very high on-current and on/off ratios using III-V FinFET devices and highlights the potential of fabricating such a device on Si. Concurrent experimental I-V and C-V measurements on InAs FinFETs on bulk and on insulator-on-silicon are currently in progress and will be discussed in our presentation.

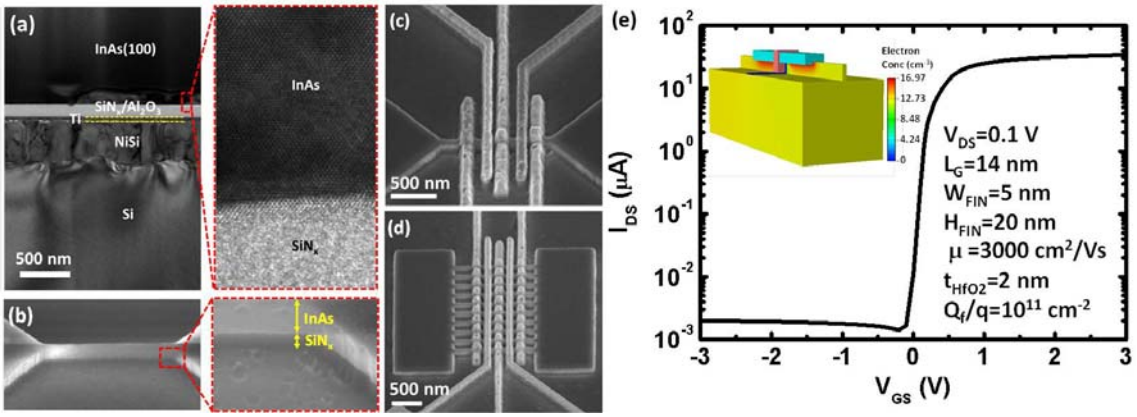

Mo1120

Surface Studies of Polytypic InAs Nanowires

M. Hjort[1**], S. Lehmann[1], J. Knutsson[1], R. Timm[1], K.A. Dick[1], E. Lundgren[1], K. Deppert[1], L. Samuelson[1], A. Mikkelsen[1]

[1]*Nanometer Structure Consortium (nmC@LU), Lund University, Box 118, 221 00 Lund, Sweden*

Regardless of the many nanowire (NW) device concepts, such as solar cells and light emitting diodes, that have been designed and processed, very little is known about the surfaces of NWs; a factor which becomes increasingly important as the dimensions shrink and the surface to bulk ratio increases. Since III-V NWs can be grown both in the zinc blende (Zb) crystal structure - the stable bulk form - as well as in wurtzite (Wz) structure [1, 2] they give access to surfaces not found in other geometries[3,4]. Surfaces that are, to a large extent, unknown thereby posing a great challenge for surface scientists. The need for complete structural and electronic determination of all NW surfaces is crucial in order to e.g. reduce the risk of surface scattering of electrons acting to lower device performance[5].

We have previously published the first atomic scale images of III-V NW surfaces [3] and are now expanding our experimental toolbox for surface analysis in order to get a full understanding of the relation between structure and electronic properties.

We have grown well defined Au-seeded polytypic InAs NWs with axial stacking of Wz and Zb segments and analyzed those structures using scanning tunneling microscopy/spectroscopy (STM/S). The NWs were prepared in a metal organic vapor phase epitaxy system using trimethylindium and arsine as precursors for the growth. The crystal structure of the NWs was tuned to include all low index side facets in the same NW.

After oxide removal using atomic hydrogen[3] we were able to investigate the atomic scale structure of all common low index facets available for Wz and Zb InAs NWs, Fig. 1(a,b) as well as obtained information about the surface electronic structure using STS measured both at room temperature and at 4K, Fig. 1(c).

In our previous investigations of InAs NW surfaces[3] we could observe excellent agreement between STM images and DFT calculations based on unreconstructed {11-20} and {10-10} surfaces. The STS results should therefore give us information about the bulk electronic properties of the material without being masked by surface states arising from reconstructions. In the present study we have observed well defined band gaps for both the ZB and the WZ segments and conclude that the surface is clean and without states in the band gap.

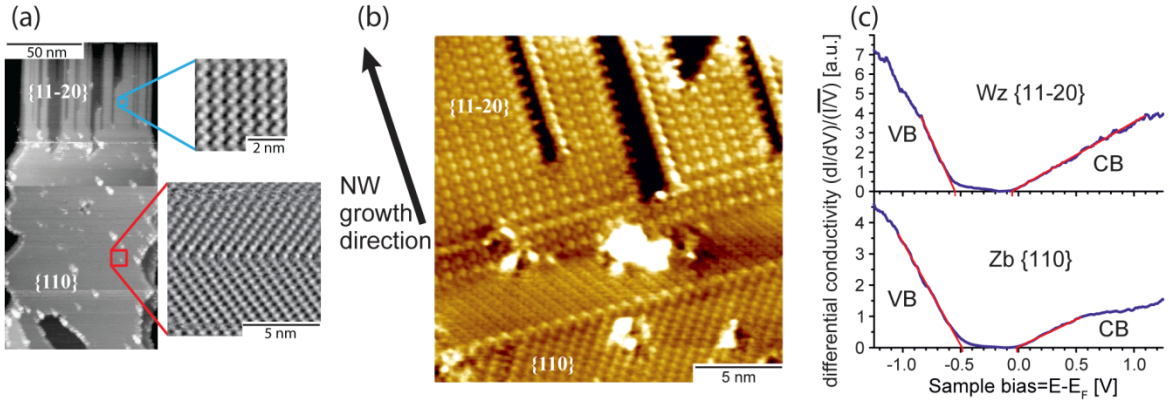

Figure 1. STM/S results obtained from a single polytypic InAs NW with axial stacking of Wz and Zb segments. (a) STM image obtained from the side facet of a NW showing the interface between a Zb{110} and a Wz{11-20} facet, U_{sample} = -1.7 V. U_{sample} = -2.2 V for the Zb inset and U_{sample} = -2.5 V for the Wz inset. (b) STM image at the interface between a {11-20} and {110} facet, Usample =-2.2 V. (c) STS data obtained from two close lying facets on the same NW depicting the local density of states. Tunneling from (to) valence band (conduction band) are marked VB (CB).

* Corresponding author email: martin.hjort@sljus.lu.se

[1] K. A. Dick *et al., J. Vac. Sci. Technol. B* **29**, 04D103 (2011).
[2] P. Caroff *et al., IEEE J. Sel. Top. Quant. Electron* **17**, 829 (2011).
[3] E. Hilner *et al., Nano Lett.* **8**, 3978 (2008).
[4] T. Xu *et al., Nanotechnology* **23**, 095702 (2012)
[5] M. Hjort *et al., ACS Nano* (accepted)

Mo1125 Invited

Probing Semiconductor Surface Charge Transport Using Crystalline Nanomembranes

Max G. Lagally

University of Wisconsin-Madison, Madison WI 53706
Email: lagally@engr.wisc.edu

Surfaces and interfaces can strongly influence semiconductor nanostructure electronic properties and charge transport. To investigate this influence quantitatively, very thin two-dimensional crystalline sheets (termed nanomembranes) provide the ideal vehicle, because in such sheets the influence of the "bulk" is strongly diminished and because they can be prepared with a well defined surface condition, with precise surface orientations and thicknesses and with known doping levels, unlike other nanostructures, such as nanoparticles and grown nanowires. The free surfaces of nanomembranes can be chemically modified in a homogeneous and predictable fashion, drawing on the long history of surface science. The sensitivity of electronic properties to the surface suggests the possibility of using charge transport measurements on very thin sheets as a form of precision spectroscopy to obtain surface electronic-structure information under well-defined conditions. This talk will explore this approach. (1) It will be specifically demonstrated, using Si(001) nanomembranes, that the surface conductance in the atomically clean, reconstructed Si(001) surface ((2x1) reconstruction) can be reliably determined and a surface charge carrier mobility extracted. Measurements use a van der Pauw configuration in ultrahigh vacuum, with a back gate. The back gate combined with a thin sample makes it possible to deplete the "bulk" of the thin silicon sheet completely. This is a generic result: given a non-zero bandgap, there exists a thickness beneath which a back-gate will be able to deplete the sheet fully.

The clean-surface results, possible only in UHV, provide the baseline for other surface terminations that do not require UHV. We show how termination of the surface Si bonds by H influences the surface transport. Complementary measurements can be made on multiple identical end-attached but otherwise free-standing nanoribbons prepared from nanomembranes (2) and on sheets still attached to the host substrate, as they are in silicon-on-insulator. We suggest that the combination of charge transport measurement with nanomembranes to determine surface electronic properties and surface charge transport can be applied to many materials systems beyond silicon, to extract the role of surfaces in modifying or controlling nanostructure electrical properties.

(1) W. Peng, Z. Aksamija, S. A. Scott, J. J. Endres, D. E. Savage, I. Knezevic, M. A. Eriksson, and M. G. Lagally, Nature Communications, submitted
(2) C.-H. Lee, C. S. Ritz, M.H. Huang, M. Ziwisky, R. Blise, and M. G. Lagally, Nanotechnology 22, 055704 (2011).

Mo1155

Trench structure formations around InAs QDs on GaAs(001) observed by STMBE

Takashi Toujyou[1*], Koichi Yamaguchi[2], and Shiro Tsukamoto[1]
[1] Center for Collaborative Research, Anan National College of Technology, Anan, Tokushima 774-0017, Japan
[2] Department of Electronic Engineering, The University of Electro-Communications, Chofu, Tokyo 182-8585, Japan
*Corresponding author: toujyou@anan-nct.ac.jp

Quantum dots (QDs) are unique nano structures that have received special attentions in recent years because these are strong candidates for advanced semiconductor quantum devices. Recently, trench structures around InAs QDs were confirmed after fabricating QDs at particular growth condition [1]. Furthermore, the lattice mismatch concerned in the QD formation and a large stress on the QD edge were well known. The trenches around the InAs QDs would be formed via diffusion of the most highly strained materials near the QD edges as same as the Ge/Si QD [2]. But, the precise mechanism of forming the trenches was not well understood yet. In order to confirm that the substrate temperature after the QD formation affect to the trench formation, we performed true *in situ* imaging during theses processes by a STMBE: a scanning tunneling microscope (STM) inside a molecular beam epitaxy (MBE) growth chamber [3], and investigated trench depth.

Samples were prepared by a following procedure; after removing oxides at 650 ^{o}C under As_4 fluxes, a GaAs buffer layer was grown at 590 ^{o}C and then InAs QDs were grown at 500^{o}C. After forming the QDs, the substrate temperature of Sample A was decreased from 500 ^{o}C to 300 ^{o}C without As_4 irradiation. On the other hand, the substrate temperature of Sample B was decreased from 500 ^{o}C to 200 ^{o}C. After a half hour, the substrate temperature was increased from 200 ^{o}C to 300 ^{o}C. After the substrate temperature was stabilized at 300 ^{o}C, we observed Sample A and B by the STMBE. After STM observations, we took Sample B out to the air and observed its surface by an atomic force microscope (AFM) at room temperature also. Fig. 1 shows the distribution of QD diameter vs. trench depth within Sample A. The trench depth mainly distributed from 0.4 nm to 1.0 nm. On the other hand, 65% of the QDs within Sample B were without the trench structure and 35% of the QDs showed the shallow trench with a depth of 0.1 - 0.3 nm. These results indicate that, after the QDs fabrication, the decreasing process of the substrate temperature affects the trench structure formations.

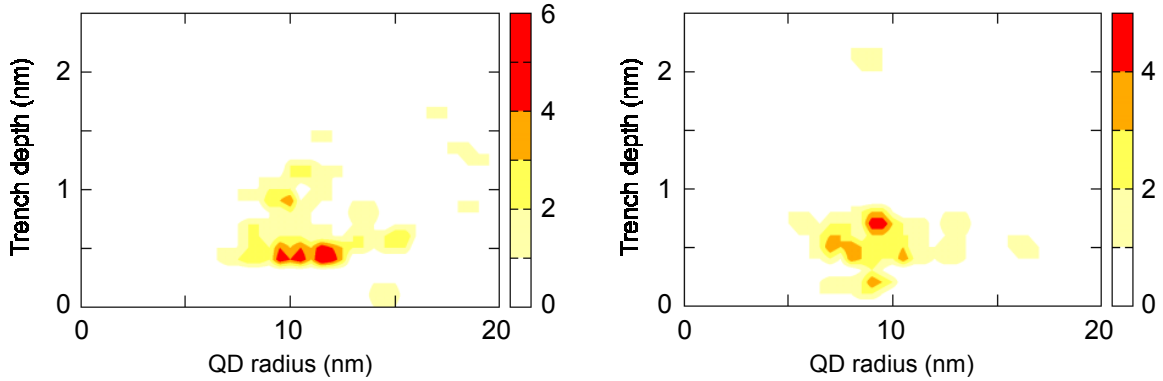

(a)[110] (b)[1-10]

Figure 1 Distribution of radius vs. trench depth within Sample A, (a) along [1-10] direction, (b) along [110] direction.

[1] E. Placidi, F. Arciprete, V. Sessi, M. fanfoni, F. patella, and A. Balzarotti, Appl. Phys. Lett. 86, 241913 (2005).
[2] S.A.Chaparro, Y.Zhang, and J.Drucker, Appl. Phys. Lett. 76, 3536 (2000).
[3] S. Tsukamoto and N. Koguchi, J. Cryst. Growth 201, 118 (1999).

Mo1200

Atomic structure and electronic properties of ringlike antimony clusters on the Si(111)7×7 surface

Martin Franz*, Stephan Appelfeller, and Mario Dähne

Institut für Festkörperphysik, Technische Universität Berlin, 10623 Berlin, Germany

*Email address: martin.franz@physik.tu-berlin.de

Self-assembled magic clusters on surfaces are on the one hand very interesting because of their zero-dimensional electronic properties. On the other hand they are promising candidates for the application in future nanodevices and for catalysis.

Here, the atomic structure as well as the electronic properties of antimony induced ringlike clusters on the Si(111)7×7 surface were studied for the first time using scanning tunneling microscopy (STM).

These clusters grow self-organized using the 7×7 reconstructed Si(111) surface as a template. This results in the formation of magic clusters, i.e. clusters that show an enhanced stability at certain sizes. Each cluster occupies one half unit cell of the 7×7 reconstruction with a strong preference for the faulted half, due to a lower energy of the cluster on this half unit cell. For preparation, submonolayer amounts of antimony were deposited at substrate temperatures between 350 °C and 500 °C.

The ringlike antimony clusters do not form centered within the triangular half unit cells but their center is located close to the center of one edge. In filled state STM images they appear as structureless features, while in empty state images a ringlike appearance is observed. This is due to the presence of a depression in the cluster center. In high resolution empty state STM images the ring appears as six single protrusions. By detailed analysis of the STM images it was found, that the apparent height of different ringlike clusters is varying. This behavior is particularly enhanced in empty state images and has not been observed before for clusters from other materials on the Si(111)7×7 surface.

We were able to develop an atomic structure model for the ringlike antimony clusters, explaining our observed filled and empty state STM images and also the varying apparent heights of the clusters. Assuming the same basic atomic structure the height variation is assigned to different antimony contents of the clusters. Hereby, the most antimony-rich clusters appear with the lowest height, while the highest appearing clusters are assigned to the most silicon-rich ones.

This project was supported by the Deutsche Forschungsgemeinschaft through FOR 1282 project D.

Mo1205

Strain Analysis of Compositionally Tailored Interfaces in InAs/GaSb Superlattices by Aberration Corrected Transmission Electron Microscopy

K. Mahalingam, H. J. Haugan, G. J. Brown and K. G. Eyink

Air Force Research Laboratory, Wright-Patterson AFB, OH 45433-7707 USA

InAs/GaSb superlattices possess interesting optoelectronic properties which are useful for a wide range of optoelectronic devices, such as infrared detectors and lasers. The band alignment in these materials is type II, wherein the conduction band of InAs is below the valence band of GaSb by about 150 meV. This permits tunability of properties through appropriate choice of the constituent layer thicknesses. However, interfaces are known to also have a significant influence on these properties, which is attributed to the local interfacial strain caused by the change in atomic species in both cation (In/Ga) and anion (As/Sb) sublattices across each interface. Considering typical growth on a (100) GaSb substrate this change in atomic species results in two types of interfacial bonds: Ga-As and In-Sb, depending on growth conditions. Although the lattice constants for GaSb (a_{GaSb} = 0.6095 nm) and InAs (a_{InAs}=0.6059 nm) are closely matched, the mismatch at interfaces can be significant, being tensile for GaAs-like interface (a_{InAs}=0.565 nm) and compressive for an InSb-like interface (a_{InAs}=0.647 nm). Considerable effort is now being directed at optimizing the structural and optoelectronic properties via precise tailoring of interface composition.

Here we present a systematic study of the local strain distribution across interfaces in several InAs/GaSb superlattices, with InAs and GaSb layer thicknesses ranging from 1.5 nm - 4.5 nm, using recently developed quantitative techniques based on aberration-corrected transmission electron microscopy. Three different sets of superlattices were investigated, consisting of (1) structures in which the interfaces were grown under nominal conditions with no composition control, (2) structures with interface composition control involving controlled exposure of each interface to a As/Sb flux before depositing the next InAs/GaSb layer and (3) structures with interface composition control wherein each interface is tailored to be “InSb-like” through a controlled deposition of 0.1 nm -0.35 nm of InSb at each interface prior to growth of the subsequent layer. The samples were examined by conventional high-resolution transmission electron microscopy (HRTEM) using the negative-spherical aberration imaging mode (performed using a Titan 80-300 TEM) and by scanning transmission electron microscopy (STEM) using high-angle annular dark-field imaging (HAADF) (performed using the double corrected TEAM 0.5 TEM at NCEM, Berkeley). The strain profiles across interfaces were acquired at the atomic scale using the peak-pair algorithm [1]. The results indicate that in samples with no interface control, the GaSb-on-InAs interface was GaAs-like, with a tensile strain of 1.8%, and also accounts for about 27% of the overall superlattice strain. In contrast, the InAs-on-GaSb interface was nearly strain neutral. The effect of interface composition control was observed to have significant effect on the strain distribution across the GaSb-on-InAs interface. Furthermore, the overall superlattice strain determined from strain distribution for each sample was found to be in good agreement with the respective measurements by X-ray diffraction. Finally, a comparison of results between HRTEM and HAADF-STEM will also be presented.

References:

1. P. L.Galindo et al. Ultramicroscopy 107 (2007) 1186.

Spintronics with Organics

Mo1400 Invited

Spin transport and carrier-mediated magnetism in vanadium tetracyanoethylene (V[TCNE]$_{\sim 2}$)

Ezekiel Johnston-Halperin
Department of Physics, The Ohio State University, Columbus, OH

The development of organic-based magnets with room temperature magnetic ordering and semiconducting functionality promises to broaden the field of semiconductor spintronics, providing a route to all-organic spintronic devices and hybrid organic/inorganic structures capable of exploiting the multifunctionality and ease of production in organic systems as well as the well established spintronic functionality of inorganic materials. A key to exploiting this functionality is the interplay between localized magnetic moments and delocalized free carriers. Here we present two complementary explorations of this correlation: the demonstration of electrically driven spin injection from a V[TCNE]$_{\sim x}$ electrode (x~2, TCNE: tetracyanoethylene; T_C > 400 K, E_G ~ 0.5 eV, σ~ 10^{-2} S/cm) into a III-V heterostructure [1] and the observation of free-carrier mediated magnetism in bulk V[TCNE]$_{\sim 2}$ films.

In the first study, a spin-polarized current is detected by monitoring the polarization state of the photons emitted from a buried light-emitting diode (LED) structure and tracks the magnetization of V[TCNE]$_{x\sim 2}$, is weakly temperature dependent, and exhibits heavy hole / light hole asymmetry. In the second study, we present an investigation into the connection between the presence of free carriers and an anomalous temperature dependence of the magnetic properties of bulk V[TCNE]$_{x\sim 2}$ films. The samples are synthesized via chemical vapor deposition and reveal the onset of sharp switching and square hysteresis at temperatures *above* 110 K, coincident with the onset of thermal activation of free carriers. This correlation suggests the onset of an additional carrier-mediated exchange pathway beyond the *s-d* coupling previously discussed for this system.

These results open the door to a new class of active, hybrid spintronic devices with multifunctional behavior defined by the optical, electronic and chemical sensitivity of the organic layer. Spin transport in hybrid structures provides the opportunity to leverage well-characterized inorganic materials as a probe of spin physics in organic and molecular systems and carrier-mediated magnetism indicates a potentially important pathway for *active* spintronic functionality in all-organic heterostructures.

[1] "Electrical Spin Injection from an Organic-Based Ferrimagnet in a Hybrid Organic-Inorganic Heterostructure," Lei Fang, K. Deniz Bozdag, Chia-Yi Chen, P.A. Truitt, A.J. Epstein and E. Johnston-Halperin, *Phys. Rev. Lett.* **106**, 156602 (2011).

Mo1430

DIPOLE INTERACTIONS AT THE INTERFACE WITH FERROELECTRIC CRYSTALLINE POLYMERS*

P.A. Dowben *Department of Physics and Astronomy and the Nebraska Center for Material and Nanoscience, Univ. of Nebraska, Lincoln, Nebraska, 68588-0299*

The dipole and molecular band offsets that result from a heteromolecular interface provides an unparalleled opportunity to build novel organic devices with nonvolatile functionalities. The engineering of these interfaces and possible voltage control of the heteromolecular interface provides a means for reducing the barriers for charge injection into organic electrics [1] as well as opening the door to voltage controlled surface chemistry at a heteromolecular interface [2]. Organic heterojunction diodes [3] and transistors [4] have now been reliably fabricated with the crystalline ferroelectric copolymer poly(vinylidene fluoride with trifluoroethylene), and the device show that reversable voltage controlled molecular band offsets are possible. As the copolymer poly(vinylidene fluoride with trifluoroethylene) (P(VDF-TrFE)) is a ferroelectric, organic heterojunctions transistors that include this polymer exhibit gate voltage dependent hysteresis [4]. Dipole interactions are implicated at the interface between copper phthalocyanine (CuPc) and poly(vinylidene fluoride with trifluoroethylene), P(VDF-TrFE), and affect the band offsets and diode properties. By combined local moment molecular systems and molecular ferroelectrics, the organic multiferroic is now within our grasp [5]. The interactions as the heteromolecular orbital interface are not simply dipolar interactions, however, the the details of the electronic struycture matter, including frontier orbital symmetries [2].

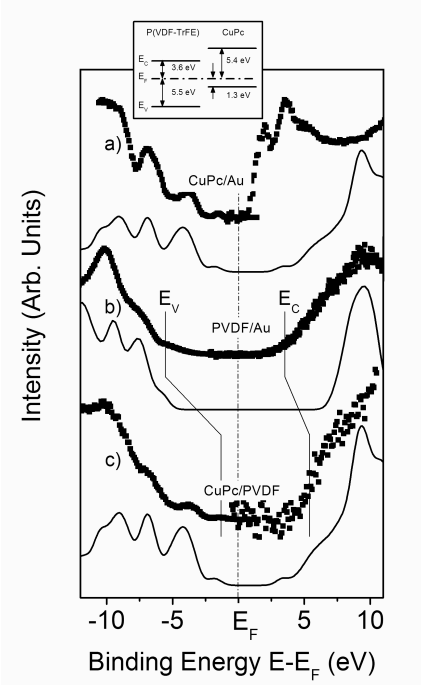

Figure 1. Photoemission (left) and inverse photoemission (right) spectra of copper metal phthalocyanine (CuPc) adsorbed on Au (a), poly(vinylidene fluoride with trifluoroethylene) P(VDF-TrFE) on Au (b) and CuPc on the crystalline ferroelectric P(VDF-TrFE) (c). For comparison, the calculated ground state density of states of CuPc is shown. The relative shifts in the edges of valence band and conduction band are indicated by vertical bars for PVDF on Au and CuPc on PVDF.

* Work undertaken with Zz. Zhang, L. Rosa, , Jie Xiao, A. Sokolov, P. Jacobson, C. Ilie, Bo Xu, J. Zhang, Ya.B. Losovyj and I. Yakovkin. This work was supported by the National Science Foundation through grants CHE-0909580 and DMR-0851703

[1] L. Routaboul, P. Braunstein, J. Xiao, Z.z.g Zhang, P. A. Dowben, G. Dalmas, Victor DaCosta, O. Félix, G. Decher, L. G. Rosa, B Doudin, *J. Am. Chem. Soc.* **134** (2012) 8494–8506

[2] Z.z.g Zhang, R. González, G. Díaz, L. G. Rosa, I. Ketsman, X. Zhang, P. Sharma, A. Gruverman, P. A. Dowben, *J. Phys. Chem. C* **115** (2011) 13041-13046

[3] J. Xiao, A. Sokolov, P.A. Dowben, *Appl. Phys. Lett.* **90** (2007) 242907

[4] P.A. Dowben, L. G. Rosa, C. C. Ilie, J. Xiao, *J. Electron Spectrosc. Rel. Phenom.* **174** (2009) 10-21.

[5] X. Zhang, T. Palamarciuc, P. Rosa, J.-F. Létard, N. Wu, B. Doudin, Z.Z. Zhang, J. Wang, P. A. Dowben, *J. Phys. Chem. C* (2007), in press

Mo1435

Manipulating Fermi level of CuPc Molecules by Dosing Gaseous Oxidant

Jun H. Park[1], Sang W. Park[1], Tyler Kent[1], William C. Trogler[2], Andrew C. Kummel[2]
[1]Materials Science and Engineering Department, University of California San Diego
[2]Department of Chemistry and Biochemistry, University of California San Diego

Background: Metal phthalocyanines (MPc) have been widely employed as channel materials in organic thin film transistor (OTFT) for chemical vapor sensing due to their novel gas adsorption properties. Theoretically, MPc molecules at electron donors during reaction with oxidative analytes which is the basis of their chemical sensing[1]. However, this sensing reaction has not been fully understood on the atomic level. This study presents molecular scale observation of NO adsorption and field doping on CuPc monolayers using ultra-high vacuum (UHV) scanning tunneling microscopy (STM).

Bonding Site: CuPc monolayers were deposited on Au (111) surfaces and HOPG by organic molecular beam epitaxy in ultra-high vacuum (UHV) and subsequently dosed at 150 K substrate temperature with NO (5%: diluted by He of 95 %) via a supersonic molecular beam source (MBS). After dosing NO for 1 min, STM images reveal small NO chemisorption sites on the CuPc metal centers; ~4 % of CuPc molecules are reacted with NO (Fig 1 (a)). As shown in Figure 1 (a), the un-reacted central Cu^{2+} ion of CuPc appears as dark hole in both of empty and filled state(not shown) STM images. After chemisorption of NO, the topographic appearance of core metal ion is modified into a bright spot, while the 4-leaf pattern of the ring still remains. If dosing duration is increased to 10 min, the coverage of chemisorption sites increases to ~7 % (Fig. 1 (b). However this coverage increase is sublinear and further dosing does not increase the coverage consistent with a chemisorption induced change in electronic structure. As shown in Fig. 1 (c), annealing CuPc surface for 10 min at 320 K induces almost complete desorption of NO. This desorption of NO indicates binding energy of NO with central metal is weak consistent with the reversible sensing of most molecular adsorbates on MPc.

Electronic Structure Changes NO/CuPc/Au(111): In order to study the electronic structure of NO chemisorption onto CuPc molecules, site specific scanning tunneling spectroscopy (STS) data was also obtained. In STS, the Fermi level corresponds to zero voltage bias so changes in band offsets as well as band edge state formation are readily observed. In Fig. 2, unreacted CuPc/Au(111) has a Fermi level (E_F) almost in the middle of the band gap. However, after NO chemisorption, this E_F shifts to the highest occupied molecular orbital (HOMO) near the valance band edge. This change in electronic structure by NO is in good agreement with previously published theoretical predictions and is consistent with the high sensitivity of CuPc film to strong oxidants in CuPc OTFT chemical sensors[2].

Electronic Structure Changes NO/CuPc/HOPG: This movement of the Fermi level shows that thin film of strong oxidants chemisorbates on MPc which have irreversible adsorption might be employed for electrostatic doping of 2 dimensional semiconductors. In Fig. 3 (a), after dosing NO for 10 min on CuPc mono layer deposited on HOPG at 150 K, NO chemisorbates which have bright protrusion on central metal ion are observed and topographic appearance of these chemisorption sites are similar with on CuPc monolayer deposited on Au(111). However, the coverage of NO chemisorbates is significantly lower (~ 0.1%) on HOPG. It is known that nobel metals, for instance Au, have large densities of states and free electrons; therefore metal substrates can transfer electron density to CuPc increasing chemisorption probability of NO. Conversely, graphene has low density of states and π-electron, so it can provide electron to CuPc molecules much less than Au[3]. This low electron density of graphene results in lower coverage of NO chemisorbates on CuPc monolayer. However, as shown in Fig. 3 (b), once NO chemisorbs on metal center of CuPc, positive charge carriers are injected from NO to CuPc molecules, similar to NO/CuPc deposited on Au(111). After dosing NO on CuPc monolayer, Fermi level shifts to HOMO and reacted the CuPc molecules appear p-type in STS. During this positive charge movement, excessive hole can be diffuse to HOPG which is under CuPc layer, and HOPG substrates may be doped to p-type.

(1) Yang, R. D.; Park, J.; Colesniuc, C. N.; Schuller, I. K.; Royer, J. E.; Trogler, W. C.; Kummel, A. C. *J Chem Phys* **2009**, *130*.
(2) Nguyen, T. Q.; Escano, M. C. S.; Kasai, H. *J Phys Chem B* **2010**, *114*, 10017.
(3) Castro Neto, A. H.; Guinea, F.; Peres, N. M. R.; Novoselov, K. S.; Geim, A. K. *Rev Mod Phys* **2009**, *81*, 109.

Mo1440

Coexistence of Ferromagnetism and Ferroelectric Polarization in Epitaxial $NiTiO_3$ thin films with the $LiNbO_3$-Type Structure

Tamas Varga[1], Timothy C. Droubay[2], Mark E. Bowden[1], Scott A. Chambers[2], Robert J. Colby[1], Bernd C. Kabius[1], Edoardo Apra[1], William A. Shelton[1], and Vaithiyalingam Shutthanandan[1]

[1]Environmental and Molecular Sciences Laboratory (EMSL), Richland, WA 99352

[2]Pacific Northwest National Laboratory, Richland, WA 99352

In a search for new multiferroic materials where the direction of magnetization can be switched by an applied electric field, we have looked for materials in which polarization and magnetization are strongly coupled. Recent theory calculations predicted that the family of compounds $MTiO_3$ (M = Mn, Fe, Ni), in a certain polymorphic structure (acentric *R3c,* also called $LiNbO_3$-type), are promising candidates where a polar lattice distortion can induce weak ferromagnetism (WFM). Guided by these insights, the $LiNbO_3$-type (LBO) phase of $NiTiO_3$ has been prepared in epitaxial thin film form. The synthesis of these $NiTiO_3$ films, their full structural characterization, physical property measurements along with first-principles DFT calculations to predict the desired $NiTiO_3$ structure, its stability, and the effect electronic structure on the ferroic properties are presented. Optical second harmonic generation imaging of the $NiTiO_3$ films indicates a polar lattice. AC magnetic susceptibility and temperature-dependent magnetization measurements suggest a Neel transition consistent with the LBO structure in $NiTiO_3$. Our field-dependent magnetization results show a residual magnetism below the Neel temperature suggesting the presence of a ferromagnetic moment induced by the polar lattice distortion. These results validate theory predictions about the coexistence of WFM and ferroelectric polarization in $MTiO_3$ compounds with the LBO structure and constitute a significant step toward establishing LBO-type $NiTiO_3$ as a multiferroic in which the direction of magnetization can in principle be switched by reversing an applied electric field.

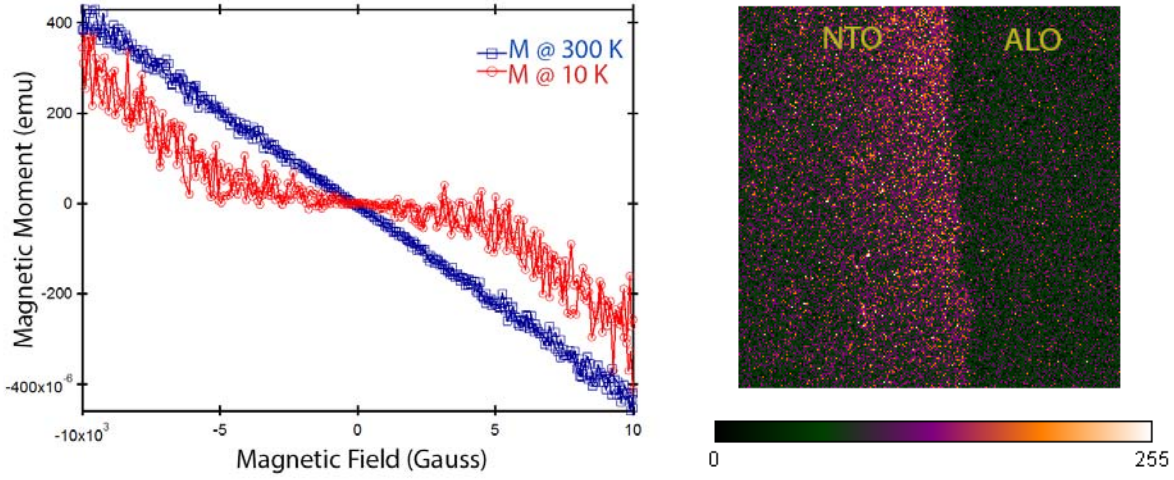

Figures: *Left:* Field-dependent magnetization curves for $NiTiO_3/Al_2O_3$ film above and below the Neel temperature indicating residual magnetization at low T. *Right*: Optical SHG image of a $NiTiO_3/Fe_2O_3/Al_2O_3$ film showing SHG signal for the film only.

Mo1445

Photoluminance, Aging and Magnetization effect on the low temperature surface phase transitions on $BiFeO_3$

Avneesh Anshul, Ashok Kumar*, Bipin K. Gupta, R. K. Kotnala

National Physical Laboratory, K. S. Krishnan Marg, New Delhi 110012, India

email: ashok553@gmail.com

Bismuth Ferrite ($BiFeO_3$, (BFO) is a well established magneto-electric multiferroic at room temperature. Although it was discovered in the late fifties in bulk and single crystal form with low polarization and large leakage current but it was rediscovered in this decade with very high polarization, magnetization and weak magnetoelectric in thin film matrix. Single crystal, bulk ceramics, and thin film form of BFO all together has been showing several functionalities such as photovoltaic, piezoelectric, magnonic logic, metal-insulator phase transition, magnetoelectric, ferroelastic, spin glass, insulating domains with conducting domains wall for nanoelectronics, terahertz applications, strip domains, etc. We have found two surface phase transitions and relaxor-like behavior in BFO below room temperature utilizing interdigital electrode in parallel configuration. After one year, same set of samples show well behaved relaxor behavior in dielectric loss spectra with shift from 150 K to 200 K (from 1 kHz to 20 kHz) in loss peaks that move towards higher probe frequency side with increase in temperature. It was hypothesis that the surface phase transition was mainly due to skin effect and spin reorientation transition. Our experimental data support the aging effect based surface phase transition which mainly due to the skin effect. Skin effect is closely related to the aging of the samples. Effect of external magnetic field on the surface phase transition is negligible till 0.5 T and within the experimental errors. The optical properties of BFO interdigital electrode has been investigated through different spectroscopy techniques. BFO is observed to produce a highly efficient yellow emission peaking at 584 nm at 325 nm excitation. The optical bandgap of 2.55 eV was confirmed through obtained PL spectrum for BFO with some indirect band edge at 2.67 eV. Moreover, we have successfully demonstrated the PL intensity can be tune through in-situ applied external DC field. Conduction band is effectively populated under the application of external electric field; the photoelectrons subsequently leave the conduction band which is supported by decrease in the intensity of photoluminescence with increase in electric field. Time resolved emission spectroscopy measurement indicated a PL decay time in the range of microseconds, suitable for making many advanced opto-magnetic as well as optoelectronic devices.

Mo1450

Graphene as substrate for organic semiconductor films

C. Teichert[1,·], G. Hlawacek[1,2], M. Kratzer[1], F. S. Khokhar[2], R. van Gastel[2], B. Poelsema[2], H. Zandvliet[2], B. Vasić[3], A. Matković[3], U. Ralević[3], R. Gajić[3]

[1]*Institute of Physics, Montanuniversität Leoben, Franz Josef Str. 18, A-8700 Leoben, Austria*
[2] *Physics of Interfaces and Nanomaterials, MESA+ Institute for Nanotechnology, University of Twente, NL-7500AE, Enschede, The Netherlands;* [3]*Institute of Physics, University of Belgrade, Pregrevica 118, 11080 Belgrade - Serbia*

· email: teichert@unileoben.ac.at http://www.unileoben.ac.at/~spmgroup/

Organic semiconductors offer the possibility to fabricate low-cost organic light emitting diodes (OLEDs) and solar cells. The novel material graphene bears the potential to be used as transparent flexible electrodes in such devices. Thus, the investigation of the growth of organic molecules on graphene is an up-to-date research topic.

Here, Low Energy Electron Microscopy (LEEM), micro Low Energy Electron Diffraction (μLEED), and Atomic-Force Microscopy (AFM) have been employed to study in situ the initial growth of the organic semiconductor para-sexiphenyl (6P) on Ir(111) supported graphene. In contrast to the formation of terraced growth mounds composed of standing molecules [1], here indeed layer-by-layer growth of lying molecules is observed as it is desired for OLEDs [2]. After formation of a low-density layer, the full first monolayer already shows a bulk like structure. Up to at least four monolayers grow in this fashion at a substrate temperature of 240 K as is illustrated in Fig. 1.

The nucleation of the 6P islands occurs at wrinkles in the metal supported graphene layer. Larger islands composed of flat lying molecules detach from the original nucleation sites and move rapidly as entities across wrinkle free substrate areas [3]. This sequence is visible in the series of LEEM images shown in Fig. 2. At 320K, crystalline 6P needles form on a wetting layer composed again of lying molecules [4].

Further, we present results of 6P grown by hot-wall epitaxy on mechanically exfoliated graphene nanoribbons which have been transferred to silicon oxide covered Si wafers. Here, Atomic-Force Microscopy (AFM) has been used to determine the growth morphologies as a function of substrate temperature. Whereas well oriented crystalline needles form on the graphene nanoribbons, growth of upright standing molecules on the SiO_2 substrate [5] is observed,.

Finally, we demonstrate the required robustness of the electrode material for device applications employing AFM based dynamic plowing lithography in conjunction with conductive AFM and Kelvin probe force microscopy [6]. In summary, we demonstrated the potential of graphene to be used as a flexible, transparent electrode for organic optoelectronic and photovoltaic devices.

This work has been supported by the Austrian Science Fund project S9707-N20, STW and FOM project 04PR2318 and the Serbian Ministry of Science under project # OI171005.

[1] G. Hlawacek, P. Puschnig, P. Frank, A. Winkler, C. Ambrosch-Draxl, C. Teichert, Science **321** (2008) 108.
[2] G. Hlawacek, F. S. Khokhar, R. van Gastel, B. Poelsema, C. Teichert, Nano Lett. **11** (2011) 333.
[3] G. Hlawacek, F. S. Khokar, R. van Gastel, C. Teichert, B. Poelsema, IBM J. Res. Devel. **55** (2011) 15:1.
[4] F. S. Khokhar, G. Hlawacek, R. van Gastel, H.J.W. Zandvliet, C. Teichert, B. Poelsema, Surf. Sci. **606** (2012) 475.
[5] S. Lorbek, G. Hlawacek, C. Teichert, Europ. Phys. J. **55** (2011) 23902.
[6] B. Vasić**,** M. Kratzer, A. Matković, A. Pavitschitz, U. Ralević, D. Jovanović, C. Ganser, C. Teichert, R. Gajić, submitted to Nanotechnology, Sept. 2012.

Mo1455

Optical and Structural Properties of CdZnS Quantum Dots Formed by the Langmuir-Blodgett Technique

A. Milekhin[1,2], N. Yeryukov[1], L. Sveshnikova[1], T. Duda[1], D. Protasov[1], O. Tereshchenko[1], N. Surovtsev[3], S. Adichtchev[3], C. Himcinschi[4], V. Dzhagan[5], D. R. T. Zahn[6]

[1]*Institute of Semiconductor Physics, 630090, Novosibirsk, Russia*
[2]*Novosibirsk State University, 630090, Novosibirsk, Russia*
[3]*Institute of Automation and Electrometry, 630090, Novosibirsk, Russia*
[4]*Institut fuer Theoretische Physik, TU Bergakademie Freiberg, Germany*
[5]*V. Lashkaryov Institute of Semiconductor Physics, 03028 Kyiv, Ukraine*
[6]*Semiconductor Physics, Chemnitz University of Technology, Germany*

We present a study of optical and structural properties $Cd_xZn_{1-x}S$ quantum dots (QDs) in the whole composition range of the alloy (x=0-1) by means of Raman, UV-vis absorption, X-ray photoelectron spectroscopies (XPS), and scanning and transmission electron microscopies.

The Langmuir-Blodgett (LB) technology was used to prepare high quality films of CdZnS behenates on quartz and (001)-oriented Si substrates covered by a 100 nm thick Au layer. The thickness of LB films under investigation was varied in the range from 50 to 200 monolayers. The reaction of the behenates with gaseous H_2S results in the formation of CdZnS QDs in an organic matrix. Free standing QDs were obtained after removing the organic matrix by thermal annealing in an inert atmosphere at temperatures of 200 and 350°C.

The structural properties of the QDs were studied by high-resolution transmission electron and scanning electron microscopies (HRTEM and SEM). The size of the QDs determined from the HRTEM and SEM images is in the range of 2-6 nm and the shape of the QDs was found to be predominantly spherical. Thermal annealing leads to increasing QD size with increasing temperature.

The interband transition energies obtained from UV-vis spectra of the QDs lie in the spectral range from green to UV and are decreasing with increasing annealing temperature. These energies were used to calculate the size of the QDs which is found to be consistent with the data obtained by direct structural methods and the calculations performed using the Lifshitz-Slezov model [M. Lifshitz, V. Slezov, J. Phys. Chem. Solids, 19(1-2) 35-50 (1961)].

Raman spectroscopy was used to probe the optical phonon dispersion in the alloyed QDs. Raman scattering experiments were carried out using a T64000 and UV-Labram spectrometers in backscattering geometry. Ar^+ and HeCd lasers were used as excitation sources in the wavelength range from 514.5 to 325 nm. The Raman spectra of the QDs show peaks corresponding to scattering by longitudinal optical (LO) phonons localized in QDs. Their frequency positions increase gradually in $Cd_xZn_{1-x}S$ QDs with increasing Zn content confirming one-mode behavior. The frequency positions of LO phonons were used for the determination of the composition in CdZnS QDs. Interconnection of Raman data with UV-vis absorption, XPS, and electron microscopy measurements is also discussed.

Surface Passivation & High-K Dielectrics

Mo1600

Characterization of Al_2O_3/GaAs Interface and Film Prepared by ALD

R. E. Sah[1], R. Driad[1], F. Bernhard[1], V. Naumann[2], C. Hagendorf[2], H. Czap[1], T. Fuchs[1], M. Mikulla[1], and O. Ambacher[1]

[1] *Fraunhofer-Institute for Applied Solid State Physics, Tullastrassse 72, 79108 Freiburg, Germany.*
[2] *Fraunhofer Center for Silicon Photovoltaics CSP, Walter-Hülse-Str. 1, 06120 Halle, Germany.*

Continuous miniaturization of Si and III/V-based devices in the semiconductor industry has led to the requirement for interface and atomic level controlled conformal deposition of a few nm thick dielectric films. The aluminum oxide (Al_2O_3) films grown using atomic layer deposition (ALD) technique have increasingly attracted attention for this purpose. The films have also been demonstrated to provide an excellent electrical surface passivation on Si for photovoltaic applications. As a consequence of ultralow surface recombination velocity, an increased efficiency of silicon solar cells has been reported. Additionally, the films have recently been studied for applications as both a wear-resistant protective coating and a structural layer for micro- and nano-electromechanical systems.

In the present contribution, we show that the interface, surface and film properties depend on configurations of the ALD technique. Two configurations of the ALD technique, namely thermal and plasma-assisted ALD, have been used for growing films on GaAs substrates. The substrates were stripped by dilute hydrofluoric acid and immediately inserted into the ALD load-lock. Atomic layers were formed at a substrate temperature of 300 °C by sequential pulsing of trimethylaluminum precursor and oxygen source (water vapour for thermal ALD while oxygen for plasma-ALD) interrupted by short nitrogen purges. The interfaces have been investigated using x-ray photoelectron spectroscopy (XPS) and secondary ion mass spectrometry (SIMS). The film properties of interest were the intrinsic stress and electrical response. Studies on the stress in ALD-Al_2O_3 are rare despite a tremendous rise of publication on the ALD in recent years.

Fig. 1 shows the XPS measurements of 5 nm thick Al_2O_3 films grown on GaAs by thermal and plasma-assisted ALD techniques. Investigations on thinner films are under progress. The measurements show the 3p doublet peaks of As and Ga, and 2s peak of Al. Since the Al 2p signal shows no double peak or a distinct shoulder, it can be concluded that Al exists only in the oxidized state within the whole Al_2O_3 layer and at the interface. An absence of any other peak, in addition to the perfect symmetrical Al 2p signal, in the given region gives an evidence of the absence of interface sub-oxides, i. e., the as-deposited Al_2O_3/GaAs is abrupt. Further, the lower intensity of As and Ga 3p peaks and the higher intensity of the Al 2s peak for plasma-assisted ALD film compared to that for thermal ALD film present a strong hint that the plasma ALD film grows more densely than the thermal ALD film right from the start. As a consequence of the difference in the growth process, the hysteresis following the first temperature cycle dependence of stress for the plasma-assisted ALD-Al_2O_3 film was almost negligible and remained unchanged upon subsequent thermal cycles (Fig. 2). The non-negligible hysteresis following the first cycle for the thermal ALD film (Fig. 3) suggests the presence of trapped water and other volatile impurities at the interface, in the film, and on the surface. The main impurity found from the XPS measurements was the one containing carbon. The amount of carbon calculated from C 1s peak was 10.92 atom % (at-%) for the thermal ALD while it was 8.22 at-% for the plasma ALD. The amounts of Al, As, F, Ga, N and O were 22.68, 5.57, 0.99, 4.96, 0.32, 54.56 at-%, respectively for the thermal ALD, while they were 27.7, 2.60, 0.81, 1.54, 0.22 and 58.92 at-%, respectively for the plasma-ALD. Thus, the ratio of O to Al was 2.4 and 2.1 for thermal and plasma ALD, respectively. The XPS measurements performed after sputtering the film surface for a few seconds revealed a significantly reduced (to ~25 %) amount of carbon, which gave evidence that most of the carbon containing impurity was present on the surface of the film. The SIMS measurements confirmed the presence of higher amount of C, and additionally revealed higher amounts of H and OH for the thermal ALD than for the plasma ALD. Furthermore, the shift in the maxima of Cs_2H and Cs_2OH signals in the SIMS measurements was not distinct, as observed by other

researchers in the case of ALD of Al_2O_3 on Si, and hence could not be asserted that the distribution of H and OH was inhomogeneous at the interface in our samples.

The linear and reversible dependence of stress on temperature, as depicted in Fig. 2 mentioned above, indicates that the thermally induced expansion of the film and of the substrate are elastic in the measured temperature range and that the difference between both expansions is constant with temperature. The temperature dependence of stress in Fig. 2 and Fig. 3 has been described by the relation:

$$\sigma_T = \frac{E_f}{1-\nu_f}\int_{T_2}^{T_1}(\alpha_s - \alpha_f)dT\,, \qquad (1)$$

where $\frac{E_f}{1-\nu_f}$ is the elastic stiffness parameter (biaxial elastic modulus, BEM), E_f is the Young´s modulus and ν_f is the Poisson's ratio for the film, and α_s, α_f are the coefficients of thermal expansion for the substrate and the film, respectively. Using relation (1) for two different semiconductor materials, GaAs and Si, the α_f and BEM have been calculated to be 3.61 ppm/K and 297 GPa, respectively for the thermal ALD film, and 3.96 ppm/K and 703 GPa for the plasma ALD film. The higher BEM (stiffness parameter) was reflected in the measurement of I-V characteristics of MOS capacitors. The leakage current of the capacitors with plasma-assited ALD film was stable, and was 3 orders of magnitude (10^{-9} A vs. 10^{-6} A for 100x100 μm^2 devices) lower than that of the capacitors with thermal ALD film. The breakdown field strength was 20 % higher (8.5 MV/cm vs. 7 MV/cm).

In conclusion, our results show that the plasma-assisted ALD technique produces a superior quality of interface and surface, with superior mechanical and electrical properties of the films compared to the thermal ALD technique for growing high-k Al_2O_3 films on GaAs.

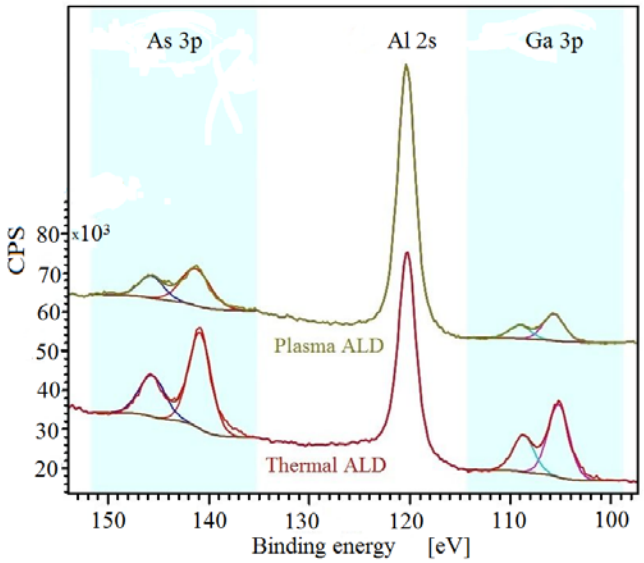

Fig. 1. High-resolution XPS spectra of the Ga and As 3p, and Al 2s photoelectron peaks of 5 nm thick plasma-assisted and thermal ALD-Al_2O_3 films grown on GaAs(100) at 300 °C.

Mo1605

Interface Characterization of Epitaxial $SrTiO_3$ on GaAs

R. Contreras-Guerrero[1], Q. Qiao[2] and R. F. Klie[2], R. Droopad[1*]
[1]Dept. of Physics, Texas State University, San Marcos, TX 78666
[2]Dept. of Physics, University of Illinois – Chicago, Chicago, IL 60607
*email: rdroopad@txstate.edu

Crystalline oxides on semiconductors represent a path towards adding functionalities onto electronic and optoelectronic devices. In addition, it is also being sought after as an alternative to SiO_2 as the gate dielectric in metal oxide semiconductor field effect transistors (MOSFETs) as they can provide an ideal interface with low density of defects. With the push for developing III-V semiconductors as new high mobility channels in complementary metal oxide semiconductor (CMOS) applications, it is an opportune time to investigate the heterointegration of crystalline complex oxides with III-V semiconductors. In this presentation, we will present results of the investigation of the effect of oxygen species on the interface between crystalline $SrTiO_3$ and GaAs. Growth of the oxide is carried out using molecular beam epitaxy on the As-stabilised c(4x4) GaAs (100) surface. With a Ti prelayer as a template, the oxide epilayer is then grown using co-deposition of the elemental fluxes with oxygen for the first 2 nm. For the growth using atomic oxygen, the plasma source is then switched on for the subsequent growth. The oxide/semiconductor interface is characterized using room temperature photoluminescence, x-ray photoelectron spectroscopy, and transmission electron microscopy.

Photoluminescence (PL) measurement of oxides on III-V semiconductors gives an indication of the relative density of states at the interface. Room temperature PL measurements of STO/GaAs samples are shown in figure 1 with an air–exposed GaAs surface shown for comparison. The increase of PL intensity for the sample grown using molecular oxygen suggests a reduction in the density of interfacial defects as compared to the sample grown using atomic oxygen and the air-exposed GaAs surface which has a Fermi level that is pinned at midgap. These results also indicate the use of atomic oxygen destroys the interface even though the interface was formed using molecular oxygen. This is similar to the growth of STO on Si where oxygen diffuses to the STO/Si interface and creates a layer of SiO_2. Figure 2 shows the photoemission data for the various oxide interfaces on GaAs. The use of molecular oxygen for STO results in the formation of Ga-O bonding with no As-O bonding detected as compared to the case for the native oxide/GaAs interface. Even with atomic oxygen Ga-O is present with an increase level but still no evidence As-O bonding. However, As-As bonding is detected suggesting As clusters is more favorable than As oxides. Figure 3 shows a TEM image for the oxide/GaAs interface of the STO/GaAs grown using oxygen plasma showing a disordered amorphous region. This study points to the possibility of using an epitaxial oxide for creating III-V interfaces that are unpinned leading to a number of future device applications involving the heterointegration of dissimilar materials.

This work is supported by the AFOSR under Grant # FA9550-10-1-0133

Mo1610 Upgraded

Passivation of missing As defect sites on InGaAs(001)-(2x4)

Mary Edmonds[1],Tyler Kent[1], Ravi Droopad[3], Evgueni Chagarov[2], and Andrew C. Kummel[1,2]
[1]Materials Science and Engineering Department, University of California San Diego
[2]Department of Chemistry and Biochemistry, University of California San Diego
[3]Department of Physics, Texas State University

$In_{0.53}Ga_{0.47}As$ has an intrinsically high electron mobility making it an attractive alternative semiconductor material for use in MOSFET applications (1). Scanning tunneling spectroscopy (STS) has been employed to show that the As-rich (2x4) surface reconstruction of $In_{0.53}Ga_{0.47}As(001)$ contains an electrically unpinned surface Fermi level both before and after dosing with the trimethylaluminum (TMA) gate oxide precursor. Huang *et al*. has shown that TMA based a-Al_2O_3 (a = amorphous) oxide growth at a single elevated temperature on As-rich InGaAs(001)-(2×4) produces a lower D_{it} as compared to the TMA dosing at elevated temperature on the In/Ga-rich (4×2) reconstructed surface (2). Therefore, it is possible that the limit on the practical D_{it} associated with InGaAs(001)-(2×4) is passivation of the numerous As missing dimer defect sites since these defect sites contain metal-metal bonds (In-Ga, Ga-Ga, and In-In). These defects sites are common to all InGaAs(001)-2x4 surfaces ranging from GaAs to InAs as shown in Table I from analysis of published images (3). Scanning tunneling microscopy (STM) and density functional theory (DFT) show that the metal-metal bond defects can be passivated with gas phase HOOH.

Figure 1(a) shows the filled state STM image of the degassed, decapped, clean $In_{0.53}Ga_{0.47}As(001)$-(2x4) surface reconstruction. The characteristic zig-zag shapes of the rows are due to the presence of the mixture of wide double ideal As dimer unit cells denoted as β2(2x4) and narrow single dimer defect unit cells denoted as α2(2x4), as shown in Fig. 1(b). Models of the double and single dimer unit cells are shown in Fig. 1(c) and 1(d). DFT was employed to model multiple bonding geometries of TMA on $In_{0.5}Ga_{0.5}As(001)$-(2x4). Fig. 2(a) shows an ideal $In_{0.53}Ga_{0.47}As(001)$-(2x4) unit cell containing two rows of As-dimers. The half coverage DMA (Fig 2b) contains As atoms with highly strained bonds and full coverage DMA (Fig 2c) shows all the As atoms have tetrahedral bonding angles. The full coverage DMA/InGaAs(001)-(2×4)(Fig 2d) has a wider bandgap (0.7 vs. 0.5 eV) than the clean surface consistent with passivating the CB edge states on the undercoordinated As atoms.

Fig. 3(a) shows full coverage DMA/InGaAs(001)-(2x4) with the missing As dimer along with its density of states showing a prominent VB state in contrast to the passivated ideal unit cells in Fig 2. The VB edge states on the passivated defect unit cells are primarily located on the In-Ga metal-metal bonds (green arrows in Fig. 3) as well as the adjacent bonds to As atoms (yellow arrows). To remove these VB states it is likely that an electronegative atom such as O must be inserted into the In-Ga bond and electropositive atoms such as Al in TMA will not work. The CB edge states are located primarily on the tricoordinated In and Ga atoms in the In-Ga bonds. To remove these CB edge states it is likely that these tricoordinated atoms must be restored to tetrahedral bonds with a passivating ligand which makes single sigma bonds such as –OH. Fig. 4 shows the DFT model of double site passivation by –OH. The double –OH passivation removed CB edge states and preserved low VB states. Experiments were performed with HOOH(g) to see if the missing As dimer defect states could be removed with just –OH passivation.

To passivate the surface with –OH, vapor from 30% $HOOH/H_2O$ was employed at 25°C to minimize any reactions with arsenic. If the In-Ga bonds and In and Ga dangling bonds were exclusively passivated, an ordered row structure without the characteristic narrow row sites of the missing As defects of InGaAs(001)-(2x4) should be observed. Fig. 5 (top) shows an STM image of the clean surface with the characteristic oscillating row thickness due to the narrow missing As dimer defect sites. After ~1000L dose of HOOH(g) at 25°C followed by annealing at 211°C for 30 min and a second anneal at 250°C for 30 min, STM was again performed (middle images in Fig. 5). No As displacement was observed and mixture of wide and narrow row sites characteristic of the defects on the clean surface is nearly gone. This is consistent with –OH bonding to the In and Ga atoms. After a further annealing at 350°C for 30 min, the surface is more ordered; again, nearly all the row sites appear wide consistent with –OH bonding to the tricoordinated In and Ga atoms. These experiments show it is possible to passivate with –OH without disrupting the As atoms.

1. J.A. Del Alamo, *Nature*, 479, 317 (2011)
2. Y. Hwang, R. Engel-Herbert, S. Stemmer, Applied Physics Letters 98 (2011) 052911.
3. Edmonds et.al, ECS Transactions, 50, 4 (2012)

Mo1630

Impact of atomic hydrogen exposure on the growth, interfacial, and electrical characteristics of HfO_2 on $Al_{0.25}Ga_{0.75}N$

Xiaoye Qin, Sarkar Anwar, Barry Brennan, Christopher L. Hinkle and Robert M. Wallace
Department of Materials Science and Engineering, University of Texas at Dallas

In this study we investigate the atomic layer deposition (ALD) of HfO_2 on the native oxide and atomic hydrogen (AH) exposed AlGaN surface. X-ray photoelectron spectroscopy (XPS) is used to determine the level of interaction between the HfO_2 and the AlGaN surfaces during deposition, by examining the initial surfaces, as well as after 10 cycles of HfO_2 by ALD (TDMA-Hf + H_2O at 250 °C). XPS is carried out *in-situ* by transferring the samples between the ALD reactor and the analysis chamber under UHV conditions (< 2 x 10^{-10} mbar) to prevent contamination due to atmospheric exposure.

Results indicate that atomic hydrogen is able to decrease the concentration of both oxygen and carbon present on the AlGaN surface without full removal, (Fig 1(a)) with both gallium and aluminium oxide still detected, although at a lower level than seen after various wet chemical treatments. Previous studies have indicated the difficulty in instigating ALD of both HfO_2 and Al_2O_3 on native oxide or wet chemically treated AlGaN surfaces,[1] however comparing the initial growth of HfO_2 on the AH exposed surface, we see ~0.5 nm of HfO_2 deposited after 10 ALD cycles as opposed to 0.2 nm on the native oxide sample (Fig 1(b)), suggesting the AH treatment produces a more facile surface for the instigation of ALD growth.

MOS capacitors were fabricated using the identical interfaces described above with an additional 9 nm of HfO_2 deposited on the AlGaN and TiN as the gate metal. C-V curves (Fig. 2) show slight differences in the electrical response depending on the surface treatment. Both samples exhibit significant charge trapping (shifts in the C-V response with each successive measurement on the same device), but the H-cracked sample exhibits a much lower EOT of the high-k oxide, most likely due to the decrease in the lower-k native oxides as a result of the atomic hydrogen treatment and specifically in Ga_2O_3.

[1] P. Sivasubramani, T. J. Park, B. E. Coss, A. Lucero, J. Huang, B. Brennan, Y. Cao, D. Jena, H. Xing, R. M. Wallace, and J. Kim, Phys. Status Solidi (RRL) 6(1), 22 (2012)

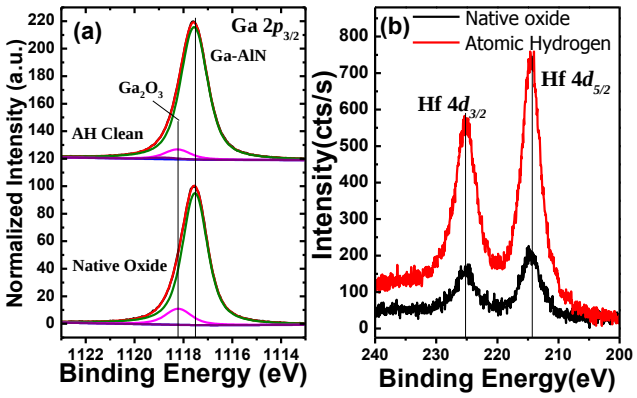

Figure 1. XPS spectra of (a) Ga $2p_{3/2}$ and (b) Hf $4d$ core levels indicating decreases in Ga_2O_3 as a result of atomic hydrogen cleaning and an increased HfO_2 thickness after 10 ALD cycles on the atomic hydrogen cleaned sample relative to that of the native oxide surface.

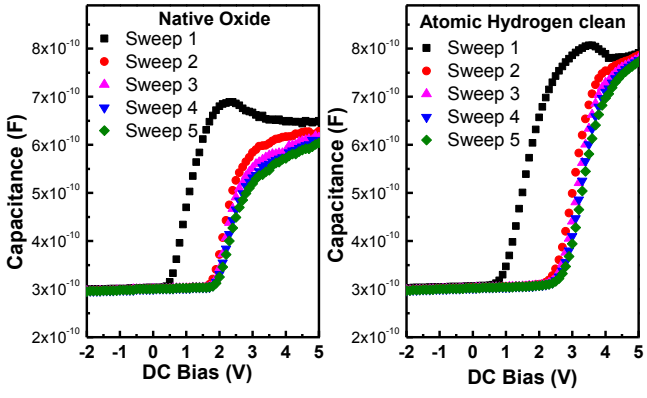

Figure 2. C-V measurements from 10 nm HfO_2/AlGaN capacitors indicating a lower EOT for the atomic hydrogen cleaned sample with respect to the native oxide sample, likely due to a decrease in the lower-k interfacial oxide with atomic hydrogen.

Mo1635

Controlling the Electrostatic Potential of Gate-Last Ge/High-k/Metal Gate Stacks through Interface Dipole Formation

S. R. M. Anwar, J. B. Burris, C. Buie, C. L. Hinkle
University of Texas at Dallas, Richardson, TX 75080

Due to its high intrinsic hole and electron mobility and relative compatibility with Si CMOS processing, Ge has long been considered as a replacement channel material for CMOS devices. High-k dielectrics in conjunction with metal gate electrodes have been implemented into recent Si integrated circuit technology and are necessary components of future Ge gate stacks as well. One of the key issues confronting Ge CMOS implementation is the creation of band-edge effective work function metal gates that do not degrade the crucial and fickle Ge channel region. In this contribution, we describe low-temperature techniques that manipulate the interface composition between HfO_2 and TiN creating two competing dipoles that allow for precise control of the electrostatic potential.

MOS devices were fabricated on p- and n-type Ge substrates with ~2 x $10^{17}/cm^3$ doping. A high-quality interface was obtained using a DI-H_2O surface functionalization by pre-pulsing the H_2O 50 times in the atomic layer deposition (ALD) chamber at 250 °C. A thin interfacial Al_2O_3 film was deposited by ALD at 250 °C followed by forming gas anneal (FGA) performed for 30 minutes at 350 °C. This FGA step converts the surface functionalized oxide to a thin layer of GeO_2 (as confirmed by XPS) resulting in improved electrical performance.[1] 2.5 nm of HfO_2 was then deposited by ALD. 10 nm of RF sputtered TiN was deposited as the gate metal followed by low-temperature anneals in various ambients to tune the effective work function (EWF) of the HfO_2/TiN gate stack. A final FGA for 30 minutes at 350 °C completed device processing. The effective work functions were determined through a variety of techniques including V_{fb} vs. EOT plots that allow for the extraction of both the EWF and fixed charge (Fig. 1). Additionally, internal photoemission (IPE) was employed to determine the band offsets at the high-k/metal interface (Fig. 2). DFT calculations and physical characterization including XPS, SIMS, XRD, and TEM have been employed to elucidate the physical mechanisms behind the device characteristics.

The low-temperature, post TiN anneals induce a myriad of effects which contribute to the controlled movement of the effective work function to any values within the Ge bandgap. The most important impact of the anneals is the diffusion of nitrogen from the TiN bulk, through nitrogen and oxygen vacancies, to the HfO_2/TiN interface and slightly into the HfO_2 itself, effectively replacing the oxygen bridge between the dielectric and the metal. SIMS analysis (not shown) confirms the movement of nitrogen and oxygen as a result of the anneals. The lower electronegativity of the nitrogen atoms compared to the replaced oxygen creates a competition between a Hf-N related dipole on one side of the interface and a Ti-N dipole on the other. Also during this process, oxygen vacancies in the HfO_2 are passivated with both oxygen and nitrogen. As can be seen in Figure 1, the temperatures must be kept quite low during the post-TiN anneal. Annealing the devices in 10% O_2 in a balance of N_2 at 450 °C can be seen to significantly reduce the EWF, increase the EOT of the gate stack, and create a very large fixed charge density (proportional to the slope of the curve). These data indicate that the Ge devices are much more sensitive to temperature and oxygen than analogous Si devices and will be discussed.[2] However, maintaining low oxygen content and sub-400 °C processing, the interfacial GeO_2 remains intact resulting in high-quality Ge MOS devices with band-edge effective work function metals. These processes have also recently been extended to 3-D structures of Ge epitaxially grown on patterned bulk Si.

This work was supported in part by the SRC GRC program and Texas Instruments, Inc.

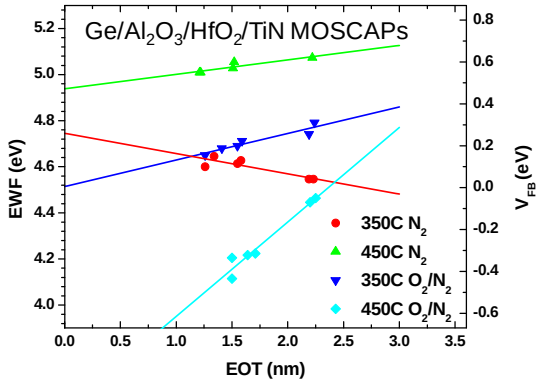

Fig. 1. V_{fb} vs. EOT of variously processed Ge/High-k/TiN gate stacks showing the wide range of EWFs due in large part to dipole formation.

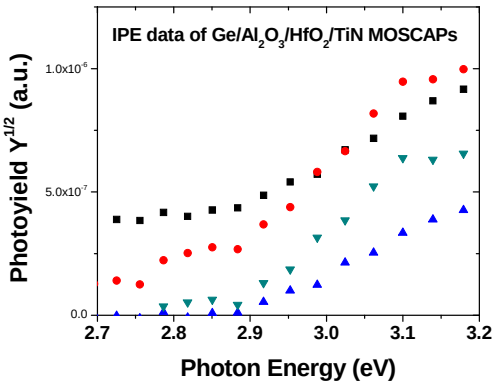

Fig. 2. IPE showing various thresholds corresponding to the HfO_2/TiN barrier height with different device processing.

1 S. Swaminathan, Y.Sun, P. Pianetta, and P. C. McIntyre, J. Appl. Phys. 110, 094105 (2011).
2 C. L. Hinkle, *et al.*, Applied Physics Letters 100, 153501 (2012).

Mo1640

Improvements in Atomic Layer Deposition Nucleation on Ge(100) via HOOH Dosing

Tobin Kaufman-Osborn[a], Joon Sung Lee[a], and Andrew C. Kummel[b]
[a]*Materials Science and Engineering, University of California, San Diego*
[b]*Chemistry and Biochemistry, University of California, San Diego*

Germanium is a promising candidate for potential channel materials due to its higher hole and electron mobility. To minimize the oxide-semiconductor interfacial defect density, a proper passivation layer must be used before the oxide layer is deposited[1]. The passivation layer must be very thin, ideally one monolayer, to allow for increased scaling of the equivalent oxide thickness (EOT). H_2O provides a well-ordered chemisorption monolayer (ML) at room temperature without disrupting surface Ge atoms if it is deposited on a clean oxide-free Ge(100)[2]. In this study, a monolayer of H_2O or HOOH chemisorbates is shown to activate TMA (trimethyl aluminum) chemisorption due to the Ge-OH bonds catalyzing the formation of an ultrathin passivation layer which can serve as an ideal ALD nucleation template on a Ge surface[3]. Figure 1a and 1b compares XPS data of a Ge surface dosed directly with TMA or prepulsed with H_2O, and it is clear that prepulsing with water nearly doubles the aluminum content on the surface demonstrating the benefit for oxidant prepulsing before TMA dosing. However, since H_2O chemisorption results in equal density of Ge-H and Ge-OH sites on the Ge(100), H_2O can only provide a maximum of 0.5 monolayer of Ge–OH sites, limiting the TMA nucleation density. By using HOOH dosing, the density of Ge–OH sites can be doubled thereby increasing the potential TMA nucleation density.

The saturation H_2O dose resulted in 0.85 ML coverage of –OH and –H species chemisorbed on the surface (Fig. 2a, blue box). The remaining unreacted portion of the surface is seen as fuzzy bright features randomly distributed on the surface. These bright features are attributed to single (Fig. 2a, green box) or double (Fig. 2a, red box) dangling bond sites. STS measurements of this surface are shown in Figure 2b. Both of the dangling bond sites have energy states in the band gap consistent with the presence of dangling bonds. Conversely, STS measurements of the H_2O sites show the conduction band edge dangling bond states are eliminated due to the passivating Ge–OH and Ge–H bonds. This room temperature dosed H_2O/Ge surface can activate TMA chemisorption on the surface and forms an ordered structure when annealed as shown in Figure 3. However, if the H_2O/Ge surface is annealed prior to TMA dosing, it can be seen that the Ge–OH and Ge–H sites on the surface have limited thermal stability (Fig 4).

A saturation dose of HOOH on Ge(100) results in a coverage of 0.95 ML of Ge–OH species chemisorbed on the surface (Fig. 5), which is more than double that of the H_2O surface. Only a few sites on the surface are unreacted dangling bond sites (Fig. 5, blue circles). STS measurements of this surface are shown in Figure 6. XPS data in Figure 7 compares oxygen content on the Ge surface after equivalent doses of H_2O and HOOH and shows that HOOH is more effective at covering the surface with Ge-OH chemisorption sites. As seen with the H_2O dosed surface, Ge–OH sites on the HOOH dosed surface passivate the conduction band edge dangling bond states, while the few dangling bond sites show energy states in the band gap. In contrast to the H_2O passivated surface, this HOOH passivated surface has increased thermal stability. Figure 8 shows the HOOH/Ge(100) surface that has been annealed to 100°C. The surface oxygen coverage remains constant to within 10% demonstrating the improved thermal stability of Ge–OH on the surface. The improved coverage of Ge–OH sites allows for increased nucleation density of O-Al bonds and also minimizes the dangling bonds which are considered as the major source of interfacial trap states (D_{it}). The improved thermal stability allows for an increased thermal budget during ALD cycles. Figure 9a shows an STM image of the HOOH/Ge surface dosed with TMA and subsequently annealed forming an ordered layer on the surface while Figure 9b shows STS of the surface demonstrating it is unpinned and has no states in the band gap.

[1] Kamata, Y., "High-k/Ge MOSFETs for Future Nanoelectronics," *Materials Today*, 11, 1-2, 30-38, Jan-Feb 2008.
[2] Lee, J.S., et al., "Effect of H_2O Chemisorption on Passivation of Ge(100) Surface Studied by Scanning Tunneling Microscopy, *Surface Science*, 605, 15-16, 1583-1588, Aug 2011.
[3] Lee, J.S., et al., "Atomic Imaging of Nucleation of Trimethylaluminum on Clean and H_2O Functionalized Ge(100) Surfaces," *Jrnl. Chem. Phys.*, **135**, 054705, Aug 2011.

Mo1645

Electronic reconstruction of Sr/Si(001) Zintl template: *ab-initio* theory and photoemission

Hosung Seo, Miri Choi, Richard C. Hatch, Agham B. Posadas and Alexander A. Demkov
Department of Physics, The University of Texas at Austin, Texas 78712, USA

A sub-monolayer of Sr on Si(001) has been extensively investigated experimentally [1] and theoretically [2] since the first demonstration of epitaxial growth of crystalline $SrTiO_3$ on Si (001) by Mckee and co-workers [3]. A charge transfer ($2e^-$/dimer) induced by a half-monolayer Sr deposition has been shown to be a key element enabling wetting of Si by $SrTiO_3$ [2,4]. However, a detailed understanding of the electronic reconstruction in the sub-monolayer Sr/Si(001) system is incomplete, and such knowledge could be extended to other epitaxial crystalline oxides on semiconductors [4,5]. Recently, using *in-situ* x-ray core-level spectroscopy, we have studied changes in the electronic structure of Si(001) induced by a sub-monolayer of Sr [1]. The analysis of the surface core level shift (SCLS) reveals that the Si 2*p* components shift toward higher binding energy by 0.49 eV after Sr deposition. This is counterintuitive from the electrostatic point of view. In this talk we will present a detailed theoretical investigation of surface core level shifts in this system. In addition, we compare the surface states with angle-resolved photoemission spectroscopy (ARPES) data.

Theoretical calculations are performed using density functional theory within the local density or generalized gradient approximations as implementer in the VASP code. We employ projector augmented wave pseudopotentials to describe Sr and Si. Experimentally, we grow sub-monolayer Sr on Si(001) using molecular beam epitaxy (customized DCA 600 MBE system) and characterize their electronic properties using *in-situ* x-ray core-level spectroscopy and angle-resolved ultra-violet photoemission spectroscopy chamber (VG Scienta R3000).

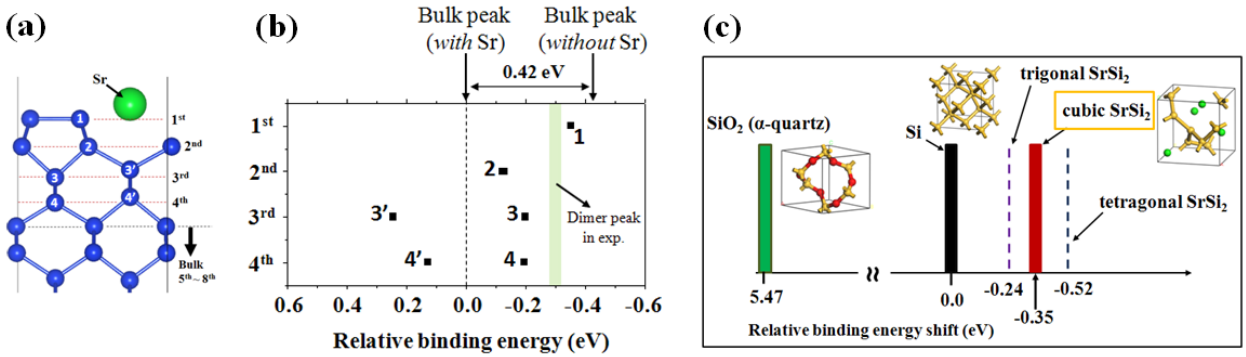

Figure 1. (a) Theoretical structure of ½ ML Sr on Si(001) obtained from the DFT calculations. (b) Surface core level shift in ½ ML Sr on Si(001) calculated using the final state theory (complete screening picture). (c) Theoretical core level shifts in the bulk $SrSi_2$ Zintl compounds in comparison with that of Si and SiO_2.

The *2p* core level binding energy in the final state theory is calculated as $E_B^{final} = E'(n_c\text{-}1) - E(n_c)$, where $E(n_c)$ is the ground state energy and $E'(n_c - 1)$ is the system's energy with a screened core hole. In order to ensure the overall charge neutrality of the system, one electron is added (complete screening picture). First, we calculate the SCLS at the Si (001) $p(2\times2)$ surface and the positions of the S_u and S_d components are -0.53eV and -0.12eV, respectively, in good agreement with our experimental results as well as existing theoretical work. For Sr on Si(001), we find that the tilted dimer rows of the Si(001) $p(2\times2)$

surface are flattened due to the charge transfer. As a result, there is only one dimer peak remaining at -0.35eV in good agreement with the -0.33eV found in the experiment as shown in Fig. 1(b).

Considering the bulk $SrSi_2$, we calculate the *2p* chemical shift induced by the charge transfer from Sr to Si to be -0.35eV as shown in Fig. 1 (c). Strikingly, however, our experiment on ½ ML Sr on Si shows that the bulk *2p* peak and all other surface 2*p* peaks shift in an opposite way compared to the bulk case. Using the initial state theory, we calculate the bulk *2p* binding energy shift to be almost zero. This can be explained by the bulk *2p* level rising up due to the surface dipole layer induced by the charge transfer, simultaneously with the Fermi level rising upward due to the change of the surface electronic structure. On the other hand, using the final state theory we calculate the bulk *2p* binding energy to be increased by 0.42eV in excellent agreement with experiment. Since there is a negligible shift in the initial state calculation, we note that the shift of 0.42eV originates from the reduced relaxation energy gain (screening effect) when the ½ ML Sr is deposited.

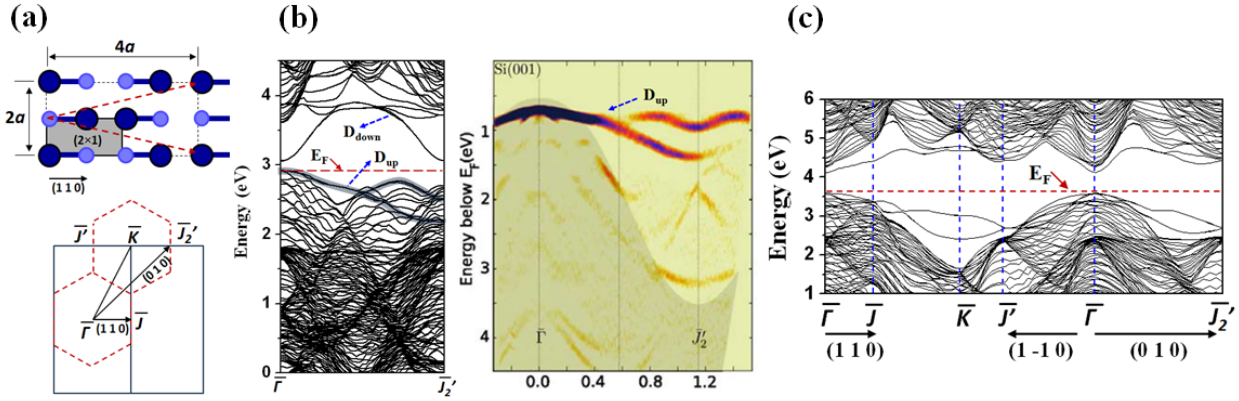

Figure 2. (a) Schematic of surface dimer structure of Si(001) *c*(2×4) reconstruction (up) with dashed arrows indicating surface lattice vectors. Corresponding surface Brillouin zone (down) are drawn with dotted lines. (b) Surface band structure of the *c*(2×4) surface (left) in comparison with ARPES data taken from Ref. [6]. The surface states appeared in the ARPES plot is highlighted with thick grey lines in the band structure plot. (c) Surface band structure of ½ ML Sr on Si (001), which is shown in Fig. 1 (a).

To shed more light on the electronic reconstruction of Sr/Si(001), we calculate the surface band structures of the clean Si(001) *c*(2×4) surface and ½ ML Sr/Si(001) (2×1) surface as shown in Fig. 2 (b) and (c), respectively. We find an excellent agreement between our theoretical band structure and the existing ARPES data as shown in Fig. 2 (b). We will present a detailed analysis for Sr/Si(001) (2×1) surface with a possible explanation for the final state effect.

Reference

[1] M. Choi, A. B. Posadas, H. Seo, R. C. Hatch, and A. A. Demkov, *submitted to Appl. Phys. Lett.*
[2] X. Zhang and A. A. Demkov, *J. Appl. Phys.* **103**, 103710 (2008).
[3] R. A. McKee, F. J. Walker, and M. F. Chisholom, *Phys. Rev. Lett.* **81**, 3014 (1998).
[4] A. A. Demkov, H. Seo, X. Zhang, and J. Ramdani, *Appl. Phys. Lett.* **100**, 071602 (2012).
[5] J. W. Reiner, A. M. Kolpak, Y. Segal, *et al.*, *Adv. Mater.* **22**, 2919 (2010).
[6] J. Eriksson, *Ph.D. dissertation* (2010).

Mo1650

Optical properties of solution-processed LaAlO/Si films using spectroscopic ellipsometry

Tae Jung Kim[1], Soo Min Hwang[2], Jae Jin Yoon[3], Soon Yong Hwang[1], Han Gyeol Park[1], Jun Young Kim[1], Jun Ho Choi[1], Young Dong Kim[1*], and Jinho Joo[2]

[1]*Nano-Optical Property Laboratory and Department of Physics, Kyung Hee University, Seoul 130-701, Korea*
[2]*School of Advanced Materials Science and Engineering, Sungkyunkwan University, Suwon 440-746, Korea*
[3]*Center for Opto-Electronic Convergence Systems, Korea Institute of Science and Technology, Seoul 136-791, Korea*
[*]*Fax: +82-(2)-957-8408 E-mail address: ydkim@khu.ac.kr*

The need to further improve the performance of complementary metal-oxide-semiconductor (CMOS) devices has triggered the development of high-*k* dielectric materials. LaAlO is one of the most promising high-*k* dielectrics because of its moderately high dielectric constant, thermal stability, and large bandgap [1]. Also, the sol-gel deposition of LaAlO is an innovative method for printed electronics, offering a simple and low-cost way of fabricating devices. However, no data on the optical properties of LaAlO grown by sol-gel processing in near infrared-visible-ultraviolet spectral region have been reported so far. In this work, we report dielectric response of LaAlO films grown by the sol-gel method as a function of the film thickness and post-annealing temperature.

The LaAlO precursor sols were prepared by using La-acetylacetonate hydrate and Al-nitrate hydrate at a molar ratio of La:Al = 5:5 with different mole concentrations of 0.05-0.2 M in order to control the film thickness. The solutions were deposited by spin coating onto dilute HF-treated p-type Si substrates, dried on a hot plate, and then sintered at 400^{o}C for 2 h in ambient air. Post-annealing was performed with rapid thermal anneal (RTA) at 700, 850, and 1000°C for 1 min in N_2 ambient to determine the dependence of the dielectric properties on the annealing temperature.

The optical properties were measured in the range of 0.70-8.98 eV by vacuum ultra-violet spectroscopic ellipsometry at room temperature. The angle of incidence was varied from 50° to 70° in steps of 10°. For extracting dielectric function of LaAlO films, we performed multilayer calculation fitting for four-phase model (air/LaAlO/interface layer/Si). The LaAlO layer could be represented accurately by the Tauc-Lorentz dispersion model. We observed the changes of the refractive index *n* and extinction coefficient *k* of the films with varying the film thickness and annealing temperature. An increase of *n* with film thickness and a formation of La-Al-Si-O interface after the RTA are observed. The change of optical properties can be related to the changes of the microstructure and chemical composition with respect the RTA temperature. Our results will be useful for optimizing the properties of LaAlO as a potential dielectric material for printed electronics.

Reference

[1] E. Cicerrella, J. L. Freeouf, L. F. Edge, D. G. Schlom, T. Heeg, J. Schubert, and S. A. Chambers, J. Vac. Sci. Technol. A **23**, 1676 (2005).

Mo1655 Upgraded

Selective TiO_2 deposition on oxidized and hydrogen passivated silicon

S. McDonnell, R. C. Longo, O. Seitz, G. Mordi, J. Kim, Y. J. Chabal, K. J. Cho and R. M. Wallace

Department of Materials Science and Engineering, The University of Texas at Dallas, Richardson, Texas 75080, USA

Advances in scanning tunneling microscopy (STM) tip-based hydrogen lithography have provided a means for changing the surface reactivity of a substrate with atomic precision. Starting with hydrogen passivated silicon, atomically precise areas of atomically clean silicon can be prepared.[1] Using STM or atomic force microscopy (AFM) in air or partial pressures of oxygen, regions of oxidized silicon can be 'written' onto the silicon surface.[2,3,4] Utilizing these techniques as nano-lithography tools, requires the use of deposition methods that can be selective over this narrow range of atomically precise patternable surfaces. Atomic layer deposition (ALD) is a useful tool for highly controllable deposition of a range of materials through chemical interactions with the substrate. ALD can be carried out under a wide range of processing conditions, which can significantly impact both the growth characteristics and physical properties of the subsequent films. Most importantly, ALD is typically carried out at temperatures low enough for hydrogen passivation to remain stable (i.e. < 300 °C). Thin metal oxide structures grown in this manner could be engaged as etch masks for the fabrication of higher aspect ratio structures using highly selective and directional reactive ion etching (RIE) techniques.

In this study, the selectivity of TiO_2 deposition, using $TiCl_4$ and H_2O, with respect hydrogen-passivated silicon and SiO_2 was studied. Initially SiO_2 and Si-H surface where prepared on Si(100) and Si(111) wafers. Depositions were carried out at room temperature, 100 °C and 150 °C. Using the Si(100) substrate, depositions were carried out on a range of different surface treatments at 100 °C. The observed selectivity is compared to density functional calculations of the $TiCl_4$ interactions with these surfaces. It was found in this work that while room temperature deposition result in significant TiO_2 deposition on hydrgon-passivated as well as oxidized silicon, the deposition at substrate temperatures of 100 °C and 150 °C resulted in only trace (< 1 Å) TiO_2 on the hydrogen-passivated surface for a deposition of 15-20 Å on oxidized silicon.

This work has been supported by Defense Advanced Research Project Agency (DARPA) and Space and Naval Warfare Center, San Diego (SPAWARSYSCEN-SD) under contract N66001-08-C-2040, and by the Texas Emerging Technology Fund of the State of Texas for the Atomically Precise Manufacturing Consortium.

References:

[1]J. Lyding, T. C. Shen, J. Hubacek, J. Tucker, and G. Abeln, Applied physics letters **64**, 2010--2012 (1994).
[2]J. Dagata, J. Schneir, H. Harary, C. Evans, M. Postek, and J. Bennett, Applied physics letters **56**, 2001--2003 (1990).
[3]H. Day and D. Allee, Applied physics letters **62**, 2691--2693 (1993).
[4]M. Yasutake, Y. Ejiri, and T. Hattori, JAPANESE JOURNAL OF APPLIED PHYSICS PART 2 LETTERS **32**, 1021--1021 (1993).

Mo1715

The atomic and electronic structure of trimethylaluminum on GaAs/InGaAs (110) surfaces

Tyler Kent[1], Mary Edmonds[1], Ravi Droopad[3], Evgeniy Chagarov[2], and Andrew C. Kummel[1,2]
[1]Materials Science and Engineering Department, University of California San Diego
[2]Department of Chemistry and Biochemistry, University of California San Diego
[3]Department of Physics, Texas State University

Abstract: The lack of intrinsic defect sites on the (110) surface may result in a lower D_{it} in MOSFETs fabricated on (110) surfaces than on (001) surfaces, and finFETs on the InGaAs(001) wafers may be dominated by (110) surfaces. One limiting factor in III-V based MOSFET performance is defect states at the oxide/III-V interface which prevent effective modulation of the Fermi level. These defects can result from missing As-As dimers on the InGaAs (2x4) surface[1] but these defects are absent from the (110) reconstruction. In this work, scanning tunneling microscopy/spectroscopy (STM/STS) is employed to study the atomic and electronic structure of trimethylaluminum(TMA) on the GaAs (110) surfaces, which lack homodimer defect sites, such as As-As dimers since (a) GaAs(110) is a good model of InGaAs(110) and it can be readily obtain by cleaving bulk wafers and (b) in general, the requirements for unpinning GaAs surface are more stringent than unpinning high In content InGaAs surfaces.

Experimental: GaAs(110) samples with $4x10^{18}$ cm^3 Si doping were transferred to the STM chamber (base pressure $1x10^{-11}$ torr) where the clean surface was imaged. 10 Langmuir of TMA was dosed at 25°C, and the sample was subsequently annealed to 135˚C for 30 min. STM was performed of the TMA dosed surface to determine the atomic bonding structure. Scanning tunneling spectroscopy (STS) used to determine Fermi level pinning of both the clean and TMA dosed surfaces. Higher doses (50 L) and annealing temperature (235˚C) were employed to get full adsorbate coverage for structural studies. A model of TMA chemisorption was developed in which a highly ordered monolayer is observed which could allow for aggressive effective oxide thickness (EOT) scaling.

Results: Fig. 1 shows a filled state STM image of the clean GaAs (110) surface. Rows in the $(1\bar{1}0)$ direction are comprised of a zigzag As-Ga chain. The filled dangling bonds of As atoms are directly observed in the image. Fig. 1 also shows the model of the GaAs (110) surface in which filled and empty dangling bonds are indicated by filled and empty red ovals; note the surface is slightly polar due to the tilting of the surface bonds. STS was performed on the clean n-type surface (see below), and it was observed that the Fermi level was located closer to the conduction band than the valence band consistent with an unpinned polar surface. Fig. 2 shows a partial coverage STM image of TMA on the (110) surface. The TMA rows are rotated 40˚ compared to the clean surface rows and have 17 A between rows. A larger dose of TMA (50ML) was deposited on the surface, and a STM image of the resulting complete monolayer is shown in Fig. 3. Ordered rows of TMA have clearly formed in the $(1\bar{1}0)$ dircection. The spacing between adjacent TMA rows is ~5.9 Angstroms, which is identical to the spacing of clean GaAs rows. A model is presented in Fig. 3 of the TMA chemisorption which accounts for the observed 5.9$\dot{A}$ spacing. DFT calculations were performed, the clean GaAs(110) surface is shown in Fig. 4. The DMA passivated surface has a conduction band edge state in the calculated DOS, shown in Fig. 5. It is believed these edge states arise from the Al-Ga bonds. To suppress the conduction band edge states –OH molecules were inserted between the Al-Ga bonds as shown in Fig. 6. The calculated density of states, Fig. 6, shows an effective suppression of the conduction band edge states.

Conclusion: It is possible to form a highly ordered monolayer of TMA on the GaAs (110) surface. The STM data is consistent with DMA molecules bonding between adjacent As and Ga atoms forming a highly ordered complete monolayer with an extremely high nucleation density which will allow for aggressive EOT scaling. STS is being performed to determine the electronic structure of this surface. Similar studies are being performed on InGaAs (110) for comparison. Additionally DFT models show that the DMA passivated surface has a large conduction band edge state which can be passivated by inserting –OH molecules into the Al-Ga bonds which should readily occur upon H_2O dosing.

Mo1720

Compensation and passivation of InN surface donors by Mg dopants and sulphur

W. M. Linhart[1], J. Chai[2], S. M. Durbin[2,3], T. D. Veal[1,4] and **C. F. McConville[1*]**

[1]Department of Physics, University of Warwick, Coventry CV4 7AL, United Kingdom
[2]The MacDiarmid Institute for Advanced Materials and Nanotechnology, New Zealand
[3]Department of Electrical Engineering and Department of Physics, State University of New York at Buffalo, Buffalo, NY 14260, USA
[4]Stephenson Institute for Renewable Energy and Department of Physics, University of Liverpool, Liverpool L69 3BX, United Kingdom

Extreme electron accumulation has been universally observed at the surface of all non-in-situ-cleaved InN films irrespective of their polarity, crystal structure and doping [1-3]. This property remains a barrier to many device applications, with attempts to passivate the surface giving only a small reduction of the electron accumulation [4, 5], apart from in one report for the N-polar surface [6]. Additionally the electron-rich surface layer impedes characterization of bulk p-type conductivity [1]. Here, we have used x-ray photoemission spectroscopy to observe a significant lowering of the surface Fermi level with increasing Mg-doping for the highest Mg concentrations ($>1\times10^{19}$ cm^{-3}), indicating a highly desirable reduction of the electron accumulation. While for moderate Mg concentrations the surface Fermi level is at the previously 'universal' value of ~1.4 eV above the valence band maximum, for [Mg]=1.2×10^{20} cm^{-20}, a value of 0.83 eV is found. Surface space-charge calculations indicate that the lowering of the surface Fermi level increases the density of unoccupied donor type surface states and that these are largely compensated by Mg-acceptors in the near-surface hole depletion rather than by accumulated electrons [7]. Moreover, we have observed a correlation between the surface In:N ratio, the Mg concentration and the surface Fermi level. The reduced surface In:N ratio at high Mg doping levels indicates the presence of fewer In-In bonds which are theoretically predicted to be the surface donors associated with the electron accumulation [8]. We have also investigated the effects of treatment with ammonium polysulphide ($(NH_4)_2S_x$) solution on the band bending at the surface of highly Mg-doped InN. The presence of sulphur at the surface shifts the position of the surface Fermi level to a lower energy, due to a transfer of charge from the InN to the more electronegative sulphur and the reduction of 70% of electron accumulation was observed in highly Mg-doped InN [7]. Our results shed new light on InN, making it more promising for fabrication of p-n junctions and associated devices.

[1] T. D. Veal, C. F. McConville, W. J. Schaff (Eds), *Indium Nitride and Related Alloys* (CRC Press / Taylor and Francis, 2009).
[2] P. D. C. King, T. D. Veal, *et al.*, Appl. Phys. Lett. **91**, 092101 (2007)
[3] W. M. Linhart, T D. Veal, C. F. McConville, *et al.*, Appl. Phys. Lett. **97**, 112103 (2010)
[4] L. R. Bailey, T. D. Veal, *et al.*, Appl. Phys. Lett. **95**, 192111 (2009)
[5] Y. H. Chang *et al.*, J. Appl. Phys. **107**, 043710 (2010)
[6] C-T. Kuo *et al.*, Appl. Phys. Lett. **98**, 052101 (2011)
[7] W. M. Linhart, *et al.*, Phys. Rev. Lett. (unpublished).
[8] D. Segev and C. G. Van de Walle, Europhys. Lett. **76**, 305 (2006)

Corresponding author*: c.f.mcconville@warwick.ac.uk

Mo1725

Structure and Optical Properties of Pure and W-Doped Gallium Oxide Films

E.J. Rubio, M. Noor-A-Alam, C.D. Barraza and C.V. Ramana,
Department of Mechanical Engineering, University of Texas at El Paso, El Paso, USA

Gallium oxide (Ga_2O_3), the stable oxide of gallium, finds attractive applications in luminescent phosphors, high temperature sensors, antireflection coatings, and solar cells. Ga_2O_3 has been recognized as a deep ultraviolet transparent conducting oxide (UV–TCO), which makes the material a potential candidate for transparent electrode applications in UV optoelectronics. While conventional transparent oxides are opaque in the UV region due to small band gap (~3 eV), Ga_2O_3 exhibits a wide band gap (~5 eV) and deep transparency to the UV region. In the present work, a detailed analysis of growth behavior, microstructure, and optical properties of pure and W-metal doped β-Ga_2O_3 films grown by sputter deposition is performed. Ga_2O_3 thin films were deposited on Si(100) and quartz substrates by keeping the growth temperature constant at 500 C and varying the flow rate of oxygen during deposition. The characteristic analysis of the samples was performed employing Rutherford Backscattering, X-ray diffraction, Spectrophotometry and Ellipsometry. From the ellipsometry analysis of the samples it was found that the thickness for the samples varied in the range of 22-29 nm and the refractive index varied from 1.78 to 2.04. For the set of conditions optimized for best stoichiometry, W-doped films Ga_2O_3 films were fabricated using co-sputtering by varying the sputtering power to W-target to vary the concentration of W-dopant. It is seen that increasing W concentrations alters the electronic structure of Ga_2O_3 as evidenced in optical and electrical measurements. The detailed analysis of W-induced electronic structure changes and associated mechanism will be presented based on the data obtained from optical spectrophotometry and spectroscopic ellipsomtry measurements.

Energy Materials

Mo1930 Invited

Compound Semiconductor Heterostructure Challenges for Ultrahigh Efficiency Photovoltaics

Harry Atwater

[1]*Light-Materials Interactions Energy Frontier Research Center and Kavli Nanoscience Institute, California Institute of Technology, Pasadena, CA USA*

Photovoltaic technology has advanced considerably, resulting in single-junction solar cells with a record efficiency of 28.8% and multi-junction cells with an efficiency (under concentrated illumination) of 44%. As impressive as these advances are, these record efficiencies and as well as efficiencies of currently manufactured cell fall far short of the thermodynamic limits to photovoltaic energy conversion. Why such a large gap?

We suggest that there is no fundamental reason, and that systematically addressing the thermodynamic efficiency losses in current photovoltaics will ultimately allow the development of solar cells with efficiencies in the 50-70% range.

A key factor limiting solar-cell performance is carrier thermalization: for a given semiconductor, light with a photon energy $E = \hbar\omega$ above the bandgap can only create a photovoltage V_{oc}, so that the $E - qV_{oc}$ mismatch energy is lost to heat. This 'quantum defect' problem can be alleviated in a multi-junction geometry. Typically, multijunction solar cells are made in a series-connected monolithic architecture, with each of 3 or 4 subcells that reduce carrier thermalization losses, but these thermalization losses are still substantial.

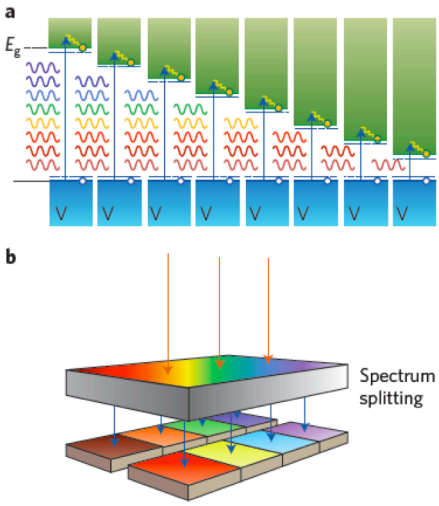

Figure 2. a, Multi-junction energy diagram. Semiconductors with different bandgaps convert different portions of the solar spectrum to reduce thermalization losses. The horizontal blue dashed lines indicate the quasi-Fermi levels defining the open-circuit voltage. The yellow dots represent the electrons. **b**, Parallel-connected architecture that can be realized using epitaxial liftoff and printing techniques of the semiconductor layers, followed by printing of a micro- or nanophotonic spectrum splitting layer.

To reach significantly higher efficiencies, the solar cell and module architecture must be radically modified. A 'full spectrum' architecture, consisting of an optically in parallel array of high-efficiency single-junction cells that form the receiver of a spectrum-splitting photonic structure, can easily accommodate a larger number (e.g., 8-10) of subcells than for conventional multijunction cells, limiting carrier thermalization to approximately 10%.

In this talk, I will discuss approaches to design and fabrication of compound semiconductor solar cells and optical spectrum splitting structures suitable for integration into a 'full spectrum' photovoltaic module.

Mo2000

Pt-based catalyst for PEM fuel cell: role of surfaces and interfaces in a novel plasma deposition method

M. Laurent-Brocq[1], N. Job[2], J.-J. Pireaux[1]
[1] Research Center in Physics of Matter and Radiation (PMR), University of Namur (FUNDP)
[2] Laboratory of Chemical Engineering–Catalytic Engineering, Liège University

Polymer exchange membrane (PEM) fuel cells are promising energy conversion devices [1]. One of the major challenges for a larger commercial distribution is the reduction of their production cost, for example by decreasing the Pt loading in the catalytic layers composing the electrodes. To do so while keeping the same catalytic properties, the dispersion of Pt nanoparticles onto the carbon support needs to be very finely tuned (particle size and distribution) and dense [2].

We apply a novel low temperature RF vacuum plasma method using organometallic solid precursors [3] to graft Pt nanoparticles on carbon black and to study the influence of the synthesis conditions on the nanoparticles physico-chemical characteristics. Catalysts were synthesized in a 'one-pot' experiment, under various plasma treatment conditions (gas and power) and characterized by X-ray diffraction, transmission electron microscopy and X-ray photoelectron spectroscopy. It will be shown that the control of the formation of the Pt nanoparticles depends on two phenomena: (i) the functionalization of the carbon black surface which is mainly influenced by the plasma gas nature and (ii) the decomposition of the organometallic precursor which results first from a thermal effect depending of the plasma power. Finally, catalysts have been annealed and the stability of the nanoparticles studied.

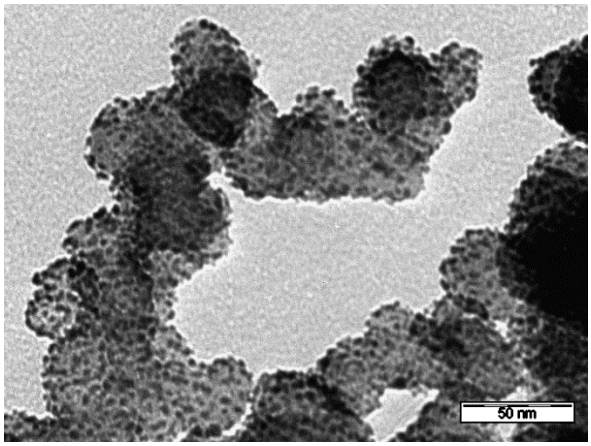

TEM micrograph of Pt nanoparticles grafted on carbon black through a low temperature plasma treatment.

1. G.W. Crabtree, MS Dresselhaus, MRS Bulletin, 33 (2008) 421
2. H.A. Gasteiger, S.S. Kocha, B. Sompalli, F.T. Wagner, Appl. Catal. B 56 (2005) 9.
3. J.-J. Pireaux, F. Reniers, J. Guillot, M. Gulas, N. Claessens, A. Batan, A. Mansour. Method for depositing nanoparticles on substrates. WO/2012/028695, 2010

Mo2005

The role of mobile ionized defects in the aging of Cu_2O/ZnO nanowire solar cells.

J.H. Joo, J. R. Richardson, E. L. Hu

A common assumption in the design of inorganic photovoltaics is that the acceptors and donors in the semiconductor are immobile, even in the presence of an electric field. For example, when a phosphorous donor atom in silicon is ionized, becoming positively charged, the phosphorous atom is assumed to remain locked in place within the silicon lattice. In silicon, ionized donors and acceptors can be assumed to be stationary even in the depletion region of a p-n junction, where mobile carriers are absent and an electric field is present. The assumption that ionized acceptors and donors do not move is typically a valid assumption in most materials, because the velocity at which these ionized species move is usually negligible. However, recent exploration into alternative materials for photovoltaic devices and nanostructured architectures for these devices challenges this assumption. This report will focus on the motion of acceptors in Cu_2O/ZnO devices, made evident through the changes in external quantum efficiency over time.

Cu_2O/ZnO photovoltaic devices, while one of the oldest photovoltaic systems, are still being actively explored today. Cu_2O is typically a p-type material with a band gap of 2.0 eV and serves as the absorber layer. ZnO is typically an n-type material with a band gap of 3.4 eV and serves as the window layer. However, copper vacancies, the species responsible for p-type doping in Cu_2O, are known to have high mobility within the Cu_2O lattice. Ionized copper vacancies residing within the depletion region are then subject to the electric field. Therefore, the acceptors in the Cu_2O move over time and change the operation of the device. For nanostructured devices, such as ZnO nanowires embedded in a Cu_2O matrix, the effects of acceptor motion can become highly exaggerated due to the large increase in junction area.

We report on the changes in electrical characteristics of both a planar and nanowire ZnO/Cu_2O device. Changes in external quantum efficiency over time show evidence of an expanding depletion region in the nanowire-based device. Photons closer to the band edge of Cu_2O are collected up to 8% more efficiently over time while higher energy photons are collected less efficiently. Copper vacancies move toward the junction, eventually forming electrically neutral defect complexes at the junction or contributing to voids that may form through the coalescence of copper vacancies. The mobile copper vacancies then leave behind a region depleted of acceptors, which increases the width of the depletion region. Minority carriers, photogenerated within this newly expanded depletion region, are now driven to the junction by the electric field. These carriers in the depletion region are collected much more efficiently than carriers relying on a diffusive driving force such as a concentration gradient.

These results have important implications for nanostructured photovoltaic devices. Devices previously thought impervious to the effects of dopant diffusion may exhibit large effects when the device architecture is nanostructured. This may counter the increase in carrier collection efficiency in such devices. The large junction area associated with nanostructured devices may cause the device to age differently. Since much more of the device resides within the depletion region, charged species are therefore more affected by these internal electric fields.

Semiconductor Nanowires for Solar Energy Conversion

Peidong Yang
Department of Chemistry
University of California
Berkeley, CA 94720

Abstract :

Semiconductor nanowires, by definition, typically have cross-sectional dimensions that can be tuned from 2–200 nm, with lengths spanning from hundreds of nanometers to millimeters. After more than a decade of research, nanowires can now be synthesized and assembled with specific compositions, heterojunctions and architectures. This has led to a host of nanowire photonic and electronic devices. Because of their unique structural, chemical and physical properties, these nanoscopic one-dimensional nanostructures can also play a significant role in terawatt energy conversion and storage. Currently the amount of energy required worldwide is on the scale of terawatts, and the percentage of renewable energy in the current energy portfolio is quite limited. Developing of cost-effective clean energy technology becomes imperative.

Nanowires, with their unique capability to bridge the nanoscopic and macroscopic worlds, have already been demonstrated as important materials for different energy conversion. One emerging and exciting direction is their application for solar to fuel conversion. The generation of fuels by the direct conversion of solar energy in a fully integrated system is an attractive goal, but no such system has been demonstrated that shows the required efficiency, is sufficiently durable, or can be manufactured at reasonable cost. One of the most critical issues in solar water splitting is the development of suitable photoelectrodes with high efficiency and long-term durability in an aqueous environment. Semiconductor nanowires represent an important class of nanostructure building block for direct solar-to-fuel application because of their high surface area, tunable bandgap and efficient charge transport and collection. Nanowires can be readily designed and synthesized to deterministically incorporate heterojunctions with improved light absorption, charge separation and vectorial transport. Meanwhile, it is also possible to selectively decorate different oxidation or reduction catalysts onto specific segments of the nanowires to mimic the compartmentalized reactions in natural photosynthesis.

In this talk, I will highlight several recent examples in this lab using semiconductor nanowires and their heterostructures for the purpose of solar energy conversion, including photovoltaics and solar water splitting.

#
#

Mo2040

Investigations on the Electronic and Structural Properties of CdS/CZTS Heterojunction Interface for Improving Solar Cell Efficiency and Stability

Ratheesh R Thankalekshmi and A.C. Rastogi
Electrical and Computer Engineering Department & Center for Autonomous Solar Power,
Binghamton University, State University of New York, Binghamton 13902, USA

Thin-film photovoltaic solar cells based on the earth-abundant Cu_2ZnSnS_4 (CZTS) quaternary p-type semiconductor as solar absorber with a high absorption coefficient ($>10^4$ cm^{-1}) and a direct~ 1.5eV band gap are being actively investigated. The CZTS solar cells modeled after $Cu(In,Ga)Se_2$ CIGS are made in the heterojunction structure with an n-CdS window layer. The CZTS solar cell power conversion efficiencies are highly dependent on the methods employed in its synthesis. For example, the vacuum deposited CZTS have yielded best efficiencies of 6.8% whereas; the majority of non-vacuum methods could produce solar cells with much lower 3-4% efficiencies such as 3.4% with electrodeposited CZTS. Although, the structure, composition and electronic properties of the CZTS films were optimized in respect of each of the methods used in synthesis, yet the reasons behind the low conversion efficiencies and low open circuit voltages of CZTS solar cells in the n-CdS/p-CZTS structure have not been fully understood. In particular, the critical role of the CdS/CZTS heterojunction interface in determining the photovoltaic properties has not received much attention. It is well known that the electronic properties of the CZTS compound are characterized by bulk native defects due to Cu_{zn} antisite, Cu vacancy, metal rich states, intrinsic defects and defect complexes. However, more specifically, their role at the CdS/CZTS heterojunction interface, especially through process induced modification has not been studied. Without such knowledge, it will be difficult to make a breakthrough in improving the photovoltaic conversion efficiency and the long-term device stability similar to those realized for CdS/CIGS solar cells.

We have investigated the structure and electronic properties of the heterojunction interface between the chemical spray pyrolysis (CSP) formed solar active p-CZTS films and n-CdS films. The non-vacuum CSP technique was used for CZTS synthesis due to its scale-up ability and potential for low cost solar cells. The herojunction interface was made by depositing thin CdS film by CSP and also by chemical bath deposition (CBD) in the CSP-CdS/CSP-CZTS, CBD-CdS/CSP-CZTS hetero-interface configurations. Interface reactions were induced by air annealing the heterojunction at 200-400ºC. The chemical composition of the interface was analyzed by x-ray photoelectron spectroscopy (XPS) in conjunction with depth profiling across the CdS/CZTS heterojunction interface. This study reveals, extensive inter diffusion of Cd and Zn. Substantial diffusion of Cd across the interface into CZTS is accompanied by depletion of Cu. At the same time, the migration of Zn across CZTS into CdS was also observed, thereby depleting Zn from the CZTS surface. Cd substituted at the Cu vacancy sites produces an n-type surface layer buried in CZTS surface. The Zn at Cu sites which contributes to the p-type character of CZTS, by migration out into CdS not only contributes to n-type surface conversion but also forms highly resistive n-CdZnS. The n-type surface conversion is confirmed from the sign of thermoelectric power and analysis of Seebeck provides detailed information on the carrier concentration consistent with the defect model of the CdS-CZTS interface. The structural defect, especially the phase segregation, studied by x-ray diffraction is consistent with the changes in the electronic property. The transformation of the required abrupt junction into a compositionally diffused interface degrades the electronic properties of the hetrojunction significantly impacting the solar cell performance. The analysis of the current-voltage characteristics of the n-CdS/p-CZTS with ITO and Mo metal contacts showed a low field region at the CdS/CZTS interface which accentuates strong carrier recombination. Such a hetrojunction device structure is not conducive for the collection of photo-excited carriers. These studies establish the modification of CdS/CZTS heterojunction interface and argue that the low efficiency may be attributed to the interface defects. This paper will report on the structure and electronic properties of the CdS/CZTS hetrojunction interface based on the detailed XPS, XRD, thermoelectric and current-voltage investigations.

Mo2045

TIN DIOXIDE δ-DOPED WITH ANTIMONY FOR THERMOELECTRIC APPLICATIONS: FIRST PRINCIPLES CALCULATIONS

L. Scolfaro[1], N. S. Castro[2], D. E. S. Silva[2], F. G. Pinto[2], and P. D. Borges[2]

[1]*Department of Physics, Texas State University, San Marcos, Texas, USA*
[2]*Instituto de Ciências Exatas e Tec. , Universidade Federal de Viçosa, Rio Paranaíba, MG, Brazil*

The rapid increase in the world's energy demand has driven the intense research recently seen in the search for alternative and sustainable energies. Thermoelectric (TE) materials have attracted great attention due to their ability to convert heat directly into electricity and vice-versa. Tin dioxide (SnO_2) showed up recently as one of the promising materials for TE application because it is chemically and thermally stable at high temperature. Multilayers and superlattices (SLs), which are built as alternate layers of different semiconductors or semiconductor/metallic materials with nanoscale dimensions are being explored as potential candidates to improve the TE figure-of-merit. In this work we study the electronic structure of Antimony delta (δ)-doped layers in SnO_2 grown along the (001) direction by performing first-principles density functional theory (DFT) calculations based on the Projector Augmented Wave approach as implemented in the Vienna Ab-initio Simulation Package (VASP-PAW). We examine the band structure and density of states of the Sb δ-doped SnO_2 SL structures using supercells which simulate doping concentrations of ~4% and ~8%, corresponding to a spacing between δ-layers of ~0.35 and ~4.0 nm, respectively. The δ-doping scheme gives a strong directionality to the carrier mobility. The induced impurity levels appearing in the gap region of SnO_2 are of Sb s-character. We observe a metallic (semiconductor) behavior of the induced bands with respect to a direction perpendicular (parallel) to the impurity delta-layers. Considering the same Sb impurity concentrations, but for a diluted alloy configuration, the metallic behavior is not observed. Our results show that the impurity-induced bands can cause an increase in the electrical conductivity for directions perpendicular to the δ-doped layers, with concomitant decrease of the thermal conductivity in virtue of the enhancement of the electron and phonon scattering. The implications of our findings in the TE applications of SnO_2 are discussed.

Presenting author's email: lscolfaro@txstate.edu

Mo2050

Interfacial Polymer Ferroelectric Dipole Induced Electric Field Effect on the Photovoltaic Performance of Organic Solar Cells

A.C. Rastogi
Electrical and Computer Engineering Department & Center for Autonomous Solar Power,
Binghamton University, State University of New York, Binghamton 13902, USA

Polymeric organic solar cells due to low cost and easy processing ability are most promising for solar electricity generation. These solar cell based on hole-conducting polymeric semiconductors (electron donor) and electron-conducting fullerene (electron acceptor) in the blended bulk heterojunction device structures, have shown conversion efficiencies of 6-8%. In the operation of organic solar cells, the donor-acceptor (D-A) interface has an important role in efficient dissociation of the photogenerated charge transfer excitons (CTE), the electron-hole pairs bound by Coulomb attraction. Photocurrent is produced when free electrons and holes generated at the interface by CTE dissociation are collected at the contacts via transport through acceptor and donor semiconductors. The main reasons for low efficiency of organic solar cells are short diffusion lengths that cause the singlet excitons to recombine before arriving at D-A interface and the nonradiative recombination of CTE at the interface before dissociation. To nullify the recombination pathways which add up to ~44% loss in conversion efficiency, most past efforts have focused on the morphology of the heterojunction interfaces at the nanoscale with limited effect.

The object of the present investigation is to improve photovoltaic performance of organic solar cells by inducing a local electric field in the vicinity of the bulk D-A heterojunction interfaces and thus (i) affect efficient CTE dissociation in generating free carriers, electrons and holes, and (ii) extract and drift free carriers apart under field to minimize loss by recombination. We have created local field by introducing the polarized ferroelectric dipoles of copolymer of vinyildene fluoride (80%) with trifluoroethylene (20%) P(VDF+TrFE) which has a large dipole moment (2.1 D) and can produce large spontaneous polarization by cooperative alignment of molecular dipoles through poling. The effect of dipolar field on photocurrent was evaluated by fabricating an organic solar cell device using 1:1 blend of donor-regioregular poly(3-hexylthiophene, P3HT and acceptor -phenyl-C61-butyric acid methyl ester (PCBM) over PEDOT coated transparent oxide conductor (TCO) glass and 0.8μm thick evaporated Al- back contact. A ~5 nm thin PVDF-TrFE interspaced between ~50 nm thick film of D-A blend forming a 3-layer stack ensures the electric field dipoles in close proximity to the D-A interface. A unidirectional electric field structure was also investigated by forming ferroelectric dipoles at the metal contact-D-A blend interface. Changes in the photocurrent under AM1.5 light were studied after ferroelectric dipoles were aligned by poling with 20 ms voltage pulses of different 20-30 V amplitude in either positive of negative polarities at TCO electrode, which induces interfacial electric field. A 30% increase in the observed photocurrent with positive poling is shown to arise from CTE dissociation under a typical electrical field of 100-250 $V\mu m^{-1}$ at the interface from additive dipoles. Correspondingly, the effect on open circuit voltage is not as significant. With ferroelectric layer at the metal- D-A blend interface, persistent dipolar orientation by compensation of charges from metal is observed to result in permanent built-in electric field. Under positive poling at different voltages, changes in conversion efficiency are also observed. This paper will report on the results of detailed photovoltaic and quantum efficiency characterizations under various poling and polarity conditions of the interface dipolar electric field which support efficient exciton dissociation at D-A interface as the main reason for improved performance of organic solar cells.

Mo2055

Thermoelectric effects of a chain of coupled quantum dots connected to metallic electrodes

D. M. T. Kuo[1] and Y. C. Chang[2]

[1]Department. of Electrical Engineering, National Central University, Chungli, 320, Taiwan
[2]Research Center for Applied Sciences, Academia Sinica, Taipei 115, Taiwan

The thermoelectric effects of a chain of coupled quantum dots (CCQD) connected to metallic electrodes are theoretically investigated in the Coulomb blockade regime. An extended Hubbard model is employed to simulate the CCQD system consisted of N quantum dots (QDs). The charge and heat currents are calculated in the framework of Keldysh Green's function technique. We obtained a closed-form Landauer expression for the transmission coefficient of the CCQD system with arbitrary number of QDs by using the method beyond mean-field theory to calculate high order Green's functions. The electrical conductance (G_e), Seebeck coefficient (S), thermal conductance, and figure of merit (ZT) are numerically calculated and analyzed in the linear response regime. The effects of electron Coulomb interactions, interdot hopping strengths, and density of states on ZT are clearly depicted. We plot the ZT as a function of temperature for different number of quantum dots in Figure 1. For the case of N=5, we also consider the variation of E_5. With increasing QD numbers, the maximum ZT is suppressed. In addition, the QD energy level fluctuation also suppresses the maximum ZT.

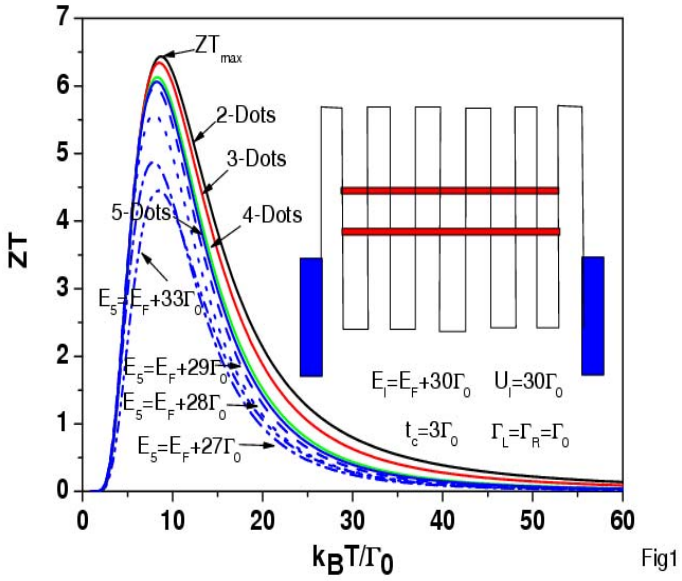

Fig. 1 ZT as a function of temperature for different quantum dot numbers. The schematic diagram for a chain of coupled quantum dots connected to metallic electrodes is shown in the inset. Notations E_l, U_l, and t_c, respectively, describe the QD energy level, on-site electron coulomb interaction, and interdot hopping strength. All energy scales are in the units of tunneling rate. E_F denotes the Fermi energy of electrodes.

Tuesday

Tu0730	Registration and Continental Breakfast
Tu0830	Tuesday Morning Session: Contacts & Nanocontacts
Tu0950	Coffee Break and Poster Viewing
Tu1050	Tuesday Morning Session: New Tools & Applications
Tu1215	Free Afternoon
Tu1930	Tuesday Evening Session: Topological Insulators I

Contacts & Nanocontacts

Tu0830 Upgraded

Ultra-low contact resistance at an epitaxial metal/oxide heterojunction through diffusion-controlled metallization of the oxide

Scott A. Chambers[a], Peter V. Sushko[b], Meng Gu[a], H. Yang[a], Nigel D. Browning[a]
[a]*Fundamental and Computational Sciences Directorate, Pacific Northwest National Laboratory, Richland, WA 99352 USA*
[b]*Department of Physics and Astronomy and London Centre for Nanotechnology, University College London, Gower Street, London, WC1E 6BT, United Kingdom*

Epitaxial Cr metal overlayers form a nearly ideal Ohmic contact to *n*-$SrTiO_3$(001) when deposited in ultrahigh vacuum at a substrate temperature of ~550^{o}C [1]. The contact resistance at room temperature, as measured by the van der Pauw method, is ~65 mΩ/square. Cr nucleates with the epitaxial relationship expected based on lattice parameters, $(001)_{Cr}$ || $(001)_{STO}$ and $[110]_{Cr}$ || $[100]_{STO}$, with an in-plane mismatch of +4.2%. Au is also expected to grow epitaxially on STO(001) as it has the same in-plane lattice mismatch as Cr. Yet, Au does not nucleate epitaxially [2], nor does it form an Ohmic contact. Rather, it makes a Schottky barrier on STO [3]. What is the difference between the two heterojunctions? Previous experimental studies have concluded that both interfaces are atomically abrupt [2,4]. Yet, their electronic properties are completely different. We have carried out a detailed investigation of Cr/STO(001) using scanning transmission electron microscopy/electron energy loss spectroscopy (STEM/EELS), together with x-ray photoelectron spectroscopy (XPS) and first-principles theory, to gain understanding. Cr is found to diffuse into the STO and occupy interstitial sites within the first three atomic planes (two TiO_2 and one SrO) without significantly disturbing the STO surface structure. Density functional theory calculations reveal that Cr interstitial species are particularly stable in the first TiO_2 plane. More than that, these interstitial species stabilize the epitaxial Cr films relative to the perfectly abrupt interface. Both theory and experiment show that Cr metallization results in charge transfer to structural Ti(IV) near the interface, effectively metalizing the STO, preventing Schottky barrier formation, and generating a ultra-low resistance Ohmic contact. In contrast, Au interacts very weakly with STO and does not diffuse into the STO, precluding STO metalization near the interface. The resulting Au/STO structure constitutes a textbook model of the metal/semiconductor interface, and Schottky barrier formation naturally follows. These results demonstrate the value of defect species that can increase thermodynamic stability of interfaces and modify their electronic properties without affecting their geometrical structures. Exploiting such defects-controlled interface structures will help to engineer more complex systems with desirable electronic properties.

[1] C. Capan, G. Y. Sun, M. E. Bowden, and S. A. Chambers, *Appl. Phys. Lett.* **100**, 052106 (2012).
[2] F. Silly and M. R. Castell, *Phys. Rev. Lett.* **96**, 086104 (2006).
[3] Y. Hikita, M. Kawamura, C. Bell, and H. Y. Hwang, *Appl. Phys. Lett.* **98**, 192103 (2011).
[4] Q. A. Fu and T. Wagner, *Surf. Sci.* **601**, 1339 (2007).

Tu0850

Barrier Height Measurement of Metal Contacts to Silicon Nanowires Using Spectrally-Resolved Scanning Photocurrent Microscopy

KunHo Yoon[1], Jerome K. Hyun[1,2], Justin G. Connell[1], Sarah L. Howell[1], and Lincoln J. Lauhon[1]

(1) Department of Materials Science and Engineering, Northwestern University, Evanston, IL 60208, USA

(2) Present address: Department of Materials Science and Engineering, KAIST, Daejeon 305-7-1, Republic of Korea

The challenge of efficient charge injection and extraction through metal contacts to semiconductors has been recognized since the early days of semiconductor devices, and the alignment of electronic energy levels at interfaces between the metal and the nanostructure is essential for engineering high performance electronic devices. The presence of a Schottky barrier limits the charge injection and, thus, key metrics in many types of devices. Conventionally, internal photoemission spectroscopy (IPS) is used to measure the barrier height of Schottky contacts [1]. However, the application of IPS has been limited to bulk and thin film semiconductor/dielectrics. As existing models of electrical contacts need to be modified for one-dimensional nanostructures (i.e. nanowires) due to significant deviations in geometries and electrostatics from conventional planar devices [2], methods are needed to measure barrier heights at reduced dimensions.

Scanning photocurrent microscopy (SPCM) was used to measure the barrier height between metal contacts and a Si nanowire. Photoexcitation below the semiconductor bandgap in SPCM induces internal photoemission at the metal-semiconductor junction, enabling separation of the contacts response from that of the semiconducting channel. The scaling of the photocurrent with photon energy is consistent with internal photoemission, enabling extraction of a quantitative barrier height.

Planar single nanowire devices were fabricated using n+ Si nanowires of varying diameters to systematically examine the influence of nanowire diameter on barrier height. As the diameter decreases, the measured effective barrier height decreases below the reported value for the Ni barrier height on bulk Si. Furthermore, we investigated the effect of near-surface doping, which is the primary method to achieve Ohmic contacts. For this purpose, Si nanowires were grown with an n+/i junction in the middle. With the same metallization, a Schottky contact was formed on the intrinsic portion, whereas an Ohmic contact was formed on the doped portion. As expected, the effective barrier height is lowered by the near-surface doping, which is expected to induce tunneling by reducing the barrier width [3].

The measurement of the barrier height of Schottky and Ohmic contacts on nanowires is an important step in understanding band profiles at nanoscale junctions, highlighting the potential for spectrally resolved SPCM measurements to investigate the physics of devices incorporating nanostructured materials with electronically active interfaces.

References

[1] J. C. Brewer, R. J. Walters, L. D. Bell, D. B. Farmer, R. G. Gordon, H. A. Atwater, *Appl. Phys. Lett.* **2004**, *85*, 4133–4135.

[2] F. Léonard, A. A. Talin, *Nature Nanotechnology* **2011**, *6*, 773–783.

[3] J. M. Shannon, *Appl. Phys. Lett.* **1974**, *24*, 369.

Tu0905 Invited

The Nanoelectronics Research Initiative: Prospects for Logic Beyond CMOS

Thomas N. Theis
IBM Thomas J. Watson Research Center,
P.O. Box 218
Yorktown Heights, NY, USA
thomas.theis@src.org

***Abstract*— The continuing evolution of silicon CMOS technology is clearly approaching some important physical limits. Since roughly 2003, the inability to reduce supply voltages according to constant-field scaling rules, combined with economic constraints on areal power density and total power, has forced designers to limit clock frequencies even as devices have continued to shrink. Subthreshold voltage operation cannot fundamentally alter this new *status quo*. The device physics must change in a more fundamental way if we are to realize fast digital logic with very low power dissipation. The Nanoelectronics Research Initiative (NRI) is a consortium of leading semiconductor companies established in 2005 to guide and fund fundamental research at U.S. universities with the goal of finding the "next switch" to replace the CMOS transistor for storing and manipulating digital information. The National Institute of Standards and Technology (NIST) and the National Science Foundation (NSF) have partnered with NRI to fund this research. To date, NRI has funded the exploration of many novel device concepts, and has guided research comparing the capabilities of these devices. Although no single device has yet emerged as a clear winner with the potential to eclipse the field-effect transistor, results are sufficiently promising that member companies have recently renewed their commitment to NRI. Based on the learning to date, a vision for the next five years of research has emerged.**

Tu0935

New Experiments and Applications Made Possible by a Low Temperature 4-Tip STM with UHV-SEM Navigation

B. Guenther, A. Bettac, J. Koeble, J. Hilton, A. Feltz

Omicron NanoTechnology GmbH, Germany, *e-mail address: a.bettac@omicron.de

A major challenge in the development of novel devices in nano- and molecular electronics is their interconnection with larger scale electrical circuits required to control and characterize their functional properties. Local electrical probing by multiple probes with STM precision can significantly improve efficiency in analyzing individual nano-electronic devices without the need of a full electrical integration. Recently we developed a new microscope stage that merges the requirements of a SEM navigated 4-probe STM and at the same time satisfy the needs for high performance SPM at low temperatures.

Besides SEM/STM probe fine navigation and imaging with atomic resolution at temperatures of T<5K, the excellent STM performance level of the LT NANOPROBE expands applications to tunneling spectroscopy and even the creation or modification of nano-structures or single atoms by an ultimately precise STM probe. In this contribution we will focus on measurements that prove the performance level of the instrument as well as on tunneling spectroscopy and atom manipulation experiments on Ag(111) at temperatures of T < 5K.

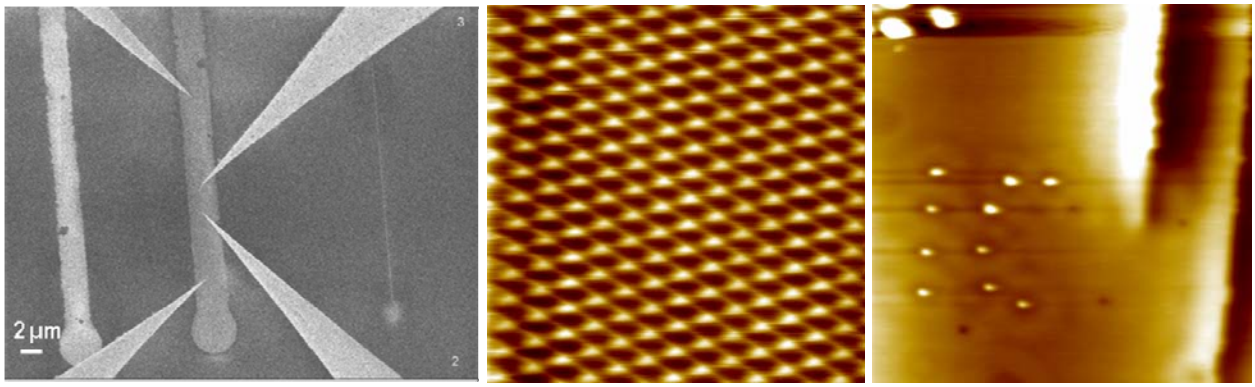

Figure:

Left: SEM image of 4 STM probes placed on a Fe-nanowire for 4-point conductance measurements at T < 5 K.

Middle: High resolution STM image of a Ag(111) surface at T<5K. Imaging parameters: Scan area: 5.7nm x 5.7nm, U_{gap}= 25mV, $I_{setpoint}$=2nA

Right: Atom manipulation of Ag-particles on a Ag(111) surface at 5K. Imaging parameters: Scan area: 48.3nm x 48.3nm, U_{gap}= 90mV, $I_{setpoint}$=5.4nA

Tu0940

Surface Characterization of Functionalized Gold Nanoparticles

Ali Rafati,[1] Sirnegeda D. Techane,[1] Lara J. Gamble,[1] Donald R. Baer[2] and David G. Castner[1]

[1]National ESCA and Surface Analysis Center for Biomedical Problems
Departments of Bioengineering and Chemical Engineering
University of Washington, Seattle, WA, USA

[2]Environmental Molecular Sciences Laboratory,
Pacific Northwest National Laboratory, Box 999, Richland WA 99352

Nanoparticles exhibit unique surface properties and require well-controlled surface properties to achieve optimum performance in complex biological or physiological fluids. Thus, there is a need to develop rigorous and detailed surface analysis methods for their characterization. The surface chemistries of carboxylic acid (COOH), amine (NH_2) and oligo(ethylene glycol) (OEG) terminated self-assembled monolayers (SAMs) on Au nanoparticle (AuNP) surfaces were characterized with x-ray photoelectron spectroscopy (XPS), time-of-flight secondary ion mass spectrometry (ToF-SIMS) and low energy ion scattering (LEIS). The size, shape, and size distribution of the AuNPs was determined by transmission electron microscopy (TEM).

For COOH-SAM covered AuNPs, as the diameter decreased and SAM chain length increased, the XPS atomic C/Au ratio and the ToF-SIMS intensity ratio of $C_{1-4}H_xO_y$ ions/Au-containing-ions both increased. Since the XPS C/Au atomic ratio depends on the SAM structure as well as the curved nature of the AuNPs, special XPS data analysis methods must be developed to accurately analyze SAM covered AuNPs. Simulated Electron Spectra for Surface Analysis (SESSA) was used for this purpose. Quantities such as SAM density, thickness, surface roughness, etc. were tuned in SESSA to optimize agreement between simulated and experimental XPS compositions. The SESSA results for 16 carbon chain length COOH-SAMs showed that the total overlayer thicknesses was 3Å thinner on the 14nm diameter AuNPs (18.5Å) compared to a flat Au surface (21.5Å). Included in the measured total overlayer thicknesses was the presence of a 1.5Å CH_2-contamination layer. LEIS was also used to measure the total overlayer thickness on the SAM covered AuNPs. The thickness measured by LEIS (18Å for the C16 COOH SAMs on 14nm AuNPs) was in excellent agreement with the total film thickness measured by SESSA/XPS.

Both methoxy (CH_3O-) and hydroxyl (HO-) terminated OEG SAMs with chains containing 11 methylene and 4 ethylene glycol units were examined. ToF-SIMS clearly differentiates the two OEG SAMs based on the $C_3H_7O^+$ peak attributed to the CH_3 terminated SAM, while XPS didn't detect a significant difference between the two SAMs on the same surface. However, XPS did show a significant difference between the same SAM on different sized AuNPs. Both OEG SAMs were more densely packed on the 40 nm diameter AuNPs compared to the 14 nm diameter AuNPs. FTIR experiments indicates the methylene backbone groups are well-ordered on all gold surfaces, but the OEG groups are more ordered on the 40 nm diameter AuNPs. Together the XPS and FTIR results suggest the OEG SAMs form a thicker and/or higher density SAMs on the 40 nm AuNPs compared to the 14nm AuNPs. SESSA and LEIS experiments are currently underway to quantify the thickness and structure differences of the OEG SAMs on the AuNPs.

Tu0945

New Milestones in Scanning Probe Microscopy: Graphene on Rh(111) studied by DFT, STM and NC-AFM using KolibriSensor™ and Tyto™

Elena Voloshina[1], Yuriy Dedkov[2], Torben Hänke[2], Thomas Schulmeyer[3], Andreas Thissen[2]
[1]*Physikalische und Theoretische Chemie, Freie Universität Berlin, 14195 Berlin, Germany;*
[2]*SPECS Surface Nano Analysis GmbH, Voltastraße 5, 13355 Berlin, Germany*
[3]*SPECS Surface Nano Analysis Inc., 20 Cabot Boulevard, Mansfield, MA 02048, USA*
E-mail: Thomas.Schulmeyer@specs.com

Graphene, a single layer of carbon atoms ordered in a "chicken-wire" lattice [1], is proposed to be used in many technological applications. One of the promising systems on the basis of graphene is its interface with metallic substrates [2]. Here graphene can be used as a protection layer for the underlying substrate, as a spin-filtering material separating two layers of a ferromagnetic material, or, in case of its growth on a lattice mismatched surfaces [for example, Ir(111), Rh(111), or Ru(0001)], as a template for the preparation of ordered arrays of clusters.

For graphene on Rh(111) [Fig.1(a-c)] several regions of different arrangements of carbon atoms above a Rh(111) substrate can be found: ATOP [A; carbon atoms are above Rh(S-1) and Rh(S-2) atoms], HCP [H; carbon atoms are above Rh(S) and Rh(S-2) atoms], FCC [F; carbon atoms are above Rh(S) and Rh(S-1) atoms], and BRIDGE [B; Rh(S) atoms bridge the carbon atoms]. These places are marked in Fig.1(a) by circle, down-triangle, square, and stars, respectively. Among them, the BRIDGE positions are expected to be the most energetically favorable for the nucleation of deposited atoms on top of a graphene layer.

In this contribution we present the combined study of the graphene/Rh(111) system via application of the state-of-the-art DFT calculations, STM, and NC-AFM. The calculated imaging contrast for STM between all high-symmetry positions for graphene/Rh(111) is in very good agreement with experimental results and this contrast does not depend on the sign of the bias voltage applied between a tip and the sample. As opposed to the latter observation, the imaging contrast in atomically-resolved AFM measurements depends on the frequency shift of the oscillating tip that can be understood on the basis of measured force-spectroscopy curves.

For this the KolibriSensor™, a new quartz sensor that excels in its performance reliability is used either for RT to HT studies in an SPM Aarhus 150 or for LT studies in the new Tyto scan head mounted into a JT-SPM.

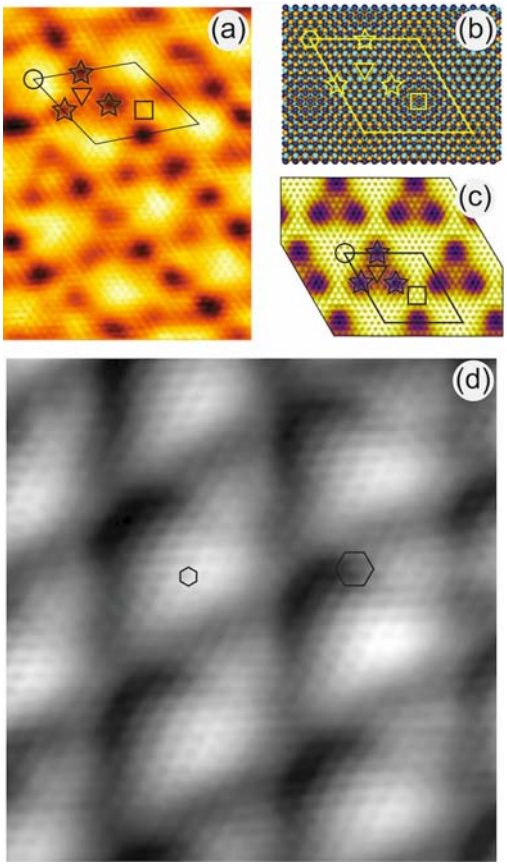

Fig.1. (a) STM image, (b) crystallographic structure, (c) calculated STM image, and (d) NC-AFM image of the graphene layer on Rh(111).

References

[1] A. Geim, Science **324**, 1530 (2009).
[2] J. Wintterlin and M. L. Bocquet, Surf. Sci. **603**, 1841 (2009).

New Tools & Applications

Tu1050 Upgraded

In-situ Characterization of Semiconductor Nanostructure Devices

R. Timm, O. Persson, J. Webb, M. Hjort, C. Thelander, L. Samuelson, and A. Mikkelsen

The Nanometer Structure Consortium, Department of Physics, Lund University
P.O. Box 118, 221 00 Lund, Sweden rainer.timm@sljus.lu.se

Semiconductor nanostructures are of continuously increasing technological importance and will enable superior device application in information technology, optoelectronics, and energy harvesting. Among them, free-standing nanowires are especially promising due to the possibility to combine III-V semiconductor material properties with Si technology [1]. With their small diameter and their very large surface-to-volume ratio, the device behavior of nanowires is strongly determined by their surface structure. However, electrical performance of nanowire heterostructures on the one hand [2] and their local surface properties like atomic structure and local density of states (LDOS) on the other hand [3] could only be studied separately yet.

Here, we go further and present a novel setup correlating local electronic properties across a semiconductor nanostructure interface with simultaneously measured *I-V* data of the same nanostructure device: We are using combined atomic force microscopy (AFM) and scanning tunneling microscopy (STM) and spectroscopy (STS) on individually contacted nanowires for mapping the atomic surface structure and the local band alignment along the nanowire heterostructure under device performance, as sketched in Fig. 1(a).

We show initial results of this unique approach on InAs-GaSb nanowire tunnel diodes [2], where we could prove Esaki behavior of a nanowire (Fig. 1c) while it was investigated by STM/AFM (Fig. 1d). From a set of STS spectra we determined the position of the Fermi level along the nanowire for different applied biases, showing an abrupt drop directly at the material interface (Fig. 1e). In a reverse experiment, we used the STM/AFM tip as local gate and measured the resulting source-drain current through the nanowire for different biases.

In some material systems, however, it is not possible to obtain Ohmic contacts to nanowires by conventional processing techniques, thus making conductivity studies very challenging. For these cases, we have developed an alternative setup where the STM tip is used to first image free-standing nanowires on their growth substrate [4] and then form an Ohmic point contact with the top of the nanowire. We will show examples of this method, measuring the conductivity of individual InP and InAs nanowires as well as the barrier height and ideality factor of Au-GaAs nanowire Schottky barriers.

[1] Wernersson *et al*., Proc. IEEE **98**, 2047 (2010)
[2] Borg *et al*., Appl. Phys. Lett. **101**, 043508 (2012)
[3] Hilner *et al*., Nano Lett. **8**, 3978 (2008);
Hjort *et al*., ACS Nano, *accepted*
[4] Fian *et al.,* Nano Lett. **10**, 3893 (2010)

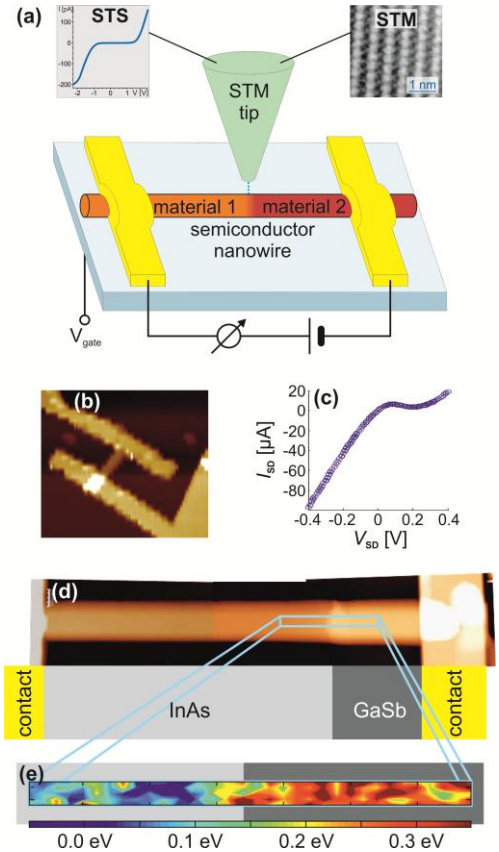

Figure 1: STM/S on nanowire devices: (a) sketch, (b) 3.5 µm x 3 µm AFM image of a contacted nanowire, (c) *I-V* curve of an InAs-GaSb nanowire, (d) 2.6 µm x 0.5 µm AFM image of the same nanowire as measured in (c), and (e) map of the local Fermi level distribution, obtained from various STS spectra, with V_{bias} = 0.3 V applied to the right contact.

Tu1110

Ultrafast Spectroscopy of Intermediate Band Solar Cell Prospects

Roy Clarke[1], Vladimir Stoica[1], Rachel Goldman[1], Jamie Phillips[1], and Richard Schaller[2]

[1]University of Michigan Center for Solar and Thermal Energy Conversion

[2]Center for Nanoscale Materials, Argonne National Laboratory

Intermediate band solar cells (IBSC) have been suggested as a way to improve the efficiency of conventional single-band-gap photovoltaics such as Si and CdTe. The idea is to introduce an additional set of electronic states, the intermediate band (IB), within the gap of the semiconductor so that more of the solar spectrum can be captured while minimizing thermodynamic heat losses. Various approaches to establish an intermediate band have been suggested including the formation of nanostructures, such as arrays of ZnS quantum dots, within the bulk of a semiconductor (e.g., ZnTe), or simply doping the semiconductor (e.g., with oxygen) to sufficient density to form an impurity band. A key question is whether the states in the IB are extended or localized and what is the lifetime of the carriers in these states. These parameters are crucial because, for the IBSC concept to be realized, sequential transitions from valence to IB and IB to conduction band must be achieved efficiently. Ultrafast laser pump-probe spectroscopy is an ideal way to study the characteristics of the IB, including carrier lifetimes, recombination dynamics and absorption cross-sections. We report here new femtosecond spectroscopy results on oxygen doped ZnTe epitaxially grown on GaSb, demonstrating that the IB to conduction band transition is accompanied by a corresponding depletion of the IB population. The pump-probe measurements performed by asynchronous optical spectroscopy are complemented by ultrafast photoluminescence measurements performed at Argonne National Lab's Center for Nanoscale Materials

Proximal probe characterization of thermal conductivity in ErAs/GaAs superlattice grown by molecular beam epitaxy

K. W. Park, H. P. Nair, S. R. Bank, and E. T. Yu*

Microelectronics Research Center, The University of Texas at Austin
10100 Burnet Road, Building 160, Austin TX 78758

Recent years have witnessed intense and growing interest in research addressing thermal transport in a variety of nanostructured materials ranging from semiconductor nanowires to certain types of layered compounds to nanocomposite materials. However, the fundamental understanding of and ability to control thermal transport behavior is at a relatively early stage of development. This arises in part from the difficulty of characterizing thermal transport behavior at the nanoscale, both in nanostructures and in more conventional thin-film or bulk materials. We report here studies in which the 3ω technique for measuring thermal conductivity has been implemented using a functionalized probe in an atomic force microscope.[1] This approach has allowed us to achieve very high spatial resolution in measuring thermal conductivity – ~100nm laterally and ~150nm in depth, limited by the size of the probe tip apex – and, with calibration using materials of known thermal conductivity, quantitative accuracy of approximately ±20% in the range of thermal conductivities of interest in this work.

The sample structure employed in this work was grown on a GaAs (001) substrate by molecular beam epitaxy, and consisted of a GaAs buffer layer grown at 580°C followed by an ErAs/GaAs superlattice consisting of 40 repetitions 0.5ML ErAs/5nm GaAs grown at 450°C. Under these growth conditions, the ErAs layers form 3-4ML (~0.9-1.1nm) high nanoparticles with diameters of ~3nm. Proximal probe measurements were performed under ambient conditions using a functionalized probe in which a thin patterned Pd film on the probe tip served as a localized heater and thermometer. In a manner analogous to the standard 3ω measurement in a thin-film geometry, an electrical excitation signal at frequency ω induces variations in the resistance of the functionalized probe tip, corresponding to changes in its temperature, at frequency 3ω that were detected using a Wheatstone bridge circuit configuration and lock-in amplifier. By modeling the thermal transport between the probe tip apex and the sample, it is possible to extract information about the sample thermal conductivity. Quantitative determination of sample thermal conductivity is possible via a calibration process in which (i) samples of known thermal conductivity, e.g., GaAs, Si, SiO_2, are measured along with the actual sample of interest; (ii) the 3ω component of voltage response is modeled as a function of sample thermal conductivity; (iii) the model is calibrated, with one fitting parameter, to data obtained for samples of known thermal conductivity; (iv) the sample thermal conductivity is obtained from its measured 3ω response and the model calibrated to samples of known thermal conductivity.

Using this approach, we determined the thermal conductivity of the ErAs/GaAs superlattice structure to be 9±2W/m·K, approximately 5× lower than that for GaAs (~50 W/m·K) despite the low (~3%) average concentration of ErAs within the structure. This value is in reasonable agreement with elementary numerical modeling we have performed of the influence of phonon scattering by ErAs nanoparticles embedded in GaAs,[2,3] which predicts thermal conductivities in the range of 15-18 W/m·K. To verify that these measurements were sensitive to the thermal transport properties of only the superlattice structure, and not the underlying substrate, shallow-angle focused ion beam etching was used to fabricate a ramped structure in which the ErAs/GaAs superlattice thickness at the sample surface varied continuously from 200nm to 0nm over a lateral distance of 2000nm. These measurements confirmed that measurements performed at the surface of the original 200nm ErAs/GaAs superlattice structure were sensitive only to the thermal conductivity of the superlattice, and in addition allowed us to determine the depth sensitivity of the proximal probe measurement of thermal conductivity to be ~150nm – considerably better than that for a traditional 3ω measurement, for which the depth sensitivity would be expected to be several tens of μm at typical measurement frequencies.

---

[1] E. Puyoo, S. Grauby, J.-M. Rampnoux, E. Rouvière and S. Dilhaire, *J. Appl. Phys.* **109**, 024302 (2011).

[2] W. Kim, J. Zide, A. Gossard, D. Klenov, S. Stemmer ,A. Shakouri, A. Majumdar, *Phys. Rev. Lett.* **96**, 045901 (2006).

[3] W. Kim and A. Majumdar, *J. Appl. Phys*. 99, 084306-1-7 (2006).

* Author contact information:
Edward T. Yu, The University of Texas at Austin, Austin, TX 78758. ety@ece.utexas.edu

Tu1120

Atom Probe Tomography: Applications to Interfaces

D.J. Larson[1], V.S. Smentkowski[2], K. Inoue[3], D.A. Reinhard[1], T.J. Prosa[1], D. Olson[1], D. Lawrence[1], P.H. Clifton[1], R. M.Ulfig[1], I. Martin[1], D. Snoeyenbos[1] and T.F. Kelly[1]

[1]Cameca Instruments Inc., 5500 Nobel Drive, Madison, WI 53711 USA
[2]General Electric Global Research Center, Niskayuna, NY 12309 USA
[3]Institute for Materials Research, Tohoku University, JAPAN

Atom probe tomography (APT) has been used for over 45 years, "to determine the composition of small volumes of metals, semiconductors, and some ceramics" [1]. Although this statement is still true some 12 years after it was written, it does not adequately capture the recent expansion and maturation of APT into non-metallurgical applications. Historically, the low analysis success rate in non-metallurgical applications has limited the utility of the technique for such materials. However, recent innovations have been shown to provide substantially higher analysis yield on a wide variety of materials [2] enabling a range of meaningful new applications of APT such as quantum wells (QWs) and transistors. Defects are known to have a significant effect on properties of InGaN multi-quantum-well devices [3]. The availability of low-pulse-energy laser pulsing has allowed for high-quality and low-noise imaging of a V defect centered on a threading dislocation, below left. This defect deleteriously affects the local properties of the QWs due to the significant compositional perturbations and resultant segregation/depletion of magnesium dopants. Characterization of complicated microelectronic structures, such as transistors, which contain a variety of materials and interfaces, has been severely limited because of analysis yield limitations. The recent introduction of UV laser pulsing using a highly focused, diffraction-limited spot has provided improved yield allowing for routine analysis of real devices such as the n- and p-MOS transistors shown below right.

In addition to the above examples of light-emitting diode [4] and microelectronics [5,6] applications, examples of APT applications advances in solar cells [7,8], and geology [9] will also be presented. These examples will illustrate one of the greatest applications areas for APT: buried interfaces.

[1] M.K. Miller, Atom Probe Tomography: Analysis at the Atomic Level, Kluwer Academic /Plenum Publishers (2000) p.2.
[2] R.M. Ulfig et al., *Microscopy and Microanalysis* 17(S2) (2011) 714.
[3] C.J. Humphreys et al., *Springer Proc. Physics* 120 (2007) 3.
[4] T.J. Prosa et al., *Applied Physics Letters* 98 (2011) 191903.
[5] D.J. Larson et al., *Inst. Phys. Conf. Series* 326 (2011) 012030.
[6] H. Takamizawa et al., *Applied Physics Letters*, 99 (2011) 133502.
[7] P.P. Choi et al., *Microscopy Today* 20(3) (2012) 18.
[8] D.J. Larson et al., *Microscopy & Microanalysis* (2012) 18(S2) (2012) 928.
[9] D. Snoeyenbos et al., *22nd Goldschmidt Conference on Geochemistry* (2012), submitted.

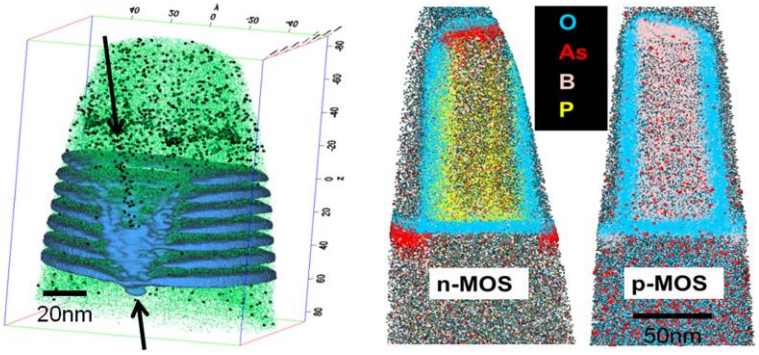

Left) InGaN multi-quantum well dislocation defect (green=GaN, black=Mg, blue=In>0.25 at.% iso-composition surface). Right) Atom maps for a pair of transistors with oxide (blue) and dopants (red=As, yellow=P) visible.

Tu1125

Atom Probe Tomographic Analysis of InGaN Quantum Wells and GdN Nanoislands in GaN

J. R. Riley[1], T. Detchprom[2], T. F. Kent[3], R. C. Myers[3], C. M. Wetzel[2], and L. J. Lauhon[1]

1. Dept. of Materials Science and Engineering, Northwestern University
2. Smart Lighting Engineering Research Center, Future Chips Constellation, Dept. of Physics, Applied Physics, and Astronomy, Rensselaer Polytechnic Institute
3. Dept. of Materials Science and Engineering, Dept. of Electrical and Computer Engineering, The Ohio State University

Gallium nitride and related alloys are materials of rapidly increasing importance in existing and emerging device technologies. For example, InGaN shows great promise as a basis for efficient solid-state lighting, and epitaxial GaN/ferromagnetic heterostructures are being explored for application in spin-based devices. In both cases, knowledge of the distribution of the alloying elements is essential to optimizing growth processes and developing quantitative and correct models of materials properties and device performance. Here we apply atom probe tomography (APT) to analyze the distribution of alloying elements in three dimensions, providing important structural information that has not been revealed by other analysis techniques. Pulsed laser atom probe analysis was carried out with a Cameca LEAP4000x system in the NUCAPT facility at Northwestern University. The samples were analyzed using 0.01 pJ laser pulse energy, 200 kHz laser pulse repitition rate, and 27 K base temperature.

3 nm InGaN quantum wells were grown between 20 nm GaN spacer layers by MOCVD [1,2] on c-axis oriented GaN. Ga (0001) planes were observed in APT spatial distribution maps and used in the reconstruction to achieve excellent agreement with x-ray diffraction measurements of layer spacing. The APT analysis reveals that not all quantum wells are continuous (Figure 1a,b). In addition, the In distribution within the quantum wells exhibits fluctuations that are larger than expected from a random alloy (Figure 3c). Electroluminescence measurements show a peak emission wavelength of 529 nm, and an x-ray diffraction analysis reveals an InN-fraction of 10% for these typical c-plane quantum wells. For comparison, the average In QW concentration is 8.5–12 at.% by APT. However, 35% of the volume of the quantum well has a composition of greater than 12 at.% In, highlighting the need for 3-D composition analysis to properly account for the nature of emission in these devices.

APT was also used to analyze the distribution of Gd in GaN thin films grown by molecular beam epitaxy. GdN islands were formed by depositing the equivalent of 2.4 monolayers of GdN under conditions that enable Gd diffusion and GdN island self-assembly. The presence of islands was confirmed by cross-sectional transmission electron microscopy and x-ray diffraction. APT measurements revealed additional features in the Gd distribution (Figure 2). One-dimensional composition profiles (not shown) of the reconstruction shown in Figure 2a revealed that the GaN spacer layers are doped with 0.5% Gd. In addition to islands, we observe the formation of $Ga_{0.485}Gd_{0.005}N$ layers in regions where island formation is not complete. In island free layers, the Gd distribution is consistent with that of a random alloy (Figure 2b). We also observe long-range atomic ordering of Gd along the growth axis, which was recently reported by another group [4]. A comparison of APT and SQUID magnetometry measurements suggest that there are multiple magnetic phases corresponding to regions of the sample with distinct Gd concentrations and distributions.

[1] T. Detchprohm, M. Zhu, W. Zhao, Y. Wang, Y. Li, Y. Xia and C. Wetzel. Phys. Status Solidi C 6, (S2), S840–S843 (2009). [2] M. Zhu, S. You, T. Detchprohm, T. Paskova, E. A. Preble, and C. Wetzel, Phys. Stat. Sol. A 207(6), 1305–1308 (2010). [3] Kent et al, *Appl. Phys. Lett.* **100**, 152111 (2012). [4] Ishimaru et al, *Appl. Phys. Lett.* **101**, 101912 (2012).

Tu1130

Imaging 'Invisible' Dopant Atoms in Semiconductor Nanocrystals

A.A. Gunawan[1], A.W. Wills[2], M.G. Thomas[3], D.J. Norris[4], K.A. Mkhoyan[1]

[1]*Department of Chemical Engineering and Materials Science, University of Minnesota, Minneapolis, MN 55455*
[2]*Department of Chemistry, University of Minnesota, Minneapolis, MN 55455*
[3]*Cornell Center for Materials Research, Cornell University, Ithaca, NY 14853*
[4]*Optical Materials Engineering Laboratory, ETH Zürich, 8006 Zürich, Switzerland*

Electronic devices have long relied on the intentional incorporation of impurities, or dopants, to control semiconducting materials. As the size of these devices shrink, nanometer-scale volumes of semiconductor can contain only a few impurity atoms, presenting new possibilities for doped nanostructures. In particular, solotronic devices now aim to exploit solitary dopants in a semiconductor to obtain new electronic, magnetic, and optical capabilities. However, in doped nanostructures, statistical fluctuations in the number and position of the impurities can have a dramatic effect on the overall behavior. Thus, the ability to locate the dopants through atomic-scale visualization is often critical for understanding the physics of these materials. For example, identification of the lattice sites of dopant atoms in lightly doped complex oxide thin films can be critical for understanding their unusual transport behavior.
Only a few techniques allow imaging of a single dopant within a semiconductor.

Scanning transmission electron microscopy (STEM) has potential, especially with the resolution achievable with aberration-correction. A highly focused electron beam is scanned across the sample while scattered electrons are collected with an annular dark-field (ADF) detector. This allows high-resolution images with atomic-number (Z) contrast to be obtained. Indeed, single dopants within a crystalline semiconductor have been imaged with the ADF-STEM approach [1]. An atomic column that contains an impurity appears with slightly different contrast in the image. However, despite its success, this approach suffers from a fundamental limitation. The dopant must have a large Z-contrast with the surrounding semiconductor atoms to ensure its visibility. Other methods are needed for the many cases when this condition is not satisfied, including doped semiconductor nanocrystals.

We combine electron energy loss spectroscopy (EELS) with ADF-STEM to image individual Mn impurities inside ZnSe nanocrystals. While Mn is invisible to conventional ADF-STEM in this host, our experiments and detailed simulations show consistent detection of Mn [2]. Thus, a general path is demonstrated for atomic-scale imaging and identification of individual dopants in semiconductors nanostructures. The results indicate that STEM-EELS presents a technique for imaging individual dopants in semiconductor nanostructures. It should be broadly applicable to the many impurities that have a suitable EELS edge, typically those with energy less than 1 keV.

[1] P. M. Voyles et al., *Nature,* **416** (2002) 826.
[2] A. A. Gunawan et al., *Nano Letters,* **11** (2011) 5553.

Tu1135 Upgraded

Abstract: **Non-contact electrical measurements at selected inner sites and interfaces**

H. Cohen, Weizmann

The inability of existing electrical tools to probe selected *inner* domains is a critical problem in device characterization and nanoscale fundamental studies. In particular, measuring internal junction fields is essential for realistic construction of band diagrams and device optimization. An answer to this problem is provided by chemically resolved electrical measurements (CREM),[1,2] an essentially non-contact technique that extracts electrical information from x-ray ejected photoelectrons. Applied to multi-interfacial solar cells, key features of the CREM methodology are introduced, including detailed evaluation of the internal fields and band offsets and, furthermore, the quantification of internal dynamic distortions under external stimuli. Problem solving gained by this improved feed-back tool is demonstrated.

Approaching *atomic-scale* electrical information,[3] CREM further proposes useful advantages for molecular-based systems. In a combined CREM plus transistor device study of bio (protein) monolayers, site-dependent transport controllability is demonstrated via targeting small 'dopant' molecules to a specific protein site. Remarkable details of the leading transport mechanisms across the single protein molecule are thus revealed.

The above capabilities, together with additional features unique to CREM, to be briefly described, present a highly attractive tool, relatively simple and commonly available to a broad research community.

1. I. Doron Mor, A. Hatzor, A. Vaskevich, T. van-der Boom-Moav, A. Shanzer, I. Rubinstein, H. Cohen, *Nature* **406**, 382 (2000)
2. H.Cohen, *Appl. Phys. Lett.* **85**, 1271-3 (2004).
3. Neta Filip-Granit et al., *Nano Lett.* **6**, 2848-51 (2006).

Tu1155

Resonant Coupling For Contactless Measurement of Materials Parameters.

R. K. Ahrenkiel [1,2], S. W. Johnston[1], and A. Feldman[2]
1. National Renewable Energy Laboratory, Golden, CO
2. Colorado School of Mines, Golden, CO.

A contactless method is very desireable in that the material under test is not contaminated or degraded by the measurement. This principle is applicable to both conventional inorganic and organic or biological materials. We have developed a technique for measuring the transport properties and recombination kinetics of semiconductors and photoconductors [1]. Our technique is called resonance-coupled photoconductive decay (RCPCD) and was developed [2,3,4] at the National Renewable Energy Laboratory (NREL). The technique provides the rapid measurement of recombination lifetimes and these data are of vital importance to a wide range of optoelectronic technologies. In the medical field, a group of workers has developed a similar technique [5] to measure the intraocular pressure (IOP) of the human eye using a MEMS device that is attached to the eye. The operating frequency of all of the above devices is about 350 to 450 MHz.

The basic principle of operation can be described by the impedance of a series resonant RLC circuit of very high quality factor, Q. The resonant frequency ω_0 is a well known function of R, L, and C and the frequency is changed markedly by a small change of any of the above parameters. The material under test can undergo small changes in complex dielectric constant that will shift the resonant frequency significantly when Q is large. The operating frequency is chosen to be at the points of maximum slope on the impedance-frequency curve of the RLC circuit. However, the response time increases as 2LQ/sqrt(LC) so a compromise must be reached between the latter and sensitivity. The circuit may be active and incorporated into an oscillator circuit or passive and incorporated into a detector circuit. For the semiconductor measurements, the sample photoconductivity is varied by an external light source producing the desired changes in sample conductivity.

For carrier lifetime measurements, we use the frequencies of 400 to 450 MHz, which completely penetrate most semiconductor wafers with common doping levels. This provides depth probes of of standard (300 to 400 μm) samples thicknesses. Depth profiles may be performed by varying the optical excitation wavelengths. The method is very linear in sample conductivity, and we have measured a linear response over more than three orders of magnitude of carrier concentration. This attribute allows us to measure the carrier recombination lifetime over many decades of injection level. We have applied RCPCD to more than several thousand samples, ranging from small-area thin films and carbon nanotubes to 350-μm-thick, 250-mm-diameter silicon wafers. In addition, the lifetimes in semiconductor ingots of irregular shape have been successfully measured as no particular size or shape is needed. The technique has been especially successful in measuring some small-band semiconductors such as InAs and mismatched InGaAs grown on InP substrates. Here, we will discuss results and other possible applications of the resonant coupling technique.

---

1. R. K. Ahrenkiel and S. W. Johnston, Materials Science and Engineering **B102**,161172(2003).
2. U. S. Patent 5,929,652, Richard Ahrenkiel, July 27, 1999.
3. U. S. Patent 6,275,060, Richard Ahrenkiel and Steven Johnston, August 14, 2001.
4. U. S. Patent 6,369,603, Steven Johnston and Richard Ahrenkiel, April 9, 2002.
5. P. J. Chen et al, J. Microelectromech. Syst. **19**, 721-734 (2010).

Tu1200

Consequences of the simplified bond hyperpolarizability model for second harmonic generation for diamond and zincblende semiconductors*

Benedikt Pesendorfer,[1] Hendradi Hardhienata†,[2,1] David Stifter,[2,1] and Kurt Hingerl[1]

[1] *Center for surface- and nanoanalytics, Johannes Kepler University, Altenbergerstr. 69, 4040 Linz, Austria*
[2] *Christian Doppler laboratory for microscopic and spectroscopic material characterization, Johannes Kepler University, Altenbergerstr. 69, 4040 Linz, Austria*

Among various surface techniques second-harmonic-generation (SHG) has been considered as a powerful optical surface diagnostic tool due to its nondestructiveness, and its compatibility with many industrial processes. However, there is a lack of understanding the measured data, mainly because surfaces, in their full complexity, are described by 3^{rd} rank tensors, with up to 27 complex components. In a series of papers Aspnes *et. al.*[1–4] have argued consistently that azimuthal measurements of rotated samples can be described by the so called simplified bond-hyperpolarizabilty model (SBHM). The first major finding was that the then available SHG data for Si(111) could be well fitted by just using two complex parameters, the "up" hyperpolarizibility used for the up bond and the "down" hyperpolarizibility used for the three downward pointing bonds. Just using these two complex parameters is a major advantage compared to a phenomenological description by a third rank χ^2 tensor. Later on the model was critizised and was tested against experiment by using Si(111) with different offcut directions and different offcut magnitude.[5]. It turned out that the influence of steps due to the miscut is important. In our understanding this counter- argument is not fair, because it is well known that steps induce a major effect for the Si(111) case[6] and therefore at least a third parameter should be added, only describing the C_2 rotational symmetry of samples with steps. In a response to this paper Adles and Aspnes[3] included effects like retardation, spatial-dispersion, and magnetic effects, proportional to quadrupole contributions in addition to the anharmonic restoring force acting on the bond charge. This inclusion, however, enhances the number of freely fitable parameters and its strictness and simplicity is thereby lost.

We employ the model in its original form with the help of a computer algebra system and recalculate the s- and p- polarized radiated dipole fields for Si(111) surfaces, correcting a typographical error in one of the published terms. Furthermore we provide as a simple extension for single and double domain Si(001) surfaces their respective azimuthal SHG dependence, assuming that no surface reconstruction is present. Contrary to the original work, however, we stress the importance of summing up all *eight* bonds within the unit cell, especially for obtaining the correct result for Si(011). Also contrary to ref.[3] we point out that spatial dispersion in crystals with a single atom basis cannot be present. As an example spatial dispersion effects in metals with either pc, bcc or fcc structure have to vanish. For completeness we also list the SHG response of (unreconstructed) bcc and fcc structures and it is shortly discussed, how reconstructed surfaces can be treated with an *ad-hoc ansatz* for the hyperpolarizibilities. Finally, we apply Huygens principle for SHG, which leads, by considering the phase relation between the fundamental field and the coherently driven SHG field originating at the atomic dipoles to a considerable simplification of the results, showing that SHG radiation of a stratified layer is only allowed into one transmission and reflection direction. Finally we propose a phase sensitive measurement capable of testing the major approximation of the SBHM saying that the charges are only allowed to move along the bond direction.

---

* email: kurt.hingerl@jku.at

[1] G. D. Powell, J.-F. Wang, and D. E. Aspnes, Phys. Rev. B **65**, 205320 (2002).
[2] H. J. Peng, E. J. Adles, J.-F. T. Wang, and D. E. Aspnes, Phys. Rev. B **72**, 205203 (2005).
[3] E. J. Adles and D. E. Aspnes, Phys. Rev. B **77**, 165102 (2008).
[4] B. Gokce, E. J. Adles, D. E. Aspnes, and K. Gundogdu, PNAS **107**, 17503 (2010).
[5] J. F. McGilp, Journal of Physics: Condensed Matter **19**, 016006 (2007).
[6] C. W. van Hasselt, M. A. Verheijen, and T. Rasing, Phys. Rev. B **42**, 9263 (1990).

† on leave from Theoretical Physics Division, Institut Pertanian Bogor, Indonesia

Tu1205

Bulk dipole contribution to second harmonic generation in diamond lattices

Hendradi Hardhienata,[1,2] David Stifter,[1,2] and Kurt Hingerl[2]

[1]*Christian Doppler laboratory for microscopic and spectroscopic material characterization, Johannes Kepler University, Altenbergerstr. 69, 4040 Linz, Austria*

[2]*Center for surface- and nanoanalytics, Johannes Kepler University, Altenbergerstr. 69, 4040 Linz, Austria*

The recent high interest in surface science techniques capable to probe surfaces *in-situ* has renewed the interest in linear and nonlinear optical techniques such as second harmonic generation (SHG). This interest has been accompanied by theoretical efforts to model the measured data, interpreting them either in a classical picture or taking into account quantum mechanics by involving transitions between initial and final states.[1] Especially for SHG the interpretation and the origin of the data is controversial. Some authors[2] claim that part of the SHG response arises from the surface and bulk quadrupoles or from magnetic dipole effects, whereas others[3] are mainly considering surface contributions. To our knowledge, however, all the literature has up to now neglected bulk dipole transitions in materials with inversion symmetry[4,5] using the following argument: Materials with inversion symmetry are described by potentials with even powers of the coordinates (i.e. $\vec{r}^2$, $\vec{r}^4$, etc.). Because a second harmonic contribution providing response to an incident field oscillating with frequency ω could origin, due to inversion symmetry, only from forces which are quadratic, or potentials which are cubic in a component of $\vec{r}$, this effect has been directly excluded.

To our knowledge it has never been discussed in the context of SHG that the potential of atoms in the diamond structure is, due to their tetrahedral bonding, intrinsically inversion asymmetric. This asymmetry can be observed, e.g., by plotting the potential within in the (111) plane - i.e. in the plane of the polarization of the driving field- as equi-contour plot. (Fig.1c).

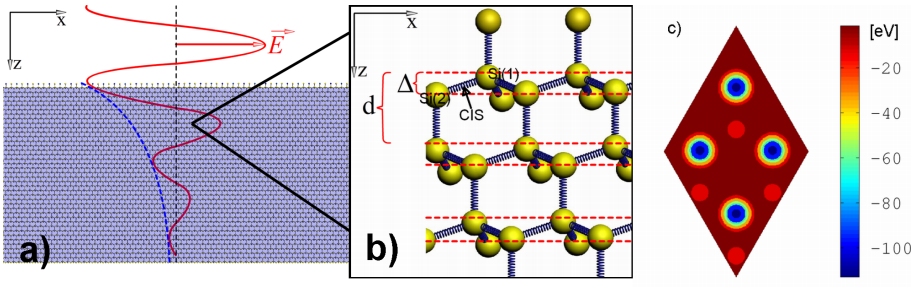

FIG. 1: a) The incoming electric field decays along the propagation direction. b) Layers are shown where one Si atom (Si(1)) is covalently bound to one from above and to three Si atoms underneath, where one is called Si(2). The center of inversion symmetry (CIS) is located in the middle between Si(1) and Si(2). c) Contour plot of the *ab-inito* potential for Si in the (111) plane (VASP calculation).

Si(111), respectively its atoms, can be described in a simple picture by four equivalent covalent bonds with a sequence of layers, which are alternatingly bound by one up bond or by three down bonds to the next layer (see FIG. 1b). For our model it is insignificant, if we imagine the bonds either as rigid, such that the electrons can only move along the bond direction[6] or as sp^3-hybridized orbitals[7], or as extended coherent wavefunctions, describing the probability density for finding the electron in a given spatial interval. **Because the exciting field decays along z due to absorption when penetrating into the bulk,** the nonlinear radiation of the Si(1) atom **is not fully canceled** by the radiation of the deeper in the bulk positioned atom Si(2), because this atom experiences a lower field. So, in the antenna picture for the Si (111) case the two waves, originating at Si(1), respectively Si(2) do not fully destructively interfere. It has to be mentioned that even for the case that the photon energy is smaller than half the bandgap, the occurrence of SHG implies absorption of the linear wave. This effect occurs at each bilayer and can be analytically summed. Finally we propose an experiment, exploiting the different dispersion for the fundamental as well as frequency doubled radiation to determine this effect.

---

[1] J. F. McGilp. *Journal of Physics: Condensed Matter*, 22(8):084018, 2010.
[2] P. Guyot-Sionnest and Y. R. Shen. *Phys. Rev. B*, 38:7985–7989, 1988.
[3] M. Corvi and W. L. Schaich. *Phys. Rev. B*, 33:3688–3695, 1986.
[4] R. W. Boyd. *Nonlinear Optics*. Academic Press, 2003.
[5] Y. R. Shen. *Nature*, 337:519–525, 1989.
[6] G. D. Powell, J.-F. Wang, and D. E. Aspnes. *Phys. Rev. B*, 65:205320, 2002.
[7] J. E. Mejia, C. Salazar, and B. S. Mendoza. *Revista Mexicana de Fisica*, 50(2):134–139, 2004.

Tu1210

Comparison of Cathodoluminescence, imaging micro-photoluminescence and Confocal Photoluminescence Microscopy for Determination of Interfacial Defect Densities in Semiconductors

O.C. Noriega,[1] A. Savage, [2] J. Chai[2] K.-K. Lee,[2] K. Doyle,[2] C. Smith,[1] N. Chau,[1] J. Pena,[1] A. Dedigama,[2] J.H. Dinan,[2] T.H. Myers[2],

[1] *Department of Physics,[2] Material Science, Engineering, and Commercialization Program, Texas State University-San Marcos, TX 78666, USA*

It can be argued that dislocation density is the single most important characteristic of epitaxial layers intended for optoelectronic device applications, particularly true for devices that require long minority carrier lifetimes of which infrared detectors are a classic example. The relationship between the responsivity of photovoltaic detectors and minority carrier lifetime in the epilayer has been well documented. The direct dependence of lifetime on dislocation density completes this link. Defects can also dominateThe classic method of measuring dislocation density is to dip a wafer or epilayer in a chemical etchant tailored to produce an etch pit at the intersection of a dislocation with the surface. The measurement of dislocation density then becomes a measurement of etch pit density (EPD). For conventional materials such as Si, GaAs, and even HgCdTe, recipes for generating etch pits are commonplace. For other materials, dislocation etching is not as reliable or well-established. Determining the efficacy of a given dislocation etch also requires extensive correlation between dislocations measured by other techniques, such as transmission electron microscopy (TEM), and the measured EPD. Finally, defect etching is difficult to use for evaluating interfacial defects.

Cathodoluminescence (CL) has been shown to be an effective tool for measuring dislocation density. CL generated by the electron beam in an SEM can be detected and images of CL intensity can be obtained. Dislocations that intersect interfaces strongly reduce the intensity of the intrinsic CL. Dark spots correspond to reduced CL associated with a threading dislocation. In addition, this technique measures other non-radiative features such as precipitates or inclusions. Both dislocation etching and CL have drawbacks, particularly in a production environment. Dislocation etching actually destroys the surface through etching, requiring a repolish or other further processing. CL involves inserting the sample into an SEM environment and exposing it to an electron beam, involving significant handling and potential for damage or contamination. In addition, the deep penetration of the electron beam can result in the inability to accurately image interfacial dislocation density.

We are investigating the use two types of photoluminescence (PL) mapping to measure non-radiative defects (in principle equivalent to EPD) at interfaces between semiconducting materials, and correlate the measurements with CL. The primary impetus is to develop an optical technique that can be used without degrading sample surfaces while producing accurate dislocate densities. The first approach is imaging microPL, where a microscope equipped with appropriate camera is used to directly image the PL from the laser through the microscope objective. Again, dark spots in the image indicate dislocations and other non-radiative defects. While viable, we have had issues with resolution due to laser inhomogenaity and due to the fact that we are collecting PL scattered within the sample along with the direct PL. Confocal microscopy (c-PL), on the other hand, is a point mapping PL measurement where the microscope is operated in an optical configuration that significantly enhances both lateral and depth resolution and returns crisp PL images with high contrast. This technique revolutionized fluorescent imaging in biology, and has the potential to become an important semiconductor interface characterization tool. We will present a direct comparison of CL, micro-PL and c-PL on various semiconductor samples. We will illustrate the utility of each technique while contrasting the strengths and weaknesses. Figures 1-3 on the following page illustrates results measured by the three techniques on the same samples illustrating the formation of dislocations at the ZnTe/GaSb interface due to exceeding the critical thickness.

Topological Insulators I

Tu1930 Upgraded

Topological insulators: an overview of experimental progress

Nitin Samarth
The Center for Nanoscale Science and Department of Physics, The Pennsylvania State University, University Park, Pennsylvania 16802-6300, USA

The influence of spin-orbit coupling on bulk electronic band structure [1] forms the basis for many phenomena of relevance to semiconductor spintronics [2]. Early theoretical work showed how spin-orbit coupling can also be used to engineer a band inversion with very profound effects on the two dimensional interface states of a compositionally modulated semiconductor, yielding a massless Dirac spectrum in heterostructures of (Pb,Sn)Te and (Hg,Cd)Te [3]. This physics has experienced a rebirth in the more contemporary context of "topological insulators," driven by a recognition of connections between surface or edge states and topological invariants [4]. I will survey experimental progress in the study of three dimensional topological insulators such as Bi_2Se_3 that ideally have gapped bulk states and metallic surface states with a spin textured Dirac cone dispersion created by the spin-momentum coupling. These surface states are revealed in spin- and angle-resolved photoemission spectroscopy dispersion [6], while scanning tunneling spectroscopy shows evidence for the suppression of backscattering [7]. I will address recent advances in electrical transport measurements [8] probing topological insulator states, and describe progress towards epitaxial heterostructures [9] and other configurations that interface topological insulator surface states with superconductivity [10,11] and ferromagnetism [12-14].

[1] Spin-Orbit Coupling Effects in Two- Dimensional Electron and Hole Systems, R. Winkler, Springer Tracts in Modern Physics (Springer, Berlin, 2003).

[2] D.D. Awschalom and N. Samarth, Physics **2**, 50 (2009).

[3] B. A. Volkov and O. A. Pankratov, JETP Lett. **42**, 178 (1985).

[4] M. Z. Hasan and C. L. Kane, Rev. Mod. Phys. **82**, 3045 (2010); X. -L. Qi and S. -C. Zhang, *ibid* **83**, 1057 (2011).

[6] D. Hsieh *et al.*, Nature (London) **460**, 1101 (2009).

[7] P. Roushan *et al*. Nature (London) **460,** 1106 (2009).

[8] J. G. Checkelsky *et al.*, Phys. Rev. Lett. **106**, 196801 (2011).

[9] A. Richardella *et al.*, Appl. Phys. Lett. **97**, 262104 (2010).

[10] Duming Zhang *et al.*, Phys. Rev. B **84**, 165120 (2011).

[11] B. Sacepe *et al*. Nat. Comm. **2**, 575 (2011).

[12] S. Y. Xu *et al.* Nat. Phys. **8**, 616 (2012);

[13] D. M. Zhang *et al.* Phys. Rev. B **86**, 205127 (2012).

[14] J. G. Checkelsky *et al.*, Nat. Phys. **8**, 729 (2012).

Tu1950 Invited

Topological quantum computing with Majorana particles

Roman Lutchyn, Station Q, Microsoft Research

Abstract:
Research in quantum computing has offered many important new physical insights as well as the potential of exponentially increasing the computational power that can be harnessed to solve important problems in computer science, physics, mathematics and material science. The largest fundamental barrier to building a scalable quantum computer is errors caused by decoherence. Topological quantum computing evades this barrier by exploiting topological materials that by their nature limit errors. I will discuss how to realize a topological superconductor in the laboratory by exploiting the properties of an interface between a semiconductor and an s-wave superconductor. I will show that the non-trivial topological superconducting state emerging in such a system supports Majorana zero-energy modes. The unique properties of Majoranas can be exploited for implementing fault-tolerant quantum computation schemes that are inherently decoherence-free.

Tu2020 Invited

Transport properties of magnetically doped topological insulator films

Yayu Wang

Department of Physics, Tsinghua University, Beijing 100084, China

Topological insulators (TI) are a new class of quantum materials with topologically nontrivial band structures originated from strong spin-orbit coupling. The surface states of three-dimensional TIs have a spin-helical, massless Dirac-like dispersion and are thus robust against time reversal invariant perturbations. These unique properties make the TIs ideal candidates for novel spintronic and quantum computational applications. Breaking the time reversal symmetry (TRS) in TIs has been predicted to create a variety of exotic topological magnetoelectric effects such as the image magnetic monopole and quantized anomalous Hall effect. Therefore, the magnetically doped topological insulators have quickly emerged as a new low dimensional magnetic system with both fundamental interests and application potentials.

In this talk we report transport properties of magnetically doped TI ultrathin films grown by molecular beam epitaxy (MBE). In the Bi_2Se_3 films doped with Cr, no ferromagnetism is observed, but the quantum transport behavior of the TIs is strongly altered. There is a systematic crossover from weak antilocalization (WAL) to weak localization (WL) induced by magnetic doping. We show that the evolution from WAL to WL indicates the transformation of the system from a topologically nontrivial TI to a topologically trivial dilute magnetic semiconductor. In a new ternary TI system $(Bi_{1-x}Sb_x)_2Te_3$ with depleted bulk carriers, Cr dopants induce a long-range ferromagnetic ordering. More interestingly, the ferromagnetism exists both in the presence of hole- and electron-type Dirac fermions with widely varied carrier concentrations. The carrier-independent ferromagnetism in TIs is consistent with the Van Vleck mechanism mediated by the band electrons. This picture is further supported by recent observations a topology-driven magnetic quantum phase transition, in which ferromagnetic ordering is strongly favored by the nontrivial bulk band topology. These results demonstrate the manipulation of the topological band structure and quantum transport properties of the TIs by TRS-breaking perturbations, and pave the road for realizing the proposed topological quantum effects.

Wednesday

We0730	Registration and Continental Breakfast
We0830	Wednesday Morning Session: Topological Insulators II
We0945	Coffee Break and Poster Viewing
We1045	Wednesday Morning Session: Spintronics Inorganic & Organic
We1210	Lunch and Poster Viewing
We1330	Wednesday Afternoon Session: Nanowire Growth & Strain Effects
We1445	Coffee Break and Poster Viewing
We1515	Wednesday Afternoon Session: Epitaxy & Graphene I
We1700	Conference Banquet Luau

Topological Insulators II

Angle-Resolved Photoemission Spectroscopy of Correlated Oxide Interfaces and Thin Films

Kyle M. Shen, Eric J. Monkman, John W. Harter, Daniel E. Shai, Yuefeng Nie, Philip D. King, Masaki Uchida, Carolina Adamo, Alex J. Melville, Luigi Maritato, David A. Muller, Darrell G. Schlom

Departments of Physics, Materials Science & Engineering, Applied & Engineering Physics, and the Kavli Institute for Nanoscale Science
Cornell University
Ithaca NY, 14853, USA

Engineering interfaces between complex oxides has proven to be a powerful technique for tuning their electronic and magnetic properties. To fully understand how these interfaces can control these electronic properties, one requires advanced spectroscopic tools to uncover their electronic structure. Angle-resolved photoemission spectroscopy (ARPES) is the leading tool for probing energy and momentum resolved electronic structure. To understand the physics of these complex oxide interfaces, we have developed an approach which combines state-of-the-art oxide molecular beam epitaxy with high-resolution ARPES.

As one example, I will describe our work on digital manganite superlattices ($[LaMnO_3]_{2n}$ / $[SrMnO_3]_n$), comprised of alternating $LaMnO_3$ and $SrMnO_3$ blocks. Our ARPES measurements reveal that by controlling the separation between the $LaMnO_3$-$SrMnO_3$ interfaces, we can tune the effects of the quasiparticle interactions, driving the interfacial states from a 3D ferromagnetic metal, to a 2D polaron liquid, and finally to a pseudogapped ferromagnetic insulator.

I will also describe some of our work on thin films on novel magnetic materials including spin-polarized $Eu_{1-x}Gd_xO$ and the *4d* ferromagnet $SrRuO_3$. I will also describe our recent work on the "infinite layer" cuprate $Sr_{1-x}La_xCuO_2$, which we can stabilize epitaxially, allowing us to address fundamental issues regarding the asymmetry between doping electrons and holes in the high-Tc cuprates, as well as our work on the quasi-2D analogue of $SrTiO_3$, carrier-doped Sr_2TiO_4.

We0900 Upgraded

Limits to Coherent Electronic Transport in Bi_2Se_3 in the Topological Regime

Dohun Kim[1], Qiuzi Li[2], Paul Syers[1], Nicholas P. Butch[1], Johnpierre Paglione[1], S. Das Sarma[1,2], and Michael S. Fuhrer[1]

[1]*Center for Nanophysics and Advanced Materials, Department of Physics, University of Maryland, College Park, MD 20742-4111, USA*
[2]*Condensed Matter Theory Center, Department of Physics, University of Maryland, College Park, MD 20742-4111, USA*

ABSTRACT

Bi_2Se_3 is a three-dimensional strong topological insulator (TI) which exhibits a metallic two-dimensional surface state with a Dirac electronic spectrum, and is of interest for novel topological electronic, spintronic, and optoelectronic devices. We have probed the limits to topological electronic transport in the surface state of Bi_2Se_3 set by (1) electron-acoustic phonon scattering, and (2) tunneling between top and bottom topological surfaces of a thin film. Experiments are performed on thin exfoliated Bi_2Se_3 in the absence of bulk conduction (topological regime) achieved by charge transfer *p*-type doping with 2,3,5,6-tetrafluoro-7,7,8,8-tetracyanoquinodimethane (F4TCNQ) organic molecules. When the gate-tuned chemical potential is near the Dirac point the carrier density is strongly temperature dependent reflecting thermal activation from the nearby bulk valence band, while unipolar *n*-type surface conduction is observed above the Dirac point with negligible contribution of bulk carriers. In this regime linear resistivity vs. temperature reflects intrinsic inelastic electron-acoustic phonon scattering in the topological surface states. Quantitative comparison with a theoretical transport calculation including both phonon and disorder effects gives the ratio of deformation potential to Fermi velocity $D/\hbar v_F = 4.7$ Å^{-1} , which gives an intrinsic limit for the conductivity at room temperature of ~550 μS per surface, corresponding to a mean free path $l \approx 5\lambda_F$ where λ_F is the Fermi wavevector. The results set strong limits on the observation of topological effects in Bi_2Se_3 requiring coherent electronic transport at room temperature.

At cryogenic temperatures where phonons are frozen, we observe clear signature of 2D weak anti-localization (WAL) behavior in the low field magneto transport, which stems from topological surface states. By investigating gate-tuned WAL behavior in devices ranging in thickness from 5 to 17 quintuple layers, we tune the inter-surface tunneling time determined by the surface hybridization-induced energy gap. The thickest devices show WAL consistent with two decoupled topological surfaces. As the devices become thinner, the tunneling time decreases and we identify two crossovers: when the tunneling time becomes shorter than the phase coherence time, we observe WAL for a single 2D system (coherently coupled top and bottom states), and at an even smaller thicknesses the hybridization gap becomes large enough that topological order is lost altogether and WAL disappears for small chemical potentials. The results can be used to understand the regimes of temperature and film thickness in which topological coherent transport can be observed.

We0920

Periodic conductance fluctuations in Bi_2Se_3 channels with self-organized, correlated surface morphology

A. Kandala, A. Richardella, D. M. Zhang, T. Flanagan, N. Samarth
Center for Nanoscale Science and Dept. of Physics, Pennsylvania State University,
University Park PA 16802 USA

Long known as a thermoelectric, Bi_2Se_3 has been a material of renewed interest since its demonstration as a three-dimensional topological insulator by angle resolved photoemission spectroscopy. Its growth by molecular beam epitaxy (MBE) on a number of substrates reveals a self-organized surface structure replete with correlated triangular terraces and steps. Coherent scattering off these step edges has been demonstrated by scanning tunneling microscopy, making it a rich playground for studies of quantum interference.

We report our studies of magneto-transport in mesoscopic, diffusive, straight channel devices of epitaxial Bi_2Se_3. Although the channels are not explicitly patterned into loops, we observe a periodic magneto-fingerprint: a signature of Aharonov-Bohm orbits. Periodic conductance fluctuations have previously been observed only in patterned diffusive rings and ballistic nanostructures. Long range correlations are observed in the film surface morphology over length scales that are broadly consistent with the path length of the Aharonov-Bohm orbits. This suggests that scattering at the step edges which encompass the triangular pyramids creates these orbits. Our hypothesis is bolstered by control measurements on mesoscopic devices fashioned from Bi_2Se_3 films on vicinal substrates with an uncorrelated surface morphology. These devices yield a conventional, aperiodic magneto-fingerprint, characteristic of universal conductance fluctuations (UCF) arising due to scattering off random disorder. Funded by ONR and DARPA.

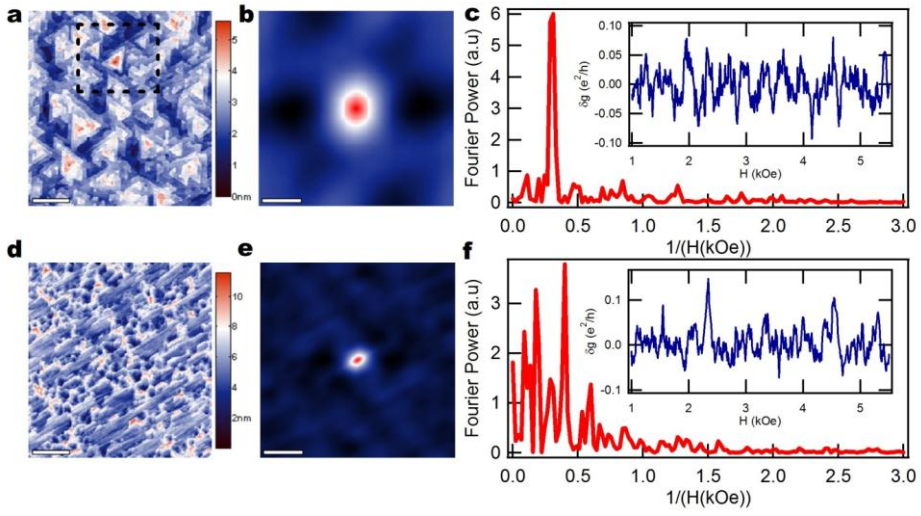

Figure: Bi_2Se_3 thin films revealing long rang correlations in surface morphology depict periodic conductance fluctuations. Conventional, aperiodic UCF observed in Bi_2Se_3 films with uncorrelated surface structure.

We0925

Opening a Topological Surface State Gap with Magnetic Heterostructures

Anthony Richardella, Abhinav Kandala, Joon Sue Lee, Duming Zhang, Dave Rench, Nitin Samarth
The Pennsylvania State University, University Park, PA 16802

Topological Insulators (TI) are characterized by conducting surface states with a Dirac-like dispersion protected by time reversal symmetry. A magnetic perturbation that breaks this symmetry can open a gap at the Dirac point with a hedgehog spin texture.[1] This situation is described by a massive Dirac Hamiltonian which depends on the orientation of the out-of-plane magnetization and which leads to a chiral 1D edge states at a domain walls where the mass changes sign.[2] A variety of magnetic heterostructures have been proposed to exploit the unique physics that occur when the surface states are gapped, such as half integer quantum Hall conductance, magnetic monopoles, and inverse spin-galvanic effect, among others.[3,4,5]

Such structures are difficult to create however due to the difficulty in finding insulating magnetic materials that are compatible with topological insulators. We discuss our efforts to create such structures using the insulating ferromagnet GdN, highly resistive GaMnAs, and the antiferromagnet MnSe grown *ex-situ* or epitaxially with the topological insulator Bi_2Se_3. The easy axes of ferromagnets are found to be in-plane but with magnetization can be pulled out-of-plane at relatively low applied fields. After characterizing the interfaces by high resolution TEM and the magnetic properties by SQUID, we see a rich variety of behavior in transport some of which appear to be related to decoupled spins at the interface, but which show a surprising commonality between magnetic species, and others which suggest a crossover to weak localization from the typical antilocalization of the surface states consistent with the opening of a surface state gap.[6] (Funded by ONR and DARPA.)

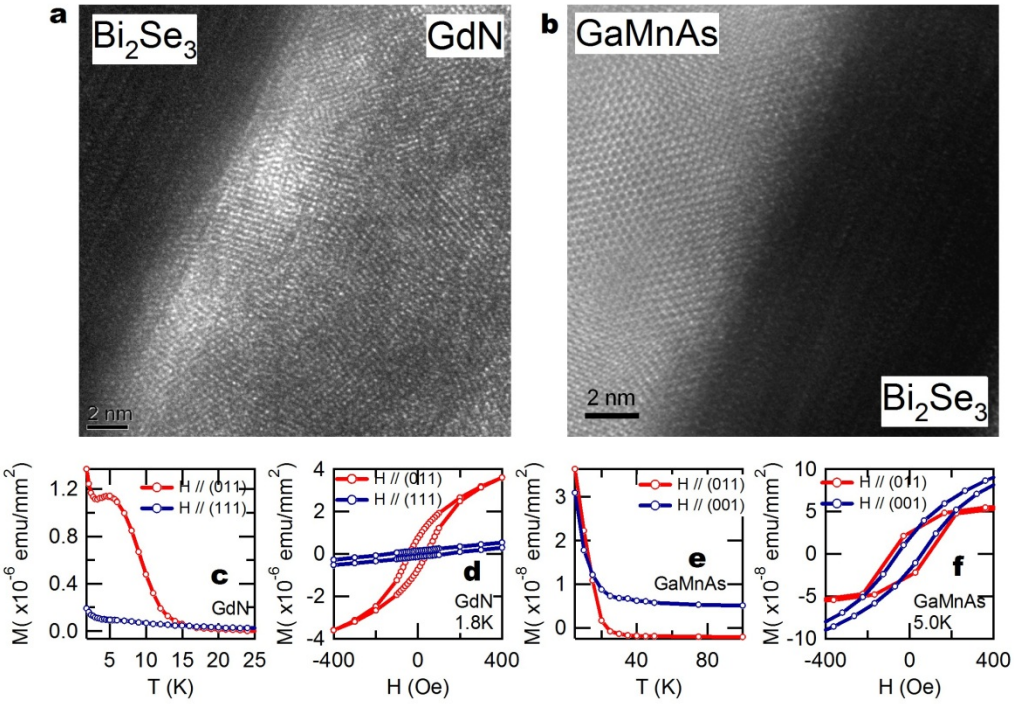

1. S.-Y. Xu, *et al.*, Nature Physics 8, 616 (2012)
2. M. Z. Hasan, C. L. Kane, Rev. Mod. Phys. 82, 3045 (2010)
3. X.-L. Qi, T. L. Hughes, and S.-C. Zhang, Phys. Rev. B 78, 195424 (2008)
4. X.-L. Qi, *et al.*, Science 27, 1184 (2009)
5. I. Garate, M. Franz, Phys. Rev. Lett. 104, 146802 (2010)
6. H.-Z. Lu, J. Shi, S.-Q. Shen, Phys. Rev Lett 107, 076801 (2011)

We0930

Epitaxial Growth and Surface Characterization of Zero-Gap Semiconductor, Half Heusler Compound LuPtSb

S. Patel, B.D. Schultz, C. Palmstrom, U.C, Santa Barbara

Three dimensional topological insulators have recently drawn great interest in the field of condensed matter physics. Three dimensional topological insulating behaviors have been predicted in a relatively new class of gapless semiconducting half-Heusler materials[1]. Ternary half-Heusler compounds are a relatively new class of materials that allow for a tuning of important properties like band gap and band inversion strength in topological insulators[1]. It is important to study the bulk electronic properties of these materials in order to create an insulating bulk, so that topological surface states can be observed through electronic measurements. Molecular beam epitaxy (MBE) is an ideal tool to use to grow highly epitaxial and highly crystalline films of these half-Heusler compounds, with which we can study the fundamental electronic properties of the bulk of these films, and obtain highly ordered smooth surfaces for topological measurements. Here we present the growth and characterization of highly epitaxial, single crystal films of the gapless semiconductor LuPtSb (001) on both lattice-matched $Al_{0.1}In_{0.9}Sb$ (001)/GaAs (001) and tensile strained 0.6% on InSb (001)/GaAs (001) buffer layers. X-ray diffractions studies confirm highly epitaxial, single crystal films nearly lattice matched on $Al_{0.1}In_{0.9}Sb$ (001) and strained on InSb (001). These highly ordered films show both a (1x3) and c(2x2) surface reconstruction which is dependent on both substrate temperature and Sb overpressure. These surfaces have been characterized by reflection high energy electron diffraction (RHEED), low energy electron diffraction (LEED), and scanning tunneling microscopy (STM). Bulk electrical properties were studied by Hall effect measurements to better understand the electronic structure of the bulk gapless semiconductor.

This work was funded in part by the Office of Naval Research under award number XXXXXXXXXXXXXXXXXX in collaboration with the University of Illinois, Urbana-Champaign.

[1] Chadov S., *et al.* Nature Materials. **9**, 541–545 (2010).

We0935

Ferromagnetism in Mn-doped Topological Insulator Bi_2Te_3 Thin-Films

Joon Sue Lee, Anthony Richardella, Dave Rench, Duming Zhang, Nitin Samarth

Department of Physics, The Pennsylvania State University, University Park, PA 16802, USA

We report ferromagnetism in magnetically doped topological insulator Bi_2Te_3 thin films grown by molecular beam epitaxy (MBE) doped with Mn. Bi_2Te_3 is a candidate 3D topological insulator which has Dirac surface band in its band gap. Mn atoms are uniformly distributed within the Bi_2Te_3 film, confirmed by Rutherford backscattering measurements and secondary ion mass spectroscopy. The range of the Mn concentration is between 2% and 10%.

Firstly, we studied different Mn concentrations at a fixed film thickness of 22 nm. Superconducting quantum interference device (SQUID) measurements show that the films are ferromagnetic with Curie temperatures (Tc) of 10~16 K and with the magnetic easy axis out-of-plane along the c-axis of the crystal, as shown in Figure. (a) and (b). Films with more Mn concentrations show higher Tc's. We observe strong anomalous Hall effect (AHE) from electrical transport measurements with large coercive fields of around 3000 Oe at 0.5 K shown in Figure. (c), and the onset of AHE is at about the same temperature observed by SQUID measurements-(Figure. (d)). In Figure (e), magneto-conductivity with out-of-plane magnetic field shows hysteresis below 3~6 K and also shows the crossover of weak anti-localization to weak localization, which has been predicted and observed as a result of magnetic doping at the surface of a topological insulator.

Secondly, we vary the thickness of Mn-doped Bi_2Te_3 films from 3 nm to 60 nm and thicker. Interestingly, we were able to grow films of different carrier types. Films thinner than 50nm were n-type, but some films thicker than 50 nm at a certain Mn concentration turned out to be p-type. Shifts in x-ray diffraction in n-type films indicate Mn going between quintuple layers, but the p-type films appear to be purely substitutional. Figure. (f) depicts temperature dependent AHE of a p-type film. The ability of tuning the Fermi level in the ferromagnetic topological insulator films provides an avenue to study ferromagnetism at the surface state and the experimental realization of the quantum anomalous Hall effect. Funded by ONR and DARPA.

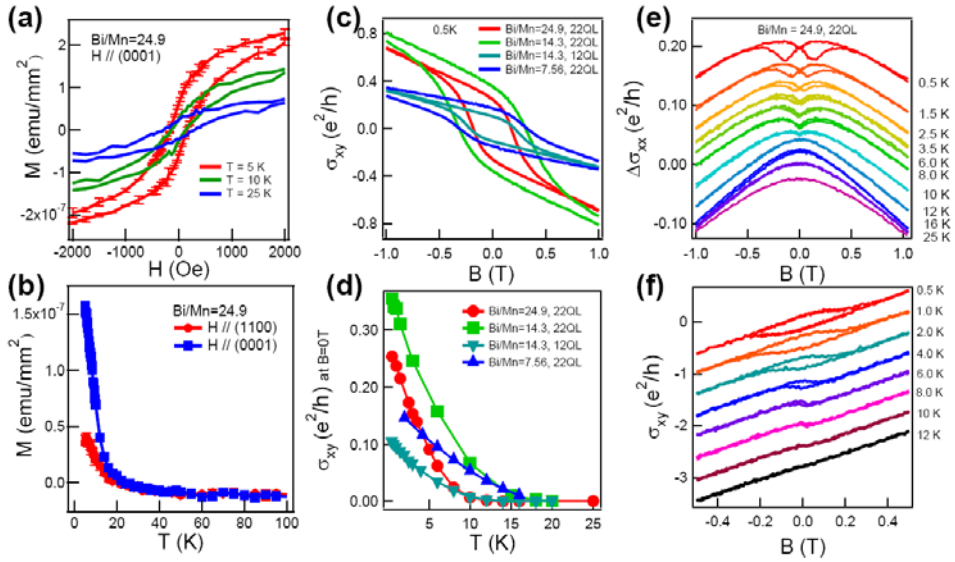

Figure. (a) Out-of-plane magnetic monent measured by SQUID and (b) temperature dependence of magnetization in a Mn-Bi2Te3 film with 2% Mn concentration. (c) AHE at 0.5 K for various Mn concentrations. (d) Hall conductivity at zero magnetic field with respect to temperature. (e) Channel conductivity in an n-type film and (f) Hall conductivity in a p-type film at different temperatures (offset for clarity).

We0940

Gapless states between two topological insulators protected by mirror symmetry

Ryuji Takahashi, Shuichi Murakami
Tokyo Institute of Technology

Topological insulators have metallic surface states while the bulk is insulating. The effective theory for the surface states is illustrated by the massless Dirac equation. The energy is linear in wavenumber similarly to photon, and the Fermi velocity depends on materials. For the surface dispersion, a chirality which takes two values is defined from the spin texture of the Dirac cone. This degree of freedom corresponds to the sign of the velocity of the surface states.

First, we consider the refraction phenomenon of the surface electronic wave at the boundary between two different topological insulators whose chiralities are the same (Fig.1). We study the transmittance and reflectance at the boundary. We find perfect transmittance when the incident wave is normal to the boundary, unlike optics. Second, when one of the topological insulators has the opposite chirality from the other, we find gapless interface states (Fig.2) between them [1]. We give a general proof [1] of the existence of the gapless states by means of the mirror Chern number [2], and we show that the gapless states are topologically protected by the mirror symmetry. Furthermore, as an example, we calculate the gapless state in the Fu-Kane-Mele model on the diamond lattice structure.

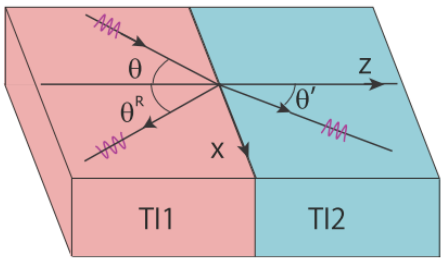

Fig. 1 Schematic of the refraction of the surface states at the boundary of the two topological insulators, TI1 and TI2.

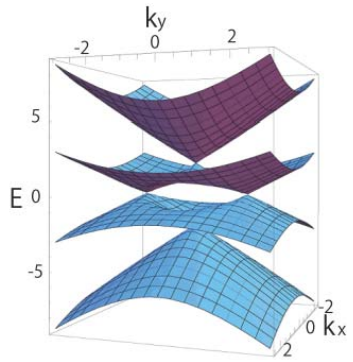

Fig. 2 The energy dispersion at the interface. The gapless states consist of two Dirac cones.

References

[1] R. Takahashi, S. Murakami, Phys. Rev. Lett. 107**,** 166805 (2011).

[2] J. C. Y. Teo *et al.*, Phys. Rev. B 78, 045426 (2008).

Spintronics Inorganic & Organic

We1045 Invited

Electrical and Thermal Spintronics in Silicon

Ron Jansen

National Institute of Advanced Industrial Science and Technology (AIST), Spintronics Research Center, Tsukuba, Ibaraki 305-8568, Japan.

Almost a century after its discovery, a basic quantum mechanical property of the electron, namely its spin, is being considered as an alternative to charge for encoding digital information. The use of electron spin in electronic devices has already had a major technological impact on magnetic data storage. In parallel, the research field, now called "spintronics", continues to produce fascinating phenomena that arise from the combination of magnetic, electric, optical and thermal effects in a wide variety of materials.
Of particular interest is the integration of magnetism and mainstream semiconductors such as silicon, as this has the potential to radically transform information technology. We will review the remarkable progress made in recent years with spins in semiconductors, focusing on the implementation of spin-based electronic functionality in silicon devices and the associated challenges. Two of our recent advances will be highlighted:

- The electrical injection and detection of spin polarization in n-type and p-type Si at room temperature using a ferromagnetic tunnel contact, and the manipulation of the spins in a transverse magnetic field (Hanle effect).
- The creation of spin polarization in Si by a thermal spin current and the associated discovery of Seebeck spin tunneling, allowing thermal transfer of spins from a ferromagnetic contact into non-magnetic materials without a charge tunnel current.

References:

S.P. Dash, S. Sharma, R.S. Patel, M.P. de Jong and R. Jansen,
Electrical creation of spin polarization in silicon at room temperature,
Nature **462**, 491 (2009).

J.C. Le Breton, S. Sharma, H. Saito, S. Yuasa and R. Jansen,
Thermal spin current from a ferromagnet to silicon by Seebeck spin tunnelling,
Nature **475**, 82 (2011).

R. Jansen, A.M. Deac, H. Saito and S. Yuasa,
Thermal spin current and magnetothermopower by Seebeck spin tunneling,
Phys. Rev. B **85**, 094401 (2012).

R. Jansen,
Silicon Spintronics,
Nature Mater. **11**, 400 (2012) - Review.

R. Jansen, S.P. Dash, S. Sharma and B.C. Min,
Silicon spintronics with ferromagnetic tunnel devices,
Semicond. Sci. Technol. **27**, 083001 (2012) - Review.

We1115

Efficient spin injection with an AlO_x tunnel barrier prepared by the oxidation of an ultra-thin Al epitaxial layer on GaAs

N. Nishizawa and H. Munekata
Imaging Science and Engineering Laboratory, Tokyo Institute of Technology
4259-J3-15 Nagatsuta, Midori-ku, Yokohama 226-8503, Japan
E-mail: nishizawa@isl.titech.ac.jp

It is widely recognized that the interface takes a crucial role in spin transport across a junction consisting of dissimilar materials [1]. For a Fe/GaAs system, formation of a Fe_xAs_y interface layer composed of diamagnetic $FeAs_2$, antiferromagnetic FeAs and Fe_2As, is inferred to reduce the spin polarization of carriers injected in a GaAs from a Fe layer [2]. Reported in this paper is that inserting an ultra-thin AlO_x layer between Fe and GaAs suppresses significantly the degradation of spin polarization of electrically injected spins. We discuss that the AlO_x layer prepared by the method described in the next paragraph suppresses formation of the Fe_xAs_y interface layer and realize efficient injection of spin polarized carriers from ferromagnetic layers.

Molecular beam epitaxy (MBE) was utilized to prepare a spin detecting structure and a AlO_x layer. The spin detecting structure (so called spin-LED) consists of a GaAs-based double heterostructure (DH) incorporating a 500-nm thick $In_{0.03}Ga_{0.97}As$ active layer in which spin-polarized electrons recombine with un-polarized holes. A 1.0-nm thick AlO_x layer was formed as follows: (i) epitaxial growth of a 5.5-Å thick Al layer at room temperature in a growth chamber, (ii) oxidation of the first Al layer in dry air for 10 hours at atmospheric pressure in the entry chamber, (iii) deposition of a second, 2.3-Å thick Al layer in a growth chamber, followed by finishing oxidation. A 100-nm thick Fe layer was then deposited by e-beam evaporation on the AlO_x layer.

Figure 1 shows a cross-sectional transmission electron microscopy (TEM) image around the interface of our interest. A very uniform AlO_x layer is noticeable. Chemical shifts measured by electron energy loss spectroscopy indicate oxidized Al and un-oxidized Fe layers. *I-V* curves studied with separate metal/1nm-AlO_x/*n*-GaAs(001) samples showed carrier transport dominated by the tunneling across the AlO_x layer with barrier height of 1.42 eV.

The overall spin polarization was evaluated by measuring circular polarization P_{opt} of electroluminescence (EL) emitted from a cleaved side-wall of a spin-LED, as shown schematically in insets Figs.2 [3]. A magnetic field of 5 kOe was applied prior to the measurement to magnetize a Fe spin-injection layer along the easy axis, so that directions of remanent magnetization and optical spins are both parallel to the in-plane, GaAs[110] axis. Shown in Figs.2(a) and (b) are, respectively, EL spectra obtained at 5 K from spin-LEDs with and without an AlO_x layer. EL from the sample with an AlO_x layer shows helicity dependent spectra with P_{opt} ~ 14 % which corresponds to spin polarized electrons of P_{ele} ~ 29 %. The sample without an AlO_x layer exhibits almost no helicity dependence. These results strongly suggest that an oxidized Al epilayer works as the layer which helps efficient spin injection.

[1] J. P. Velev *et al.*, Surf. Sci. Rep. **63**, 400 (2008).
[2] A.T.M.K. Jamil, *et al.*, Thin Solid Films **516**, 3015 (2008).
[3] W. Terui, *et al.*, stat. sol. c **8**, 396 (2011); T. Hanna, *et al.*, J. Cryst. Growth **323**, 383 (2011).

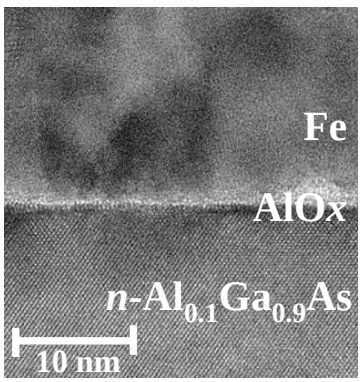

Fig.1 Cross-sectional TEM image around Fe/AlO_x/*n*-AlGaAs.

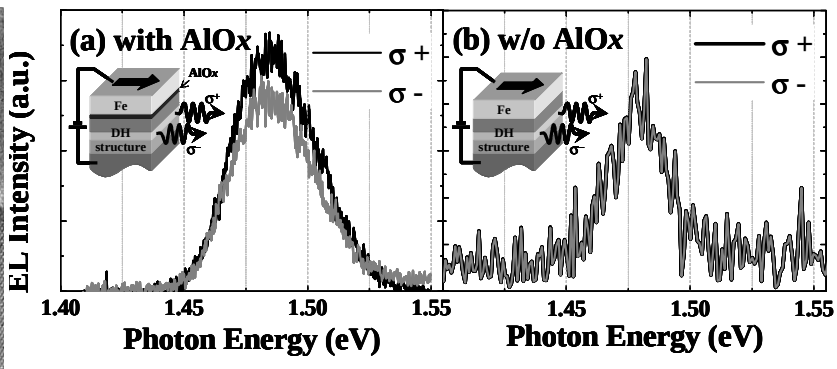

Figs.2 σ+ and σ- EL spectra from the side-wall of Spin-LED (a) with and (b) without AlO_x with no external magnetic field. Insets schematically illustrate experimental configurations with magnetization vectors and optical axes.

We1120

Surface-termination Effect on Nitrogen-Vacancy Charge in Diamond

Shanying Cui and Evelyn Hu

School of Engineering and Applied Sciences, Harvard University, Cambridge MA 02138 USA

The nitrogen-vacancy (NV) defect center in diamond has attracted much attention in recent years due to its long spin coherence time. The ability to initialize and read out NV spin states optically at room temperature is a significant advantage for applications of quantum information processing (QIP)[1] and single-spin magnetometry[2]. NV centers can exist in a negative (NV^-) or neutral (NV^0) state, but only the negative state is spin-active (S=1). Efficiently coupling of the NV to another spin for magnetometry or to a waveguide for QIP requires the NV to lie close to a surface, within a few nanometers. It is therefore imperative to understand the effect of surface chemistry on the charge state of NV and to try to maximize the number of NV^- states over NV^0.

While a few studies have compared NV charge in hydrogen-terminated versus oxygen-terminated surfaces[3], not much has been studied on other terminations. Currently, all researchers working with surface-NVs terminate with oxygen as a final step to increase NV^- signal. In this work, we compare oxygen-terminated surfaces to halogen-terminated surfaces.

We start with a high purity single crystal diamond sample ([N] < 5 ppb) and implant NVs to a depth of 14±5nm[3]. Oxygen-termination is achieved by a variety of techniques: boiling acid, oxygen plasma, or pirhana clean. Chlorine- and fluorine-termination is achieved with Cl_2 and CF_4 plasma, respectively. Our surface NVs are excited with 532nm laser at room temperature, and the photoluminescence spectrum is acquired via an objective normal to the surface. The photoluminescence spectrum shows both NV^0 and NV^- zero-phonon lines (Fig 1a).

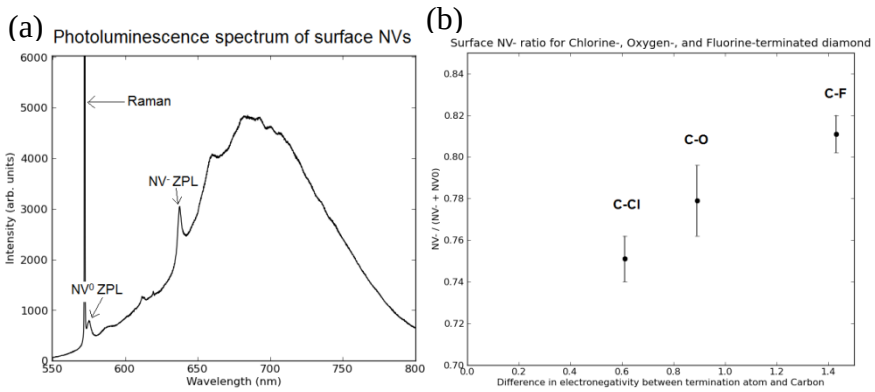

Figure 1. a) Photoluminescence of oxygen-terminated diamond with NVs 14±5nm from surface. b) Ratio of NV^- ZPL area to total ZPL area.

Comparing different terminations on the same sample, we find that relative to oxygen-terminated surfaces, chlorine leads to a lower NV^- concentration whereas fluorine seems to increase it (Fig 1b). We also found that NV^- concentration varied more between different oxygen-terminated surfaces than fluorine-terminated samples, especially depending on the method of oxygen termination. X-ray photoelectron spectrometry (XPS) was used to confirm chemical termination of the diamond lattice.

Understanding how surface chemistry affects NV charge is crucial for all applications that depend on the long-lived, stable coherence of the NV^-. These studies of halogen termination of diamond should prove important in extending that stable coherence.

[1] B.B. Buckley, G.D. Fuchs, L.C. Bassett, D.D. Awschalom, *Science* **330**, 1212 (2010)
[2] G. de Lange, D. Riste, V.V. Dobrovitski, R. Hanson, *PRL* **106**, 080802 (2011)
[3] K.-M. C. Fu, C. Santori, P.E. Barclay, R.G. Beausoleil. *APL* **96**, 121907 (2010)

Manganese Phthalocyanine on Cobalt: An Interesting Model Interface for Organic Spintronics

Francisc Haidu[a], Axel Fechner[a], Benjamin Mahns[b], Georgeta Salvan[a], Martin Knupfer[b], and Dietrich R. T. Zahn[a]

[a]*Semiconductor Physics, Chemnitz University of Technology, D-09126 Chemnitz, Germany,*
[b]*Electronic and Optical Properties Department, IFW Dresden, D-01171 Dresden, Germany*
E-mail: francisc.haidu@physik.tu-chemniz.de

As a candidate for organic spintronics Manganese Phthalocyanine (MnPc) attracts a lot of interest having an unusual spin state S=3/2 [1, 2] and ferromagnetic properties at low temperatures [2]. The spin state could even be changed to S=5/2 by alkali metal doping [1] or, as theoretical calculations show to S=1/2 by reaction with molecular oxygen [3].

In this study we focus on the interface of MnPc with the ferromagnetic metal Cobalt which is an important one for spin injection [4]. The occupied and unoccupied electronic states of MnPc can be determined combining Ultraviolet Photoelectron Spectroscopy (UPS) and Inverse Photoemission Spectroscopy (IPS). MnPc was deposited via Organic Molecular Beam Deposition in Ultra High Vacuum.

The thickness dependent UPS and IPS spectra in Fig. 1 show the secondary electron cutoff from which the formation of an interface dipole can be deduced [5, 6]. The features developing near the Fermi edge are the Highest Occupied Molecular Orbital and the Lowest Unoccupied Molecular Orbital in the UPS and IPS regions, respectively, and their onset defines the transport gap [6]. A band gap opening with increasing film thickness saturating above 4 nm is observed. The results obtained are compared to those of a previous study of Copper Phthalocyanine deposited on Silicon substrate [7].

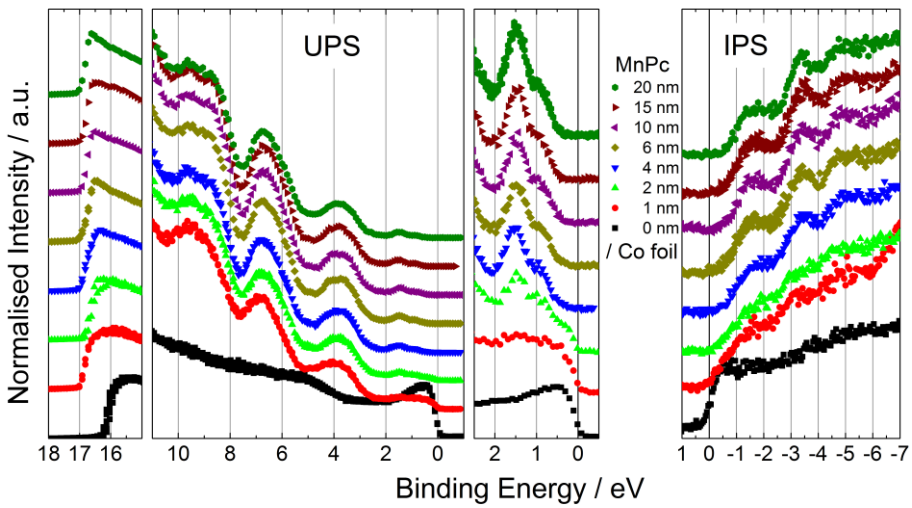

Fig. 1. UPS and IPS measurements of MnPc at different thicknesses deposited on Co foil.

[1] Y. Taguchi *et al.*, J. Am. Chem. Soc. **128** (2006) 3313-3323;
[2] N. Ishikawa, Struct. Bond. **135** (2010) 211–228;
[3] R. Friedrich *et al.*, J. Chem. Phys. **136** (2012) 064704;
[4] C. Barraud *et al.*, Nature Physics **6** (2010) 615;
[5] M. Grobosch *et al.*, J. Phys. Chem. C **113** (2009) 13219;
[6] D. R. T. Zahn *et al.*, Chem. Phys. **325** (2006) 99–112;
[7] M. Gorgoi and D. R. T. Zahn, Organic Electronics **6** (2005) 168.

Energy Level Alignment and Charge Transport at Metal/Alq_3 Interfaces: Implications for Organic Spintronics

J. S. Jiang, Materials Science Division, Argonne National Laboratory

The alignment between the electrode work function and the organic lowest unoccupied molecular orbital (LUMO) or highest occupied molecular orbital (HOMO) is a crucial parameter in determining the nature of charge transport in organic electronics. However, experimental determination of LUMO is challenging. [1] For the archetypal electroluminescent organic semiconductor tris-(8-hydroxyquinoline) aluminum (Alq_3), various techniques gave significantly different HOMO-LUMO gap values. [2] Using ballistic electron emission spectroscopy (BEES), we have directly determined the energy barrier for electron injection at clean interfaces of Alq_3 with Al and Fe to be 2.1 eV and 2.2 eV, respectively. We quantitatively modeled the sub-barrier BEES spectra with an accumulated space charge layer, and found that the transport of non-ballistic electrons is consistent with random hopping over the injection barrier. [3] I will discuss the implication of these results on recent reports [4] of spin transport in "organic spin-valve" structures that have been taken as the basis for organic spintronics.

Supported by U.S. DOE Office of Science Basic Energy Sciences, under Contract No. DE-AC02-06CH11357.

[1] J. C. Scott, *J. Vac. Sci. Tech*, **A 21**, 521 (2003).
[2] I. H. Campbell, D. L. Smith, *Appl. Phys. Lett*. **74**, 561 (1999); I. G. Hill *et al. Chem. Phys. Lett.* **327**, 181 (2000); S. F. Alvarado *et al. IBM J. Res. Dev.* **45**, 89 (2001); Kahn *et al. J. Poly. Sci.* **B 41**, 2529 (2003).
[3] Jiang, Pearson, Bader, *Phys. Rev.* **B 77**, 035303 (2008); Jiang, Pearson, Bader, *Phys. Rev. Lett.* **106**, 156807 (2011).
[4] V. Dediu, *Nature Mater*. **8**, 707 (2009).

Hysteretic control of organic conductance due to remanent magnetic fringe fields

M. E. Flatté[1,*], F. Macià[2], F. Wang[1], N. J. Harmon[1], M. Wohlgenannt[1], and A. D. Kent[2]

[1]Optical Science and Technology Center and Department of Physics and Astronomy, University of Iowa, Iowa City, Iowa 52242, USA

[2]Department of Physics, New York University, 4 Washington Place, New York, NY 10003, USA

[*]Email: michael-flatte@uiowa.edu

Manipulation of the remanent (zero external magnetic field) magnetization state of a thin ferromagnetic film is shown to control the room-temperature conductance of a thin film of organic semiconductor deposited on top. For the organic semiconductor Alq_3 the fringe magnetic fields from a multidomain, remanent magnetization state of the film enhance the device conductance by several percent relative to its value for the magnetically-saturated ferromagnetic film. The effect of fringe fields is insensitive to ferromagnetic film's thickness (which varies the fringe field magnitude proportionately) but sensitive to the magnetic domain's correlation length. We thus demonstrate a new magnetic mechanism for controlling an organic film's conductance at zero external magnetic field, useful for magnetic sensors and memory devices. The effect originates from spin precession and correlated electronic transport in the presence of a magnetic field gradient.

Room-temperature electronic transport in disordered semiconductor films is strongly affected by spatially-varying, randomly oriented fields, such as hyperfine fields in organic semiconductors, which can lead to changes in conductance of several percent at room temperature in external fields as small as 10 mT[1-3]. The sensitivity of electronic transport in disordered films to such inhomogeneous random fields suggests that the fringe fields from a ferromagnetic film might similarly modify electronic transport. This effect, dubbed "fringe-field organic magnetoresistance", was identified in measurements where the fringe fields from a single unsaturated ferromagnetic film dramatically influenced an organic film's conductance[4].

We have now characterized the effect of *remanent* fringe fields from the ferromagnetic film on the organic conductance. Our devices consist on an organic material (Alq_3) on a ferromagnetic electrode and a non-magnetic top electrode. The ferromagnetic electrode has perpendicular anisotropy and forms small scale ($\sim$ 500 nm) domains near the electrode's coercive field. There are strong fringe fields emanating from the ferromagnetic electrode when it is in a multi-domain state. At zero applied field, these remanent fringe fields increase the conductance of the organic semiconductor Alq_3, whereas fringe fields from a similar domain configuration generated at the coercive field (where the film magnetism begins to switch) lead to a decrease in Alq_3's conductance. The thickness of the ferromagnetic film (and thus the proportionally increasing fringe field magnitudes) is not critical to the observed effect and can be varied by a factor of four without significantly changing the magnitude of the fringe field magnetoresistive effect. These results are consistent with the correlation length of the fringe fields being the most important factor influencing the magnetic-field-dependence of the electronic transport in the organic layer. Further, we created specific remanent states in the ferromagnetic electrode with different domain configurations and measured the conductivity of the semiconductor organic layer. Remanent states in the magnetic electrode are achieved by setting a partially magnetized state; departing from a saturated magnetized state we ramped the field to a value near the electrode coercive field and then returned the field to zero. A transport theory based on spin precession and correlated electron transport in the presence of a magnetic field gradient reproduces many of these features.

This work was supported by an ARO MURI.

[1] T. L. Francis *et al.,* New J. Phys. **6**, 185 (2004)
[2] V. N. Prigodin *et al,* Synth. Met. **156**, 757 (2006)
[3] F. L. Bloom *et al.,* Phys. Rev. Lett. **99**, 257201 (2007).
[4] F. Wang *et al.,* Phys. Rev. X **2**, 021013 (2012).

We1205

Integrating MBE materials with graphene to induce novel spin-based phenomena

Adrian G. Swartz,[1] Kathleen M. McCreary,[1] Wei Han,[1] Patrick M. Odenthal,[1] Jen-Ru Chen,[1] Yufeng Hao,[2] Rodney S. Ruoff,[2] Jaroslav Fabian,[3] and Roland K. Kawakami[1]

[1]*Department of Physics and Astronomy, University of California, Riverside, CA 92521, USA*
[2]*Department of Mechanical Engineering and the Texas Materials Institute, The University of Texas at Austin, Austin TX 78712*
[3]*Institute for Theoretical Physics, University of Regensburg, D-93040 Regensburg, Germany*

(Dated: October 14, 2012)

Abstract

Proximity based interactions between nearby systems (i.e. films, adsorbates, molecules) and graphene could lead to the realization of novel phenomena[1, 2]. Graphene, a single atomic layer of sp^2 bonded carbon with conducting π orbitals that extend out of the plane, is ideal for investigating proximity related behavior. Such effects, which rely on atomic orbital overlap, require highly controlled surfaces and interfaces. Here, we are primarily concerned with the interactions of functional oxides and adsorbates with graphene because of the possibility of induced spin splitting via exchange, magnetism, and spin-orbit coupling.

First, we have examined functional oxide films integrated with graphene. The ferromagnetic insulator EuO has been predicted to cause exchange splitting in graphene when the two are brought into contact and many theorists have suggested spintronic applications for such a structure including spin manipulation, spin filtering, and spin transfer torque. However, deposition of oxide materials on graphene is a major challenge as typical deposition techniques generally result in rough films (due to graphene's large surface energy) and defected graphene (caused by the violent nature of common evaporation techniques such as sputtering, *e*-beam, and PLD). Here, we have taken advantage of the low energy deposition technique molecular beam epitaxy (MBE) in order to solve the difficult issue of oxide deposition on graphene. We have examined the feasibility of integrating the ferromagnetic insulator EuO with graphene and have found that under a special growth regime that flat and crystalline films can be realized[3]. The films are characterized with RHEED, Auger, XRD, AFM, and MOKE, while the properties of the underlying graphene layer is investigated through Raman spectroscopy and charge transport. Raman spectroscopy shows the absence of defects and resistivity measurements indicate that the mobility is not strongly affected by the EuO deposition. The direct integration without the aid of a buffer layer is a key advance towards experimental observation of the exchange proximity effect at the EuO/graphene interface. Further, this work demonstrates a route for realizing high quality oxide materials with graphene as gate dielectrics.

Second, we have taken advantage of atomic scale control provided by MBE and investigate submonolayer deposition of adsorbates and their interactions with graphene. Adatoms can possibly induce local effects such as magnetism, spin-orbit coupling, charge impurity potentials, and orbital hybridization. In order to understand the effect of the adsorbates on spin-based properties and phenomena, we have performed systematic *in-situ* deposition of adatoms onto graphene non-local

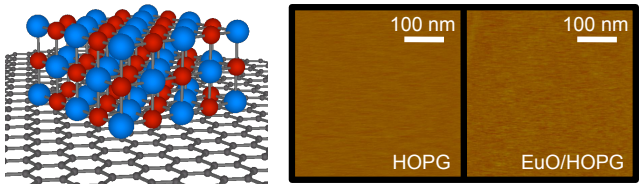

FIG. 1. a) Schematic of EuO crystal deposited on top of graphene. b) Atomic force microscopy (AFM) of HOPG(0001) substrate with rms roughness 0.1 nm. c) AFM of 5 nm EuO(001) film on HOPG(0001) with rms roughness 0.2 nm. The films are determined to be flat and crystalline. Films are also grown on exfoliated and CVD grown graphene. The graphene is characterized by Raman spectroscopy and charge transport which indicate negligible defects introduced by the EuO overlayer.

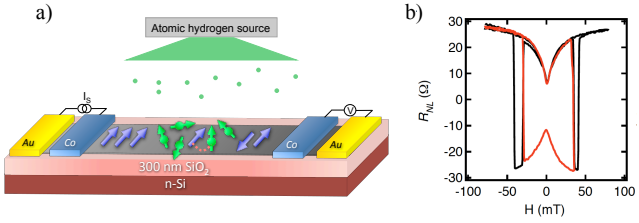

FIG. 2. a) Schematic of non-local graphene spin valve device with *in-situ* deposition of atomic hydrogen. Blue arrows represent injected spins diffusing along the graphene channel and green arrows represent magnetic moments formed by p_z-orbital defects. b) Non-local resistance at T=12 K after the introduction of atomic hydrogen to the graphene device. Exchange coupling with the magnetic moments causes increased spin scattering around zero applied field and creates the observed dip. The minor loop (red curve) is symmetric around zero spin signal indicating that the behavior is due spin scattering as opposed to changes in resistivity.

spin valves. This approach has significant advantages over other experimental techniques as it probes the spin-degree of freedom locally on the graphene flake and can be properly characterized before and after the adsorbates are introduced. In particular, we have deposited atomic hydrogen[4] and Mg adsorbates[5]. We have found that atomic hydrogen can induce magnetic moments in graphene and that these moments couple via exchange to the injected spin current. This coupling results in an exchange field which causes the spins to precess rapidly with an observed effective g-factor as large as $\sim$20. This is the most convincing evidence for magnetic moment formation in graphene, which has been a controversial issue experimentally. On the other hand, Mg adsorbates do not form magnetic moments, but act as atomic scale charge impurity scatterers. Thus, Mg adosrbates allow us to investigate the origin of spin relaxation in graphene. This is one of the most important issues in graphene spintronics because of the unexplained discrepancy in spin lifetime between theory (1 μs) and experiemnts (1 ns), which limits graphene's potential for commercial applications. By monitoring the spin lifetime with increasing Mg coverage, we have found that in the current regime of spin relaxation of $\sim$1 ns, charge impurity scattering has negligible effect on the spin relaxation time. These results together demonstrate the power of molecular beam epitaxy in realizing novel graphene properties and functionality through careful control over the key interfaces and proximity materials.

[1] O.V. Yazyev and L. Helm, *Phys. Rev. B* **75**, 125408 (2007).

[2] H. Haugen, D. Huertas-Hernando, and A. Brataas, *Phys. Rev. B* **77**, 115406 (2008).

[3] A. G. Swartz, P. M. Odenthal, Y. Hao, R. S. Ruoff, and R. K. Kawakami, *ACS Nano* in review (2012).

[4] K. M. McCreary, A. G. Swartz, W. Han, J. Fabian, and R. K. Kawakami, *Phys. Rev. Lett.* in press, arXiv:1206.2628 (2012).

[5] A. G. Swartz, J. R. Chen, K. M. McCreary, W. Han, and R. K. Kawakami, *Appl. Phys. Lett.* in review (2012).

Nanowire Growth & Strain Effects

We1330

XPS and PL investigations of ZnO nanowire arrays

D.R. Jones, R.A. Brown, J-T Heiva Minster-Blondeau C.J. Barnett and T.G.G. Maffeis

College of Engineering, University of Swansea, Singleton Park, Swansea, SA28PP

ZnO nanostructures have a great potential for novel electronic and optoelectronic devices because of the large (3.37 eV) direct band gap of ZnO and the availability and ease of fabrication of high quality single crystalline nanostructures. Controlling the surface properties of ZnO nanomaterials is crucial to the realisation of this potential because of the enhanced surface to volume ratio of nanostructures. In this paper we present an investigation of the surface properties of ZnO nanowire arrays using X-ray Photoelectron Spectroscopy (XPS) and Photoluminescence (PL). Specifically we focus on the O 1s core level which can be deconvoluted into a bulk lattice component and a surface component, and the visible band of the ZnO PL spectra which has been attributed to surface states and/or lattice oxygen vacancies or other defects and impurities [1]. The origin of the visible band is still poorly understood. We show that annealing in air up to 400C results in a large decrease in the visible band, but without affecting the overall shape of the visible peak. However, annealing over 400C increases the visible contribution and changes the shape, indicating a change in the recombination mechanism. Annealing in vacuum at 400C removed most of the yellow to red emission, leaving only green in the visible band. This result suggests that the green contribution is mostly caused by oxygen vacancies. XPS analysis shows enhanced surface sensitivity due to the vertically aligned structure of the array, making the effective escape depth of the photoelectrons very small. This was confirmed by scanning at normal emission and 60 degrees off normal emission, with the high binding energy component smaller at 60 degrees off normal emission. Annealing in air and vacuum affect the surface oxygen differently but complete removal of the high binding energy feature is not possible, even after annealing at 700C in vacuum. We suggest that the high binding energy shoulder is made up of a surface component and a sub-surface defect contribution. The PL and XPS results show that the surface and optical properties of ZnO nanostructures can be manipulated by annealing in various ambient, which could have important implications for devices such as white LEDs or optical sensors.

[1] A. B. Djurisić and Y. H. Leung, “Optical properties of ZnO nanostructures.,” *Small (Weinheim an der Bergstrasse, Germany)*, vol. 2, no. 8-9, pp. 944-61, Aug. 2006.

Novel InGaAs/GaAs quantum dots in a GaP(001) matrix

H. Eisele*, C. Prohl, A. Lenz, D. Roy, J. Schuppang, M. Dähne, G. Stracke, A. Strittmatter, U. W. Pohl, and D. Bimberg,

Technische Universität Berlin, Institut für Festkörperphysik, Hardenbergstr. 36, 10623 Berlin, Germany,
*Email address: holger.eisele@physik.tu-berlin.de

Due to the comparably low lattice mismatch, GaP is a promising material for the direct integration of optical III-V-semiconductor applications into silicon-based technology. Hence, the development of epitaxially grown quantum dots on GaP(001) substrates for opto-electronic devices is an interesting new task. Furthermore, In(Ga)As/GaP quantum dots are also promising for new nano-memory cells due to an expected high hole localization energy at the quantum dots, as compared with InAs/GaAs quantum dots, resulting in reasonable long storage times. In order to understand the growth of quantum dots in this new material system, we analyzed InGaAs/GaAs/GaP nanostructures at the atomic scale using scanning tunnelling microscopy (XSTM).

The investigated sample was grown by metal organic vapor phase epitaxy (MOVPE) on a GaP(001) substrate. It contains a stack of three layers, each consisting of nominally 3.0 monolayers (ML) GaAs, followed by 2.0 ML of $In_{0.25}Ga_{0.75}As$. The thin GaAs interlayer prior to InGaAs deposition was used to encourage the *Stranski-Krastanow* growth mode for quantum dot formation.

The high-resolution XSTM images show quantum dots, being confined by a truncated pyramidal shape. A wetting layer being connected to the quantum dot at its base is present, clearly demonstrating a *Stranski-Krastanov* growth mode, even if for highly strained systems typically rather the *Volmer-Weber* growth mode would be expected. The average quantum dot base length is found to be 12 nm, and the height is up to 10 ML. A statistical analysis leads to a high quantum dot density of 2.4×10^{11} cm^{-2} within the sample. Even though the strain energy in this system is relatively high as compared with the InGaAs/GaAs system, no structural defects, such as e.g., dislocations or nano-void formation, could be found. The analysis of the local stoichiometry shows different material compositions for the wetting layer and the quantum dots: The wetting layer consists of almost pure GaAs (no Indium) with a sharp interface at the bottom, where the growth was started. At the top side, the GaAs segregates into the GaP capping layer. The quantum dots show a truncated, reversed-cone stoichiometry profile of intermixed InGaAs with a high Indium content at its top center. Their compositional structure is very similar to InGaAs/GaAs quantum dots, but due to the higher strain here their size is scaled down. Overall, a phase separation process into Indium-rich quantum dots and an Indium-free wetting layer occurs during the growth.

MOCVD Regrowth of InP on Hybrid Silicon Substrate

Chong Zhang[1*], Di Liang[2], John E. Bowers[1]
[1] Electrical & Computer Engineering Department, University of California, Santa Barbara, CA
[2] Intelligent Infrastructure Lab, HP Labs, Palo Alto, CA

Epitaxial growth/regrowth technology is important for many photonic integration applications to realize high-performance active components and low-loss passive part on single substrate [1, 2]. But a compatible regrowth process is still lacking for hybrid Silicon system, in which a low temperature (<400°C) wafer bonding technology is usually adopted [3]. MOCVD growth of InP typically requires temperature higher than 550°C, which is too high for the bonded III/V-on-Silicon sample. Serious material degeneration can result from bonding interface bubble generation due to trapped gas molecules and the difference in the coefficients of thermal expansion between the bonding materials at that temperature. In this work we discuss the effort of MOCVD regrowth of InP on the hybrid Silicon substrate.

Hybrid Silicon substrate was prepared by epitaxially transferring a 2μm-thick III/V layer on a SOI substrate by a low-temperature (300°C) bonding process [4]. Vertical outgassing channels (VOCs) were adopted on SOI substrate (Fig. 1(a)) to trap gases generated at the bonding interface [4]. It is noted that 2μm is supposed to be below the critical thickness for InP layer considering the thermal coefficient mismatch between InP and Silicon at 600°C. Prior to transferring the sample into MOCVD reactor, another critical step is to release trapped gases in VOCs by etching through III/V. Otherwise, trapped gases expand and cause severe III/V delimitation at bonding interface (Fig. 1(c)). We also observed that a higher density of outgassing channels was needed for higher processing temperatures. This indicates increasing amount of gas generation at higher temperature, which is equivalent to a shorter diffusion length of new generated gas at bonding interface. Another method to take bonded sample to regrowth environment is to use long and dense in-plane outgassing channels (Fig. 1(b)) to allow bonding-generated gases to diffuse freely at elevated temperature. Fig. 1(d) shows that the smooth, bubble-free III/V surface is preserved on the bonded sample with in-plane channels after 10-min anneal at 600°C. As shown in Fig. 2, the corresponding photoluminescence (PL) from quantum wells (QWs) within the III-V stack kept 80% of the intensity and similar full-width at half maximum after the anneal. A 10nm blue shift could result from a strain change in the system. By using this strategy, 1μm selective regrowth of InP was operated at 600°C on mesa-patterned hybrid Silicon substrate for the first time. Cross section SEM of regrown sample was shown in Fig. 3. No bubbles or debonding were seen at the bonding interface and 50-80% of the PL intensity was measured, compared with that of the bonded sample before regrowth. This regrowth demonstration paved the way to integrate more functionality on the hybrid Silicon platform and may even provide a useful technique for III/V-on-silicon heteroepitaxy.

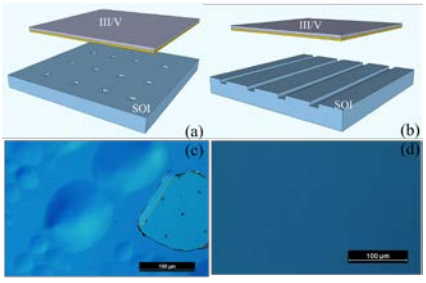

Fig.1 Diagram of (a) vertical and (b) in-plane outgassing channels; and 2-μm thick bonded III/V surface after 10min anneal at 600°C with (c) VOCs and (d) in-plane outgassing channels

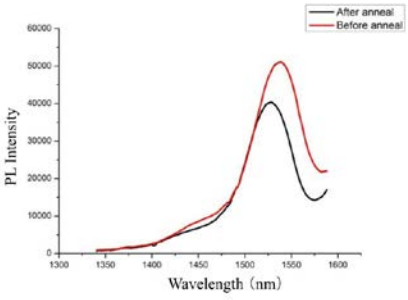

Fig.2 PL of the bonded III/V with QW active region on SOI with in plane channels before and after 10min anneal at 600°C

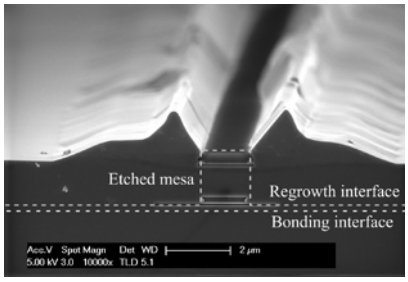

Fig.3 Cross-section SEM of 1μm selective InP regrowth on the etched III/V mesa on bonded III/V layer stack on SOI substrate

[1] R. Nagarajan, et al., IEEE Journal of Selective Topics in Quantum Electronics, 11, 326, 2005
[2] L. Coldren, et al., Journal of Lightwave Technology, 29, 554, 2011
[3] D. Liang, et al., Materials, 3, 1782, 2010
[4] D. Liang, et al., Journal of Electronic Materials, 37, 1552, 2008

*czhang@ece.ucsb.edu

We1345

News from the non-polar GaN$(10\bar{1}0)$ surface: Hidden surface states and intrinsic versus extrinsic Fermi-level pinning

Ph. Ebert[1], L. Lymperakis,[2] P. H. Weidlich,[1] H. Eisele,[3] M. Schnedler,[1] J.-P. Nys,[4] B. Grandidier,[4] D. Stievenard,[4] R. E. Dunin-Borkowski,[1] and J. Neugebauer,[2]

[1] *Peter Grünberg Institut, Forschungszentrum Jülich GmbH, 52425 Jülich, Germany*
[2] *Computational Materials Department, Max-Planck-Institut für Eisenforschung GmbH, Max-Planck-Str. 1, 40237 Düsseldorf, Germany*
[3] *Institut für Festkörperphysik, Technische Universität Berlin, Hardenbergstr. 36, 10623 Berlin, Germany*
[4] *Institut d'Electronique, de Microélectronique et de Nanotechnologie, CNRS, UMR 8520, Département ISEN, 41 bd Vauban, 59046 Lille Cedex, France*

GaN-based semiconductors nowadays are the materials of choice for green to ultraviolet optoelectronic devices. However, due to the built-in spontaneous polarization field combined with discontinuities of the piezoelectric polarization arising from strained hetero interfaces along the [0001] direction, the wave functions for electrons and holes are spatially separated in the active region of an optoelectronic device, hence reducing the internal quantum efficiency. This can be avoided by growing the optoelectronic nanostructures on the *m*-plane, where the normal component of the polarization field is zero. As the chemical reactivity during growth (i.e. growth kinetics, incorporation of impurities/dopants and defects) depends sensitively on the electronic and geometric properties of the surfaces, a detailed knowledge of the energetic position of surface states is critical.

Unfortunately, the electronic structure of the GaN$(10\bar{1}0)$ surface and in particular the presence of a surface state within the fundamental band gap is highly debated and hence the fundamental properties remain unclear.[1] Density functional theory (DFT) calculations within the local density approximation (LDA) predict two surface states shifted out of the fundamental band gap,[2,3] whereas recent DFT calculations based on modified pseudopotentials find the upper (empty) surface state in the whole Brillouin zone within the band gap.[4] On the other hand STM experiments suggest the absence of surface states in the band gap,[3,5,6] raising the question if STM or the theoretical calculations provide a realistic picture of the physically relevant part of the surface states.

By combining scanning tunneling spectroscopy (STS) and first principles calculations we clarify the controversial issue of the electronic structure of *m*-plane GaN surface. We indeed find the paradoxical situation that conventional STM mapping modes fail to probe the physically most relevant parts of a surface state, which is fully within the fundamental band gap. Based on a detailed analysis of the calculated dispersion and decay into the vacuum of the surface and bulk states, we tailor the design of the STM experiments, in order to boost the sensitivity thus allowing to probe the apparently hidden surface state. Finally, we discuss the implications of this apparently hidden surface state on the Fermi-level pinning and its measurement by STS.

[1] H. Eisele and Ph. Ebert, Phys. Status Solidi RRL **6**, 359 (2012).
[2] J. E. Northrup and J. Neugebauer, Phys. Rev. B **53**, R10477 (1996).
[3] M. Bertelli, P. Löptien, M. Wenderoth, A. Rizzi, R. G. Ulbrich, M. C. Righi, A. Ferretti, L. Martin-Samos, C. M. Bertoni, and A. Catellani, Phys. Rev. B **80**, 115324 (2009).
[4] D. Segev and C. G. Van de Walle, Europhys. Lett. **76**, 305 (2006); C. G. Van de Walle and D. Segev, J. Appl. Phys. **101**, 081704 (2007).
[5] L. Ivanova, S. Borisova, H. Eisele, M. Dähne, A. Laubsch, and Ph. Ebert, Appl. Phys. Lett. **93**, 192110 (2008).
[6] Ph. Ebert, L. Ivanova, and H. Eisele, Phys. Rev. B **80**, 085316 (2009).

Atomic Layer Epitaxy of III-N Semiconductors: How Low (in T) Can You Go?

C.R. Eddy, Jr.[1], N. Nepal[2], N.A. Mahadik[1], L.O. Nyakiti[2],
S.B. Qadri[1], M.J. Mehl[1] and J.K.Hite[1]

III-N materials continue to play a significant and growing role in a range of advanced device technologies from rf electronics to visible and UV emitters and detectors. Such a broad application space continues to motivate explorations into new ways to grow III-N materials with improved quality (reduced extended and point defects) and flexibility (ternaries and quarternaries with full stoichiometric ranges and, for each, with thicknesses varying from nanometers to micrometers). In this work, we explore the synthesis of binary III-nitride semiconductors (GaN, AlN and InN) by atomic layer epitaxy where we find growth temperatures for high-quality crystalline layers are less than half that of conventional growth methods and where that new parameter space leads to the discovery of new crystalline phases of some binaries.

Atomic layer epitaxy (ALE) is a method in which the precursors for growth are introduced in a sequence of gas pulses added to an inert carrier gas flow. ALE is simply atomic layer deposition (ALD) at higher temperatures sufficient to promote surface diffusion processes that allow either homo- or hetero-epitaxial growth. Here, we use pulses of trimethylgallium (TMG), trimethylaluminum (TMA) and trimethylindium (TMI) in group III pulses and plasma-activated nitrogen in group V pulses carried on an ultra-high purity (UHP) argon carrier gas and separated by purge steps with UHP Ar only flowing. All precursors are of UHP or semiconductor grade. This pulse sequence is investigated to define self-limited growth conditions for each binary semiconductor. A variety of substrates (silicon, sapphire, GaN templates on sapphire, etc.) are subjected to the pulse sequences at a range of temperatures from 150°C to 500°C in a customized Cambridge Nanotech, Inc. Fiji plasma-assisted ALD reactor. Growth rates and their dependencies on process conditions were assessed. Resulting films were assessed by a variety of techniques for structural, chemical, and electrical properties.

In all cases, preparation of the substrate surface is essential to growth of high quality films. We investigated a number of *ex situ* and *in situ* surface treatments and find that GaN surfaces pre-treated *ex situ* with HF and HCl and *in situ* with alternating pulses of trimethylgallium and hydrogen plasma followed by an hour of annealing at 500°C (emulating a Ga-flash-off process) resulted in the best surfaces. With these proper surface preparations, we are able to grow high quality, wurtzitic AlN at 500°C. These thin films (~36 nm) demonstrated smooth surfaces (~0.7 nm rms roughness for 10x10 μm^2 scan area) and (0002) peak rocking curve width of about 630 arc-sec, but contained a high fraction of carbon (8%) and small fraction of oxygen (0.6%). Similar efforts were demonstrated for GaN films grown between 350 and 450°C. For InN, two growth regimes were defined. One between 175 and 185°C, for which a new cubic phase of InN was realized by XRD and TEM, and a second regime between 220 and 260°C for which quality wurtzitic materials (262 arc-sec for (0002) reflection) were grown. As with AlN, both films contained high fractions of carbon (3%), but little-to-no oxygen (0.1%). Finally, initial efforts to grow ternaries of InAlN were conducted using a digital alloying approach where quality, crystalline ternaries were realized over the entire stoichiometric range. These early results suggest great potential for ALE growth of III-N semiconductors.

[1]U.S. Naval Research Laboratory, 4555 Overlook Ave., SW, Washington, DC 20375,
[2]American Association for Engineering Education, 1818 N Street, NW, Washington, DC 20036 Postdoctoral Fellow (residing at NRL)

We1355 Invited

Polarization-induced nanowire light emitting diodes with mid-deep UV emission

S. C. Carnevale[1], T. F. Kent[1], C. Marginean[2], F. Akyol[3], P. J. Phillips[4], R. F. Klie[4], S. Rajan[1,3], R. C. Myers[1,2,3]

1. Dept. of Materials Science and Engineering, The Ohio State University, Columbus, Ohio
2. Dept. of Physics, The Ohio State University, Columbus, Ohio
3. Dept. of Electrical and Computer Engineering, The Ohio State University, Columbus, Ohio
4. Dept. of Physics, University of Illinois, Chicago, Illinois

Among the direct and wide band gap semiconductors, III-Nitrides emerged as the material of choice for short wavelength light emitting diodes (LEDs), where a central challenge is hole doping (Mg). Secondly, dislocations limit their performance. Addressing both difficulties, we developed a pn-diode not requiring impurity doping, polarization-induced nanowire LEDs (PINLEDs) not containing dislocations and exhibiting hole conductivity in AlGaN without acceptor doping. If the composition of (Ga,Al)N is graded along the polarization dipole direction (c-axis), a slab of bound polarization charge is uniformly distributed in the crystal, which is compensated by free charges. By grading the composition in a back and forth manner within a nanowire (GaN→AlN→GaN) a polarization-induced pn-junction is formed. Unlike other pn-diodes, PINLEDs can be formed without intentional impurity doping, do not freeze out at low temperature, yet still exhibit rectification and ultraviolet light emission at the band gap (Carnevale et al, *Nano Lett.*, **12**, 915 (2012)). Since the junction material is AlN, in principle any wavelength in the AlGaN band gap range can be achieved by adjusting the composition of AlGaN quantum wells inserted in the junction region of the nanowires. To date, PINLEDs with EL from 360 nm to 250nm have been shown by varying the AlGaN composition in the quantum well. These UV LEDs can be electrical integrated onto silicon wafers, or grown on molybdenum substrates. Temperature and time-dependent photoluminescence spectroscopy measurements of the quantum efficiency and carrier lifetimes in the AlGaN quantum disk active regions of UV PINLEDs will be discussed.

In PINLEDs, the polarity of the nanowires determines the carrier type in each graded section, and therefore diode orientation (n/p versus p/n). Atomic resolution STEM measurements of a random selection of wires exhibit the N-face orientation. However, selective etching and scanning conductance mapping reveal that most of the wires are N-face (n-top/p-bottom), but some are Ga-face (p-top/n-bottom). When all the nanowires are connected in parallel, applying positive bias to the top of the nanowires leads to forward bias and recombination from the Ga-face wires, while large negative bias leads to forward bias of the N-face wires only. This leads to an unusual situation where either polarity applied to the ensemble devices shows EL; in reality, many pn diodes are connected in parallel with different orientation. Following from the polarity investigation, the current density in individual nanowire LEDs and the efficiency can be determined. New devices designed for optimal N-face nanowire orientation are discussed, where p-bottom contacts are formed automatically for PINLEDs that are grown directly on Mo-coated substrates.

Morphology and Evolution of Surface Reconstruction of an InAs-GaAs Wetting Layer at High Temperatures

Tomoya Konishi[1], Gavin R. Bell[1,2], Shiro Tsukamoto[1]

[1] Center for Collaborative Research, Anan National College of Technology, Tokushima 774-0017, Japan.
[2] Department of Physics, University of Warwick, Coventry, CV4 7AL, UK.

For optimal use of semiconductor quantum dots (QDs), it is desirable to arrange them in a highly dense and site-controlled array. However, important gaps remain in the understanding of the Stranski-Krastanow-like growth mechanism of InAs-GaAs QDs, particularly the effects of surface reconstruction (SR) in the wetting layer (WL) preceding QD nucleation. It is reported that the (n×3) SRs favor intermixing of Ga and In atoms. Furthermore, *ab initio* Monte Carlo simulations have shown that the migration barrier energy of mobile In adatoms becomes higher on Ga defects, implying that QD nucleation occurs preferentially on Ga-rich fluctuations within the WL, associated with ×3 SR [1].

In order to confirm the ansatz experimentally, we carefully measured the spatial distribution of ×3 SR in the WL using a unique scanning tunnelling microscopy / molecular beam epitaxy (STMBE) system. If QD nucleation is induced by ×3 SR, it is likely that the spatial distribution of QD precursors resembles that of ×3 SR [2]. In this study, we analyzed the spatial distribution of the SR on the 100×100 nm^2 STMBE images by using image processing techniques (Fig. 1). The SR is distinguished by As dimer row pitch (×2, ×3 and ×4 regions). We finally obtained a precise map of SR patterns. We demonstrate that the frequency distribution of the measured pitches is comparable with the RHEED patterns and Fourier transformed STM images (Fig. 2).

From the SR map of WL, the spatial distribution function of ×3 SR pattern was calculated and was compared to that of QD nucleation pattern. The similarity in the both functions suggested that QD nucleation is likely induced by Ga-rich fluctuations forming ×3 SR.

[1] S. Tsukamoto, T. Honma, G. R. Bell, A. Ishii, and Y. Arakawa, Small, **2** 386 (2006).
[2] T. Konishi, S. Tsukamoto, Surface Science **605** L1–L5 (2011).

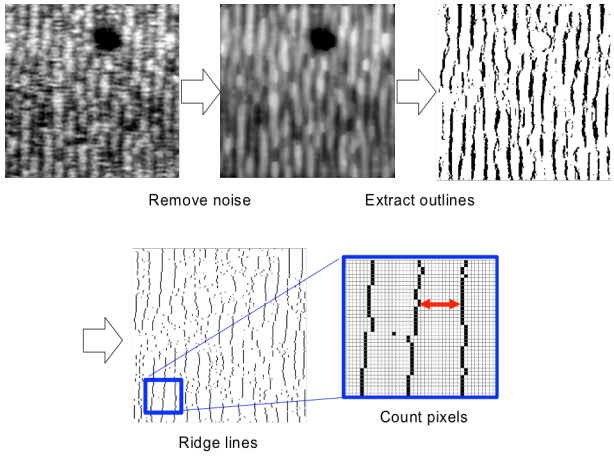

Fig. 1: Schematic diagram of surface reconstruction map generation on an example 20×20 nm^2 region.

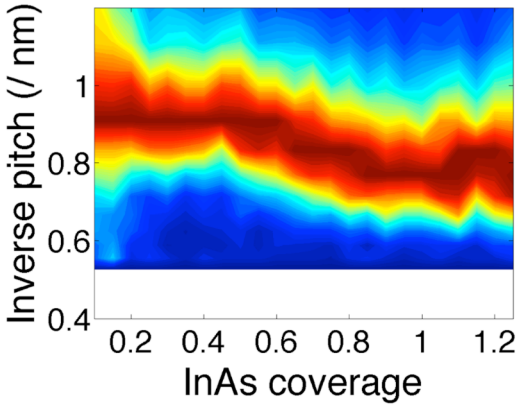

Fig. 2: Evolution of As dimer row pitch as a function of InAs coverage. It is shown that the surface reconstruction changes from ×2 to the mixture of ×3 and ×4.

Title: Surface Morphology of GaAs and GaSb (111)A Grown by Molecular Beam Epitaxy

Authors: Law, J. J. M.;[1] Calderon, I.;[1,3] Huang, C. –Y.;[1] Lu, H.;[2] Rodwell, M. J. W.;[1] and Gossard, A. C.[1, 2]

[1]*ECE and* [2]*Materials Departments, University of California, Santa Barbara*

[3]*Santa Barbara City College*

For equivalent oxide thicknesses (EOTs) below 1 nm, the higher density of states of Si will provide more drive current per gate width than higher injection velocity III–V materials, e.g., $In_xGa_{1-x}As$, InP, etc. By utilizing the effective mass anisotropy of the satellite X– and L–valleys of III–V materials, it may be possible to have simultaneously large density of states and high injection velocities. Rotating the wafer to the (111) orientation, the maximum anisotropy between the longitudinal and transvers effective mass of one of the L–valleys can be harnessed to either allow for several L–states or a Γ– and an L– state to be aligned.[1] Atomically smooth heterointerfaces grown on the (111) are required as the quantum–well thicknesses required to align the first Γ– and L–eigenstate are approximately 1–2 nm.[2]The extremely low–energy of formation of inverted domains or stacking faults due to the 60° rotational symmetry of the (111) plane hinders the growth of atomically flat, defect–free crystals and heterojunctions. Particular care must be taken to encourage bonding and/or growth along step edges in order to preclude the formation of stacking faults.[3] We have used previously reported growth conditions[4] for smoothing of GaAs grown on GaAs (111)A to improve surface morphology of GaAs growth on vicinal GaAs (111)A substrates and heteroepitaxial GaSb on on–axis GaAs (111)A.

Samples were grown on semi–insulating GaAs (111)A substrates. Substrates were nominally on–axis (± 0.2 °), 2°±0.5° off–axis towards (100), and 2°±0.5 off–axis towards $(\bar{1}\bar{1}2)$. All GaAs samples were grown at ~ 600 °C (temperature measured by pyrometer) while all GaSb samples were grown at ~ 535 °C. Increasing the V:III beam equivalent pressure (BEP) ratio during growth helped improve the surface morphology of both the GaAs and GaSb. Optimized GaAs and GaSb samples were grown with V:III BEP ratios of ~70 and 15, respectively. Increasing the ratio of As_4 to As_2 and Sb_4 to Sb_2 by decreasing the As and Sb cracking zones from 850 to 600 °C and 900 °C to 760 °C, respectively, improved surface morphology of both on–axis GaAs and on–axis GaSb. In the case of on–axis GaAs, decreasing the cracking zone temperature decreased stacking fault densities from 1.24 to 0.78×10^8 cm^{-2}, as evidenced by the reduction of hexagonal or triangular surface features in AFM images. Surface terminations of stacking faults, as seen by AFM, were eliminated entirely by introducing a 15 min. 640 °C post–growth anneal. Surface morphologies from optimized growths showed 0.5–1 μm wide steps with RMS roughnesses of 0.054 nm (~0.5 μm^2). GaAs grown on vicinal substrates showed stacking–fault–free morphologies without post–growth annealing. Samples off–cut to (100) showed bowed and/or kinked step edges with large surface mounds at the apex of the kinks. These samples had 5×5 μm^2 RMS roughnesses of ~ 0.63 nm; samples off–cut to $(\bar{1}\bar{1}2)$ showed kink–free step edges with surface roughness of ~ 0.24 nm. Increasing the Sb_4 to Sb_2 ratio and post–growth annealing (for 15 min. to 600 °C) improved the morphology of GaSb grown on optimized on–axis GaAs (111)A; however, while the density of stacking faults decreased, the triangular surface features indicative of stacking faults were not entirely eliminated. Additionally, large and ~ 50 nm deep surface pits were reduced in lateral (~ from 1–2 to 0.5–1 μm) dimension, but they were not entirely eliminated using these techniques.

[1] M. J. W. Rodwell *et al.* 2010 IEEE Device Research Conference (DRC) 2010, June 2010, South Bend, Indiana, pp. 149.
[2] S. Mehrotra *et al.* 24th IEEE Conference on Indium Phosphide and Related Materials (IPRM), August 2012, Santa Barbara, California, pp
[3] Y. Okano *et al.*, Jpn. J. Appl. Phys. **29** L1357 (1990).
[4] P. J. Simmonds *et al.* Appl. Phys. Lett. **112** 054313 (2012).

We1435

Use of atomic hydrogen to prepare GaSb(211)B and GaSb(100) substrates for subsequent ZnTe growth by MBE

T.H. Myers[1], J. Chai,[1] K.K. Lee[1], O.C. Noriega,[2] J.H. Dinan,[1] A. Savage,[1]
J.J. Kim[3], and D. J. Smith[3]

[1]Material Science, Engineering, and Commercialization Program, Texas State University-San Marcos, TX 78666,
[2]Physics Department, Texas State University-San Marcos, TX 78666, USA
[3]Department of Physics, Arizona State University, Tempe, AZ 85287-1504, USA

ZnTe is a material of much current interest for photovoltaic applications and it is also considered as a possible buffer layer for growth of HgCdTe or HgCdSe. Moreover, the ZnTe/GaSb heterostructure itself is of potential interest for cascade solar cells. Thus, different approaches geared towards optimizing the epitaxial growth of high quality ZnTe/GaSb are under active investigation. We have investigated the use of atomic hydrogen for surface preparation of GaSb for subsequent growth of ZnTe and ZnTeSe. We have carried out a detailed microstructural study of these ZnTe/GaSb(211)B samples using cross-section transmission electron microscopy as well as x-ray photoelectron spectroscopy, x-ray diffraction, atomic force microscopy and imaging photoluminescence measurements. We will present results indicating that we are able to get smooth, clean and stoichiometric GaSb surfaces suitable for subsequent epitaxial growth without using an Sb overpressure. In particular, ZnTe layers with thicknesses of 350 nm and below have highly coherent and sharp interfaces with the GaSb, and exhibit very low densities of dislocations. We have grown thick ZnTeSe/GaSb layers with dislocation densities in the mid-10^4 cm^{-2}. We are also growing additional ZnTe samples on GaSb(100) substrates by MBE and will report that study as well during the presentation.

Epitaxy & Graphene I

We1515

Epitaxial growth and electronic band structure of the semiconducting Half Heusler compound CoTiSb

J. K. Kawasaki,[1] L. M. Johansson,[2] M. Hjort,[2,3] R. Timm, [2,3] B. D. Schultz,[4] T. Balasubramanian,[5] A. Mikkelsen,[2,3] and C. J. Palmstrøm[1,4]

[1]Materials Department, University of California Santa Barbara
[2]Nanometer Structure Consortium (nmC@LU), Department of Physics, Lund University, Sweden
[3]Division of Synchrotron Radiation Research, Department of Physics, Lund University, Sweden
[4]Department of Electrical and Computer Engineering, University of California Santa Barbara
[5]MAX-Lab, Lund University, Sweden

We demonstrate the first epitaxial growth of the Half Heusler compound CoTiSb. CoTiSb belongs to the family of Half Heuslers with 18 valence electrons per formula unit that are predicted to be semiconducting despite being composed of all metallic components. However due to challenges in growing high quality single crystals, clear semiconducting behaviour has not yet been demonstrated. Here the CoTiSb films were grown by molecular beam epitaxy on a lattice matched $In_xAl_{1-x}As$ buffer layer. The films are epitaxial and single crystalline, as measured *in situ* by reflection high energy electron diffraction (RHEED), low energy electron diffraction (LEED), and scanning tunnelling microscopy (STM). The CoTiSb(001) surface reconstructions change as a function of temperature and Sb overpressure in a manner similar to that observed for traditional compound semiconductors. The electronic band structure of the films was measured by angle resolved photoemission spectroscopy (ARPES) at the MAX-Lab synchrotron facility in Lund, Sweden. A protective Sb capping and decapping scheme was developed to maintain the surface quality of the films as the samples were transported to the characterization facility and exposed to air. The CoTiSb films are demonstrated to be semiconducting, with a valence band maximum 0.6 eV below the Fermi level, and the measured bulk band dispersion is in general agreement with density functional theory and tight binding calculations. The CoTiSb films also have metallic surface states that cross through the Fermi level at the $\bar{X}$ points, consistent with scanning tunnelling spectroscopy (STS) measurements.

This work was supported in part by the Office of Naval Research, the Air Force Office of Scientific Research, the National Science Foundation, and the Swedish Research Council.

Epitaxial Growth Cubic InN Films via Plasma-Assisted Atomic Layer Epitaxy

N. Nepal[1], N.A. Mahadik[1], J.K. Hite[1], S.B. Qadri[2], M.J. Mehl[2], and C.R. Eddy, Jr[1].

[1]Electronics Science & Technology Division, U.S. Naval Research Laboratory, Washington, DC 20375, USA

[2]Material Sciences and Technology Division, Naval Research Laboratory, Washington, DC 20375, USA

Among III-nitride semiconductors, indium nitride (InN) has the smallest direct band gap, largest electron saturation velocity and mobility, and smallest electron effective mass. It has long been an attractive semiconductor material for application in optical, electrical, and optoelectronic device technologies such as solar-cells and high electron mobility and high frequency devices. Cubic InN has even smaller band gap and superior electronic properties as its lattice is isotropic and possesses lower phonon scattering compared to hexagonal InN [1-2]. The most thermodynamically stable phase of the InN is a wurtzite structure (a hexagonal phase). Fairly low growth temperature is required to grow meta-stable phases and prevent its dissociation. A zincblende (a cubic phase) InN on InAs/GaAs has been demonstrated at 450 °C by plasma assisted molecular beam epitaxy (MBE). However, there are no previous reports on epitaxial growth of InN by true-ALE at low temperatures (<300 °C), which would allow growing novel phases of materials. Here, we report on growth of a new face centered cubic InN with NaCl-type structure.

InN layers (5-60 nm thick) were simultaneously grown by ALE on a-plane sapphire, Si(111), and GaN/sapphire templates using a Cambridge Nano Tech Fiji 200 atomic layer deposition/epitaxy system at temperatures from 175 to 260 °C. The InN layers were characterized using spectroscopic ellipsometery (SE), x-ray photoelectron spectroscopy (XPS), x-ray diffraction (XRD), Laue diffraction (LD), Hall Effect, atomic force microscopy (AFM), and transmission electron spectroscopy measurements. Based on SE measurements, there are two ALE growth temperature windows between 175 - 185 °C and 220 – 260 °C in which the growth process is self-limiting. In the lower temperature ALE window, InN on a-plane sapphire crystallized in a face centered cubic lattice with a NaCl type structure, which has never been previously reported. InN grown on other substrates predominantly formed the more common hexagonal phase. The NaCl-phase and the epitaxial nature of the InN films on a-plane sapphire grown at 183 °C are confirmed independently by x-ray diffraction, transmission electron microscopy, and numerical simulations. These results are very promising and demonstrate the tremendous potential for the PA-ALE in the growth of crystalline III-N materials with novel phases unachievable by other deposition techniques.

1. Talwar, D. N., Sofranko, D., Mooney, C. & Tallo, S. *Mater. Sci. Eng. B* **90**, 269-277 (2002).
2. Nanishi, Y., Saito, Y. & Yamaguchi, T. *Jpn. J. Appl. Phys.* **42**, 2549-2559 (2003) and the references therein.

Single Crystal Zinc Oxide Formed Epitaxially on Single Crystal Gold

Kathryn J. Greenberg, John H. Joo, Mor Baram, David R. Clarke, and Evelyn L. Hu

The interface between metal and oxide or metal and semiconductor can play a critical role in the performance of electrical and optical devices. Most metal-oxide interfaces are formed using vapor phase deposition techniques which do not result in an epitaxial relationship. These techniques have limitations such as the incorporation of contaminants at the interface and alloying of the metal with the material on which it is deposited. The aqueous growth method presented here overcomes several of these problems.

Until now, there has been very limited research done on the epitaxial growth of zinc oxide (ZnO) on metals. We demonstrate the ability to epitaxially grow ZnO on single crystalline gold as shown in Figure 1. The gold plates, which are up to 100µm in width, are grown using a thermolysis technique from a gold-surfactant complex. Before the growth of ZnO, a nucleation step is performed using either microwave heating, for fast nucleation, or oven heating, for slow nucleation. The speed of the nucleation determines the roughness of the zinc oxide film. The single crystalline ZnO is then grown in an aqueous solution at 90°C for several hours depending on the thickness of the ZnO desired. The lattice mismatch between the close packed directions of gold and ZnO is 12.7%, but even with this mismatch an epitaxial relationship between the two materials is obtained. To further study and confirm the epitaxial relationship, scanning electron microscopy, electron backscatter diffraction, transmission electron microscopy, and electron diffraction are used. Both the in-plane hexagonal symmetry and the out of plane orientation of the zinc oxide are studied. Micro-photoluminescence spectroscopy is used to probe the optical properties of the epitaxial zinc oxide.

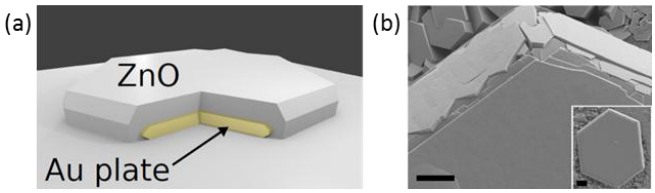

Figure 1: (a) Schematic representation of ZnO grown on single crystalline gold plate. (b) SEM image of microwave nucleated ZnO on a gold plate after the growth step. Scale bar = 5µm. Insert shows the entire gold plate with smooth and flat ZnO grown on top. Scale bar = 20 µm.

In addition to confirming the epitaxial relationship between the metal and oxide, the interface between the gold and zinc oxide is further investigated using a range of techniques. Removal of the ZnO from the gold microplates using a stamping and wet etching process creates single crystalline ZnO membranes, the thickness of which is determined by the growth time. The roughness of the membrane surface is observed to depend on the type of nucleation. As well as allowing study of the zinc oxide-gold interface, these membranes can themselves be used to fabricate high quality optical devices such as optical cavities. Reflection measurements of the ZnO on single crystalline gold are performed and compared to those of ZnO on polycrystalline gold, in which there is no epitaxial relationship. Since interfaces between metals and oxides are found in numerous types of devices, it is also important to study the electrical properties of the interface between the gold and ZnO. The contact resistance is calculated along with the carrier injection into the epitaxial zinc oxide for both ZnO on single crystalline gold plates as well as on polycrystalline gold. There is a wide range of applications for metal-oxide interfaces. The high quality ZnO-gold interfaces fabricated here have the potential to enhance the performance of existing devices, such as improving electrical contacts to high bandgap materials and increasing light extraction from planar LEDs.

Quantum Transport and Correlated Phenomena in Bilayer and Trilayer Graphene

Graphene, a two - dimensional single atomic layer of carbon, has recently emerged as a new model system for condensed matter physics, as well as a promising candidate for electronic materials. Though single layer graphene is gapless, bilayer and trilayer graphene have tunable band gaps that may be induced by out-of-plane electric fields or arise from collective excitation of electrons. Here I will present our results on transport measurements in bilayer and trilayer graphene devices with mobility as high as 400,000 cm^2/Vs. We demonstrate the presence of an intrinsic gapped state in bilayer graphene at the charge neutrality point, evidence for quantum phase tranisition, and stacking-order dependent transport in trilayer graphene. Our results underscore the fascinating many-body physics in these 2D membranes, and have implications for band gap engineering for graphene electronics and optoelectronic applications.

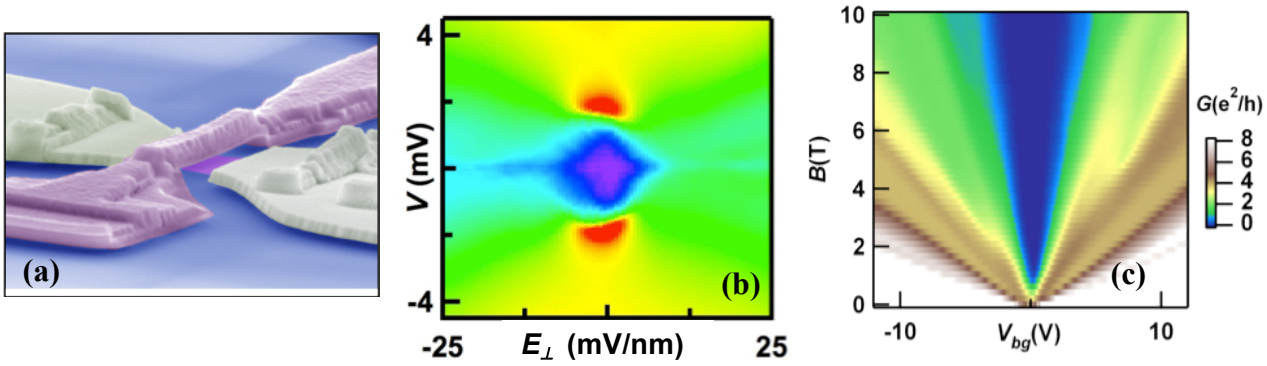

Fig. 1.(a) SEM image of a suspended graphene membrane with suspended top gate. (b). $G(V, E_\perp)$ for a BLG device at the Dirac point. (c). Landau level fan diagram of a double-gated trilayer graphene device. The plot displays conductance (color) vs gate voltage and magnetic field with symmetry-broken Landau levels.

References:

1. W. Z. Bao, Z. Zhao, H. Zhang, G. Liu, P. Kratz, L. Jing, J. Velasco, D. Smirnov, and C. N. Lau, *Phys. Rev. Lett.* **105**, 246601 (2010).
2. W. Bao, L. Jing, Y. Lee, J. V. Jr., P. Kratz, D. Tran, B. Standley, M. Aykol, S. B. Cronin, D. Smirnov, M. Koshino, E. McCann, M. Bockrath, and C. N. Lau, *Nat. Phys.*, 7, 948 (2011).
3. J. Velasco, L. Jing, W. Bao, Y. Lee, P. Kratz, V. Aji, M. Bockrath, C. N. Lau, C. Varma, R. Stillwell, D. Smirnov, F. Zhang, J. Jung, and A. H. MacDonald, *Nature Nanotechnology*, 7, 156 (2012).
4. W. Bao, J. Velasco Jr., F. Zhang, L. Jing, B. Standley, D. Smirnov, M. Bockrath, A. MacDonald, and C.N. Lau, *Proc. Nat. Acad. Sci.*, to appear (2012).

Email: lau@physics.ucr.edu

J. Lau, Univ. of California, Riverside

Effects of surface geometry on the wettability of water on graphene

Tomohiro Yonemaru[1,2], Hiroki Shimizu[1], and Jun Nakamura[1,2]
[1]*The University of Electro-Communications (UEC-Tokyo), Tokyo, Japan*
[2]*Japan Sceience and Technology Agency (JST), CREST, Saitama, Japan*

Interactions between water molecules and material surfaces, especially between graphene and water molecules, have been studied widely. Recently, it has been revealed experimentally that a uniform structured-water layer exists at the graphite/water interfaces, while graphene is a hydrophobic substrate [1]. The structure and dynamic properties of interfacial water at the graphene surface have also been investigated using molecular dynamics (MD) simulations. The first layer of water on graphene is more structured than the liquid bulk and well-oriented with respect to the surface, forming a local ice structure with the Ih symmetry [2]. On the other hand, the water layer on the atomically-featureless graphite wall is not flat, with some hydrogen atoms pointing perpendicularly to the surface plane [3]; the local structure of interfacial water is quite different from the ice Ih structure.

In this study, we have investigated effects of the potential corrugation of graphene on the ordering of water molecules using the MD simulations. Figures 1(a) and 1(b) show the equilibrated structures of water on the graphene and the geometry-less graphene, respectively. As shown in Fig.1(b), the water molecules form a liquid droplet on the geometry-less graphene, being superficially consistent with the hydrophobic nature of graphene. But, the water layer on the graphene with the atomic geometry shows high wettability even at 300K as shown in Fig.1(a). These results show that the atomic corrugation of graphene plays a crucial role in the wetting and ordering properties of the water molecules. When the number of water molecules is increased, the water forms a liquid droplet on the graphene at 300K, as seen in Fig.2. What has to be noticed is that the water molecules proximal to the surface still form layered structures even in such a droplet structure, which reminds us the so-called Stranski-Krastanov fashion in the crystal growth for hetero systems. Viewed in this light, we reasonably conclude that the graphene is hydrophilic from a microscopic point of view, while hydrophobic if we look down from a macroscopic stand point.

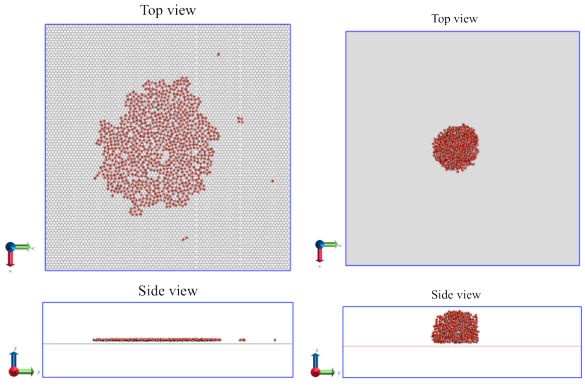

Fig.1 Snapshot of the equilibrium states for the water molecules (a) on the graphene and (b) on the geometry-less graphene at 300K. 864 water molecules are adsorbed on the graphene and the geometry-less graphene. The unit cell size is 20 nm x 20 nm.

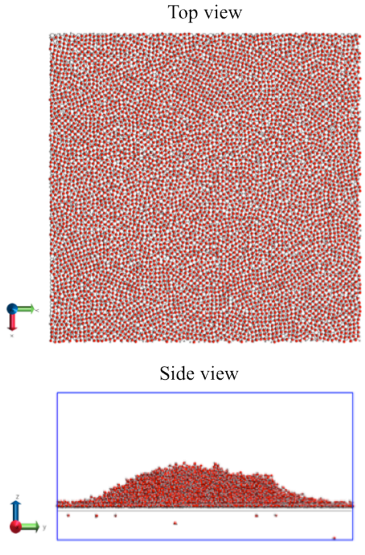

Fig.2 Snapshot of the equilibrium state for the model of 11,440 water molecules on the graphene.

References

[1] K.Suzuki *et al.*, Applied Physics Express **4**, 125102 (2011)
[2] L. M. Alarcón *et al.*, Chem. Phys. **388**, 47 (2011)
[3] M.C. Gordillo and J. Martí, J. Chem. Phys. **117**, 3425 (2002)

Corresponding author: Tomohiro Yonemaru
Department of Engineering Sciences,
The University of Electro-Communications (UEC-Tokyo)
1-5-1 Chofugaoka, Chofu, Tokyo 182-8585, Japan
e-mail: yonemaru@natori.ee.uec.ac.jp
Tel.& FAX: +81-42-443-5156

We1605

Electronic Effects of Non-Covalent Molecular Modification of Graphene NanoElectronic Devices

Christina A. Hacker, Michael A. Walsh, Curt A. Richter[1],

[1]*Semiconductor and Dimensional Metrology Division, Physical Measurements Laboratory, National Institute of Standards and Technology, Gaithersburg, Maryland 20899,*

Graphene is a two-dimensional material with many intriguing properties making it of interest for electronic and optical applications. Researchers have made electronic devices out of graphene demonstrating high speed applications, and photovoltaics demonstrating its use as a transparent electrode. Of particular interest is the ability to couple organic molecules to the graphene surface to 1-use organic molecules to modulate the electronic properties of graphene in a static fashion or 2-use organic molecules to create dynamic electronic materials. There are two typical routes for incorporating molecular layers on graphene, covalent or non-covalent/ π-π stacking attachment of organic monolayers. Covalent attachment provides robust linkages between the substrate and the organic molecules while also disrupting the 2-dimensional network and degrading the electronic properties, such as mobility. Non-covalent molecular attachment, on the other hand, preserves the integrity of the graphene layer but can also bond molecules to the graphene surface in an uncontrolled and unstable fashion. Pyrene is a typical molecule used to alter the electronic properties of graphene and carbon nanotube as it π-π stacks nicely, is easily functionalized with a variety of moities, and provides a nice balance of aromaticity and solubility.[1] Researchers recently synthesized cobalt-centered redox molecules that contain pyrene moieties which are capable of assembling on graphene and demonstrated electrochemical activity on the surface.[2] Synthetically altering the molecule to contain three pyrene substituents enabled the tripod like Co molecule to assemble on the graphene surface with higher integrity making it an ideal candidate for tailoring the electronic properties of graphene with an assembled monolayer.

We report the electronic properties of graphene structures functionalized with π-π stacking of Co-containing molecules shown in Figure 1. Cobalt bis-terpyridine [$Co(tpy)_2$] containing tripodal compounds have been designed to noncovalently adsorb to graphene through three pyrene moieties. The presence of the molecules was verified by XPS. FTIR and Raman spectroscopies were performed on the graphene both, prior to and following, monolayer adsorption to verify the structure. Electrical properties of graphene were characterized by using a hall bar setup with the measurements performed under vacuum. Local electronic changes were investigated with scanning probe microscopy. The presence of the cobalt molecules impacts the electrical properties of the graphene causing an average downward shift in the charge neutrality point of -12V suggesting the molecules induce an n-doping while the carrier mobility is relatively unchanged. The combination of redox active molecules and graphene nanoelectronic devices provide a key step toward developing dynamic electrode surfaces for sensing, electrocatalysis, and electronic applications.[3]

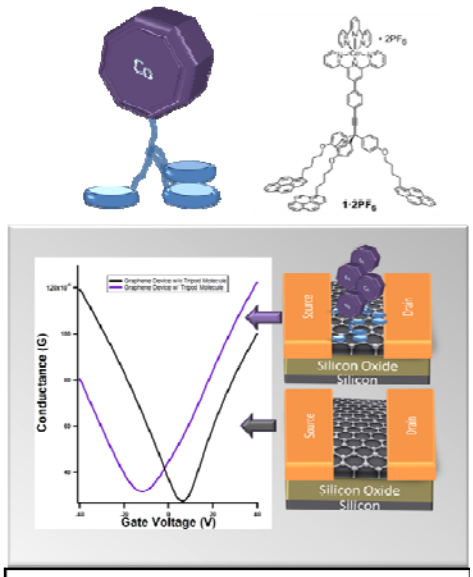

Fig. 1: Tripod molecules shown at the top can alter the electronic properties of nanoelectronic architectures with molecular layers physically adsorbed to the graphene surface (bottom). Representative conductance-voltage data (left) and corresponding schematic (right) of graphene nanoelectronic devices.

We1610

Imaging of Electron Beam Induced Current in Epitaxial graphene

Shin Mou, John Boeckl, Weijie Lu, J.H. Park, W.C. Mitchel
Air Force Research Laboratory, Materials and Manufacturing Directorate, Wright-Patterson AFB, OH 45433, USA

Stephen Tetlak
Wyle Laboratories, Dayton, OH 45431 USA

Abstract

It has been known and observed that there forms a Schottky junction between graphene and SiC in epitaxial graphene due to the work function difference and the charge transfer between them. As a result, it is viable to apply the electron beam induce current (EBIC) technique on the epitaxial graphene due to the fact that the built-in field at the Schottky junction sweeps out the excited carriers generated by the electron beam. EBIC is an important characterization technique, which identifies electrically active impurities/defects, detects local built-in fields, and measures minority carrier diffusion lengths. In this paper, we use a FEI SEM equipped with a current amplifier to investigate the spatial distribution of EBIC which is collected in a two terminal geometry. The incident electron beam generates excited electron-hole pairs in SiC and the minority carriers are collected through the Schottky junction before flowing into graphene. EBIC imaging reveals microscopic domains of bright and dark contrast areas due to the local EBIC polarity and magnitude, which is believed to result from the spatial fluctuation of the carrier density in graphene. We also investigate the EBIC intensity as a function of the electron energy. Using an analytical drift-diffusion current model to fit the electron energy dependent data, we are able to extract the minority carrier diffusion length in the SiC, which is on the order of a few micro meters and agrees well with published data.

Growth of III-N Semiconductors on XeF_2 Functionalized Epitaxial Graphene

N. Nepal, V. D. Wheeler, T.J. Anderson, F.J. Kub, M. A. Mastro, R. L. Myers-Ward, S.C. Hernandez, F. Bezares , J. A. Freitas, L.O. Nyakiti, A. D. Koehler, D. K. Gaskill, K.D. Hobart, and C. R. Eddy, Jr.

U.S. Naval Research Laboratory, 4555 Overlook Ave., SW, Washington, DC 20375, USA

In hot-electron transistors (HET) with a heavily doped semiconductor base layer, the ballistic or quasi-ballistic transportation of hot electrons is inhibited by impurity and carrier-carrier scattering [1]. Whereas for HETs with a metal base layer, the quantum mechanical reflection at the interface between metal and semiconductor partially prevents hot-electron from being transmitted to the collector region [2]. Replacing the base layer of HET with graphene provides the possibility of overcoming these limitations and enable high-speed operation (>1THz). For high-power, high-voltage applications, the HET emitter is required to be a robust, wide bandgap material. III-nitride semiconductors are very promising materials for such applications due to their robustness and properties supporting high power and rf device application. Thus, a III-nitride HET incorporating a graphene base layer could outperform current state-of-art InP based heterojunction bipolar transistor [3-4]. However, a key technological hurdle inhibiting the realization of such a device is the growth of semiconductor quality material on the relatively inert sp^2-bonded graphene surface, which lacks out-of-plane bonds. There have been previous efforts to grow GaN on oxygen plasma treated graphene [5], but the resulting GaN layer was polycrystalline, with a rough and irregular surface. In this work, we report the first ever epitaxial growth of III-N semiconductor layers on epitaxial graphene (EG) to enable a range of potential heterojunction devices.

A thin AlN nucleation layer was grown on functionalized EG [6] using atomic layer epitaxy. This thin layer enabled subsequent growth of a thick GaN epilayer by metalorganic chemical vapor deposition (MOCVD). The surface morphology of these GaN/AlN/graphene layers reveals smooth and uniform surfaces with steps and terraces, typical of the underlying silicon carbide substrate after EG growth [7]. Raman measurements taken after GaN growth show the presence of the graphene 2D peak at 2719 cm^{-1} confirming the preservation of the graphene. X-ray diffraction analysis reveals [0001] oriented hexagonal GaN with a rocking curve full width at half maximum (FWHM) of (0002) and (0004) peaks of about 544 and 641 arc-sec, respectively. These FWHM values are similar to values observed for GaN grown by MOCVD on sapphire [8]. The GaN layer has a strong room temperature photoluminescence (PL) band edge emission at 3.40 eV, which supports high optical quality GaN layer on graphene. Successful demonstration of GaN growth on graphene opens up possibilities of III-nitride/graphene heterostructure-based devices.

1. Y. Miyamoto et al., Jpn. J. Appl. Phys. 42, 7221 (2003).
2. M. Tonouchi, H. Sakai and T. Kobayashi, Jpn. J. Appl. Phys. 25, 705 (1986).
3. C. Kunook, L. Chul-Ho, and Y. Gyu-Chul, *Science* **330,** 655 (2010).
4. Pending F.J. Kub, "Transistor Having Graphene Base," U.S Patent Application 2012/0068157 21 Sept. 2011.
5. W. Mehr et. al., Electron Device Letters, 33, 691-693 (2012).
6. V.D. Wheeler et al., *Carbon* **50**, 2307-2314 (2012).
7. L.O. Nyakiti et al., *Nano Letters* **12**, 1749-1756 (2012).
8. J. N. Kuznia et al., *J. Appl. Phys*. **73,** 4700-4702 (1993).

Finite-ranged Impurity Effect to Hall Conductivity in Graphene

M. Noro, S. Murakami and T. Ando

Department of Physics, Tokyo Institute of Technology

We study the Hall effect in a weak magnetic-field of graphene containing scatterers with finite potential range in the real space. In our previous study, the effect of long-ranged impurities to longitudinal conductivity is shown and it solves the so-called missing-π problem which has been discussed for a long time [1]. In this work, the scattering effects to Hall conductivity are taken up by using Green's function technique within a self-consistent Born approximation in the same way as in the previous study. To see explicit dependence on the potential range, we consider scatterers with a Gaussian potential with range *d*.

Figures show the results of the Hall conductivity in graphene as a function of Fermi energy. The Hall conductivity has two peaks around the Dirac point for the scattering strength *W=0.15*. It shows an increase for the high energy region. The result of short-ranged limit converges for high-energy region which corresponds to that of impurities with δ-functional potentials [2]. For *W=0.2*, the peak structure around the Dirac point vanishes because of strong scattering from high-energy region. Such an increase for the high-energy region or the vanished peak of the Hall conductivity does not appear in the short-ranged case.

We also show the Hall conductivity in single Dirac fermions. In this case, we consider the Zeeman splitting term which in the graphene case does not affect the Hall conductivity.

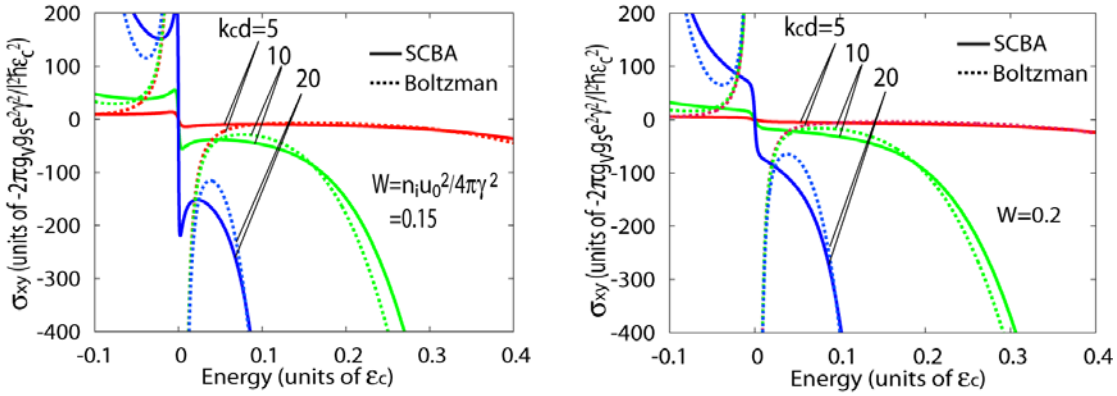

Fig.: Hall conductivity for dimensionless scattering strength *W*=0.15(left) and 0.2(right). g_v (=2) and g_s (=2) are the valley degeneracy and spin degeneracy. ε_c, k_c are the cut-off energy and the wave number, respectively. $k_c d = 5(20)$ corresponds to short (long) ranged case.

[1] M. Noro, M. Koshino and T. Ando, J. Phys. Soc. Jpn. 79, 094713 (2010)
[2] T. Fukuzawa, M. Koshino and T. Ando, J. Phys. Soc. Jpn.**78**, 094714 (2009)

Controlled Interface Manipulation for Epitaxial Graphene on 4H- & 6H-SiC using Scanning Tunneling Microscopy

P. Xu, M. L. Ackerman, S. D. Barber, J. K. Schoelz, D. Qi, and P. M. Thibado[a)]
Department of Physics, University of Arkansas, Fayetteville, Arkansas 72701, USA

V. D. Wheeler, L. O. Nyakiti, R. L. Myers-Ward, C. R. Eddy, Jr., and D. K. Gaskill[b)]
Naval Research Laboratory, 4555 Overlook Ave., SW, Washington, DC 20375, USA

Epitaxial graphene grown on SiC has been identified as one of the most likely avenues to graphene-based electronics. A detailed understanding of the morphology of the graphene is therefore important. In our work, epitaxial multilayer graphene grown on the polar and non-polar surfaces of 4H-SiC and 6H-SiC, respectively, was investigated using scanning tunneling microscopy (STM). Bunched nano-ridges ten times smaller than previously recorded were observed throughout the 4H-SiC surface. A new STM technique called electrostatic-manipulation scanning tunneling microscopy (EM-STM) was performed to alter the morphology of the nano-ridges; and a demonstration of this is shown below in Fig. 1. A raised area above the long narrow trench can be seen in the upper middle section of Fig. 1(a). After collecting this image, an EM-STM measurement was carried out directly on top of the raised area. For EM-STM, the bias voltage was ramped from 0.1 V to 3.0 V while the feedback loop was left on (constant current mode). After EM-STM (data not included), the surface topography changed as shown in Fig. 1(b). Namely, the raised region has now collapsed. The surface height in this region has dropped by ~0.1 nm. At the atomic scale, STM images reveal an apparent lattice constant dilation. We will show that this dilation is due to the STM tip electrostatically dragging the graphene surface. Similar lattice dilation results were obtained for graphene grown on the a-, m-, and r-crystallographic oriented surfaces of 6H-SiC. By modeling the electrostatics involved in the EM-STM measurement, we estimate that a force of ~5 nN and energy of ~10 eV was required to alter the local interfacial bonding.

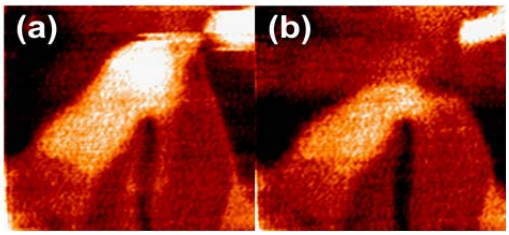

Fig. 1. A chronological series of filled-state STM images of graphene on 4H-SiC, measuring 250 nm × 250 nm and taken with a tip bias of 0.1 V and a setpoint current of 0.1 nA. (a) STM image take before EM-STM was performed; (b) STM image take after EM-STM was performed. The EM-STM data consists of height vs. voltage data taken with the feedback on (constant current mode). The EM-STM data is not shown.

This work is supported in part by ONR grant N00014-10-1-0181 and NSF grant DMR-0855358.

[a] Electronic mail: thibado@uark.edu
[b] Electronic mail: gaskill@nrl.navy.mil

The Evolution of PCSI—A Perspective of the Last 40 Years

David K. Ferry

School of Electrical, Computer, and Energy Engineering, Arizona State University
Tempe, AZ 85287-5706, ferry@asu.edu

PCSI was born in the Fall of 1973 as an idea to focus scientific attention on the questions surrounding the surfaces and interfaces of compound semiconductors, with the first conference being held in Fort Collins, CO, in January 1974. Since then, the conference has grown and evolved, but still focuses upon important current questions about the science of surfaces and interfaces. Over the intervening years, many breakthroughs, as well as the consolidation of various ideas, have come from the conferences. In this talk, I will highlight a few of these, as well as discuss some ideas that failed to be recognized at the time, perhaps because the world wasn't ready for them. Perhaps the key significance of the conference over the years has been its continued importance, as many attendees have remained constant over long periods of time, and it has been a site of important, and continued, discussions that have led to major advances in the field.

Thursday

Th0730	Continental Breakfast
Th0830	Thursday Morning Session: Spin Torque & Graphene
Th0930	Coffee Break and Poster Viewing
Th0830	Thursday Morning Session: Graphene II
Th1145	Conference Ends

Spin Torque & Graphene

Th0830 Invited

Giant Spin Hall Effects and Spin Transfer Torques in Heavy Metal/Ferromagnet Thin Film Devices

Dan Ralph, Luqiao Liu, Chi-Feng Pai, Alex Mellnik, Yun Li, Hsin-Wei Tseng, OukJae Lee, and Robert A. Buhrman

The spin Hall effect is a phenomenon that can occur in heavy metals due to the presence of spin-orbit coupling. When a charge current flows through such a material, electrons with different spin orientations can be deflected along different spatial paths, with the result that the flow of charge current generates a transverse flow of pure spin current. Usually the strength of this effect is characterized in terms of the spin Hall angle $\theta_{SH} = \left[J_S / (\hbar/2)\right] / \left[J_e / e\right]$, the dimensionless ratio of the transverse spin current density to the applied chard current density. I will first discuss a simple approach that our group has developed for measuring θ_{SH}. We fabricate bilayer devices consisting of a thin film of a spin Hall metal with a ferromagnet such as permalloy on top. We apply a current in the film plane that, because of the spin Hall effect, generates a vertically-propagating spin current in the spin Hall metal that can travel to the ferromagnet and be absorbed by it, to apply a spin transfer torque. By measuring the amplitude of the resulting magnetic deflections we can accurately measure the strength of the spin torque and hence the amplitude of the spin Hall spin current. We find by this technique that the strength of the spin Hall effect in Pt was vastly underestimated in almost all previous experiments (the Saitoh group at Keio University got it right). Furthermore, we find that the spin Hall effects in tantalum and tungsten are even stronger than in Pt, so that currently the largest spin Hall angle that we have measured, in the high-resistivity beta form of tungsten, is $\theta_{SH} \approx 0.3$.

Spin Hall angles on this order are very interesting for applications, because the strength of the spin torque per unit applied current in spin Hall devices can be much greater than the torque due to spin-filtered spin currents that flow in conventional magnetic tunnel junctions (MTJs). In a conventional MTJ, the strength of the spin torque is limited to be at most 1 unit of $\hbar/2$ angular moment transferred per unit charge in the current; whereas in spin Hall devices the efficiency can be an order of magnitude or more greater. This highly-efficient spin Hall torque can be used to make magnetic memory and signal-processing devices that can be manipulated with low values of current and energy. Since the spin current and charge current in a spin Hall device travel in perpendicular directions, spin-Hall-torque devices are also inherently more reliable than conventional MTJ-based memory structures – unlike in conventional MTJs the magnetic manipulation process in spin-Hall-torque structures does not involve applying a large voltage to a tunnel barrier, that can result in dielectric breakdown. I will present our group's latest results showing that the spin Hall torque can produce efficient switching of both in-plane and perpendicularly-magnetized thin-film magnetic devices, and it can also generate steady-state magnetic oscillations in response to a direct current. Furthermore, the spin Hall torque can be combined with voltage-controlled magnetic anisotropy to generate even more efficient, very high-density magnetic memory devices, and also frequency-tunable nanomagnetic oscillators. I will close by asking some questions about how to search for even stronger spin-Hall materials.

Th0900 Invited

Multiferroic tunnel Junctions

A. Chanthbouala [1], A. Crassous [1], V. Garcia [1,2], K. Bouzehouane [1],S.Fusil [1], L. Bocher [3], A.Gloter [3], C. Deranlot [1], S. Xavier [4], N. Mathur [2], M.Bibes [1] and A. Barthélémy [1]

1) Unité Mixte de Physique CNRS/Thales, Campus de l'école polytechnique, 1 av. A. Fresnel, 91767 Palaiseau, France
2) University of Cambridge, Cambridge CB2 3EQ, United Kingdom
3) Laboratoire de Physique des Solides, Université Paris Sud, 91405 Orsay, France
4) Thales Research and Technology, 1 Av. Augustin Fresnel, 9167 Palaiseau, France

The phenomenon of electron tunneling has been known since the advent of quantum mechanics. Its interplay with magnetism, i.e., spin-dependent tunneling observed in magnetic tunnel junctions has aroused considerable interest and led to important advances in the field of magnetic random access memories. In 1971, Esaki *et al.* proposed to couple another ferroic order, ferroelectricity, with quantum-mechanical tunnelling in ferroelectric tunnel junctions composed of metallic electrodes with a ferroelectric tunnel barrier. The recent advances in the growth of ferroelectric thin films and the possibility to achieve stable and switchable ferroelectric polarization in nanometer-thick films have now allowed achieving this goal.

In these ferroelectric tunnel junctions, large changes in the resistance are observed and correlated with the direction of the ferroelectric polarisation of the barrier [1]. This give rise to large electroresistance phenomena (TER) that amounts to 75000% for a 3nm $BaTiO_3$ tunnel barrier as revealed by scanning probe microscopy. This resistance switching in solid-state ferroelectric tunnel junctions is large, fast, stable, reproducible and reliable electroresistance offering new opportunities for ferroelectrics in future data storage [2].

When a ferromagnetic counter electrode of Fe is added to obtain a ferroelectric magnetic tunnel junction, a modulation of tunnel magnetoresistance reflecting changes in the spin polarisation of the electrode when the ferroelectric polarisation is switched have been observed [3]. These junctions provide an interesting opportunity to obtain a robust room temperature magnetoelectric effect and to achieve an electric control of the spin polarisation. We will review recent advances in this field.

1] Nature 460, 81 (2009) ; Appl. Phys. Lett. **96**, 042901 (2010)
2] Nature Nanotechnology 7, 101 (2012); Nature Materials (2012) accepted
3] Science 327, 1106 (2010) ; Nature Materials 10, 753 (2011)

We acknowledge financial support from the European Research Council (ERC Advanced Grant FEMMES, No. 267579)

Graphene II

Th1015 Invited

Graphene Barristor:
a New Device Structure for High On- and Off- current Ratio

Dr. Hyun-Jong Chung

Research Staff Member, Graphene Center
Samsung Advanced Institute of Technology

Abstract:

Graphene has been considered as one of the potential post Si-materials due to its high mobility. [1] However, since graphene is semi-conductor with zero band gap, it is difficult to achieve high I_{on}/I_{off} ratio, one of the most important requirements for commercial devices. There have been many attempts to open its band gap for high I_{on}/I_{off} ratio, but most of them end up lowering the mobility. [2-5] Thus, we proposed and demonstrated a new device structure for graphene transistor based on one of the unique properties of graphene for high I_{on}/I_{off}: using this approach, we were able to achieve the ratio over 10^5. [6] Our device has several major advantages over previously proposed graphene based electronic devices. Since our device does not alter the given properties of graphene, such as opening the band gap, it has no fundamental issues on mobility degradations. In addition, our device is fully compatible with current Si technology and we were able to fabricate the devices with 6" wafer scale with CVD (Chemical Vapor Deposition) grown graphene. In this presentation, we will discuss about the details of our graphene device including the device structure and the detailed understanding of working mechanism. We will present device characteristics including I-V curves with 10^5 on/off ratio. We will also present the performance of an inverter based on our devices. Finally, we will discuss the current issues and their potential solutions.

[1] K. Kim, J.-Y. Choi, T. Kim, S.-H. Cho, and H.-J. Chung, Nature (2011), 479, 338
[2] Y. Zhang, T.-T. Tang, C. Girit, Z. Hao, M. C. Martin, A. Zettl, M. F. Crommie, Y. R. Shen, and F. Wang, Nature (2009), 459, 820
[3] X. Li, X. Wang, L. Zhang, S. Lee, and H. Dai, Science (2008), 319, 1229
[4] J. Cai, P. Ruffieux, R. Jaafar, M. Bieri, T. Braun, S. Blankenburg, M. Muoth, A. P. Seitsonen, M. Saleh, X. Feng, K. Mullen, and R. Fasel, Nature (2010), 466, 470
[5] L. Ci, L. Song, C. Jin, D. Jaiwala, D. Wu, Y. Li, A. Srivastava, Z. F. Wang, K. Storr, L. Balicas, F. Liu, and P. M. Ajayan, Nature Materials (2010), 9, 430
[6] H. Yang, J. Heo, S. Park, H. J. Song, D. H. Seo, K.-E. Byun, P. Kim, I. Yoo, H.-J. Chung, and K. Kim, Science (2012), 336, 1140

Unique optoelectronic applications of graphene

Huili (Grace) Xing
Electrical Engineering Department, University of Notre Dame

Graphene, an atomically thin 2D crystal with zero bandgap, has been touted for many intriguing applications, particularly for transparent touch screens and wearable electronics. Its optoelectronic properties are equally noteworthy. IR photodetectors and modulators as well as THz emitters have been proposed and demonstrated recently. As a standing alone 2DEG with tunable conductivity, we discovered it is possible to use graphene to modulate THz beam transmission/reflection from near unity to zero. The experimentally demonstrated graphene THz modulators are already among the best electrically driven devices today [1]. As the thinnest conductor on earth, graphene has much lower density of states compared with conventional thin metal films. Consequently, graphene offers unique solutions to various problems that have been historically hindered by the high DOS of metal thin film. Recently, we observed, for the first time, hole injection from Si over the oxide barrier to graphene in internal photoemission spectroscopy measurements, enabled by this properties of graphene [2].

[1] a) **Broadband graphene terahertz modulators enabled by intraband transitions.** Berardi Sensale-Rodriguez *et al. Nature Communications,* 2012. b) **Extraordinary control of terahertz beam reflectance in graphene electro-absorption modulators**. Berardi Sensale-Rodriguez *et al*. Nano Letters, 2012.
[2] a) **Determination of graphene work function and graphene-insulator-semiconductor band alignment by internal photoemission spectroscopy**. Rusen Yan *et al*. APL 2012. b) **Graphene as an electrode for direct observation of hole injection from silicon to oxide**. Rusen Yan *et al*. Submitted, 2012.

Bio: Huili (Grace) Xing is currently the John Cardinal O'Hara CSC Associate Professor of Electrical Engineering at the University of Notre Dame. She obtained B.S. in physics from Peking University (1996), M.S. in Material Science from Lehigh University (1998) and Ph.D. in Electrical Engineering from University of California, Santa Barbara (2003), respectively. Her research focuses on development of III-V nitride and 2-D crystal semiconductor growth and (opto)electronic devices, especially the interplay between the material quality and device developments. More recent research interests include THz applications. She is a recipient of AFOSR Young Investigator Award and NSF CAREER Award.

Graphene and h-BN at the Interface

Prof. Rodney S. Ruoff
Cockrell Family Regents Chair
The University of Texas at Austin
r.ruoff@mail.utexas.edu
http://bucky-central.me.utexas.edu/
http://bucky-central.me.utexas.edu/publications/index.html

Graphene-based materials are of interest because of their electronic and thermal transport, mechanical properties, high specific surface area, and that they can act as an atom thick layer, barrier, or membrane, among other reasons. Our micromechanical exfoliation approaches [1,2] conceived of in 1998 yielded multilayer graphene and one paper described in detail how monolayer graphene could be obtained [1]. Three main research areas of our group are: (i) Growth of large area graphene on metal substrates, characterization and physical properties, and studies of devices having such CVD-grown graphene as a central component; (ii) Generation, study, and use of chemically modified graphene 'platelets' (typically derived from graphite oxide) including as dispersed in liquids forming colloids, and powders derived from such colloids or separately generated by microwave or thermal treatment of graphite oxide; (iii) Generation and study of new types of carbon derived from graphene-based precursors, such as *activated microwave expanded graphite oxide* ('aMEGO')[3].

Here, I will focus on graphene-metal interfaces such as graphene-Cu, graphene-Ni, and graphene-Cu/Ni alloy, as well as on h-BN-metal interfaces from research projects underway in my group and also *briefly* describe what I think are some important new directions in carbon and *first row element* research, for the next 10-20 years, that will introduce new issues involving interfaces for these new material classes that have not yet been made experimentally.

Support of our work by the W. M. Keck Foundation, NSF, DARPA 'iMINT', DARPA 'CERA', ONR, SWAN NRI, ARO, AEC, DOE, and the SRC, is appreciated.

1. Lu XK, Yu MF, Huang H, and Ruoff RS, *Tailoring graphite with the goal of achieving single sheets,* Nanotechnology, **10**, 269-272 (1999).
2. Lu XK, Huang H, Nemchuk N, and Ruoff RS, *Patterning of highly oriented pyrolytic graphite by oxygen plasma etching,* Applied Physics Letters, **75**, 193-195 (1999).
3. Zhu, Yanwu; Murali, Shanthi; Stoller, Meryl D.; Ganesh, K. J.; Cai, Weiwei; Ferreira, Paulo J.; Pirkle, Adam; Wallace, Robert M.; Cychosz, Katie A.; Thommes, Matthias; Su, Dong; Stach, Eric A.; Ruoff, Rodney S. *Carbon-Based Supercapacitors Produced by Activation of Graphene.* Science **332**, 1537-1541 (**2011**).

Short bio. Rod Ruoff joined The University of Texas at Austin as a Cockrell Family Regents endowed chair in September, 2007. He earned his Ph.D. in Chemical Physics from the University of Illinois-Urbana in 1988, and was a Fulbright Fellow in 1988-89 at the Max Planck Institute fuer Stroemungsforschung in Goettingen, Germany. Prior to joining UT-Austin, he was the John Evans Professor of Nanoengineering in the Department of Mechanical Engineering at Northwestern University and director of NU's Biologically Inspired Materials Institute from 2002-2007. He has co-authored 321 peer-reviewed publications devoted to chemistry, physics, materials science, mechanics, engineering, and biomedical science, is co-founder of Graphene Energy, Inc. and the founder of Graphene Materials, LLC. and Nanode, Inc. Dr. Ruoff is on the editorial board of *Composites, Science, and Technology*; *Carbon*; *Journal of Nanoengineering and Nanosystems*; and is a Managing Editor and Editorial Board Member of *NANO*. He was a Distinguished Chair Visiting Professor at Sungkyukwan University's Advanced Institute of NanoTechnology (SAINT) for several years and has recently been re-named to this position.

Dr. Ruoff's research interests include, among others:

- Synthesis, characterization, and properties of novel materials (e.g., graphene, nanotubes, sp^2-sp^3 hybrid materials, negative curvature carbons; composites)
- Energy and the environment
- Nanomanipulation and new tools for the biomedical sciences
- Technology transition

Author Index